TOPICS IN WHITE DWARFS

By

D. E. O'Donoghue

Thesis submitted in partial fulfillment of the requirements
for the Ph.D. degree at the University of Cape Town

Acknowledgements

Many people have assisted in the production of this thesis : Gary Wegner started me on the idea of modelling white dwarfs using Kemic's tables ; Chris Koen provided helpful discussions on that work ; Don Kurtz provided me with the routine to do Deeming's unequally spaced data power spectra and other helpful discussions ; Tony Fairall got some time resolved IPCS spectra of L 19-2 for me which were, unfortunately, too noisy to be useful. Tony Putman and Nick Townsend did a little of the photometry. D. T. Wickramasinghe made available preprints of his work with B. Martin. B. Lasker and J.T. Mc Graw kindly sent us their data on L 19-2. It is my pleasure to thank all of these people. I am indebted most of all to Prof. Brian Warner from whom I've learnt a lot of astronomy, the rudiments of observing and who has provided help and advice at every stage of the work as well as about half the observations of L 19-2. He has also obtained considerable financial support for me from various sources without which this work would not have been done.

The financial support of the University of Cape Town and the Council for Scientific and Industrial Research is gratefully acknowledged as are the computing facilities of the U.C.T. computer centre (where the very considerable amount of computing needed for this work was done) and the observing facilities of the South African Astronomical Observatory.

Declaration

I hereby declare that any work in this thesis which is not referenced or otherwise disclaimed, is my own.

Signed

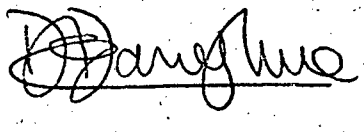

Abstract

The observations of the 12 known magnetic white dwarfs are reviewed and a list of mechanisms is discussed which could give rise to the observed absorption and polarization spectra. Particular emphasis is placed on the observations of, and mechanisms important in the 3 magnetic white dwarfs to be modelled - BPM 25114, G 99-47 and GD 90. The calculation of continuum flux and polarization in these stars is discussed : the ATLAS computer programme (Kurucz,1970) is outlined and the linear theory of circular dichroism (Lamb and Sutherland,1974) is described together with its effects on radiative transfer. The line absorption and polarization is treated in the context of Unno's (1956) equations and the line broadening theory and method of solution of the equations are presented. The computer programme to combine all aspects of the models is described in some detail, the calculated absorption and polarization spectra are presented and compared with the observations. Good overall agreement was achieved. The successes and failures of the approach are discussed together with suggestions for future work.

The current observational and theoretical picture for the ZZ Ceti stars is discussed and the analysis of ZZ Ceti (Robinson et al.,1976) is examined in detail. An extensive programme of high-speed photometry on L 19-2 is reported, and the data reduction techniques described. Initial analysis of the reduced data with the approach of Robinson et al. was found to be fraught with difficulties. Instead, frequency analysis was performed using the technique of power spectra of unequally-spaced data (Deeming,1975). Five oscillation periods were discovered : 350, 192, 143, 113 and 118 seconds. Each of these was found to be amplitude variable. The 192 s oscillation was found to be comprised of a nearly equally spaced triplet of frequency components. Second-order effects in the frequency splitting were discovered. Thus, strong evidence was provided for the presence of rotational splitting of oscillation modes in the low amplitude ZZ Ceti stars. The remaining four oscillation modes were found to have two components each, with a third suspected in two cases. No equal frequency splitting was seen in any of these. No other frequencies with amplitudes exceeding 0.0001 mag were detected in the 100 to 1000 s period range. A proposed mode identification is given and the uncertainties in the theory discussed. L 19-2 was found to have no detectable period variations over the 4.5 year interval spanned by all available observations and was thus found to be another very stable white dwarf pulsator.

Table of contents

1. Introduction To The Magnetic White Dwarfs 1-1
1.1. The Magnetic White Dwarfs And Outline Of This Work 1-1
1.2. The Observations Of Magnetic White Dwarfs 1-2
1.2.1. Grw +70 8247 1-3
1.2.2. G 195-19 1-3
1.2.3. G 99-37 1-3
1.2.4. G 240-72 1-4
1.2.5. G 227-35 1-4
1.2.6. GD 229 1-4
1.2.7. LP 790-29 1-4
1.2.8. PG 1015+01 1-5
1.2.9. Summary Of The Type II Objects 1-5
1.3. Feige 7 And The DA Magnetic White Dwarfs 1-6
1.3.1. GD 90 1-6
1.3.2. G 99-47 1-6
1.3.3. Feige 7 1-7
1.3.4. BPM 25114 1-7
1.4. Principles Deduced From The Observations 1-8
1.4.1. Absorption Features 1-8
1.4.2. Polarization Features 1-9
1.4.3. Type I And II Magnetic White Dwarfs 1-11
1.4.4. Variability In Magnetic White Dwarfs 1-11

2. The Atmosphere And The Continuum 2-1
2.1. The ATLAS Computer Programme 2-1
2.2. Computing The Magnetic White Dwarf Atmospheres 2-2
2.2.1. GD 90 2-2
2.2.2. BPM 25114 2-3
2.2.3. G 99-47 2-3
2.3. Magnetic Circular Dichroism 2-3
2.4. Radiative Transfer Of Circularly Polarized Radiation 2-7

3. The Polarization And Absorption Lines 3-1
3.1. The Unno Equations 3-1
3.2. The Line Cpacity And Broadening 3-3
3.3. Boundary Conditions And Solution Of Unno's Equation 3-5

4. The Results And Conclusions 4-1
4.1. The Line Profile Computer Programme 4-1
4.2. Model Parameters And Results 4-4
4.2.1. BPM 25114 4-4
4.2.2. GD 90 4-5
4.2.3. G 99-47 4-6
4.3. Conclusions, Suggestions For Future Work 4-7

5. Introduction To L 19-2 And The ZZ Ceti Stars 5-1
5.1. General Properties Of The ZZ Ceti Stars 5-2
5.2. The Luminosity Variations Of The ZZ Ceti Stars 5-3
5.3. The Cause Of The ZZ Ceti Stars' Light Variations 5-4
5.4. ZZ Ceti (=R 548), G 117-B15A and L 19-2 5-8

6. High Speed Photometry Of L 19-2 6-1
6.1. The Observations 6-1
6.2. The Reduction Of The Data 6-5

Table of contents

7.	Frequency Analysis Of L 19-2	7-1
7.1.	Initial Investigations Of The 192 s Period	7-1
7.2.	Power Spectra Of Unequally Spaced Data	7-5
7.3.	Frequency Structure Of The 192 s Oscillation	7-8
7.4.	Frequency Structure Of The 113 s Oscillation	7-9
7.5.	Fequency Structure Of The 118 s Oscillation	7-10
7.6.	Calculating Power Spectra Of Large Data Sets	7-11
7.7.	Power Spectra Of The Complete Data Set	7-13
7.7.1.	The 192 s Oscillation	7-13
7.7.2.	The 113 s Oscillation	7-15
7.7.3.	The 118 s Oscillation	7-15
7.8.	Analysis Of The 350 s Oscillation	7-16
7.9.	Discovery And Analysis Of The 143 s Oscillation	7-17
7.10.	Analysis Of The Data Of 1976	7-17
8.	Discussion And Conclusions	8-1

LINE PROFILES FOR 3 MAGNETIC WHITE DWARFS

1. Introduction To The Magnetic White Dwarfs

1.1. The Magnetic White Dwarfs And Outline Of This Work

Since the discovery of the first white dwarf with a magnetic field exceeding 1 MG (10^6 gauss) by Kemp et al. (1970) a great deal of effort has been expended on locating and observing similar objects and developing theory with which to interpret the observations. 12 have been discovered so far (1979.0). These form a small group in the identified white dwarfs and are designated DX magnetic white dwarfs (MWD). Observationally, they are recognised and are distinct from non-MWDs due to (1) any recognisable absorption features in the spectrum being displaced from their normal positions by the Zeeman effect resulting from the presence of the magnetic field ; (2) the presence of circular and/or linear polarization caused by magnetic circular dichroism and cyclotron absorption in the star's photosphere . It must be emphasised that white dwarfs with magnetic fields in binary systems are excluded from the MWD category. Apart from (1) and (2), the group exhibits absolute magnitudes, tangential velocities and photometric colours which are typical of white dwarfs in general (Angel,1977).

It is the intention of this work to discuss all the various mechanisms giving rise to (1) and (2), emphasising the inherent assumptions and limits of applicability of the theory. Within these limits, the theory will be applied to three members of the MWDs to synthesize in detail their spectra (both intensity and polarization) for comparison with the observations. Briefly, the procedure to be followed is similar to that of Martin and Wickramasinghe (1978) whose work was published during the course of this investigation. The ATLAS computer programme (Kurucz,1970) is used to compute an atmosphere (temperatures, pressures, opacities etc.) for each star given its effective temperature, surface gravity, chemical composition and dominant opacity sources. The result is a table of temperature, gas and electron pressure, density, partition functions and monochromatic opacities versus Rosseland optical depth. These data are then used to calculate a spectrum according to the following procedure : consider an area element on the star's surface sufficiently small that the magnetic field permeating the photosphere is approximately constant over the area element. At each wavelength of interest, the contribution to the continuum polarization is calculated using Lamb and Sutherland's (1974) treatment of magnetic dichroism combined with a linearized extension of Shipman's (1971) zeroth order approach to the radiative transfer. The wavelengths of each Zeeman component of the first four Balmer lines are found from Kemic's (1974) calculations and are combined with an assumed line profile to yield the line opacity at the wavelength under consideration. This line opacity is used in Unno's (1956) polarized radiative transfer equations to provide the contribution of the line polarization and intensity. These contributions are summed to give a spectrum for each area element, extending over the range of wavelengths which are to going to be compared with the observations. Finally, a magnetic field distribution over the stellar surface is assumed and a similar calculation takes place for each area element, all of which are

integrated to yield the final synthesized spectrum.

The above program is an attempt to account fully for the significant physical processes operating in the photospheres of MWDs and to test the modelling of these processes by predicting what the observations should be. It should be noted that many assumptions have been made in the above scheme and these will be justified as the development of the models is discussed together with possible areas of breakdown. The procedure is applied to only 3 of the 12 known MWDs and the reasons for this will be made clear in the following section which is devoted to a description of the observations of all the MWDs and a brief discussion of the main features of the current hypothesis explaining these observations. Chapter 2 explains the main points of the ATLAS programme, the continuous polarization process and the treatment of the radiative transfer. The next chapter traces the derivation of the radiative transfer equations for the lines ; discusses the process of Zeeman splitting and what line broadening theory is used in the models and concludes with the method of solution of the equations and the boundary conditions used. In chapter 4, salient features of the computer programme for the lines are pointed out, the synthesized spectra are presented and compared with the observations and the successes and failures of the technique are discussed along with suggestions for future work.

1.2. The Observations Of Magnetic White Dwarfs

Before plunging into the details of the observational work on each star, it is helpful to have the broad overview of them in mind. Observationally, the MWDs divide into two groups (Angel,1977). The stars of the first group have about 1% circular polarization, no detectable broad band linear polarization and absorption spectra with lines or molecular bands which have been identified (in some stars tentatively, in others more conclusively) with Zeeman shifted lines due to hydrogen and/or helium, or Zeeman shifted bands of carbon based molecules. The magnetic fields causing these effects have been estimated to be in the range 1 to 50 MG. At 1 MG, the Zeeman shift is less than 2 Angstroms (abbreviated A without the superscripted circle) in the first four members of the Balmer series while the continuous circular polarization is less than 0.05% (Preston, 1970 ; Angel,1977). Members of the second group have large circular polarization (1-5%), may have linear polarization of comparable size and have spectra either that are apparently continuous or that have features which have not as yet been identified. The physical reasons for this grouping will be discussed in section 1.4 and it suffices to say for the present that the presence of the linear component and the size of the circular polarization suggests that the strength of the magnetic fields in these stars exceeds 50 MG. It is proposed to classify the former group as type I MWDs and the latter as type II. Because the main thrust of this work is in synthesizing absorption spectra (largely absent in type II stars) and because the calculation of polarization and Zeeman splitting is only reliable for magnetic field strengths under 50 MG, only members of type I stars will be modelled while type II stars will be mentioned to contrast with type I and in relation to MWDs as a whole.

Prior to 1970, it was suggested that if magnetic flux was

conserved in the collapse to the white dwarf state of evolved stars, many white dwarfs should exhibit very large surface magnetic fields. First efforts to verify this suggestion proved fruitless in spite of the reasonably sensitive equipment used, and an upper limit of about 0.1 MG was set on the mean longitudinal magnetic field in DA white dwarfs while 0.5 MG was the corresponding limit for DB white dwarfs measured by Greenstein and Trimble (1967) (Preston,1970 ; Angel and Landstreet,1970a).

1.2.1. Grw +70°8247

In mid 1970 this star was discovered to be a MWD (Kemp et al.,1970). It displays 1-3% circular polarization in the visible and is a peculiar object with an almost featureless spectrum except for a controversial band at 4135 A and two more at about 5855 A. The first attempt to explain how continuous polarization could arise from a thermal source in a magnetic field was Kemp's (1970a) magnetoemission theory from which a field of about 10 MG was inferred to be present in Grw +70° 8247 (Kemp et al.,1970). Since then, further observations and discussion in the literature have suggested that the absorption features are Zeeman shifted molecular helium bands or atomic helium lines. The strong circular polarization feature at 3400 A is suspected to be due to a continuous absorption edge in helium of the 2^3P transition (Greenstein,1970 ; Angel and Landstreet,1970b ; Kemp and Swedlund,1970 ; Kemp,1970b ; Shipman,1972 ; Wegner,1971 ; Angel,1972 ; Angel,Landstreet and Oke,1972 ; Wickramasinghe et al.,1972 ; Landstreet and Angel,1975 ; Wegner,1976). The star exhibits appreciable linear polarization and its magnetic field has been found to vary between 10 and 50 MG. Questions raised by observations of the star are not fully resolved and further theoretical work on molecular bands is awaited. Angel (1977) has categorised this star as a type II MWD.

1.2.2. G 195-19

In 1971, a second MWD, G 195-19, was discovered (Angel and Landstreet ,1971a ; Kemp et al.,1971 ; Greenstein,Gunn and Kristian,1971) to have variable circular polarization of order 0.5% (Angel and Landstreet,1971b). Because of the variability, further observations were made and a 1.33 day periodicity was detected suggesting that rotation was the cause of the variability (Angel,Illing and Landstreet,1972). The featureless continuous spectrum places this object in the type II group.

1.2.3. G 99-37

Also in 1971, G 99-37 was discovered to be an MWD with about 1% circular polarization. It has molecular bands of C_2 and CH in its spectrum. From the polarization measurements, its magnetic field strength is estimated to be about 4 MG, clearly a type I object (Landstreet and Angel,1971 ; Angel and Landstreet,1974 ; Liebert,1976).

1.2.4. G 240-72

The DC white dwarf G 240-72 was discovered to exhibit linear polarization of about 1.5% and circular polarization of about 0.5% (Angel et al.,1974a) . The circular polarization in the blue and the red are of opposite sign. The spectrum has a very broad shallow depression (20%) in the region 4400-6300 A. Because of this and the presence of the sizeable linear component , this star is thought to be a type II MWD.

1.2.5. G 227-35

The white dwarf suspect G 227-35, which has no detectable absorption features, was found to be a MWD with strong circular polarization (Angel et al.,1975). There is a 3% maximum at 4500 A and the polarization rises again to 8% in the near infrared. There is no linear polarization and the star is again thought to be of type II from the strength of the polarization .

1.2.6. GD 229

Swedlund et al. (1973) discovered circular and linear polarization in this object indicating that it is a MWD. Subsequent observations (Greenstein et al.,1974) revealed a striking spectrum of broad absorption features, the strongest being 50% deep at 4185 A and 250 A wide. The features are unidentified as yet but it has been argued that the strongest is due to cyclotron absorption in a 250 MG magnetic field. This contention is supported by a coincident feature at 4185 A in the circular polarization spectrum and a large broad V band linear polarization measurement of 3% which can only be formed in such a high field (see section 1.4). On the other hand, a number of σ components of an atomic line could be the cause but there is no obvious identification (Angel,1977). The latest observations by Greenstein and Boksenberg (1978) argue that the cyclotron absorption hypothesis is unworkable because only an unrealistically homogeneous magnetic field over the stellar surface could form such a feature. The star's circular polarization is about 1% and varies with wavelength while the linear component is 3% over a broad band. Both are suspected to be variable (Swedlund et al.,1973) but this has not been confirmed (Kemp et al.,1974). Both this object and Grw +70 8247 are hot stars and their spectra have been compared (Greenstein et al.,1974). Wegner (1976) takes up this theme and gives an extensive discussion of the possible causes of the various absorption features in their spectra.

1.2.7. LP 790-29

Another MWD with similar characteristics is LP 790-29. Discovered by Liebert and Strittmatter (1977), it was observed by Liebert et al. (1978b) and found to have about 10% circular

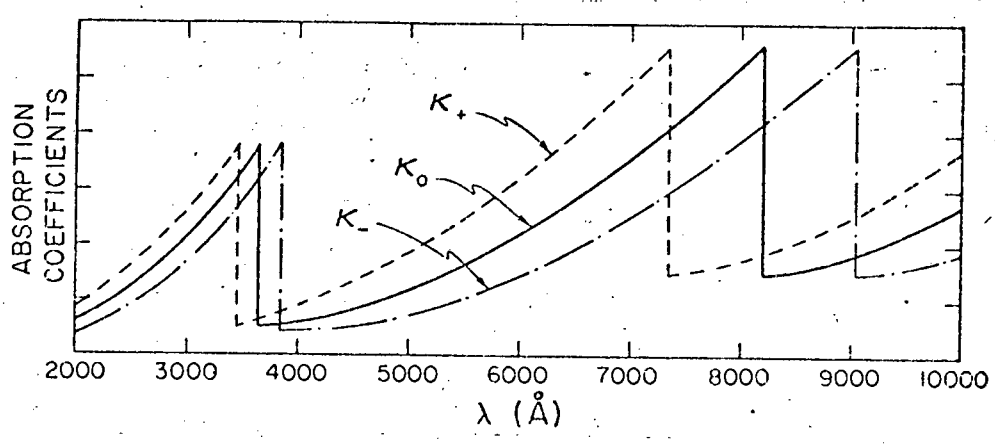

Figure 1. The behaviour of the absorption coefficients for bound-free absorption in a magnetic field (much exaggerated).

polarization and a very broad, 75% deep absorption feature of 850 A equivalent width, together with other less significant features. The principal one is thought to be due to the Swan bands of C_2 while the others are possibly due to Zeeman shifted band heads in a field of 100 MG. It is clearly a type II object.

1.2.8. PG 1015+01

Green et al. (1978) report that this star is a MWD with 1.5% circular polarization which is periodic (about 100 minutes) again suggesting rotation. The star's temperature is about 10000K and it has shallow but definite absorption components which cannot obviously be identified with H or He, even if Zeeman shifted in a field up to 50 MG (Angel,1978b). The star is thus believed to be of type II.

1.2.9. Summary Of The Type II Objects

With the exception of G 99-37, all the above stars are suspected to be type II objects. It is obvious that they are not a homogeneous group and have only the presence of a magnetic field as a common property as inferred from the strength of the circular and/or linear polarization. In many cases, the size of this field is known only to order of magnitude. In addition, many have featureless spectra or spectra with unidentified absorption components or spectra of molecular bands. The present work is aimed at constructing models of stars with hydrogen absorption features and field strengths typical of type I stars. Thus, all the above stars are individually of no special interest to this scheme. The remaining four of the group of 12 MWDs display absorption lines that are strongly suspected to be due to Zeeman shifted components of atomic hydrogen or helium. In addition, the magnetic fields thought to exist in these stars are < 50 MG, for which Kemic (1974) has calculated the positions and strengths of the Zeeman components of hydrogen and helium , while the linearized theories of magnetic circular dichroism are also adequate in this regime. Thus, models of these stars can be made according to the previously mentioned scheme and the observations of them are of special interest and will be discussed in the next section.

It should be noted that these 12 stars are not the only high magnetic field degenerates. An additional 4 are listed in Angel (1978b). However , these are all in complex systems where accretion disks and mass transfer are important and they are thus outside the scope of this work.

1.3. Feige 7 And The DA Magnetic White Dwarfs

The majority of white dwarf stars are designated DA because of the predominance of hydrogen in the chemical composition of their atmospheres and in the absorption lines in their spectra. None of the stars discussed so far can be designated DA. Indeed Elias and Greenstein (1974) could find no magnetic stars among the list of

DAs that they tested. However, Angel et al. (1974b) identified the first DA MWD : GD 90.

1.3.1. GD 90

This star has well resolved identifiable Zeeman structure in $H\beta$, $H\gamma$ and $H\delta$. It also has circular polarization with maxima of about 5% which are coincident with the absorption features while no linear polarization has been detected. There is no evidence of spectrum variability which suggests that the magnetic field of the observable disk is constant in time. The Zeeman shifts are compatible with a field varying over the stellar surface between 4 and 9 MG (Angel et al.,1974b). The authors also conclude from the depth of the absorption features that the field is constant over a substantial fraction of the stellar disk, at least 20%. Recent observations by Brown et al. (1977) have extended the list of absorption features. They also compute the predicted continuum polarization from Kemp's (1970a) magnetoemission theory using a value of the magnetic field derived from the Zeeman splitting. This is then compared with the observations and consistency can only be achieved if Balmer edge effects are included in the calculation. They find no evidence for time variability in the magnetic field.

1.3.2. G 99-47

The star G 99-47 is an interesting object because it is a very cool white dwarf. It was found to be magnetic with 0.4% circular polarization (Angel and Landstreet,1972). It was classified as featureless, type DC, by Greenstein et al. (1971) and has an effective temperature of 5700k according to Greenstein (1974). In 1974 and 1975, Liebert et al. (1975) detected an $H\alpha$ Zeeman pattern in the star. They interpret the single feature in their spectra as being due to the π component (unpolarized) of $H\alpha$ shifted 21 A shortward by a mean longitudinal field of 16 MG. The two σ components will be too weak to be detected except by their circular polarization and this is found to be present at wavelengths on both sides of the absorption feature indicating a surface field varying between 8 and 25 MG. The authors explain the absence of the other Balmer lines by the fact that the Balmer decrement steepens as the effective temperature decreases. This, combined with the broadening due to the magnetic field (see section 1.4), is likely to make higher series members undetectable. The star is, in fact, so cool that it is near the temperature below which the Balmer lines disappear, even in non-magnetic atmospheres (Liebert et al.,1975). The authors modelled the intensity and polarization spectrum crudely, and found a good fit to the data although the polarization measurements were made in channels at least 160 A wide. They report a discrepancy in the field strength calculated from the continuum cirular polarization and that found from the modelling of the single absorption feature which they attribute to errors in the former due to some uncertainty in the magnetic circular dichroism theory and the effects of radiative transfer in a cool atmosphere.

1.3.3. Feige 7

The star Feige 7 was discovered to be a MWD by Liebert et al. (1977). It was originally classified DC (no features deeped than 10%) but is now known to have a rich spectrum of weak absorption features and variable circular polarization. The latter varies sinusoidally with zero mean, 0.3% amplitude and a period of 2.2 hours. The spectrum is interpretable in terms of Zeeman shifted hydrogen and helium lines in a field of 18 to 20 MG. The spectrum varies slightly over the polarization period and this suggests that the variability is due to rotation. The authors propose that the star is an oblique rotator with the magnetic axis inclined at 24° to the rotation axis which is in the plane of the sky. The star is very hot, with an effective temperature as high as 28000K which makes it the hottest magnetic degenerate star. The star is unique among white dwarfs in that it has both neutral hydrogen and helium lines of comparable strength in its spectrum. From this, helium must be the dominant atmospheric constituent but the H/He abundance may well vary over the stellar surface due to the presence of the magnetic field which must be very homogeneous due to the relative sharpness of the absorption features (Liebert et al.,1977 ; Angel,1977). Surface varying photospheric abundances due to magnetic fields have been found to play an important part in explaining the spectra of some magnetic A stars. Liebert et al. propose some possibilities to test this hypothesis for Feige 7. A centred dipole with an orientation as described above has been found to fit these constraints rather well. Because a dipole configuration is strongly suggested by the data and because its high effective temperature indicates that it is recently formed, the authors point out that this white dwarf is a significant test for theories explaining the origin and evolution of magnetic fields in MWDs, especially for the hypothesis that argues that the fields are quite complex initially with high order field multipoles decaying with time.

The latest observations by Greenstein and Boksenberg (1978) have been compared with a number of model atmospheres and a significant continuum depression has been observed shortward of 5000 A. This has been explained by absorption of unresolved Zeeman components of H and He.

1.3.4. BPM 25114

The final DA MWD is the most clearcut and recent example : BPM 25114. Suggested by Wickramasinghe and Bessell in 1976, it has been confirmed to be a magnetic DA by further observations (Wickramasinghe and Bessell, 1976 ; Wickramasinghe et al.,1977 ; Wegner,1977a) and has been modelled fairly successfully by Wickramasinghe and Wegner along the guidelines attempted in this thesis (Wegner,1977a ; Martin and Wickramasinghe,1978). The star is found to be variable in its photometric colours, its specrtum and its circular polarization spectrum. Its spectrum shows a well resolved Zeeman triplet in $H\alpha$ and other distinct features shortward of this which, the above models suggest, are due to Zeeman split components of $H\beta$ and $H\gamma$. All the variations are found to be periodic on a time scale of 2.84 days (Wegner,1977a) and in phase with each other. The models give good spectral

agreement and the star is thought to be an oblique rotator with a polar field of about 40 MG, the dipole being inclined at an angle to the line of sight which varies by as much as 30 degrees during a rotation period (Martin and Wickramasinghe,1978). In unpublished work, Wegner and O'Donoghue attempted to explain the light variations on the basis of the oblique rotator, by modelling the U,B,V colours from calculations of the spectrum changes in one rotation period. It was found, however, that the spectral changes were not sufficiently large to fully account for the colour variations observed. The star is hot (effective temperature around 20000K) and strong wavelength dependent circular and linear polarization is predicted on the basis of the models. At the moment, sufficiently detailed polarization observations are lacking, and these are awaited to provide a check on the models so far (Martin and Wickramasinghe,1978).

This completes the review of the data to be intepreted. The next section makes some general commments on the MWDs in an attempt to explain the general features of the observations on the basis of what is theoretically predicted about their behaviour.

1.4. Principles Deduced From The Observations

1.4.1. Absorption Features

A particularly striking fact about some of the MWDs is the absence of the usual Stark broadened and well defined absorption lines but instead, the presence of very shallow features spreading across many tens and even hundreds of Angstroms. Other MWDs have no absorption features in their spectra at all. This is explained by the phenomenon of 'magnetic broadening'. The magnetic field removes the energy level degeneracy in the radiating atoms and splits each Balmer line into a number of sub-components whose wavelengths are shifted away from the field-free values by amounts depending on the strength of the field. At relatively low fields, the linear Zeeman effect is dominant which results in a triplet structure with one component, the π component, remaining at the field-free value while two σ components appear on either side of the π component, and shifted from it by equal increments in frequency (or energy). At progressively higher fields, the quadratic Zeeman effect becomes of increasing importance. This term is dependent upon the fourth power of the principal quantum number n, and so the quadratic Zeeman effect is equal to the linear at 10 MG for H_γ while almost negligible for H_α (Angel,1977). The quadratic shift is always a blue shift and so each triplet component is now further split into many more sub-components : thirty components in all for H_δ for example. At 10 MG, the furthest apart of these thirty lines are separated by nearly 300 A (Kemic,1974). The result is that in a star with a completely homogeneous field of 10 MG, there are now thirty components of varying strength spread over 300 A, in the place of the original single line (see also fig. 3). In a star with a distribution of field strength over the disk, each of these components is shifted by varying amounts (depending on the local field strength), with the result that a shallow, extremely broad absorption feature is

formed. In Wegner's (1977b) models of Hβ line profiles, he shows how the classical Zeeman triplet, which is still recognizable in a dipole field of polar field strength 20 MG, rapidly becomes unrecognizable as the field is increased to 50 MG. From these considerations we may conclude that : (i) MWDs with low fields will have recognizable absorption features ; (ii) Stars with high fields will exhibit a complicated line structure; (iii) Stars with inhomogeneous magnetic fields will have any recognizable absorption features made less conspicuous due to the smearing out these features because of the varying wavelength shifts in the Zeeman sub-components; (iv) MWDs with fields in excess of 50 MG may well exhibit only continuous spectra because their lines have been split and 'washed out' by the very strong inhomogeneous magnetic field to such an extent that they merge with the continuum. The wavelength dependence of the line absorption coefficient is more similar to that of a continuous absorption coefficient than to the normal field free line absorption coefficient.

1.4.2. Polarization Features

MWDs display continuous circular polarization which is due to two causes : circular polarization because of bound-bound transitions in atoms or molecules in the photosphere and continuous circular polarization as a result of the circular dichroism exhibited by continuous absorbers in a magnetic field (more fully discussed in the next chapter). The former may exhibit a Zeeman triplet structure in low fields with polarization of 10 to 20%. In high fields, this structure may become washed out as described in the discussion of the absorption features, with a consequent reduction in size to a few percent or less. The latter cause will also result in polarization of order 1% which is smoothly continuous with wavelength, associated with the continuous absorption processes. There may be discontinuities if the bound-free absorption coefficient has edges, e.g. the Balmer jump. Thus the spectrum of circular polarization will be smooth except for those features due to absorption lines or bands , or due to bound-free absorption edges.

As mentioned previously, linear polarization is also seen in the MWDs. Again , there are three mechanisms responsible : (i) polarized radiation from absorption lines, emitted perpendicularly to the magnetic field. This follows from Unno's equations of polarized radiative transfer. It will obviously be evident only at wavelengths where the line absorption coefficient is significant, and may be strong (10%) over these regions. The field geometry is very important in determining the strength of this source of linear polarization since linear polarization produced in two oppositely directed fields will cancel ; (ii) magnetic linear dichroism. This is quadratic in the field strength and is negligible in the visible below fields of 10 MG. Furthermore, any linear polarization produced in the photosphere by the above mechanisms is likely to be severely attenuated by Faraday rotation (Sazonov and Chernomordik,1975). This causes a rotation in the plane of polarization as it propagates through the photosphere. The result is that linear polarization that is emitted at different depths in the photosphere will be rotated by different amounts by the time it reaches the surface thus

scrambling up any ordered structure rendering it undetectable ; (iii) cyclotron absorption. Free electrons spiralling around magnetic field lines are accelerated and thus may absorb radiation and re-emit both linear and circular polarization. In the visible , the effect is not significant below 10 MG. Above 10 MG, it may become very significant (Lamb and Sutherland,1974 ; Angel,1977). Models of cyclotron and synchrotron (relativistic cyclotron) radiation emitted from the corona and the magnetosphere have been built to explain observed linear and circular polarization in MWDs (Ingham et al.,1976 ; Rosi et al.,1976).

In summary, the following points may be noted : (1) Circular polarization arises in MWDs because of absorption features, magnetic circular dichroism and cyclotron absorption. This will be smoothly continuous except at wavelengths where the line absorption features are not washed out by field inhomogeneities, or where bound-free absorption edges occur or where cyclotron absorption is not washed out by field inhomogeneities (cyclotron absorption takes place at discrete frequencies for a fixed field strength). (2) Linear polarization arise because of line or band absorption, magnetic linear dichroism and cyclotron absorption. It is insignificant for fields under 10 MG. (3) MWDs with low fields will display continuous circular polarization of the order of 1% and little or no linear polarization while those with large fields should diplay strong circular polarization (<5%) and linear polarization of the same strength. This refers only to continuous polarization of both kinds. Low field stars may exhibit strong polarization features (linear and/or circular) in the region of absorption features although this is less likely for the linear component which is subject to Faraday rotation, the effects of which will not be incorporated in the modelling procedure of this work.

Table 1-1. Summary Of The Magnetic White Dwarfs

Name	Spectrum	Field Strength (MG)	Representative Polarization Cir (%)	Lin	Absolute Magnitude M_v	Tangential Velocity (km/s)
TYPE I						
GD 90	H	5	<0.15	-	12.63	13
G 99-47	H	20	0.4	<0.1	14.58	41
BPM 25114	H	40	1.0?	-	11.54	35
Feige 7	H,He	18-20	0.3	-	11.48	39
G 99-37	CH,C_2	4	0.8	<0.1	14.28	15
TYPE II						
Grw+70°8247	He?	50?	3	2	12.14	41
GD 229	Unident	-	1	3	11.21	19
G 240-72	Contin	-	0.5	1.5	14.49	52
G 195-19	Contin	-	0.8	<0.13	13.62	83
G 227-35	Contin	-	3	<0.1	14.07	33
LP 790-29	C_2	100?	5	-	-	-
PG1015+01	Unident	-	1.5	-	-	-

1.4.3. Type I And II Magnetic White Dwarfs

The summary points in the discussion of absorption and polarization features above, form a foundation for the typing of MWDs as introduced earlier and as displayed in table 1 of Angel (1977) reproduced above as table 1-1. Type I stars have fields below 50 MG. This means that they show continuous circular polarization of 1% or less, show no continuous linear polarization because of their low fields and display absorption features that may be recognized. Type II stars show strong circular and linear polarization in accordance with their high field strengths (the only exception is G 227-35 which shows little linear but strong circular polarization : this anomaly is unresolved as yet), and continuous spectra or spectra with inidentified absorption features. Note that the field strengths are undetermined but are deduced as being high because of the strength of the observed polarization. The uncertainties in the magnetic circular dichroism theory, particularly evident at high field strengths, together with the lack of supporting evidence from the spectra, make the task of identifying the polarization sources and deducing the magnetic field strength an extremely difficult undertaking in these type II stars.

It should now be clear that observations of MWDs may be strongly influenced by selection effects thus possibly explaining why there is an apparent lack of DA MWDs. To classify a white dwarf as DA, necessitates identifying Balmer lines in the star. In type II stars, this would be near impossible because of the washing out of the lines by the strong field. In type I stars, depending upon the field strength, the task is difficult due to the significant Zeeman shifts which result from fields in excess of 1 MG (Borra,1976 ; Borra,1973 ; Angel,1977). There may indeed be a genuine lack of magnetic DAs relative to non-magnetic DAs due to some as yet unknown cause, but at this stage, the above considerations make it hard to decide if this is true or not. Only type I stars are recognizable as DA and 3 out of 5 of these have been classified as having hydrogen spectra anyway.

Because this work is concerned only with type I stars, mechanisms which are only significant in type II stars will be omitted from the modelling process. Thus, cyclotron absorption and magnetic linear dichroism will not be studied here.

1.4.4. Variability In Magnetic White Dwarfs

Three of the twelve show variability in polarization and/or spectra. This is attributed to a different magnetic field geometry being presented to the observer, almost certainly due to rotation. In the case of the variable DAs (or semi-DAs), BPM 25114 and Feige 7, an oblique rotator model seems to fit the data quite well. This refers to the case when the magnetic axis of symmetry is not coincident with the axis of rotation , causing different aspects of the field geometry to be presented to the observer as the star rotates. This results in both polarization and spectrum variability. In the case of the type II star G 195-19, the periodically varying polarization has been attributed to variable composition over the stellar surface. On the other hand, it has also been explained by the existence of a magnetic

'spot', a region of enhanced field, which rotates with the star (Landi Degl'Innocenti,1976).

In conclusion, the observational data for the 12 MWDs have been briefly reviewed in this chapter and a list of mechanisms which could produce the observed features, has been discussed. It remains now to choose the correct mechanisms for each star and combine them in their appropriate degree of importance to model the observed behaviour. The three stars which are going to be studied are BPM25114, GD 90 and G 99-47. The modelling procedure is certainly appropriate for Feige 7. However, the process is not as simple as for the former three due to the considerable abundance of helium in this star which is not as simple to deal with as hydrogen. Moreover, it was learned that D.T. Wickramasinghe and his co-workers were working on this star and as a result, it was not considered further.

The first aspect of the models to be constructed is the behaviour of the continuum and this is the subject of the next chapter.

2. The Atmosphere And The Continuum

2.1. The ATLAS Computer Programme

It should be pointed out at the outset that no attempt is made to include the effects of magnetic pressure on the run of temperature, gas pressure etc. with mean optical depth through the atmosphere. This course is also followed by Martin and Wickramasinghe (1978) who point out that these effects could be significant if the field varies with depth setting up a magnetic pressure gradient. Their model of BPM 25114 suggests that a variation in field strength by a factor greater than two, the spread due to a dipole configuration, is needed to explain the observations and that this could come about if the magnetic field has a dominant influence on the structure of the star leading to a distorted configuration as suggested by Mestel (1967) for the magnetic Ap stars. Nonetheless, we shall assume that the atmospheres of the modelled white dwarfs are not significantly different from non-magnetic white dwarfs of the same atmospheric properties. To include the effects of magnetic pressure would make the problem excessively complicated especially when it is recalled that the pressure is non-isotropic and does not directly affect neutral gas.

It is not the intention here to give a detailed account of model atmosphere theory or even describe the derivation of the algorithms used in the ATLAS computer programme. Instead, a brief outline of the stages in calculating a model atmosphere will be traced and, in the next section, the particular application to MWDs will be discussed.

The first step in any calculation is the choice of an initial temperature distribution. In ATLAS, this is the grey temperature distribution. Next, the equation of hydrostatic equilibrium is solved iteratively until self-consistency is achieved in the distribution of total pressure and mean optical depth. It is at this stage that magnetic pressure is omitted from the total pressure. The assumption of local thermodynamic equilibrium (LTE) is adopted and this is fully justified in white dwarfs where scattering is unimportant due to the high density of the photosphere. It breaks down at very small optical depths of course, but these regions do not contribute significantly to the emergent radiation. Using the LTE assumption, the statistical equilibrium equations are solved to yield the number densities of atoms in each atomic state. In the next stage, ATLAS computes the total opacity at each specified frequency by summing up contributions from a wide variety of sources : hydrogen, helium and metals etc. whose inclusion is controlled by setting the appropriate opacity switches in the input to the programme. Once the opacities are known at each frequency, the programme calculates the radiation field : the source function, intensity and flux. The flux is integrated over frequency and it is compared to the flux from a black body of the same temperature as the effective temperature of the star (given by Stefan's law) . Finally, the temperature correction is performed. This consists of adjusting the temperature distribution to give the required flux at each optical depth. In ATLAS, three correction procedures are

employed : deep in the atmosphere, the flux is sensitive to temperature and the flux error is reduced by using the Avrett-Krook (1963) temperature correction procedure ; at the surface, the flux is no longer sensitive to temperature but the flux derivative is, so the temperature is corrected by using the Λ correction procedure of Bohm-Vitense (1964) ; a third algorithm is used to smooth out the distribution in the transition region between where the other two methods are appropriate. Having thus arrived at a new temperature distribution, ATLAS returns to the beginning to start a fresh iteration by re-solving the hydrostatic equilibrium equation. The programme then continues iterating until the errors in the flux and its derivative are down to a few percent which is about the limit of meaningful accuracy.

After convergence has been attained, everything is known about the atmosphere : ATLAS provides a table of temperature, pressure, density, electron number density, partition functions, all as a function of Rosseland mean optical depth. This table is then read in to the line calculating programme as will be seen in chapter 4. In addition to the above structural quantities, wavelength dependent quantities such as monochromatic opacity and flux are tabulated at each specified wavelength.

We now discuss those considerations which are of particular relevance to the computations of the atmospheres of the actual three MWDs modelled.

2.2. Computing The Magnetic White Dwarf Atmospheres

Since it is necessary to include the effects of hydrogen line blanketing on the structure of the atmospheres of the three stars, but at the same time needing the programme to provide a line free continuum for use in the line calculations, the following procedure is used : the programme is allowed to iterate assuming that the line absorption is the same as that in a normal non-magnetic DA white dwarf i.e. the greatly Stark-broadened Balmer lines. In this way, line blanketing is crudely included in the calculation of the atmospheric structure. Of course, the line blanketing is likely to be much greater than this in many cases. If the magnetic field is so strong that it spreads the Zeeman components over a wide wavelength range, the above line blanketing calculation will underestimate the true blanketing effect. This point will be returned to in the discussion of the results. For the final iteration, however, the line opacity is not included when computing the radiation field. In order to ensure that the temperature, pressure and other distributions are not affected by this 'incorrect' flux, the temperature correction is omitted from this final iteration. Thus, the final models yield crudely line-blanketed atmospheric structure and line-free continua.

2.2.1. GD 90

The effective temperature of this star is taken from Eggen (1968) as 12000K and the surface gravity used is log g = 8. The chemical abundances are 'normal' i.e. the same as in the sun and the dominant opacity sources are H I and the negative hydrogen ion, all other opacities provided in ATLAS (Kurucz,1970) being

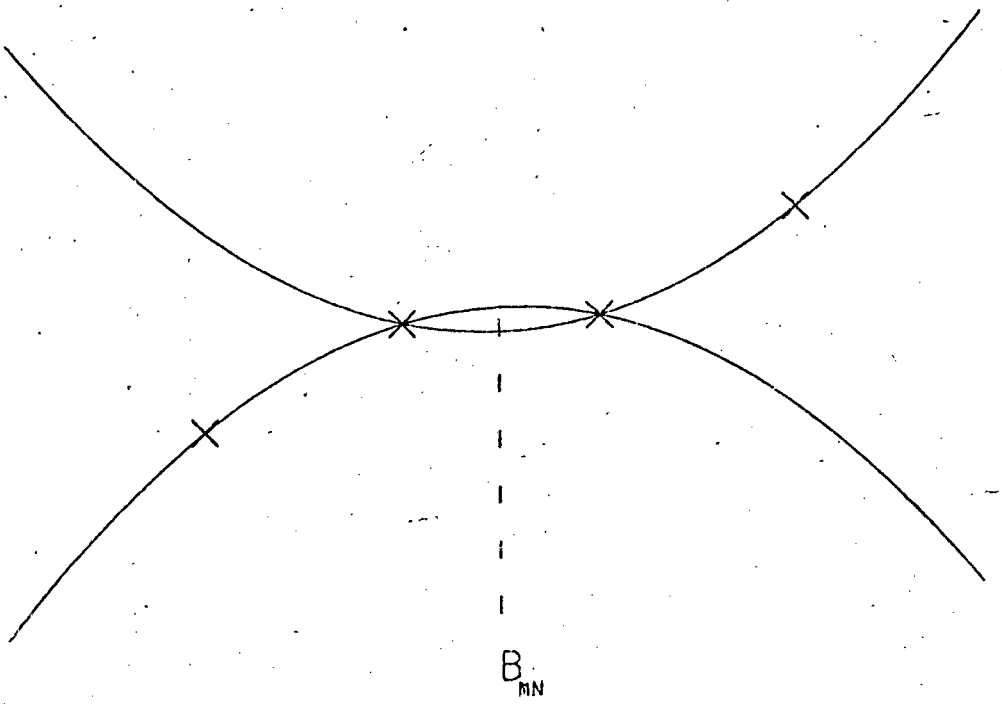

Figure 4. Illustration of the process of parabolic interpolation in Kemic's tables. The crosses represent 4 wavelengths for a particular Zeeman sub-component at four field strengths. Two parabolas are fitted through the points as shown and the interpolated value is taken as the mean of the two parabolas evaluated at the interpolated field strength B_{mn}.

insignificant. Greenstein's (1974) effective temperature of 15000K was also tried but yielded lines that were too weak.

2.2.2. BPM 25114

The atmosphere for this star is computed with log g = 8, normal abundances and dominant opacity source H I. Other opacity sources were found to be negligible. The effective temperature was varied between 17000K and 25000K . At the lower value, the lines were found to be too strong while at the upper value the slope of the continuum was unacceptable. The best agreement was found with Teff = 20000K.

2.2.3. G 99-47

Multichannel spectrophotometry by Greenstein (1974) yielded an effective temperature of 5700K. The slightly higher value of 6000K used in the present model was found to give better agreement with the observed depth of the Hα absorption feature. The non-detection of metal lines at 6000K in a non-magnetic white dwarf necessitates the metal abundance being 0.001 of the solar value or less (Weidemann,1975). As usual, log g = 8, the He/H ratio was 0.1 and the opacity sources included were H I, the cool star metal opacities of ATLAS (Kurucz,1970) and the negative hydrogen ion, the latter of which was dominant as expected.

2.3. Magnetic Circular Dichroism

This completes the description of how the atmospheres of the three DA MWDs were calculated. We next turn to a study of continuum polarization.

The first attempts at understanding the polarization behaviour of a thermalised gas in a magnetic field were made by Kemp (1970a), and refined by Chanmugam et al. (1972) and corrected by Kemp (1977). Kemp considered bound-bound transitions in a magnetic field, of harmonic oscillators maintained at uniform temperature by a thermostat. The system, a 'gray' body, has the property of constant spectral absorptivity i.e. it exhibits a flat featureless spectrum. Using both a quantum-mechanical and classical treatment, he showed that the result of imposing a magnetic field on this system was the appearance of a net circular polarization given at frequency ω by

$$q(\omega) \cong -\omega_L/\omega, \qquad \omega_L = \frac{eB}{4\pi m_e c}$$

where ω_L is the Larmor frequency. This result is a first order effect in the magnetic field and is based on the so-called 'rigidity' of the wavefunction against magnetic perturbation, a phenomenon discussed more fully a little further on. Kemp extended this model to considering free-free transitions in a magnetic field. It should be noted that this radiation is not cyclotron radiation which results from a charged particle radiating due to being accelerated into circular motion in a

magnetic field. Rather, this radiation arises from electron-nuclei collisions where the motion of the electrons between collisions is not rectilinear but circular, in rotation about a magnetic field line. The dichroism arises because the collisions in which the magnetic force on the electrons acts in the same direction as the Coulomb force, will accelerate the electrons more strongly causing them to radiate more strongly than those collisions in which the electric and magnetic forces are opposed. Since these two types have orbits with opposite senses of rotation, they radiate opposite senses of circular polarization with unequal strength (Angel,1977). By considering a reference frame rotating with the cyclotron frequency, Kemp removed the circular paths of the electrons and treated the situation as in the magnetic field-free case and deduced that the net circular polarization is proportional to the ratio of the Larmor frequency and the observed frequency, as in the harmonic oscillator case (Kemp,1970a).

A major source of continuous opacity in white dwarfs is bound-free transitions and the resultant circular dichroism due to moderate magnetic field strengths was treated by Lamb and Sutherland (1974). At optical wavelengths, the bound-free opacity of helium is well-represented by the hydrogenic result because the emission and absorption of radiation is due to transitions of an electron in an excited state while the other electron , tightly bound in the 1 S state, effectively screens the nucleus so its net charge is only +1e. The use of the hydrogenic wave-functions is thus fully justified in the case of helium. Also, as the dipole radiation approximation is fully justified for bound-free opacity in the optical (Lamb and Sutherland,1974), we need only analyse the behaviour of the dipole absorption coefficient for both hydrogen and helium bound-free opacity.

Bound-free opacity is due to the absorption of radiation of frequency ω by an electron in a bound state of negative energy ,-I, with some initial wave-function, to a continuum state of energy $\hbar\omega - I$, with some final wavefunction. Now suppose the magnetic field is weak enough so that the quadratic Zeeman effect is not significant in relation to the linear effect. Because the linear Zeeman Hamiltonian is diagonal, the initial state wave-function is unaltered by the field. This is the 'rigidity' of the wave-function against magnetic perturbation which is the basis of Kemp's harmonic oscillator treatment. In this case, only the bound state energy changes by $m_i \hbar\omega_L$ where m_i is the initial state magnetic quantum number. Now the matrix element in the absorption coefficient, see equation 2.3.1, is a weighted overlap of the bound and free electron wave functions. Thus, if the final state 'free' electron wave function is similarly unperturbed out to an atomic distance of the order of the bound state radius, the zero field free electron wave-function will be a good approximation to the free electron wave-function in the matrix element for the non-zero field case. Of course, at greater distances, the free electron wave-function is badly distorted and must spiral around the field lines. This approximation is valid if the free electron kinetic energy term is much larger than the quadratic Zeeman energy term in the Hamiltonian. In this case, the free electron wave-function is approximated by the zero field one with a linear Zeeman shift, $m_f \hbar\omega_L$, in the energy. The condition for the quadratic Zeeman effect being negligible is

$$\frac{e^2 B^2 \langle r^2 \rangle}{8mc^2} \ll \hbar\omega_L$$

where r is the bound state radius. This reduces to

$$n^4 B_7 \ll 1000$$

where B_7 is the field strength in units of 10 MG, and n is the principal quantum number. For the Balmer series (n=2), this is still valid at 50 MG. The condition on the free electron kinetic energy is

$$\frac{P^2}{2m} \gg \frac{e^2B^2}{8mc^2} \langle r^2 \rangle \quad \text{or}$$

$$\langle r^2 \rangle \ll \langle r_L^2 \rangle$$

where r_L is the Larmor radius and r the bound state wave function radius.

Having laid the foundations and stated where the approximation is valid, the derivation of the dichroism formula is straightforward. Since we are in the linear regime, each bound state is split into a triplet of states as described in section 1.4. The wave-functions for the three are identical, as established above, while the energies are linearly shifted : one state being identical to the zero field state, two others shifted above and below by $\hbar\omega_L$. There are thus three absorption coefficients : K_0, K_+, K_-. Evidently, if the zero field absorption coefficient is given in the dipole approximation by

$$K_0 = \text{const.} \times \omega \sum_{i,f} |\langle f|d_q|i\rangle|^2 \delta(E_g - E_i - \hbar\omega) \qquad (2.3.1)$$

$$= \text{const.} \times \omega f(\omega)$$

(E_i is the initial energy (-I), E_f is the final energy, $\hbar\omega$ is the photon energy and $\langle f | d_q | i \rangle$ is the matrix element of the transition) then the magnetic field leaves unchanged the matrix element and only alters the energy term in the δ-function with the result that the other two absorption coefficients are given by

$$K_\pm = \text{const.} \; \omega f(\omega \pm \omega_L) \qquad (2.3.2)$$

Lamb and Sutherland illustrate this formula for the case of hydrogen and their diagram is reproduced in fig. 1. It is now easy to see why the circular dichroism arises and to calculate quantitatively its size and spectral dependence : radiation caused by transitions from the level associated with opacity K_0, is unpolarized, while radiation from the other two levels is oppositely circularly polarized. Hence, the fractional difference in the opacities is

$$\frac{\Delta K}{K_0} = \frac{K_+ - K_-}{K_0} \qquad (2.3.3)$$

$$= \frac{\text{const.}\omega[f(\omega+\omega_L) - f(\omega-\omega_L)]}{\text{const.}\omega.f(\omega)}$$

and provided the magnetic field is small enough so that $\omega_L \ll \omega$, a Taylor expansion yields

$$\frac{\Delta K}{K_0} = \frac{2\omega_L}{f(\omega)} \frac{df}{d\omega}, \quad \frac{\omega_L}{\omega} << 1 \qquad (2.3.4)$$

This is a very useful formula : supposing that $f(\omega)$ is well represented by some simple power law over a restricted wavelength interval, say

$$f(\omega) = k\omega^{\alpha}$$

then $\Delta K/K_0$ reduces to

$$\frac{\Delta K}{K_0} = \beta \frac{\omega_L}{\omega} ; \quad \beta = 2\alpha ; \quad \frac{\omega_L}{\omega}, \frac{\Delta K}{K_0} << 1 \qquad (2.3.5)$$

Examples of β are 8 for hydrogen, 5.7 for He (Angel,1977). 2.3.5 is thus a formula of fundamental importance in magnetic circular dichroism which is valid for all sources of continuous opacity in white dwarf atmospheres, both bound-free and free-free. Of course, the constant β depends on the opacity in question. The formula is based on a linear theory and its validity is being stretched even at fields of about 50 MG.

Notice that in an atmosphere with many different kinds of continuous absorbers, the value of β is a weighted average over the various individual values, the weight being the corresponding opacity : in the case of three opacity sources, for example,

$$\Delta K_1 = \beta_1 \frac{\omega}{\omega_L} . K_1$$

$$\Delta K_2 = \beta_2 \frac{\omega}{\omega_L} . K_2$$

$$\Delta K_3 = \beta_3 \frac{\omega}{\omega_L} . K_3$$

The total ΔK is the algebraic sum of the individual ΔK_i for the same reason that the total opacity is the sum of the individual opacities and so

$$\Delta K = \frac{\omega}{\omega_L} (\beta_1 K_1 + \beta_2 K_2 + \beta_3 K_3)$$

Finally, because of the fact that

$$K_0 = K_1 + K_2 + K_3$$

then

$$\frac{\Delta K}{K_0} = \frac{\beta_1 K_1 + \beta_2 K_2 + \beta_3 K_3}{K_1 + K_2 + K_3} \frac{\omega}{\omega_L}$$

and for the general case of many absorbers

$$\frac{\Delta K}{K_0} = \left(\frac{\sum_i \beta_i K_i}{\sum_i K_i} \right) \frac{\omega}{\omega_2} \qquad (2.3.6)$$

Notice from fig. 1, the opacity near the absorption edges changes discontinuously so that the approximation $\Delta K/K_0$ is small, must fail in these regions which extend 60 A and 300 A on either side of the Balmer and Paschen edges respectively, as shaded in the graph.

Lamb and Sutherland calculate the polarization in these regions but we shall not attempt to do so because they are not in regions of the spectrum where observations exist at the moment for the stars to be modelled. We do, however, point out that such calculations justify the statements concerning continuous circular polarization features near opacity edges, made in section 1.4, and expect that features in the observations might arise due to edges, as is postulated for Grw $+70^{\circ}8247$.

Having determined, to first order at least, the effect of a magnetic field on bound-free and free-free opacity, we now proceed to demonstrate the effect of this circular dichroism on radiative transfer and calculate the circular polarization of the emergent radiation.

2.4. Radiative Transfer Of Circularly Polarized Radiation

We shall follow closely the treatment of Shipman (1971) but extend the approximation made in his calculations from zero to first order. In regions where the opacity is due to continuum sources alone and thus slowly varying with frequency, we may expand the function f in equation 2.3.2 as a Taylor series

$$K_{\pm} = \text{const.}\omega.f(\omega) \pm \text{const.}\omega.(\omega-\omega_L)\frac{df}{d\omega}$$

or $$K_{\pm} = K_0 + \delta K$$

provided $\omega_L << \omega$ or $\delta K << K_0$. Defining optical depths t, t_+ and t_- appropriate to K_0, K_+ and K_- we have

$$dt_+ = K_+ dM \quad , dM = \rho dx \qquad (2.4.2)$$
$$dt_- = K_- dM$$
$$dt = K_0 dM$$

$$\Rightarrow \quad dt_+ = K_+/K_0\, dt$$
$$dt_- = K_-/K_0\, dt$$

and from eqs 2.4.1 and 2.4.2, it follows that

$$t_+ = \int K_+ dM = \int (K_0+\delta K)\, dM = t + \delta t \text{ and}$$

$$t_- = \int K_- dM = \int (K_0-\delta K)\, dM = t - \delta t \qquad (2.4.4)$$

Using these relations, let us calculate the difference in emergent fluxes of the two oppositely polarized kinds of radiation :

$$H_+ - H_- = \tfrac{1}{2} \int_0^{\infty} S(t_+) E_2(t_+) dt_+ - \tfrac{1}{2} \int_0^{\infty} S(t_-) E_2(t_-) dt_-$$

where S is the source function and E_2 is the second exponential integral. Let us change the variable of integration to the unshifted optical depth scale t. Hence

$$H_+ - H_- = \tfrac{1}{2}\int_0^{\infty} S(t_+(t)) E_2(t+(t)) \frac{K_+}{K_0} dt - \tfrac{1}{2}\int_0^{\infty} S(t_-(T)) E_2(t_-(t)) \frac{K_-}{K_0} dt$$

Note that the dependence of S in LTE on the three optical depth scales is through the temperature distribution $T(t), T(t_+)$ and $T(t_-)$. At each physical level in the atmosphere, there is a unique temperature so the numerical value of the source function at each level is the same and may be set equal to the unshifted optical

depth's source function S(t). We may further expand the exponential integrals in a first order Taylor series yielding

$$E_2(t_+(t)) = \dot{E}_2(t) + \dot{E}_2(t)\delta t$$

$$E_2(t_-(t)) = E_2(t) - E_2(t)\delta t \quad \text{so that}$$

$$H_+ - H_- = \tfrac{1}{2}\int_0^\infty \{S(t)[E_2(t) + \dot{E}_2(t)\delta t]\frac{K_+}{K_o} - S(t)[E_2(t) - \dot{E}_2(t)\delta t]\frac{K_-}{K_o}\}dt$$

Now, assuming that the magnetic field at the surface does not vary deeper in the photosphere, $\Delta K/K_o$ from equation 2.3.5 does not vary with t. Also from equation 2.4.1, $\Delta K/K_o = 2\delta K/K_o$ so that

$$\delta t = \int \delta K dM = \frac{\delta K}{K_o}\int K_o dM = \frac{t\delta K}{K_o}$$

Using this relation and the fact that $(K_+ + K_-)/K_o = 2$ then the above relation for the fluxes reduces to

$$H_+ - H_- = \tfrac{1}{2}\int_0^\infty \{S(t)[E_2(t) + t\dot{E}_2(t)]\frac{\Delta K}{K_o}dt$$

Also to first order

$$H_+ + H_- = \tfrac{1}{2}\int_0^\infty S(t)E_2(t)dt$$

Since $\dot{E}_2(t) = -E_1(t)$, the first exponential integral, the final expression for the circular polarization is

$$q = \frac{H_+ - H_-}{H_+ + H_-} = \frac{\int_0^\infty S(t)\{E_2(t) - tE_1(t)\}\frac{\Delta K}{K_o}dt}{\int_0^\infty S(t)E_2(t)dt}$$

In the case of a linear source function and $\Delta K/K_o = 0.1$, this solution is identical to Shipman's (1971) solution and differs from the exact solution which may be evaluated analytically. In the case of a realistic temperature distribution for a 12000K model DA white dwarf at 5000 A, the values of q are respectively 4.4%, 5.2% and 4.3%. Thus the above is an improvement over Shipman's work in realistic cases.

In the present work, 2.4.5 was integrated using the results of the model atmosphere calculations which provide the dependence of the functions in the integrand on t, the Rosseland optical depth. The source function is the Planck function from the LTE assumption. The fractional circular polarization, q, was combined with the results of the polarization calculations for the line absorption which will be described in the next chapter. This, then, completes the section on the calculation of the continuum flux and polarization and we next consider the lines.

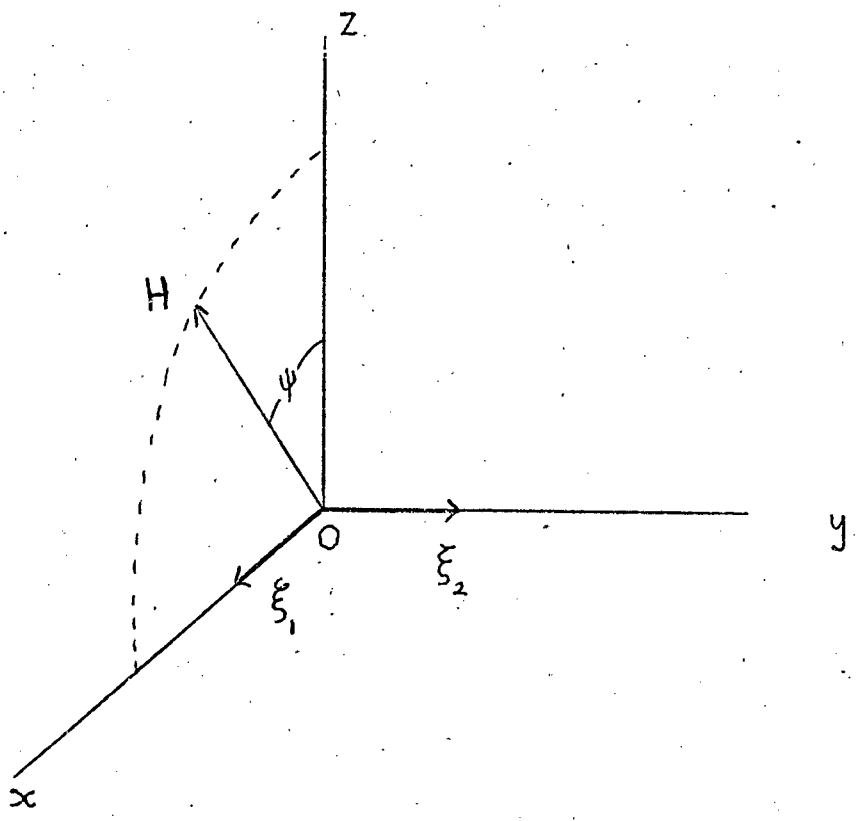

Figure 2. Co-ordinate system for representing the polarization. The z-axis shows the direction of the line of sight. The z-x plane contains the magnetic vector OH and ψ is the angle zOH.

3. The Polarization And Absorption Lines

3.1. The Unno Equations

In describing the Unno equations, we shall merely outline their derivation since the details are described in Unno (1956). Considering fig. 2, taken from Unno's work, ψ is the angle between the magnetic field and the line of sight, the z-axis. The x-axis is orientated in such a way that the magnetic field, represented by the vector H, lies in the x-z plane. ξ_1, ξ_2 and $\varepsilon_1, \varepsilon_2$ are the amplitudes and phases of the electric vector components along the x and y axes and denoted by ξ_x and ξ_y. The polarization of the radiation is fully described by the Stokes parameters I,Q,U,V where

$$\begin{aligned} I &= I_1 + I_2 \\ Q &= I_1 + I_2 \\ I_1 &= \overline{\xi_1^2}\ ,\ I_2 = \overline{\xi_2^2} \\ U &= 2\xi_1\xi_2\cos(\varepsilon_1-\varepsilon_2) \\ V &= 2\xi_1\xi_2\sin(\varepsilon_1-\varepsilon_2) \end{aligned}$$

In the classical theory of Lorentz, the absorbing and emitting electrons are assumed to be linear oscillators which undergo precession around the field lines when a magnetic field is present. Along the lines of force, the oscillators are unaffected by the magnetic field and will absorb and emit radiation as though no field were present. In the plane perpendicular, the oscillators undergo a frequency shift due to precession. In the first case, the electrons are known as p-electrons and give rise to the unshifted component, the π component. In the second case, the so-called l- and r-electrons will absorb and emit only the left- and right-handed circular polarization of the σ components which are equally shifted in frequency on either side of the π component. This is the 'classical' description of how a single spectral line becomes split into a triplet. Denoting K_p, K_r and K_l as the corresponding absorption coefficients per unit volume per unit solid angle then

$$K_p(\nu) = K_e(\nu \mp \Delta\nu_H) = K_r(\nu \pm \Delta\nu_H) = K_\nu$$

where $\Delta\nu_H$ represents the Zeeman frequency shift and K_ν is the usual absorption coefficient in the absence of a magnetic field. Further defining K as the continuous absorption coefficient we may denote

$$\eta_p = \frac{K_p}{K},\ \eta_l = \frac{K_l}{K},\ \eta_r = \frac{K_r}{K}$$

We now calculate the changes in the Stokes parameters due to the absorption of the p-, r-, l-electrons and the continuous absorption. After travelling a length Δz the result is

$$\Delta I_1 = -K\Delta z[(1+\eta_p \sin^2\psi + \frac{\eta_\ell+\eta_r}{2}\cos^2\psi) I_1 + \frac{-\eta_\ell+\eta_r}{4}\cos\psi V]$$

$$\Delta I_2 = -K\Delta z[(1+\frac{\eta_\ell+\eta_r}{2}) I_2 + \frac{-\eta_\ell+\eta_r}{4}\cos\psi V]$$

$$\Delta U = -K\Delta z[1+\frac{\eta_p}{2}\sin^2\psi + \frac{\eta_\ell+\eta_r}{4}(1+\cos^2\psi)]U$$

$$\Delta V = -K\Delta z[\frac{-\eta_\ell+\eta_r}{2}\cos\psi(I_1+I_2)+\{1+\frac{\eta_p}{2}\sin^2\psi+\frac{\eta_\ell+\eta_r}{4}(1+\cos^2\psi)\}V]$$

Pure absorption is assumed when calculating the emission and this is certainly valid in MWD atmospheres where, as we have noted, LTE is an excellent approximation. With B as the source function the resulting changes in the Stokes parameters are

$$\Delta I_1 = K\Delta z\,[1+\eta_p\sin^2\psi + \frac{\eta_\ell+\eta_r}{2}\cos^2\psi]\frac{B}{2}$$

$$\Delta I_2 = K\Delta z[1+\frac{\eta_\ell+\eta_r}{2}]\frac{B}{2}$$

$$\Delta U = 0$$

$$\Delta V = K\Delta z(\frac{-\eta_\ell+\eta_r}{2})\cos\psi B$$

We may simplify these two sets of equations by dropping the equation for U which vanishes for the emission and does not interact with the other parameters for the absorption. Introducing the continuum optical depth τ by $d\tau = -K\,dz\,\sec\theta$ we may combine the contributions for emission and absorption and simplify to get

$$\cos\theta\frac{dI}{d\tau} = (1+\eta_I)(I-B)+\eta_Q Q+\eta_V V$$

$$\cos\theta\frac{dQ}{d\tau} = \eta_Q(I-B)+(1+\eta_I)Q$$

$$\cos\theta\frac{dV}{d\tau} = \eta_V(I-B)+(1+\eta_I)V \quad \text{where}$$

3.1.1

$$\eta_I = \frac{\eta_p}{2}\sin^2\psi + \frac{\eta_\ell+\eta_R}{4}(1+\cos^2\psi)$$

$$\eta_Q = (\frac{\eta_p}{2} - \frac{\eta_\ell+\eta_r}{4})\sin^2\psi$$

$$\eta_V = (\frac{-\eta_\ell+\eta_r}{2})\cos\psi$$

A more general set of equations has been derived by the Landi Degl'Innocentis (1975) from a quantum mechanical approach and their equations reduce to the above when the terms due to anomalous dispersion are neglected. Anomalous dispersion gives rise to Faraday rotation and, as mentioned previously, the effects

of Faraday rotation will not be included in the present work.

Unno obtains analytic solutions to his equations assuming a homogeneous magnetic field, linear source function and η_p, η_r, η_l constant with optical depth. This scheme is too restrictive for the present work but it is of interest to note that when ψ is $0°$, Q is zero, V non-zero while Q is non-zero and V zero when ψ is $90°$. Since Q/I and V/I represent the fractional linear and circular polarization respectively, these results are expected from the simple linear oscillator picture for the cases when the observer looks parallel ($\psi = 0°$) and perpendicular ($\psi = 90°$) to the magnetic field.

The above equations were derived assuming that each spectral line becomes a triplet when a magnetic field is applied. In the case of the anomalous Zeeman effect, i.e. when the quadratic effect begins to separate each component of the triplet into sub-components, the same equations can be used provided that the functional forms of η_p, η_r and η_l are changed appropriately. This change merely involves calculating and summing, at each wavelength, the contributions to the opacity of each sub-component suitably broadened by Stark profiles (or other profiles where appropriate).

3.2. The Line Opacity And Broadening

The predominant broadening mechanism in white dwarfs is Stark broadening by electrons and ions. However, G 99-37 is sufficiently cool that the effects of self-broadening are important, particularly since the gas pressure is high and the electron pressure low.

The hydrogen line opacity is, as usual, for each Balmer line,

$$K_\nu = \frac{n_2}{\rho}(1-e^{-h\nu/kT})\alpha_\nu$$

where $h\nu$ is the energy of a photon in a transition from level 2 to m and is thus appropriate for the Balmer series where m=1,2...; n_2 is the number density of atoms in level 2, calculated from the Boltzmann equation and simply taken from the model atmosphere calculated previously and read in as input to the line profile programme ; ρ is the density and the parenthesized term is the stimulated emission factor. α_ν is the broadening profile and is normalised such that

$$\int_0^\infty \alpha_\nu d\nu = \frac{\pi e^2}{mc} f_{nm}$$

where f_{nm} is the usual transition probability. In order to combine Stark and self-broadening it is convenient to re-write the opacity as

$$K_\nu = \frac{n_2}{\rho} P_\varepsilon T^{-1} \zeta_1 \{1+[R(N_\varepsilon,T)+\frac{n_0}{n_\varepsilon}\zeta_2]\Delta\lambda^{\frac{1}{2}}\}\Delta\lambda^{-\frac{5}{2}} \qquad 3.2.1$$

which is taken from Cayrel and Traving (1960) and quoted in Aller (1963) who tabulates for the first four Balmer lines ζ_1, ζ_2 and $R(N_\varepsilon,T)$. In the above, n_o is the number of H atoms per gram, n_ε the number of electrons per gram and P_ε the electron pressure.

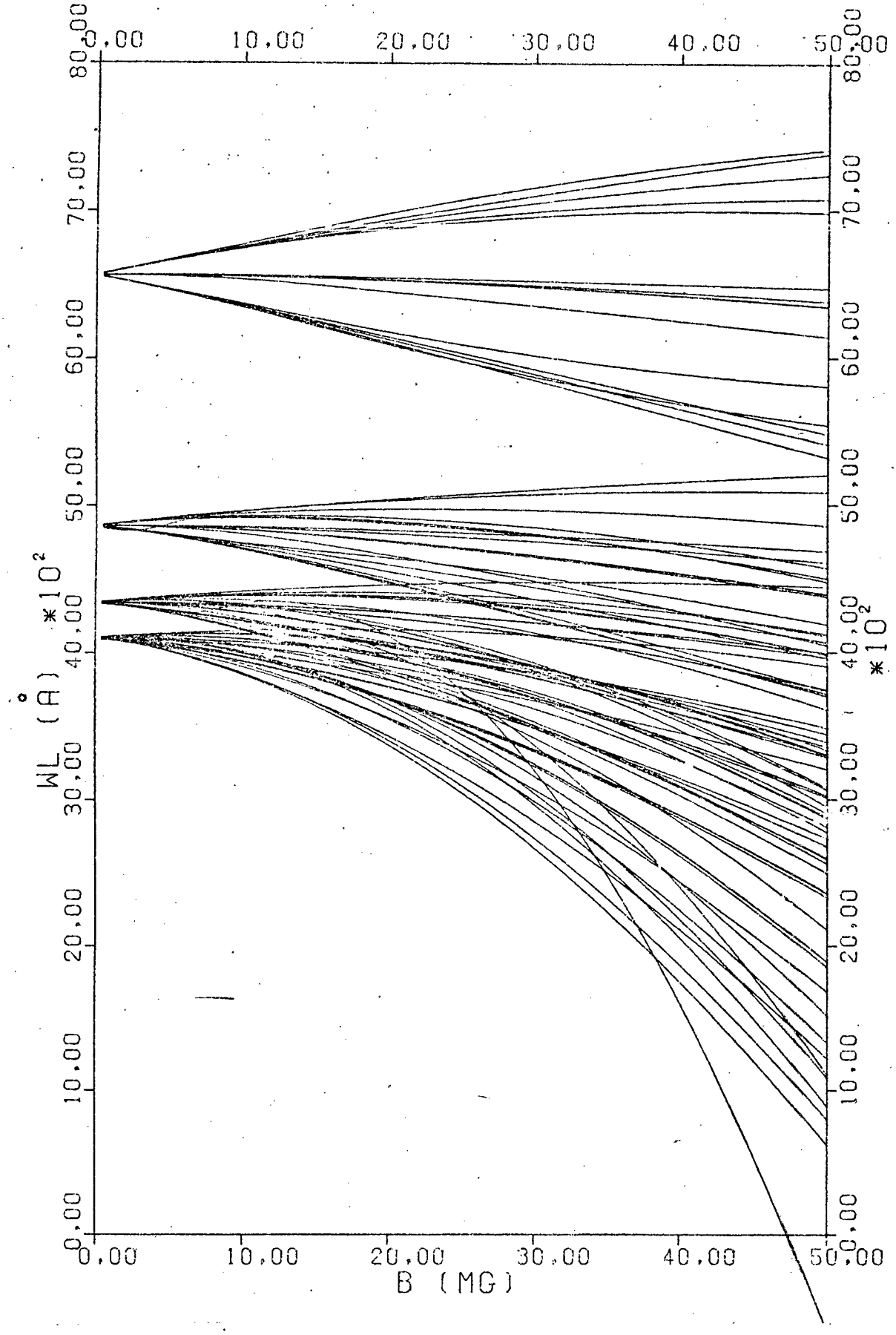

Figure 3. The wavelengths of the Zeeman sub-components of the first four Balmer lines as a function of magnetic field strength. Parabolic interpolation/extrapolation in Kemic's (1974) tables has been used. The tables only extend to 10 and 20 MG for Hδ and Hγ respectively.

This formula is an extension of the wing formula due to Kolb, Griem and Shen (1959) to include self-broadening . $R(N_e,T)$ is a slowly varying function of N_e and T. Of course, the above calculation of opacity is strictly valid only in the wings and when l-degeneracy is not removed and obviously diverges as $\Delta\lambda \to 0$ near the line cores. In order to correct this, $\Delta\lambda$ was not allowed to decrease below a certain value $\Delta\lambda_{min}$ in the evaluation of the opacity. The value of $\Delta\lambda_{min}$ was found by comparing the above profile to two others : in the case where Stark broadening is most important, i.e. in GD 90 and BPM 25114, the comparison was done with profiles from Kepple and Griem's (1968) tabulated line cores ; in the case where self-broadening is most important, the comparison profile was a standard Lorentzian with a damping constant calculated from Wickramasinghe and Bessell (1979) who studied self-broadening in a cool non-magnetic DA white dwarf. In each case, the value of $\Delta\lambda_{min}$ was determined so that the area under the truncated profile was approximately equal to the area under the comparison profile so that the above normalization condition was approximately obeyed. Of course, the above procedure may lead to some errors in the opacity. However, it is computationally inexpensive compared to inserting accurate tabulated line cores especially since at each wavelength and for each area element, the profile must be calculated 90 times, the total number of Zeeman sub-components for the first four Balmer lines. Moreover, the effective 'magnetic' broadening due to the inhomogeneity in the magnetic field is likely to be much more significant than any error in the individual profiles (Borra,1976 ; Angel,1977).

From Kemic's (1974) tables of wavelength and transition strength as a function of magnetic field, it can be seen that each Zeeman sub-component has a different strength. The line opacity formula quoted above already contains the transition probability in the ζ_l term. Thus, in order to combine each Zeeman sub-component with its appropriate strength, each transition strength was first transformed to transition probability according to the formula quoted in Kemic's tables

$$f_{ji} = \frac{304}{(2S+1)} \frac{S_{ij}}{\lambda_{ij}}$$

where f_{ji} is the transition probability, S_{ij} is the transition strength, S = 1/2 and λ_{ij} is the wavelength of the transition. Then, each transition probability was divided by the total transition probability obtained by summing over all Zeeman sub-components separately for each line. In this way, the sum of the normalized transition probabilities will sum to 1 in the zero field case as expected.

In order to test the calculations of the line opacity in the line profile programme, the line opacity calculated when the magnetic field was absent was compared with that of the ATLAS programme in the wings of the Balmer lines. Good agreement between the two values was found as expected.

Some interesting points arise from scrutiny of the wavelengths in Kemic's tables, plotted in fig. 3 with parabolic interpolation and extrapolation for field strengths other than the tabulated ones. The most obvious fact is that the Zeeman shift is very much greater for $H\delta$ than for $H\alpha$ in accordance with its dependence on the fourth power of the principal quantum number (Preston,1970). Thus, the triplet structure disappears at much lower field

strengths for Hδ than Hα. Also, the features associated with absorption by components of the former will be shallow and broader than the corresponding features associated with the latter. This effect is also related to the fact that calculations are performed for field strengths up to 100 MG for Hα but only 10 MG for Hδ. In the case where the field strength of the area element on a stellar model exceeds 10 MG, Kemic's tables must be extrapolated and this gives rise to considerable uncertainty in the positions of the components of Hδ. For Hβ and Hγ, the tables extend to 50 MG and 20 MG respectively. Thus, the wavelengths of the components must be extrapolated over a considerable range for field strengths up to 50 MG in the case of Hγ and Hδ but no extrapolation is necessary for Hα and Hβ. Indeed, in the case of BPM 25114, where fields of around 40 MG were used in the models, extrapolation shifted the wavelengths of some comonents of Hδ by thousands of Angstroms from their zero field value.

Another point of interest is that the σ^+ components at the long wavelength side of the π component may remain at approximately the same wavelength over a significant range of field strengths. This arises because the wavelength shift associated with the linear and quadratic Zeeman effect are of opposite sign for these components. At low fields, the linear red shift is dominant ; at higher fields, the quadratic blue shift begins to cancel the linear effect and this produces these 'stationary' wavelengthss . The net effect is to produce an absorption feature that is narrower than that of the other σ component. The effect is most significant for our purposes for Hβ and Hγ. For Hα and Hδ the quadratic effect is much smaller or greater, respectively, than the linear shift so that the stationary points lie at field strengths above 100 MG for the former and under 1 MG for the latter.

We now turn to the method of solution and boundary conditions for the Unno equations assuming that $\eta_I(\tau)$, $\eta_Q(\tau)$, $\eta_V(\tau)$ and $B(\tau)$ are known.

3.3. Boundary Conditions And Solution Of Unno's Equations

In the deep interior of the atmosphere, LTE is a very good approximation to the physical conditions. In this case the intensity of the radiation is given by the law of black body radiation which is isotropic, homogeneous and, most important for our purposes, unpolarized. It is clear then that suitable boundary conditions are I=B, Q=V=0 where B is the Planck function. Beckers (1969) has suggested using the Unno analytic solution evaluated in the deep interior as the boundary condition but this will closely approximate the above conditions provided that the factor $\beta = 1/B \; dB/dT$ appearing in the analytic solution is nearly zero and this should be the case in the deep interior where the temperature gradient, and hence dB/dT , is very much smaller than at small optical depths.

Two optical depth scales are important and these are $\tau_c = \int_o^\infty K_c \rho \, dx$ and $\tau_{tot} = \int_o^\infty (1+\eta_I) K_c \rho \, dx$, the continuum and total optical depth. Notice that in the case of no magnetic field, $(1+\eta_I)K_c = K_c + K_l$ where K_c and K_l are the continuous and line opacities respectively, so that $K_c + K_l$ is the total opacity. The Unno equations are integrated with τ_c as the dependent variable. However, the level in the atmosphere where the integration must begin depends on where the boundary conditions begin to diverge from the true

solution of the equations. This occurs at a level where radiation emitted from this level has an appreciable probability of escaping from the star without suffering further absorption or scattering. This takes place around a total optical depth of about 5 where an emitted photon has about a 1% probability of escape. It is important that the total optical depth and not the continuum optical depth is used to determine this level because the radiation 'feels' the total opacity and not merely the continuous opacity. Of course, in wavelength regions which are free of all lines, the two opacities are the same. In this way, the integration begins at τ_{tot} =5 at which point I is set equal to B and Q and V are set to 0. For the purposes of checking the calculations and comparing with the continuum calculations of the ATLAS programme, a continuum intensity integration was also performed, i.e. the Unno equations were solved with $\eta_I=\eta_Q=\eta_V=0$ and this integration was accordingly begun at $\tau_c=5$. It is a much quicker process because the Unno equations collapse to the usual equation of radiative transfer since Q=V=0 when the above parametric functions vanish. In this case, continuum polarization was ignored because it was calculated as in section 2.4

Beckers (1969) has used a Runge-Kutta type method of integrating the Unno equations to the surface. For the models presented here, a simpler approach was used. The value of each Stokes parameter S_n at level τ_n was found in terms of its value S_m at level τ_m by

$$S_m = S_n + \left.\frac{dSn}{d\tau}\right|_{\tau_n} (\tau_m-\tau_n) \qquad S=I,Q \text{ or } V$$

where $dS_n/d\tau_c$ is given by the Unno equations. This method was extensively tested for the case where Unno obtains analytic solutions, i.e. for a linear source function and η_I, η_Q, η_V constant with optical depth. For a wide range of line opacity, so that both line core and wing conditions were simulated, and for a wide range of source function gradients, excellent agreement was found between the numerically integrated solutions and the Unno analytic solutions provided that the integration step length was chosen to be small enough. In the case of spectral regions free of line absorption, a step of length of 0.05 was found to be satisfactory resulting in about 100 integration steps. In regions where line absorption is important, this breaks down because $dI/d\tau_c$ is much greater relative to I because of the factor $1+\eta_I$. In this case the step length was chosen to be $0.05/(1+\eta_I)$. However, approximately the same number of steps were needed because the integration begins higher up in the atmosphere where τ_{tot} =5 at which level $\tau_c= 5/(1+\eta_I)$. In practice, it was found that η_I never became so large that the starting point, τ_c , was so small as to be effectively at the surface.

To conclude this section, it is of interest to note that a new method of solution for the Unno equations has been formulated by Martin and Wickramasinghe (1979) which has a number of advantages over the method presented here and other techniques found in the literature and discussed and compared by them. The ratios η_p, η_r and η_l are defined to include both continuous and line absorption in the numerator so as to directly allow for polarization in the continuum. This eliminates the need to calculate the continuum polarization separately. Their approach assumes that over sufficiently small intervals in the atmosphere, the assumptions used to obtain the Unno analytic solutions hold and, by expanding the Unno solution in a power series and equating coefficients,

they obtain the solution at successive levels in terms of that at previous levels. In practice, they find that in a realistic atmosphere only 6 integration points are needed leading to a very substantial saving in the non-trivial amount of computer time used by other techniques. They also report better numerical accuracy in a numer of cases. Clearly, this is the best method currently available.

4. The Results And Conclusions

4.1. The Line Profile Computer Programme

The previous two chapters have described the various component calculations to produce the final synthesized intensity and polarization spectra. It is the purpose of this section to tie all of these calculations together which may conveniently be done by describing our computer programme which uses all the previously developed theory.

The programme first read in the model atmosphere for the star to be modelled as calculated by ATLAS and as described in sections 2.1 and 2.2. The atmosphere was divided up by ATLAS into 40 different layers and the independent variable describing each depth was $\int \rho dx$ which proved useful in integrating opacities to provide corresponding optical depths. The wavelength dependent opacities and intensities were calculated every 100 A. The next task was to make suitable adjustments to Kemic's tables to enable extrapolation at field strengths up to 50 MG for $H\gamma$ and $H\delta$. This was done by parabolically extrapolating the last three wavelength values to obtain values at 20 and 50 MG. The transition strengths were not parabolically extrapolated to these field strengths but simply taken as the same as at the last available tabulated point. For all four Balmer lines, the zero field strengths were taken to be the same as those at 3 MG. The transition strengths were then converted to transition probability (see section 3.2) and normalized by dividing by the sum of the transition probabilities for all the Zeeman sub-components at 0 MG for each line separately.

Having completed the preliminaries, the rest of the calculations were performed for each wavelength spanning the spectral interval being investigated. For all models, the resolution was chosen to be 10 A.

For the chosen wavelength λ, the total continuous opacity was found by linearly interpolating the two total continuous opacity values spanning the the value λ and found from the atmosphere results. The corresponding continuum optical depths were found by integrating through the atmosphere using the same procedure used by ATLAS.

Next, the visible surface of the star was divided up into 112 area elements consisting of 10 points from the centre to the limb which are equally spaced in $\sin\theta$ where θ is the angle between the normal to the area element and the line of sight. For the innermost value of θ, 4 equally spaced azimuthal points were chosen, while for the rest, 12 equally spaced azimuthal points were used. For each area element Unno's equations were integrated to yield the surface values of I,Q,V and the continuum intensity, while equation 2.4.5 was evaluated to provide the fractional continuous circular polarization. The details of these calculations will be discussed presently. The fractional continuous circular polarization was multiplied by the continuum intensity to yield an effective continuum Stokes parameter V_c and all the Stokes parameters were integrated over the visible surface taking account of the projective geometry of each area element.

The evaluation of equation 2.4.5 was straightforward. The

exponential integrals were calculated using the same coding as in ATLAS and the integrations were performed using a logarithmic optical depth scale to improve numerical accuracy.

In the integration of Unno's equations, the first step was to calculate the angle between the magnetic field and the line of sight, ψ. This depends, of course, on the adopted magnetic field geometry and provision was only made for centred or decentred dipoles inclined at an angle, α, to the line of sight which was specified with the polar field strength, B_p, in the input.

Explicitly, let ϕ be the azimuthal co-ordinate, B the strength of the magnetic field permeating the area element, A the fraction of the star's radius by which the dipole is decentred (if necessary), and consider two co-ordinate systems : the x-y-z system with the z axis along the line of sight and the x axis along the direction of $\phi=0^\circ$; and the xx-yy-zz system which has its zz axis along the axis of the dipole and the yy axis co-incident with the y axis. Then the magnetic field strength, B , and the angle between the magnetic field and the line of sight, ψ, of the area element are given, along with components in the two co-ordinate systems denoted by appropriate subscripts, for the centred and decentred dipole by the following formulae :

$$x = \sin\theta \cos\phi$$
$$y = \sin\theta \sin\phi$$
$$z = \cos\theta$$
$$xx = x\cos\alpha - z\sin\alpha$$
$$yy = y$$
$$zz = z\cos\alpha + x\sin\alpha$$

Centred Dipole :

$$B_{xx} = 3\, B_p\, xx\, zz$$
$$B_{yy} = 3\, B_p\, yy\, zz$$
$$B_{zz} = B_p\,(3\, zz^2 - 1)$$
$$B_z = B_{zz}\cos\alpha - B_{xx}\sin\alpha$$
$$B = \sqrt{B_{xx}^2 + B_{yy}^2 + B_{zz}^2}$$
$$\psi = \arctan\left(\sqrt{B^2 - B_z^2} \,/\, B_z\right)$$

Decentred Dipole :

$$d = \sqrt{1 + A^2 - 2\,A\,zz}$$
$$B_{xx} = 3\, B_p\,(1-A)^3\,(zz-A)\,xx \,/\, d^5$$
$$B_{zz} = B_p\,(1-A)^3\,(3\,(zz-A)^2 - d^2) \,/\, d^5$$
$$B_z = B_{zz}\cos\alpha - B_{xx}\sin\alpha$$
$$B = B_p\,(1-A)^3 \sqrt{3\,(zz-A)^2 + d^2} \,/\, d^4$$
$$\psi = \arctan\left(\sqrt{B^2 - B_z^2} \,/\, B_z\right)$$

Next, the ratios η_p, η_r and η_l were evaluated and summed for the four Balmer lines included in the line opacity. The details of this involved calculating the positions and transition probabilities for every Zeeman sub-component for the magnetic field strength of the area element. This calculation was done using parabolic interpolation in Kemic's tables. The tables have field strengths of 0, 3, 7, 10, 20 and 50 MG. For area elements with field strengths, B_{mn}, in the interval 3 to 20 MG, a parabola was fitted to the three points, one of which is greater than B_{mn} and the other two less than B_{mn} and the interpolated wavelength and transition probability found at B_{mn}. A second parabola was fitted to the three points, one of which is less than B_{mn}, the other two greater and another interpolated wavelength and transition probability found. The final value for each was the mean of these two values. The process is illustrated in fig. 4. For the case when B_{mn} lay outside the above interval, i.e. lay near either end of the table, only 1 parabola was fitted using the

three appropriate end of table points. For each sub-component, $\Delta\lambda$ was then calculated and the broadening profile evaluated with a weight given by the interpolated transition probability. $R(N_e, T)$, which appears in this formula, was interpolated logarithmically from the table in Aller (1963). As discussed in section 3.2, $\Delta\lambda$ was never allowed to be smaller than the cut-off $\Delta\lambda_{min}$. In the case where Stark broadening is most important (all models except that for G 99-47), the cut-offs for Hα, Hβ, Hγ and Hδ were $0.05F_o$, $0.15F_o$, $0.25F_o$ and $0.25F_o$ Angstroms respectively. F_o is $1.25\times10^{-4}n_e^{2/3}$ and is the effective electric field causing the Stark broadening with n_e the electron density. In the case where self-broadening is predominant, the cut-off was taken to be $1.25\lambda^2\gamma/4\pi c$ where λ is the wavelength for which the profile is being evaluated, $\gamma = 6.18\times10^{-5}(\lambda_{12} f_{12} + \lambda_{1n} f_{1n})N_o$ an expression from Wickramasinghe and Bessell (1979), and c is the speed of light. In the expression for the damping constant γ, N_o is the volume number density of neutral H atoms in the ground state and λ_{1n} and f_{1n} are respectively, the wavelength and transition probability of H(1-n). These cut-offs were obtained by determining where the wing formula used, equation 3.2.1, should be truncated to yield approximately the same integrated area as the appropriate Stark profile tabulated in Kepple and Griem (1968) for the Stark broadening case and as a Lorentzian profile with the above damping constant in the self-broadening case.

Having found η_ρ, η_r and η_1, η_I, η_Q and η_V were found using the calculated value for ψ and the expressions in equations 3.1.1. The total opacity was calculated with the expression $(1+\eta_I)K_c$ where K_c is the continuous opacity found previously, and this is integrated with $\rho\,dx$ to give the total optical depth throughout the atmosphere in the same way that the continuum optical depth was found.

At this stage, all the η's, the source function and the optical depths were known for the 40 levels in the atmosphere and so the integration to the surface was begun at a total optical depth of at least 5. Only two points need be made. The first is that when η_I is large, the derivative $dI/d\tau_c$ is large. When the integration begins with $I_{(s)}=B_{(s)}$ at level s, the value of I at the next level up (s-h) is $I_{(s-h)}=B_{(s)}-dI/d\tau_c \cdot h$ where h is the step length. If the derivative is large, because of line core conditions, this may lead to $I_{(s-h)}$ falling below $B_{(s-h)}$ resulting in a reversal of the intensity gradient which is unphysical. The problem is obviously that the step length is too great and is solved by reducing the step length until the value of $I_{(s-h)}$ is at least $B_{(s-h)}$. The second point is that all the values of the η's and B at points which do not coincide with one of the 40 ATLAS points are found by parabolic interpolation of the appropriate values of the 40 ATLAS points. Because the 40 ATLAS points are not equally spaced in the continuum optical depth, this may lead to poor interpolation near the surface resulting in, for example, negative opacities and other anomalies. This condition is checked for and rectified by using linear interpolation.

This completes the description of the programme. The final stage is to describe what the parameters of the models were and to present and discuss the results.

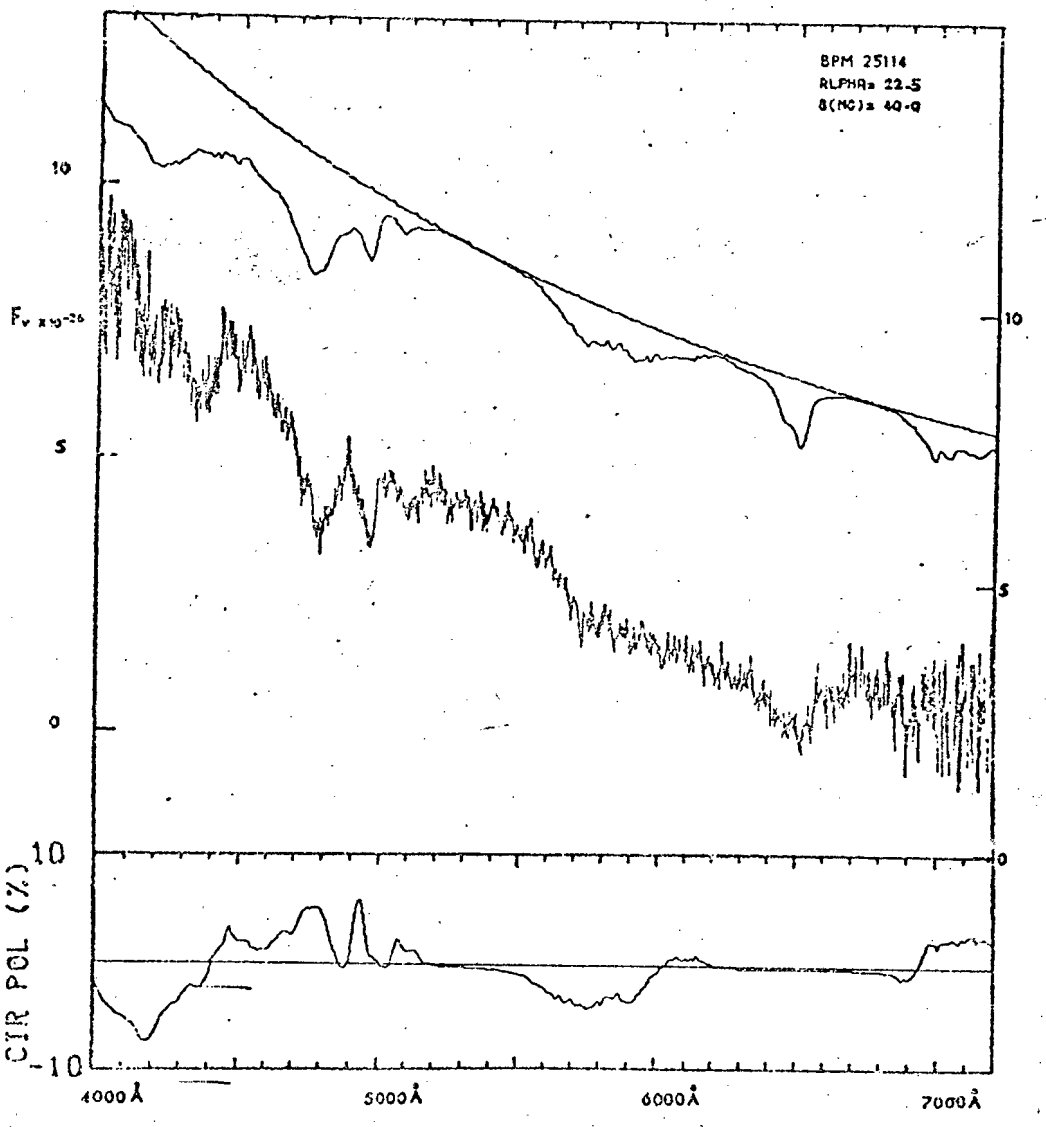

Figure 5. Observed and theoretical fluxes and theoretical circular polarization for BPM 25114. The zero of the theoretical curve, a model 20 000 K magnetic white dwarf with dipole strength 40 MG and viewing angle 22.5°, is marked as such. The zero of the observations is the upper annotated axis corresponding to +10% circular polarization. The observed and theoretical curves are normalized at 4000 A. The smooth theoretical curve is the predicted continuum.

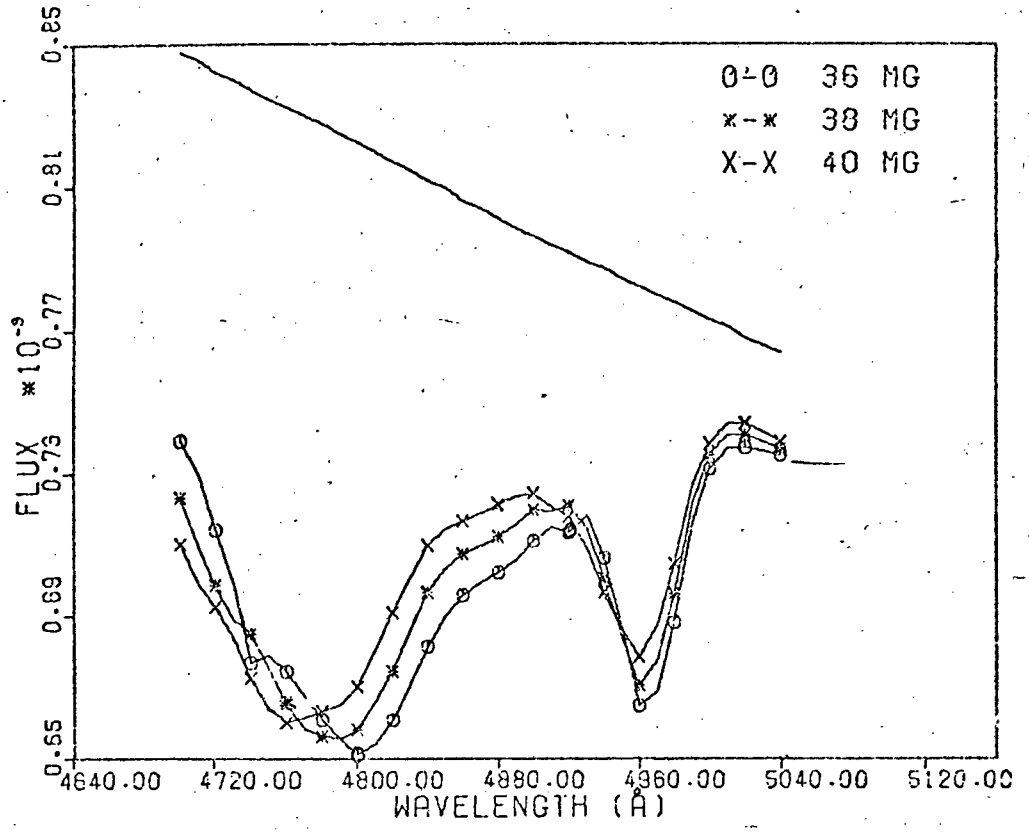

Figure 6. A section from the theoretical curve in fig. 5 with two models of different dipole field strength included. The vertical axis has an arbitrary scale.

4.2. Model Parameters And Results

As mentioned previously, the work of Martin and Wickramasinghe (1978) and Wickramasinghe and Martin (1979) became available as preprints when the first of our models of BPM 25114 were being experimented with. Their work removed much of the incentive to investigate a variety of models for each star (which would have been very expensive in computer time), and so the parameters for the models presented here follow closely the parameters used in their work.

4.2.1. BPM 25114

The observations of this star are from Wickramasinghe et al. (1977). Recall that the effective temperature which best fit the observations was 20000K in spite of some uncertainty in the absolute calibration of the observations. The adopted polar field strength, B_p, is 40 MG with α, the angle between the dipole axis and the line of sight, 22.5°. The polarization and line spectrum of this model is presented in fig. 5, together with the spectrum of Wickramasinghe et al. taken on May 21.66 (U.T.) 1976. As found by Wickramasinghe and Martin (1979), there is good overall agreement between the observed and theoretical spectra. In our results, there is a slight improvement over their modelling for the feature between 4100 and 4400 A, but this is probably fortuitous, depending critically on the extrapolation of Kemic's tables. The high magnetic field causes very rapid wavelength changes in the positions of the σ components of Hγ and Hδ, especially the σ^- components. This effect results in deeper absorption at about 4500 A in the theoretical curve than in the observations, whose overall shape seems to suggest that there is little, if any, line absorption at 4500 A.

In agreement with the previous work, the observations show a broader feature in the σ^- components of Hα around 6000 A than predicted by the theoretical spectrum. Martin and Wickramasinghe (1978) report little success in improving the agreement with a decentred dipole. They suggest that a magnetic spot or a more complicated field geometry such as a quadrupole might be the answer. The latter is unlikely however : fig. 4 of Wegner's (1977b) cruder models of the Hβ feature (4800-5000A) give good agreement with the observations while his quadrupole model of the same field strength and orientation (his fig. 6) is in poor agreement. Other orientations only make matters worse.

In order to determine the field strength more accurately, some variations were explored and so two further spectra were calculated at 36 and 38 MG over the restricted region 4700-5050 A and the results for all three models are presented in fig. 6. The feature near 4800 A is centred at 4760, 4780 and 4800 A in the 40, 38 and 36 MG models respectively. The observations indicate that this feature is centred between 4760 and 4800 A so the best estimate of the polar field strength is 38$\pm$2 MG. Additional support is provided by the relative depths of the two features in fig. 6, compared with the same quantities in the observations. Limitations on computer time prevented the exploration of other spectral regions at this field strength but it is unlikely that significant differences will occur.

Overall, the dipole seems to be a very good first approximation to the field geometry. It is of interest to note that this star is quite hot with the result that higher order multipoles of the field may not have relaxed as yet. In this connection, wavelength dependent observations of the circular polarization are eagerly awaited since these promise to be an even more sensitive indicator of the magnetic field geometry as will be seen in the case of the next star to be considered, GD 90.

4.2.2. GD 90

As discussed previously, the effective temperature used for this object was 12000K. The observations are the Digicon results reported in Angel et al. (1974) which have a resolution of 25 A, lower than tha adopted theoretical value of 10 A. It was not possible to use the higher resolution image-tube spectra reported in the same article since these have no absolute calibration.

Two models were constructed with parameters similar to those of Wickramasinghe and Martin (1979). Both have B_p = 9 MG. The inclination angle α, is 105° with a centred dipole for the one model and 90° with a decentred dipole for the other. The latter dipole is decentred by 10% of the stellar radius with the stronger pole having the field lines directed inwards. The results for each model are presented in figs. 7 and 8. Both line spectra are in good agreement with the observations except that the σ^+ component of Hβ is slightly shortward of the observed value of 4918 A. Wickramasinghe and Martin report the same discrepancy and comment that it probably occurs in the interpolation of the strongest σ^+ component of Hβ. In addition the theoretical π component of Hβ is shallower relative to the σ components than the observations suggest. The most likely explanation for this is the truncation of the line opacity near the line centre in the construction of the models.

Both models, together with those of Wickramasinghe and Martin, predict shallower central depths for the three lines than those observed. Indeed, Greenstein's (1974) data suggests an even higher effective temperature of 15000K which would weaken the theoretical lines still further. Wickramasinghe and Martin conclude that the effect of the magnetic field on the atmospheric structure is the most likely explanation, either through steepening the temperature gradient because of the increased line blanketing of the large number of Zeeman components spread over a wide wavelength region, or by affecting the hydrostatic equilibrium of the star.

It should be noted that the much greater absorption in the observations around 4000 A is due to the presence of the higher Balmer lines which were not included in the models because no Zeeman effect calculations have been done for them. Also, the theoretical polarization feature in this region may not match the observations when they become available.

It is apparent that the theoretical polarization spectrum for the centred dipole is in very poor agreement with the observed profile. Wickramasinghe and Martin reported that they were unable to get good agreement for any inclination angle. By contrast, the decentred model gives a much better fit. The model here seems to be slightly better around Hβ (4800A) than the previous work whose features are deeper than observed. It is clear therefore that a

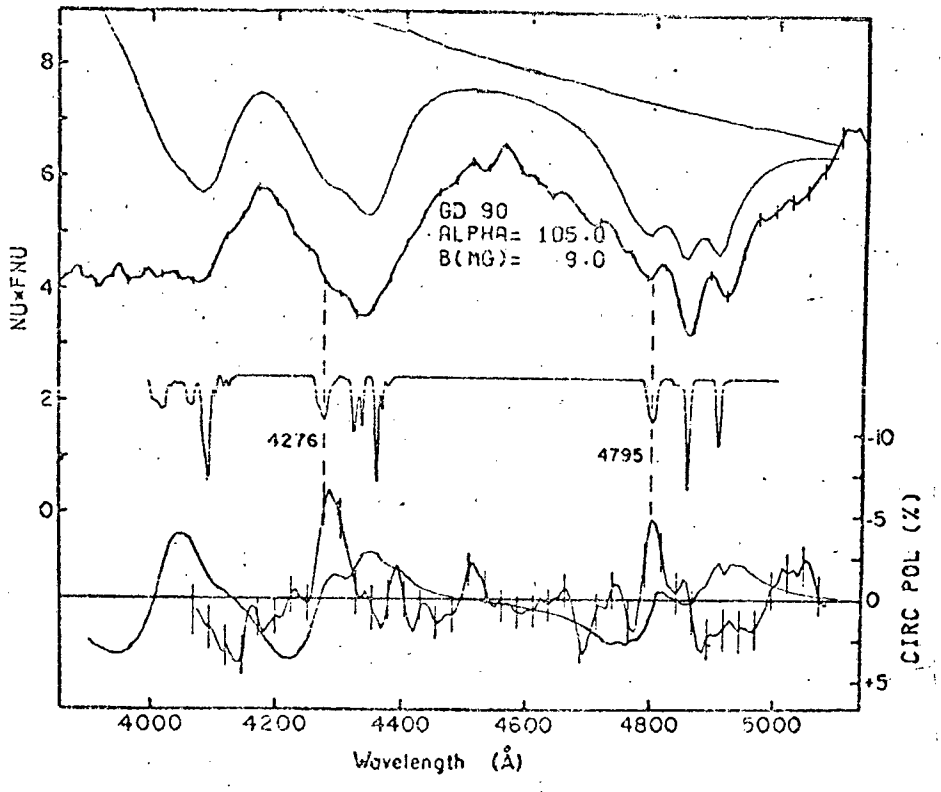

Figure 7. Observations of line and polarization profiles for GD 90 taken from Angel et al. (1974a), together with theoretical model curves. The top two represent continuum and line profiles for a 12000 K magnetic white dwarf, centred dipole of strength 9 MG and viewing angle 105°. The theoretical and observed profiles are normalized at 4600 A and the vertical axis νf_ν has an arbitrary scale. The theoretical polarization curve (no error bars) is plotted on the same axis as the observed curve.

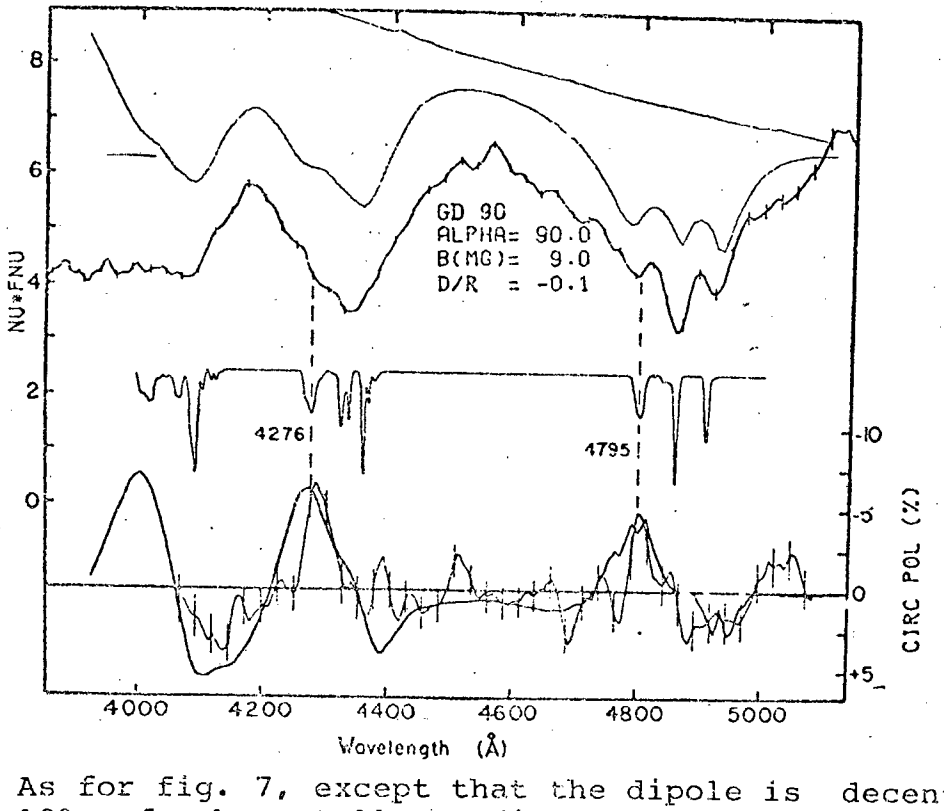

Figure 8. As for fig. 7, except that the dipole is decentred by 10% of the stellar radius and inclined at 90° to the line of sight.

decentred dipole with inclination angle 90° is a good first approximation to the field geometry in this star. This also agrees with the conclusion of Angel et al. (1974) mentioned in section 1.3.1 that the field is constant over a substantial fraction of the stellar disk. A dipole lying 'on its side' will fulfill this condition. Better polarization data must be obtained to see whether this model can achieve more detailed agreement, particularly around 4400 and 4700 A.

It is of some note that the absorption spectra for the two models presented here are quite similar while the polarization profiles are very different. Therefore, it is important to obtain wavelength dependent polarization data (in spite of its demands on telescope time) in order to be sure that a particular model is at least approximately correct.

4.2.3. G 99-47

The comparison observations for this star were taken from Liebert et al. (1975). The model consructed here has parameters $\alpha = 120°$ and $B_p = 25$ MG. The theoretical intensity and polarization spectrum are presented in fig. 9 together with the observations.

$H\beta$ and both σ components of $H\alpha$ should be unobservable according to the model and this is confirmed. As mentioned previously, the star is so cool that it is near the limit where hydrogen lines disappear from the spectrum. The π component of $H\alpha$ matches the observed feature quite well. It is deeper than the corresponding feature in Wickramasinghe and Martin's model. They suggest that agreement between their model and the observations could be improved by the inclusion of self-broadening and this is confirmed by our model. However, the feature is still slightly too shallow and this, together with the fact that the model continuum is a little flatter than observed, suggests than an even higher effective temperature is warranted. On the contrary, the value of 6000K used is higher than 5700K found from the multichannel spectrophotometry of Greenstein (1974), and there is no absorption at $H\beta$.

With the exception of the region around $H\beta$, where their curve is almost featureless, the polarization spectrum for the corresponding model of Wickramasinghe and Martin is very similar to the one in the figure. High resolution polarimetry is awaited to test the models more strictly.

The broad band polarization measurements are $0.95\pm0.15\%$ (6020-6380A) and $-0.28\pm0.15\%$ (6740-7120A) from Liebert et al. (1975). The model presented here predicts 0.67% and -0.45% for the two regions which is not as good as achieved by the previous work. This may be because their continuum polarization calculations are more self-consistent than the separate calculation used in the model here. In this regard, Wickramasinghe and Martin report no discrepancy between the magnetic field estimate inferred from the position of the $H\alpha$ π component and that inferred from the continuum polarization calculated by the magnetic dichroism theory, as found earlier by Liebert et al. (1975).

4.3. Conclusions, Suggestions For Future Work

(i) Centred or decentred dipolar field geometries have been shown to give good overall agreement with the observed line and polarization profiles of the three known magnetic DA white dwarfs.

(ii) The calculations of wavelength and transition probability for the Zeeman components of the first four Balmer lines formed in high magnetic fields have been shown to be reasonably accurate. This is an important result because it is not possible to produce such high magnetic fields in the laboratory in order to verify these caculations. The lack of detailed agreement with the observed wavelengths of some of the features is likely to be caused by errors in interpolation and more particularly extrapolation in the existing tables.

(iii) The conclusion of Borra (1976) that an approximate line-broadening theory is adequate in computing line profiles of magnetic white dwarfs is verified. Also, the inclusion of self-broadening, again in only an approximate fashion, is found to be important in the cool magnetic white dwarf, G 99-47.

(iv) The use of realistic atmospheres is found to be important in calculations of theoretical spectra of magnetic white dwarfs. Wickramasinghe and Martin (1979) find that their spectra, particularly the line strenghths , are sensitive to atmospheric structure while the model of BPM 25114 presented here is in better agreement with the observations than that of Wegner and O'Donoghue (unpublished) who merely used Unno's analytic solutions. The assumption that magnetic pressure effects are unimportant in calculating the atmospheric structure is found to be justified only as a first approximation.

(v) The dependence of the observed circular polarization on wavelength is very sensitive to the magnetic field geometry. Therefore, it is important that future models be fully tested by comparing theoretical and observed values of polarization, particularly over a range of wavelength, before any confidence can be placed in any one particular magnetic field geometry.

(vi) The model for G 99-47 illustrates how absorption features may be rendered unobservable by being 'washed out' by inhomogeneities in a strong magnetic field, particularly if the temperature is so low or high that these lines would be weak in a non-magnetic white dwarf. Thus, the lack of observable features in type II magnetic white dwarfs may be fully accounted for by this effect.

(vii) The magnetic dichroism mechanism producing continuum polarization has been shown to be well described by the linear theory at low field strengths.

There is much scope for further work : on the observational side, narrow band polarimetry should be obtained for BPM 25114 and G 99-47, while the observations of GD 90 should be improved. Of particular interest would be observations of BPM 25114 and GD 90 near the Balmer limit to detect the polarization feature predicted by Lamb and Sutherland (1974). In spite of the heavy demands on telescope time, such observations are important in testing both models presented here and the theory describing magnetic circular dichroism.

Spectra of BPM 25114, taken over the suspected rotation period of the star : 2.84 days (Wegner,1977a), would enable comparison of further models of the star using various inclination angles to be made in order to account for the spectral variations that are seen

in Wickramasinghe et al. (1977). Martin and Wickramasinghe (1978) have attempted to do this but only two comparison spectra were available while Wegner's (1977a) more extensive coverage is confined to the region near Hβ.

The search for more magnetic white dwarfs should be continued if not intensified. Discovery of examples with recognizable Zeeman patterns would provide incentive to continue building models similar to the present ones. On a wider scale, reliable statistics of the fraction of magnetic white dwarfs within the white dwarf category might provide important clues in the study of the collapse of evolved stars, especially in relation to the details of magnetic field changes during collapse.

From the theoretical point of view, the most pressing problem is surely improving Kemic's tables as is obvious from fig. 3 by performing the calculations for (1) a finer grid of magnetic field strengths ; (2) a greater range of field strengths for Hγ and Hδ as well as the higher Balmer lines (preferably up to 100 MG). Perhaps equally important is an investigation of magnetic effects on atmospheric structure. Two questions arise here. How is the atmosphere affected by (i) the increase in line blanketing that would result from line absorption (albeit quite shallow) spread over a very wide wavelength range and (ii) the inclusion of magnetic pressure as a significant, if not dominant, contribution to the total pressure appearing in the equation of hydrostatic equilibrium ? Other problems that could usefully be investigated are to experiment with quadrupole and higher multipole geometries either separately or superimposed upon the basic dipole. It would also be of interest to know if a magnetic 'spot' could give similar results to a dipole and, if so, this may explain the photometric variability of BPM 25114.

From an evolutionary point of view, magnetic white dwarfs are a significant sub-class of the white dwarfs. They are also of considerable interest in the studies of polars : cataclysmic variable systems where one component is a magnetic white dwarf. They also represent a less complex laboratory for investigations into the denser, more magnetic neutron stars. Some confident steps have been taken in understanding their physics.

OBSERVATIONS AND ANALYSIS OF L 19-2

5. Introduction To L 19-2 And The ZZ Ceti Stars

In the years around 1975, it became clear that there existed a well-defined class of luminosity variable DA white dwarfs : the ZZ Ceti stars. From extensive high-speed photometry of the prototype star, ZZ Ceti, Robinson et al. (1976) have been able to build a model of its light curve accurate to 0.001 mag and 10 s in time. The ZZ Ceti star L 19-2 and ZZ Ceti itself are both low amplitude variable stars and it is thought that they exhibit similar photometric properties (Mc Graw,1977). In order to determine whether this is so, a program of high-speed photometry of L 19-2 was undertaken and the analysis of the observations constitutes the second part of this thesis. To appreciate the significance of such a study, it is necessary to have some knowledge of the general properties of the ZZ Ceti stars as a whole. A detailed account of the discovery of these stars by Robinson and Mc Graw appears in Mc Graw (1977). Reviews by Robinson (1979) and Mc Graw (1980) bring the observational picture up to date and so only a summary of the salient points will be given here.

Table 5-1. The ZZ Ceti Stars

Star	α (1950)	δ	V	(B-V)	(U-B)	(G-R)	Refs
BPM 30551	01 04.7	-46 26	15.42	0.17	-0.50	-	1,2
ZZ Ceti	01 33.7	-11 36	14.10	0.20	-0.54	-0.43	3
BPM 31594	03 41.8	-45 58	15.03	0.21	-0.66	-	4
HL Tau-76	04 16.8	27 13	15.20	0.20	-0.50	-0.39	5
G 38-29	04 17.0	36 09	15.63	0.16	-0.53	-0.42	6
G 191-16	04 55.4	55 21	15.98	0.03	-	-0.44	7
GD 99	08 58.7	36 19	14.55	0.19	-0.59	-	8
G 117-B15A	09 21.2	35 30	15.52	0.20	-0.56	-0.45	8,9
GD 154	13 07.6	35 26	15.33	0.18	-0.59	-0.43	10
L 19-2	14 25.4	-81 07	13.75	0.25	-0.53	-	2,11
R 808	15 59.5	36 57	14.36	0.17	-0.56	-0.38	8
G 226-29	16 47.6	59 09	12.24	0.16	-0.62	-0.43	12
G 207-9	18 55.7	33 53	14.64	0.17	-0.60	-	13
G 185-32	19 35.2	27 36	13.00	0.17	-0.57	-0.42	7
GD 385	19 50.4	25 02	15.13	0.19	-0.68	-0.43	14
GD 556	23 11.8	55 12	16.21	-	-	-0.38	7
G 29-38	23 26.3	04 58	13.10	0.20	-0.65	-0.43	15

(1) Hesser et al. (1976)
(2) Mc Graw (1977)
(3) Lasker and Hesser (1971)
(4) Mc Graw (1976)
(5) Landolt (1968)
(6) Mc Graw and Robinson (1975)
(7) Mc Graw et al. (1980)
(8) Mc Graw and Robinson (1976)
(9) Richer and Ulrych (1974)
(10) Robinson et al. (1978)
(11) Hesser et al. (1977)
(12) Fontaine et al. (1980)
(13) Robinson and Mc Graw (1976)
(14) Fontaine et al. (1981)
(15) Schulov and Kopatskaya (1973)

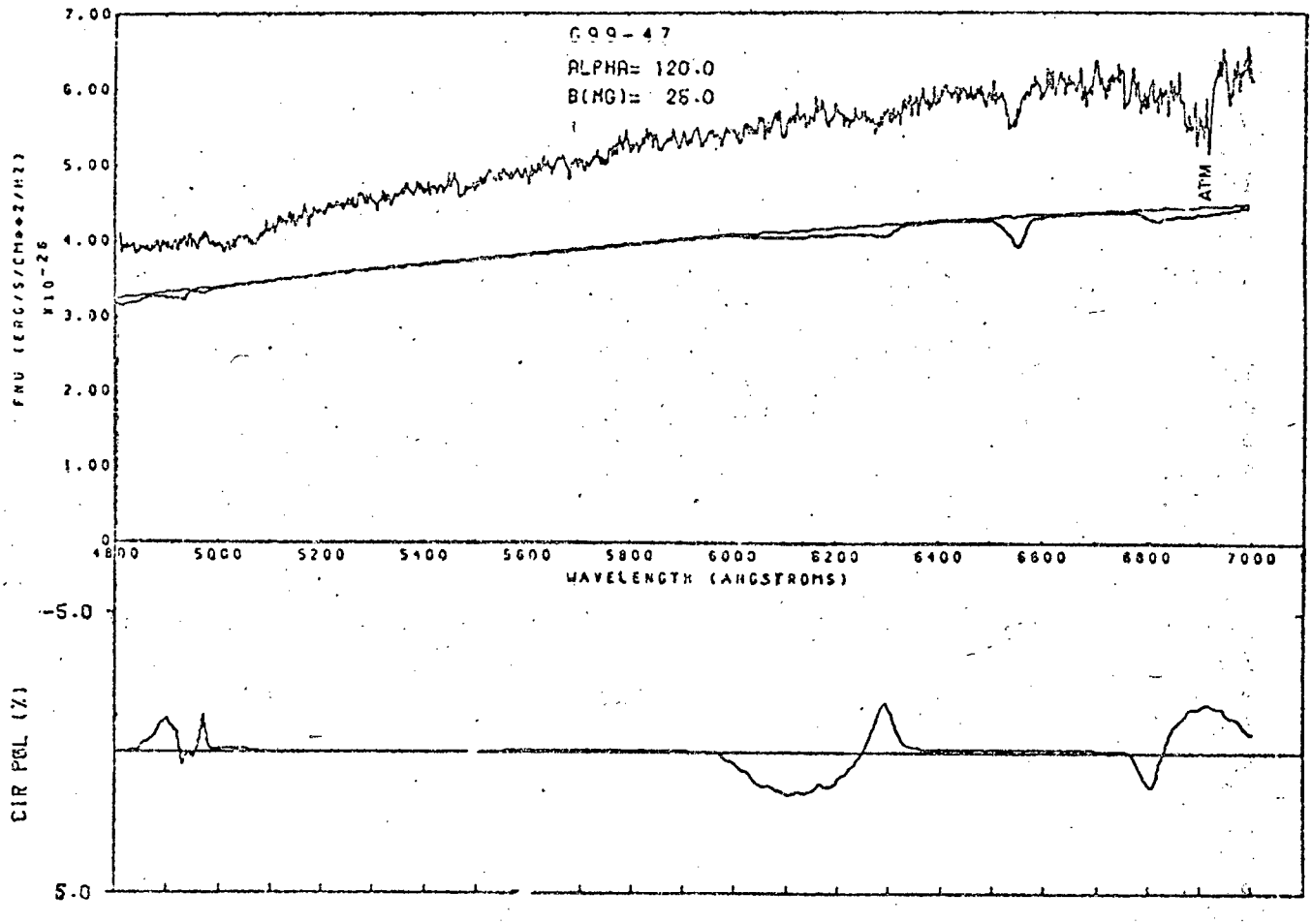

Figure 9. Observed and theoretical fluxes and theoretical circular polarization for G 99-47. The observations are from Liebert et al. (1975). The theoretical curve represents a 6000 K magnetic white dwarf, centred dipole, strength 25 MG, viewing angle 120° , and is scaled linearly to fit alongside the observed profile.

5.1. General Properties Of The ZZ Ceti Stars

The original list of 12 ZZ Ceti stars reported in Mc Graw (1977) has been extended to 17 and this new census appears in table 5-1, taken from Mc Graw (1980), along with Johnson UBV colours, Greenstein colour index G-R and references to discovery and other observations appearing in the literature. The colour, B-V, of BPM 30551 in the table is a lower value, due to Wegner (1980), than that appearing in Mc Graw (1977) while Mc Graw argues that the B-V of 0.03 for G 191-16 is unreliable. All the stars in table 5-1 are of spectral type DA. This is not a selection effect since many non-DA white dwarf stars or white dwarfs of unknown spectral type were searched for variability (nearly 50% in the initial survey).

Another important property that is apparent from table 5-1, is that for all stars for which colours are available, $0.15 < B-V < 0.25$ which is a much smaller interval than the range -0.2 to 0.6 in which DA white dwarfs are found. This property is illustrated in fig. 10, the two colour diagram taken from Robinson (1979). The crosses represent non-variable DAs while the filled circles represent the ZZ Ceti stars. The ZZ Ceti stars thus occupy a restricted region of the two colour diagram, the ZZ Ceti instability strip. The error bars in fig. 10 are large but the finite width of the instability strip has been independently confirmed by Mc Graw's (1979) Stromgren (b-y) colour measurements. A similar but more up-to-date plot appears in Mc Graw (1980). It contains degenerate stars of many different spectral types but contains no new significant information except that the red edge of the instability region, which depended on the B-V colour of BPM 30551 of 0.29 reported in Mc Graw (1977), is now better defined.

Thus far, we have seen that the ZZ Ceti stars are luminosity variable DA white dwarfs with colours near 0.2 in B-V. These criteria were well tested by numerous observations of non-DA white dwarfs and white dwarfs distributed over a wide range of colour (Mc Graw,1980), the vast majority of which were found to be non-variable. Since the ZZ Ceti stars form a physical, as well as a morphological class of variable white dwarfs, other isolated candidates for inclusion have been excluded if they do not exhibit the same spectral type, colour and type of variability (see below). Robinson (1979) discusses examples of this sort. The solid line in fig. 10 is the white dwarf cooling sequence for log g = 8 (Terashita and Matsushima,1969) and it is significant that the ZZ Ceti stars lie near the dip in this line corresponding to a maximum of Balmer line and continuum absorption. This point will be returned to after a little more discussion on the type of variability seen in these stars.

In the range of colour populated by the ZZ Ceti stars, B-V is a good temperature indicator and thus it might be expected that the ZZ Ceti stars lie in a restricted effective temperature interval. Mc Graw (1979) has measured the Stromgren colours of some of the ZZ Ceti stars and these provide effective temperatures and gravities by comparison with the model atmospheres of Wickramasinghe and Strittmatter (1972). Table 5-2, from Robinson (1979), confirms the expected temperature clustering and shows that log g lies in a narrow range from 7.8 to 8.1.

Table 5-2. Effective Gravities And Temperatures Of ZZ Ceti Stars

Star	b-y	u-b	T_e	Log g
R 548	.036	.686	12550±150	7.77±.02
HL Tau-76	.033	.634	13010±350	7.94±.02
G 38-29	.063	.678	11900±1000	7.9 ±.4
GD 99	.035	.587	13350±1000	8.1 ±.4
G 117-B15A	.032	.556	13640±350	8.14±.05
R 808	.078	.655	11730±250	7.98±.05
G 29-38	.060	.614	12630±150	8.14±.02
BPM 30551	.122	.628	10315±400	7.79±.15
BPM 31594	.028	.665	12870±400	7.80±.25
L 19-2	.071	.598	12520±400	8.24±.25

Since all DA white dwarfs must cool through the instability strip, another important property of the ZZ Ceti stars is that they must be very numerous. Using the B-V colour to define the instability strip, about 25% of the DA stars in the strip are variable (Robinson,1979). This is, of course, a lower limit since many of the non-variables may be low amplitude variables which are difficult to detect. However, some of these stars have been observed to be constant repeatedly leading to the conclusion that all of the DA stars in the B-V defined instability strip cannot be variable. An important point has been raised by Mc Graw (1980), however, which is that use of the G-R colour index, which was specifically tailored for DA white dwarfs, leads to a separation of the non-variables from the ZZ Ceti stars in the B-V defined instability region. Thus, all of the stars in the instability strip in the range $-0.45 < G-R < -0.38$ are ZZ Ceti stars. Shipman's (1979) temperature calibration leads to an effective temperature range from 11000 to 13000K. Hence, the vast majority, and possibly all, of the DA white dwarfs become ZZ Ceti variables when they cool through the range 13000 to 11000K. Apart from their variability, the ZZ Ceti stars are quite normal DA white dwarfs : (1) The colours, as seen in fig. 10, are quite normal ; (2) The spectra are typical of non-variable DAs. The $H\gamma$ line profiles were compared for a variable and a non-variable and were found to be almost identical (Robinson,1979) ; (3) There is no significant difference between the mean absolute magnitude of the ZZ Ceti stars and that of a group of non-variables with similar colours ; (4) Sion et al. (1978) have found that the ZZ Ceti stars are kinematically indistinguishable from non-variable DA white dwarfs with similar colours ; (5) Angel (1978a) has failed to detect any magnetic field in two of the ZZ Ceti stars.

5.2. The Luminosity Variations Of The ZZ Ceti Stars

The light curves of the ZZ Ceti stars have characteristic peak-to-peak amplitudes ranging from 0.02 mag to 0.34 mag. Power spectra of short sections of data (< 0.5 days) are non-stationary, i.e. two power spectra of different sections of data will not be the same. For the low amplitude variables, the changes in the power spectra usually consist of variations in the amplitudes of the small number of discrete frequencies present.

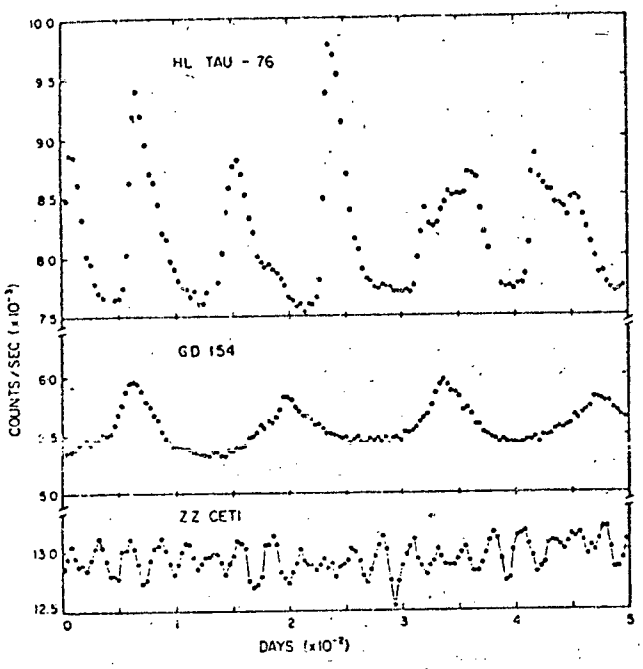

Figure 11. Typical light curves for 3 of the ZZ Ceti stars.

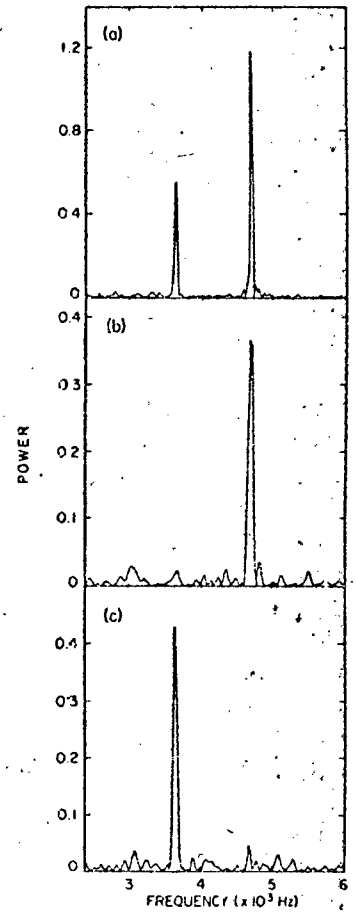

Figure 12. Power spectra of the light curve of ZZ Ceti on U.T. dates (a) 6 October,1975 ; (b) 7 October,1975 ; (c) 8 October,1975.

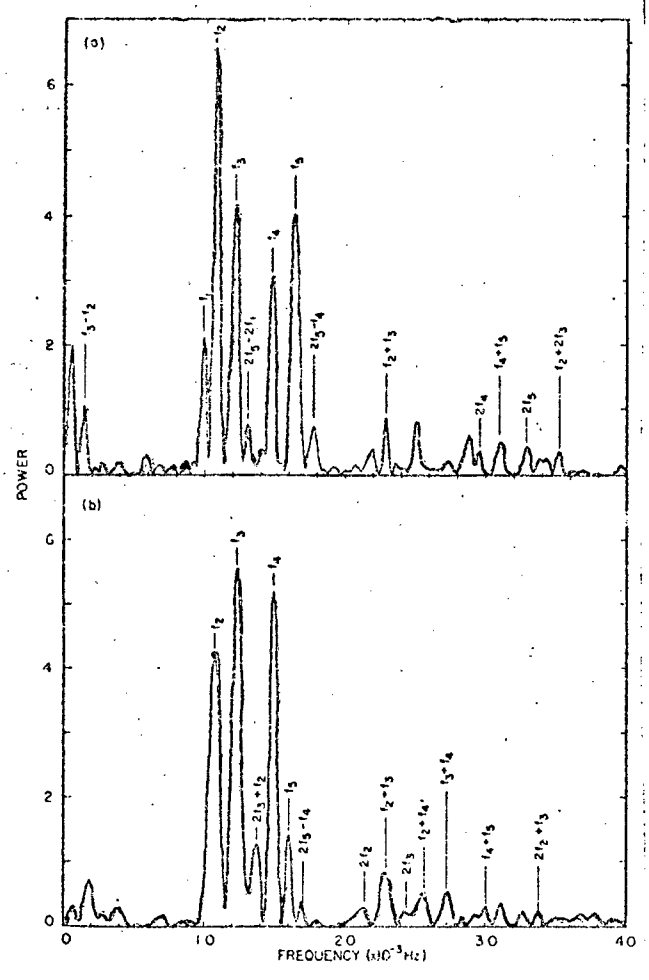

Figure 13. Two power spectra of the light curve of G 29-38. Principal frequencies and a few of the frequencies identified as harmonics and linear combinations of the principal frequencies are indicated . (a) From 16 October,1974 and (b) from 17 October,1974.

On the other hand, the power spectra of short sections of data from the same large amplitude variable may be dramatically different. The peaks in the power spectra usually fall in the 100 to 1000 s range.

Fig. 11, from Mc Graw (1980), shows typical portions of the light curves for 3 ZZ Ceti stars. The large amplitude variable HL Tau-76 has distinctly non-sinusoidal pulse shapes which are also seen in the other large amplitude variables. As the amplitude of the light variations decreases, the pulse shapes in general become more nearly sinusoidal and the periods shorter. The low amplitude variables, as illustrated by ZZ Ceti in the figure, tend to have sinusoidal, multiply-periodic light curves. The multiple periods often manifest themselves as 'beats', an effect apparent in the light curve of ZZ Ceti. The periods are generally in the range 100 to 400 s and are extremely stable (Robinson and Kepler,1980). The middle light curve in the figure is for GD 154, a typical intermediate amplitude star which exhibits a pulse shape and periods between those of HL Tau-76 and ZZ Ceti.

As mentioned above, the power spectra calculated from the light curves of the ZZ Ceti stars exhibit properties that are strongly correlated with amplitude of light variation. The low amplitude variables have power spectra that are usually quite simple. There are a small number of discrete peaks present, each of which may have a time varying amplitude (see fig. 12 from Mc Graw (1977)). The period variations with time are generally very small relative to the period itself. On the other hand, the large amplitude variables have extremely complex power spectra. Fig. 13 from Robinson (1979) shows two power spectra from consecutive nights for the large amplitude variable G 29-38, and these power spectra are typical for the large amplitude variables. Their power spectra generally show many peaks that vary in amplitude quite rapidly. In addition, in many cases the plethora of features may be sorted out into a small number of 'principal peaks' (always < 6) along with other peaks which are at frequencies which are either (i) equally spaced around one of the principal frequencies or (ii) harmonics of one of the principal frequencies or (iii) expressible in the form $mf_1 + nf_2$ where m,n are small integers and f_1 and f_2 are two of the principal frequencies. This completes the description of the general features of the light curves, power spectra and other observable properties of the ZZ Ceti stars. We now consider the interpretation of these data.

5.3. The Cause Of The ZZ Ceti Stars' Light Variations

Mc Graw (1977) has argued convincingly that the light variations are due to pulsation. There is no evidence for eclipses in any of the ZZ Ceti light curves, nor is there any stochastic flickering associated with mass transferring binary systems. The spectra are normal DA and do not show emission lines characteristic of accretion disks. Apart from pulsation, the only plausible intrinsic mechanism is the presence of star spots which rotate with the star. This possibility is ruled out due to the presence of multiple periodicities in all of the ZZ Ceti stars. In addition, the homogeneity of physical parameters in the class argues strongly in favour of pulsation. It has been pointed out on many occasions that the ZZ Ceti stars lie on the extension of the Cepheid instability strip down to the white dwarf cooling

sequence (Mc Graw,1980) and this indicates that the mechanism which causes pulsational instability in the Cepheids may be effective in the ZZ Ceti stars. However, Cox and Hansen (1979) and others have noted that this extension requires extrapolation of the Cepheid instability strip through five orders of magnitude in luminosity and may be co-incidental. Another important pointer towards pulsation is the fact that a ZZ Ceti star must have hydrogen in its atmosphere (because of the DA spectral type) and must have an effective temperature in the range where Balmer line and continuum absorption is greatest (Robinson,1980). Overall, the evidence favouring pulsation is predominant and this view is well accepted in the literature at present.

The period-mean density relation, as applied to white dwarfs, predicts periods in the range 2-20 s for white dwarfs pulsating in the fundamental radial mode. These periods become shorter with higher overtones and are confirmed by relatively realistic models of white dwarfs (Mc Graw,1977). Because the observed periods in white dwarfs are 1 to 2 orders of magnitude greater than the periods predicted for radial pulsation, this type of pulsation is not the cause of the light variations in the ZZ Ceti stars. This conclusion is further supported by Mc Graw (1979). The variations in the Stromgren colours were measured over a few pulses of two large amplitude variables and related to effective gravity and temperature changes by comparison with model atmospheres. The conclusion arising from this study is that variations in temperature during a pulsation are sufficient to account for the luminosity variations in the two stars studied while variations in the radius, manifesting themselves through effective gravity changes, are small and contribute negligibly to the luminosity variations.

On the other hand, Warner and Robinson (1972) and Chanmugam (1972) have suggested that non-radial oscillation is the most likely explanation for the luminosity variations of the ZZ Ceti stars. Non-radial oscillations may be divided into four groups : the p-modes, the single f-mode, the g^+-modes and the g^--modes (Cox,1976). The primary restoring force is pressure and gravity for the p- and g-modes respectively, with the single f-mode intermediate in frequency between the other two. The g^--modes are dynamically unstable and are related to convective instability. The periods of the f- and p-modes are all to short compared with the observed ZZ Ceti periods (Osaki and Hansen,1973 ; Harper and Rose,1970), and, like the radial modes, these periods decrease going to higher overtones or harmonics. On the other hand, the g-mode periods fall in the same range as the observed ZZ Ceti periods and realistic models (Brickhill,1975 ; Osaki and Hansen,1973) confirm this qualitative agreement.

Linear, adiabatic, non-radial oscillations may be described by a surface perturbation (Ledoux and Walraven,1958) given by

$$f(r,\theta,\phi) = f_k(r) Y_\ell^m(\theta,\phi) e^{-i\omega t}$$

where the 'mode' k specifies the number of nodes in the radial eigenfunction while l and m are related to the number of nodes on the stellar surface, quite analogous to the quantum numbers of the wave function of the hydrogen atom. Removal of the spherical symmetry, e.g. by rotation, destroys the (2l+1)-fold degeneracy in m which may take on all values from 0 to $\pm l$. The periods of the g-modes of a non-rotating star depend on k and l with P_{kl}

increasing with k and decreasing with l. Thus, a whole spectrum of periods may be observed and these periods may become arbitrarily long with increasing k. When m-degeneracy is removed, the new observed period P_{klm} is related to the old P_{kl} by

$$\frac{1}{P_{k\ell m}} = \frac{1}{P_{k\ell}} - m(1 - C_{k\ell})\Omega, \quad m = 0, \pm 1, \ldots, \pm \ell$$

where Ω is the frequency of rotation of the star and C_{kl} is a constant dependent on k,l and the structure of the star, and is of order unity. When Ω is much smaller than $1/P_{kl}$, i.e. slow rotation, the oscillation modes become equally split in frequency about the non-rotating period, P_{kl}.

There exists an additional family of non-radial modes, the Rossby or r-modes (Papaloizou and Pringle,1978). They can exist only in rotating stars. Mc Graw (1977) has argued that the periods of these modes are too short compared to the ZZ Ceti periods for the r-modes to be the cause of the light variations in these stars. Nevertheless, the peculiar frequency structure seen in an intensive analysis of G 117-B15A (Kepler and Robinson,1980), suggests that r-modes may be mixed in with the g-mode pulsations in this star.

With this very brief description of non-radial oscillations (considerable detail may be found in Ledoux and Walraven (1958) ; Unno et al. (1980) ; Cox (1980)), a natural explanation exists for the frequency structure and type of light curve seen in the ZZ Ceti stars. Mc Graw (1977) divides this explanation into phenomena associated with (i) linear oscillation and (ii) non-linear oscillation.

For the low amplitude pulsators, the sinusoidal pulse shapes in the light curves and the absence of harmonics in the power spectra suggests that the pulsations are linear. The existence of discrete, well-separated periods in these stars (e.g. 2 periods in ZZ Ceti) is attributed to the simultaneous excitation of multiple g-mode oscillations of different k and/or l. The amplitude variability of these separate oscillation modes is explained by the hypothesis that each oscillation mode is split by slow rotation into two or more very closely spaced frequencies which are unresolved on time scales associated with single high-speed photometry observing runs (<0.5 days). These unresolved frequencies will move in and out of phase with each other thus producing variations in the amplitude of each of the 'apparent' single periods seen in the power spectra. This hypothesis has had considerable success in explaining the observed photometric variations of ZZ Ceti itself over a 9 year interval (Stover et al.,1980) and will be more fully discussed in the next section.

In the case of the large and intermediate amplitude pulsators such as HL Tau-76, the non-sinusoidal shape of the pulses and the extreme non-stationarity of the power spectra suggest that non-linear effects in the oscillations are important. These effects result in the presence of harmonics of the so-called 'principal' frequencies and excitation of 'cross-frequencies' consisting of sums and differences of integer multiples of the principal frequencies. The former follows directly from the non-sinusoidal pulse shapes while the latter two are attributed to non-linear coupling of oscillation modes. It is easier to transfer energy between the principal frequencies rather than excite 'new' ones so the presence of cross-frequencies is only

seen in the large amplitude variables where the pulsation energy is sufficiently large. Of course, the non-linear coupling can only take place between frequencies of the right separation and which must both be eigenfrequencies of the g-modes at the same time ; however, the spectrum of g-modes is sufficiently dense in white dwarfs to allow both conditions to be simultaneously fulfilled. Mc Graw (1977) has argued against the hypothesis that large growth rates may be responsible for amplitude variability in the peaks of the power spectra of the ZZ Ceti stars on the basis that such growth rates would have to be unrealistically large and insists that the total pulsational energy remains constant over time scales as short as days at least.

Finally, the presence of rotation may be inferred from power spectra of some of the large amplitude ZZ Ceti stars, particularly BPM 30551. A pattern of low amplitude components, equally split in frequency about a large amplitude period has been seen in a power spectrum for this star (Mc Graw,1977). G 207-9 and G 29-38 also have power spectra with equal frequency spacing among some components although they are less striking examples. The photometric properties of ZZ Ceti may be understood in terms of slow rotation (Robinson et al.,1976 ; see next section).

A number of points summarise the discussion up to now : (1) The ZZ Ceti stars are all normal DA white dwarfs with effective temperatures between 11000 and 13000K occupying a very restricted region of the two colour diagram. There is evidence that all DA white dwarfs with temperatures in this interval are ZZ Ceti stars. (2) The presence of hydrogen in the atmosphere along with the location of the ZZ Ceti stars in the two colour diagram near the region of maximum Balmer absorption and near the extension of the Cepheid instability strip, together with the characterictics of the light curves (no flickering, eclipses), suggests that the ZZ Ceti stars are single, pulsating stars (or at least that any binary nature is not important), driven by a mechanism similar to that operating in the Cepheids. (3) The qualitative agreement between the observed periods and those expected for non-radial g-mode pulsations suggests that the latter are most probably responsible for the light variations. In addition, there is evidence that Rossby-modes are present in at least 1 ZZ Ceti star. (4) The amplitude of pulsation in the ZZ Ceti stars is strongly correlated with the presence of non-sinusoidal pulse shapes in the light curves and complexity in the power spectra. (5) For the low amplitude pulsators, the pulse shapes are sinusoidal indicating linear oscillations. With the exception of G 117-B15A, the power spectra have discrete, amplitude variable peaks at frequencies bearing no simple relation to one another. This behaviour is attributed to the simultaneous excitation of multiple g-mode oscillations that are frequency split causing the amplitude variability. (6) The large amplitude pulsators exhibit strongly non-sinusoidal pulse shapes indicating non-linear effects are present in the oscillations. These effects are manifested in the power spectra by the presence of harmonics of the principal frequencies (those that are always present in the power spectra), exchange of energy between the principal frequencies and excitation of cross-frequencies, the latter two by non-linear resonance coupling of the g-modes.

This completes the broad overview of the ZZ Ceti stars. L 19-2 is a low amplitude variable and so it is of interest to examine the observations and analysis of ZZ Ceti, also a low amplitude variable, since it is the only well-studied star with a full

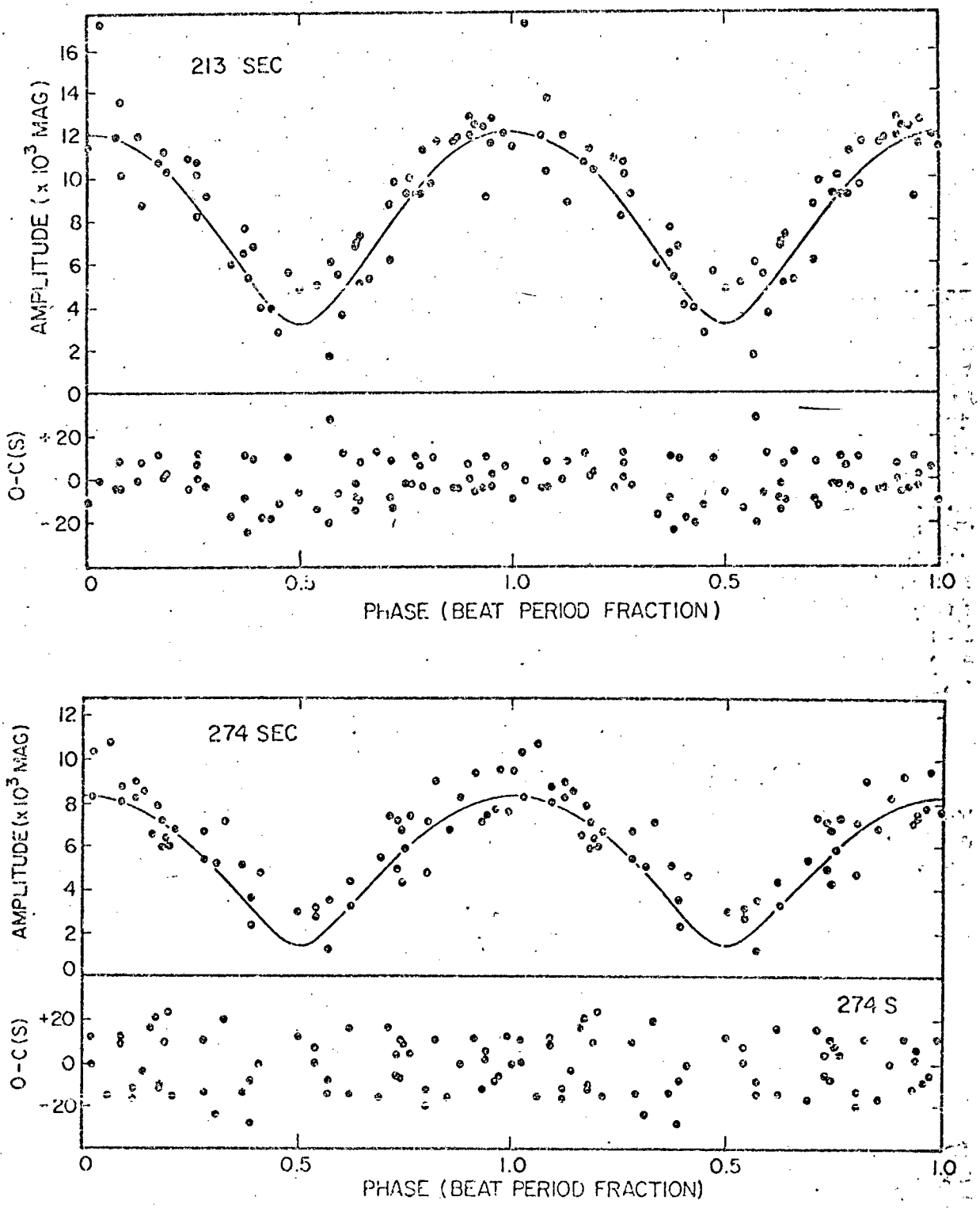

Figure 14. The points in the upper half of the top frame are the measured amplitudes of the 213 second pulsation of ZZ Ceti folded on its 1.44122 day beat period. The solid line is the amplitude that results from adding the first two components in table 5-3. The lower half of the top frame displays the difference between the observed pulse arrival times and those predicted by letting the first two components in table 5-3 beat against each other. The lower frame displays the corresponding information for the 274 second pulsation.

report in the literature to date.

5.4. ZZ Ceti (=R 548), G 117-B15A and L 19-2

Referring to fig. 12, from Mc Graw (1977), it is evident that ZZ Ceti has two amplitude varying peaks in its power spectra near 213 s and 274 s. The technique used by Robinson et al. (1976) consisted of measuring the amplitudes of these two peaks in power spectra obtained from many nights of observing ZZ Ceti. For each oscillation separately, the amplitude was plotted as a function of time and the resulting amplitude curve searched for periodicity. For the 213 and 274 s periods, a periodicty of 1.44122 and 1.66528 days respectively was found in the amplitude curve and these amplitude points were folded at the respective 'beat' periods to produce the mean amplitude curve shown in fig. 14, from Robinson (1979). It is apparent that the amplitude of oscillation of each period undergoes an almost sinusoidal variation. The most obvious explanation for this behaviour is that each periodicity is not a single amplitude varying oscillation but two closely spaced frequencies which beat with each other producing the respective 1.44 and 1.66 day variations in the amplitude-time curves. The angular frequency separation of the two closely spaced frequencies is given by

$$\omega_A = \frac{2\pi}{T} \qquad 5.4.1$$

where T is the amplitude beat period. By adding two sine waves of amplitude A_0 and A_1 and frequencies ω_0 and $\omega_0 \pm \omega_A$, it is trivial to show that the resultant is given by

$$F(t) = A_t \sin(\omega_0 t + \Omega_t) \quad \text{where}$$

$$A_t = (A_0^2 + A_1^2 + 2A_0A_1 \cos\omega_A t)^{\frac{1}{2}} \text{ and}$$

$$\phi_t = \tan^{-1}\left[\frac{\pm A_1 \sin\omega_A t}{A_0 + A_1 \cos\omega_A t}\right]$$

Indeed, the solid line through the mean amplitude curve for each oscillation is the expression for A_t in 5.4.2 with the appropriate parameters A_0 and A_1 found by least squares fitting a curve of the form $\sqrt{k_1 + k_2 \cos\omega_A t}$ to the amplitude points to obtain $k_1 = A_0^2 + A_1^2$ and $k_2 = 2\ A_0\ A_1$. By allowing two sine waves with the above amplitudes and frequencies to beat together, the difference between the expected and observed arrival times of pulses can be calculated. If the model of the light curve is a good one, these differences should show no trend or periodicity and should be randomly scattered about zero. That this is the case for the model of ZZ Ceti can be seen from the lower plots in each diagram for the separate 213 and 274 s periods. The ordinate is the difference in observed and calculated times (O-C), and the abscissa is the beat period fraction.

In this way, Robinson et al. (1976) have shown that the light curve of ZZ Ceti can be predicted to about 0.001 mag in amplitude and 10 s in time and that the behaviour of each of the 'apparent'

single periodicities in the power spectrum is entirely consistent with a model whereby each separate period is a closely split pair, approximately 0.5 sec apart. Recently, Stover et al. (1980) have combined all the observations of ZZ Ceti spanning a 9 year interval. They confirm the initial model and show that the frequencies, amplitudes and phases of the 4 components have remained remarkably constant over this interval. The present model parameters (fully tabulated in Stover et al.) are summarised in table 5-3 from Robinson (1979) along with upper limits on the period changes. The stability of the periods is among the highest for any variable star at visual wavelengths. In addition, the frequency splitting is attributed to rotation as mentioned previously. The rotation periods, of order 1 day or so, are additional evidence that white dwarfs are slow rotators (Mc Graw,1977 and references therein).

Table 5-3. The Periods In ZZ Ceti

Period (sec)	Amplitude (mag)	Period Change (sec/sec)
212.768427 ±3	0.0044 ±2	$< 7 \times 10^{-13}$
213.132605 ±2	0.0077 ±2	$< 2 \times 10^{-13}$
274.250814 ±4	0.0049 ±2	$< 3 \times 10^{-13}$
274.774562 ±6	0.0034 ±2	$< 9 \times 10^{-13}$

In a recent conference proceedings, Robinson and Kepler (1980) give a preliminary report on a similar frequency analysis of the low amplitude variable G 117-B15A. The star is described as having frequencies at $3/4\,\nu_o - \Delta\nu$, $3/4\,\nu_o + \Delta\nu$, ν_o and a further three at the frequencies of the first three increased by ν_o where ν_o = 1/215.20 Hz and $\Delta\nu$ = 0.000205 Hz. Thus there are two close pairs equally split about $3/4\,\nu_o$ and $3/4\,\nu_o + \nu_o$ and two others at ν_o and $2\,\nu_o$. The frequency splitting results in a much more rapid amplitude beat cycle of about 3/4 hour. The peculiar frequency spacing involving the factor 3/4 is not readily interpretable (Robinson and Kepler,1980) except in terms of r-modes. No further discussion of this star will be given except to note that it is apparently not morphologically very similar to ZZ Ceti in its photometric properties.

Mc Graw (1977) reports that L 19-2 exhibited similar behaviour to ZZ Ceti on the seven nights of his observations in that the amplitude of one of the periods in the star changed smoothly from 2.3×10^{-3} mag through a minimum of 0.9×10^{-3} mag and back to 2.8×10^{-3} mag. He has also found that L 19-2 has two periodicities, at 192.4 and 113.6 s. The amplitude of its light curve is low but the stability of these periods is high.

From all of this, it can be seen that L 19-2 is a candidate worthy of intensive study to determine : (1) what frequencies are seen in the power spectra of the star ; (2) are they amplitude

variable and, if so, is the nature of the variability the same as in ZZ Ceti ; (3) are there any very stable frequencies in the star ?

To answer these questions, a program of high-speed photometry of L 19-2 was begun and the description of these observations forms the basis of the next chapter.

6. High Speed Photometry Of L 19-2

6.1. The Observations

At declination -81°, L 19-2 is the most southerly of the known ZZ Ceti stars. The observations of this star were made at the Sutherland observing station of the South African Astronomical Observatory, which is located at about -30°S. Thus, a considerable advantage of observing this star is that it is visible all year from Sutherland although only 20° above the horizon at times. Hence, very long observing runs could be made on this star extending to about 11 hours a night in the middle of winter.

The observations were made using a computer-controlled pulse counting photometer (Nather and Warner,1971 ; Nather, 1973). Briefly, this equipment consists of a Nova 1200 computer which counts the pulses fed from an S 11 response photomultiplier tube at the Cassegrain focus, through a pulse discriminating amplifier. At the end of the user-specified sampling interval, the computer prints and punches on paper tape the total number of counts and initialises the counters for the next integration. The computer also controls a real time display of the raw data as it is gathered and enables Fast Fourier Transforms to be performed on any section of the raw data (up to 1024 points) so that power spectra of the raw data may be examined at the telescope. The photomultiplier is uncooled as the dark count rate for the tube is very low at the operating voltage used for the observations. The photomultiplier is mounted on an offset-guiding photometer to enable guiding without interrupting the optical path. The observations were made using the 0.75 m and 1.0 m reflectors of the S.A.A.O.. For the 0.75 m and 1.0 m telescopes respectively, the net count rate from the star was typically 3300 and 5700 c/s in 'white' light. As a result of these low count rates, no optical filter was inserted into the light beam. The bandpass was thus determined mainly by the spectral response of the photomultiplier. For most of the observing runs, the contribution from the sky was measured regularly (see below).

The full journal of observations and notes is given in table 6-1, consisting of the run number, week number, Universal Time at the start of the first integration, the Heliocentric Julian Date corresponding to this time (used in calculating the time of each integration), the telescope used and the number of integrations including sky and other 'bad' points. Altogether, L 19-2 was observed for about 292 hours in 81 runs spread over 57 nights spanning an 18 month interval. This resulted in about 105000 10 s integrations of which the author contributed about 60%.

In addition to these observations, also included in the table for the sake of completeness are the data obtained by Mc Graw (1977) and Hesser et al. (1977) kindly made available by these authors. As will be seen later, these data were not sufficiently extensive to stand alone but proved to be of value in extending the baseline of the observations.

Table 6-1. Journal Of High Speed Photometry Of L 19-2

Run Number	Week	Start Date	Start Time U.T.	Heliocentric Julian Date 2,440,000.0+	Telescope (m)	Number Of Integs
2693*	1	21 Mar 79	22:13:31	3954.42680	0.75	1091
2695	1	25 Mar 79	19:49:49	3958.32719	0.75	2127
2697	1	26 Mar 79	19:19:34	3959.30623	0.75	2500
2699	2	23 Apr 79	19:23:44	3987.31026	0.75	1041
2700	2	24 Apr 79	20:40:18	3988.36347	0.75	286
2701	2	26 Apr 79	23:08:10	3990.46622	0.75	1028
2702	2	27 Apr 79	17:25:44	3991.22845	0.75	3140
2703	2	29 Apr 79	17:18:19	3993.22336	0.75	3078
2704	3	26 Jun 79	17:32:41	4051.23376	1.0	2472
2706	3	27 Jun 79	16:59:22	4052.21061	1.0	1630
2711	3	29 Jun 79	16:57:31	4054.20929	1.0	536
2714	3	30 Jun 79	17:13:36	4055.22044	1.0	3760
2715	3	1 Jul 79	16:57:10	4056.20901	1.0	2048
2717	3	2 Jul 79	16:58:00	4057.20957	1.0	3072
2732	4	29 Oct 79	22:13:16	4176.42370	1.0	385
2733	5	11 Dec 79	19:54:31	4219.32673	0.75	1365
2734	5	12 Dec 79	19:40:09	4220.31676	0.75	2050
2735	5	13 Dec 79	19:33:01	4221.31181	0.75	1053
2736	5	14 Dec 79	20:18:27	4222.34336	0.75	1254
2737	5	15 Dec 79	19:23:18	4223.30507	0.75	946
2738	5	17 Dec 79	21:31:38	4225.39421	0.75	1007
2741	6	20 Feb 80	22:53:13	4290.45295	1.0	1501
2743	6	23 Feb 80	22:22:22	4293.43167	1.0	1693
2746	6	24 Feb 80	23:46:46	4294.49033	1.0	1180
2749	6	26 Feb 80	00:03:01	4295.50166	1.0	1104
2750	7	13 Mar 80	20:07:38	4312.33903	0.75	2580
2751	7	14 Mar 80	19:19:04	4313.30535	0.75	2807
2752	7	15 Mar 80	19:15:21	4314.30282	0.75	2190
2753	7	16 Mar 80	19:10:52	4315.29975	0.75	2945
2754	7	17 Mar 80	19:09:13	4316.29865	0.75	2957
2755	8	3 Jun 80	19:58:11	4394.33496	0.75	2906
2756	8	4 Jun 80	17:39:38	4395.23874	0.75	3832
2757	8	5 Jun 80	17:25:26	4396.22888	0.75	3910
2758	8	6 Jun 80	17:31:09	4397.23285	0.75	3871
2759	8	7 Jun 80	17:32:39	4398.23390	0.75	951
2760	8	7 Jun 80	23:11:09	4398.46896	0.75	1810
2761	8	8 Jun 80	18:17:49	4399.26526	0.75	2689
2762	8	9 Jun 80	17:52:29	4400.24766	0.75	849
2763	8	10 Jun 80	00:23:25	4400.51915	0.75	1150
2764	9	5 Aug 80	17:30:05	4457.23075	1.0	868
2772	10	29 Aug 80	17:19:26	4481.22227	0.75	1078
2774	10	30 Aug 80	17:25:03	4482.22612	0.75	1059
2776	10	31 Aug 80	17:25:47	4483.22658	0.75	1046
2778	10	1 Sep 80	17:30:32	4484.22984	0.75	1051

Run Number	Week	Start Date	Start Time U.T.	Heliocentric Julian Date 2,440,000.0+	Telescope (m)	Number Of Integs
2780	10	2 Sep 80	18:17:40	4485.26252	0.75	681
2782	10	2 Sep 80	23:16:14	4485.46985	0.75	651
2784	11	4 Sep 80	19:43:16	4487.32186	0.75	1064
2785	11	5 Sep 80	01:15:46	4487.55275	0.75	520
2786	11	7 Sep 80	17:39:31	4490.23578	0.75	546
2788	11	8 Sep 80	17:37:26	4491.23429	0.75	2240
2790	11	9 Sep 80	01:30:05	4491.56250	0.75	730
2791	11	9 Sep 80	17:37:37	4492.23437	0.75	1066
2792	11	9 Sep 80	20:39:57	4492.36098	0.75	1810
2793	11	10 Sep 80	02:32:11	4492.60557	0.75	340
2794	12	10 Sep 80	17:37:07	4493.23397	0.75	1540
2796	12	10 Sep 80	23:51:37	4493.49403	0.75	745
2797	12	11 Sep 80	02:13:37	4493.59263	0.75	456
2798	12	11 Sep 80	17:39:27	4494.23554	0.75	3505
2799	12	12 Sep 80	18:47:52	4495.28300	0.75	2340
2800	12	13 Sep 80	02:41:28	4495.61188	0.75	260
2801	12	13 Sep 80	18:57:00	4496.28930	0.75	972
2802	12	13 Sep 80	21:54:02	4496.41223	0.75	276
2803	12	14 Sep 80	17:45:25	4497.23954	0.75	2487
2805	12	15 Sep 80	02:12:15	4497.59149	0.75	403
2806	12	15 Sep 80	17:50:13	4498.24283	0.75	3400
2810	13	4 Oct 80	01:28:14	4516.56004	1.0	482
2817	13	6 Oct 80	00:16:09	4518.50990	1.0	165
The Early Data						
Mc Graw (1977) :						
2385		21 May 76	23:15:31	2920.47190	0.75	262
2457		4 Jul 76	20:01:50	2964.33717	0.75	452
2460		27 Jul 76	18:06:45	2987.25657	0.75	602
2466+		28 Jul 76	17:31:29	2988.23204	0.75	723
2470+		29 Jul 76	17:37:26	2989.23614	0.75	716
2475+		30 Jul 76	17:22:13	2990.22553	0.75	739
2479		31 Jul 76	17:16:13	2991.22133	0.75	434
2480		1 Aug 76	17:17:05	2992.22189	0.75	752
2484		2 Aug 76	18:19:05	2993.26490	0.75	432
Hesser et al. (1977) :						
C2323+		20 Aug 76	23:35:27	3011.48381	0.91	1072
C2320+		21 Aug 76	23:58:35	3012.49983	0.91	824
C2317+*		22 Aug 76	23:25:44	3013.47627	0.91	1357
C2312+		23 Aug 76	23:34:12	3014.48280	0.91	1515
C2336		17 Sep 76	23:47:41	3039.49096	1.5	796

Notes : (1) The sampling time in all the data is 10 s.
(2) Run 2459 in Mc Graw (1977) was unavailable to us.
(3) * denotes that the analysis indicated that the start times of these runs are suspect.

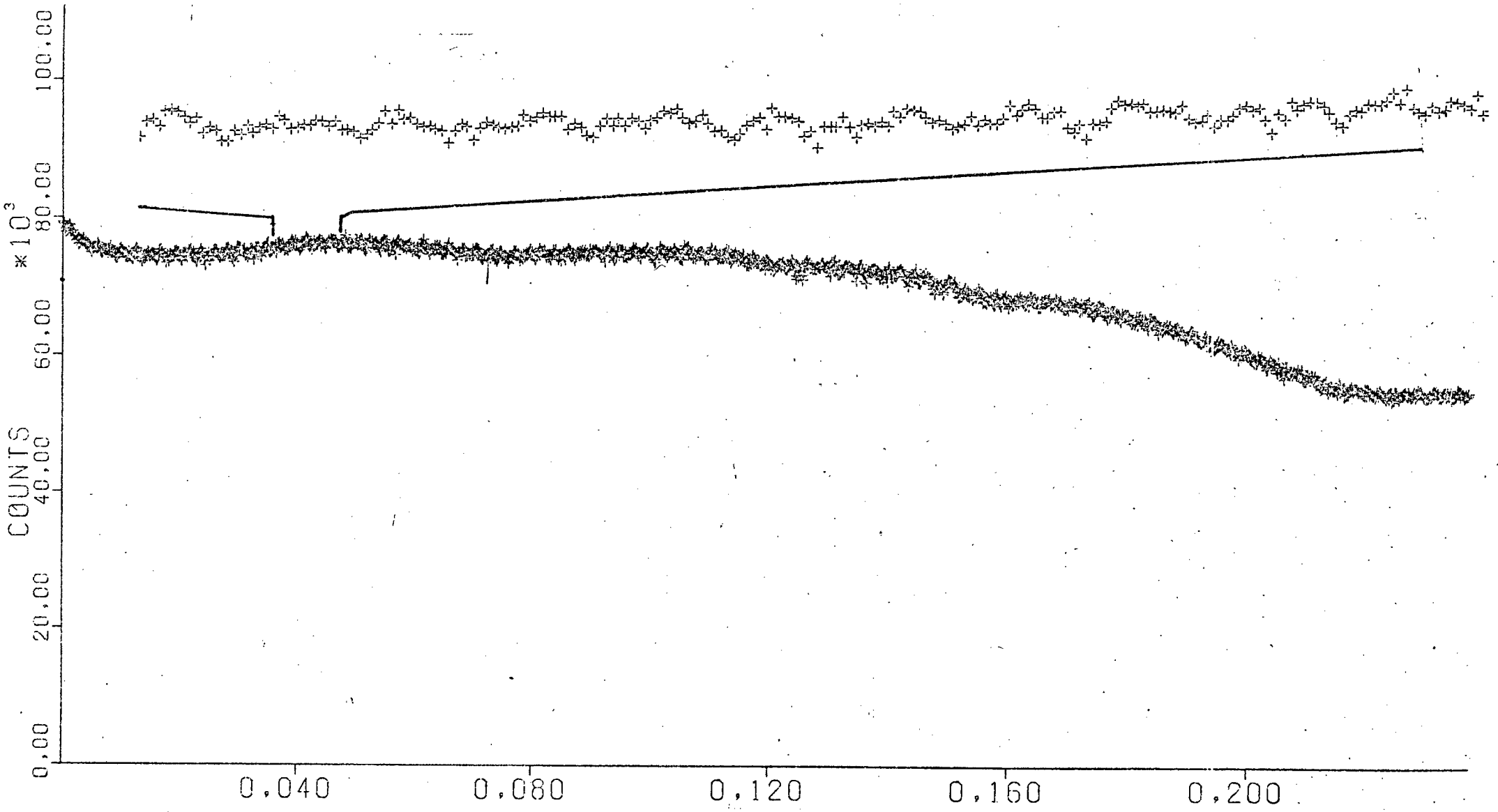

Figure 15. The complete light curve of ZZ Ceti for run 2715. The ordinate is the number of detected counts (star + sky) in 10 seconds and the abscissa is in days. The inset is a higher resolution plot of the indicated part of the light curve.

(4) + denotes that these runs were originally of sampling time shorter than 10 s and were co-added to yield a 10 s sampling time.
(5) The prefix C to the run number indicates that the observations were made at Cerre Tololo Inter-American Observatory. All others were made at the Sutherland site of the South African Astronomical Observatory.
(6) The number of integrations includes all sky and bad points within the data. Degraded data at the ends were simply discarded.
(7) Sky measurements were not made for weeks 3,5 and 7.

Fig. 15 shows the complete light curve for the raw data of run 2715 along with a small section of it plotted at higher time resolution. Each point is a 10 s integration. The abscissa is in days and the ordinate is the total number of counts (star+sky) detected in 10 s. The expanded part of the plot clearly reveals the 192 s oscillation which is strong for that part of the run but is less obvious in other parts of the light curve.

Some comments are in order at this stage about the quality of the gathered data. The most obvious is that the greater number of detected counts on the 1.0 m telescope yielded a better signal to noise (predominantly photon counting statistics) ratio than on the 0.75 m telescope. The 1.0 m data (especially that of week 3) were found to be the most useful in the frequency analysis. Also, the data were degraded at various times by loss of photons. In most cases this was due to guiding errors or sky measurements. In other cases, photons were lost due to the passage of thin cirrus in front of the star. The observations in this case were not stopped because the cloud interruptions were often brief and the real time display was a very sensitive indicator of the presence of cloud. In addition to the above, telescope aperture was lost by dome obscuration when the star was at an hour angle near 12 hours, while an increase in size of the photometer diaphragm necessitated by bad seeing led to a sudden increase in sky contribution and a discontinuity in the photometric trace. Before reduction, therefore , the raw data had to be edited and this was done in the following way : (1) in the case of guiding errors, sky measurements and cloud, the bad data were replaced by linear interpolation of the adjoining good data ; (2) Telescope aperture loss was handled by fitting a straight line through the downward sloping photometric trace (from the time when the dome began to obscure the telescope) and multiplying each observed count rate by the ratio of the mean count rate (found by extrapolating the unobscured data) and the count rate indicated by the straight line ; (3) The observed counts following an increase in size of the diaphragm were reduced by the difference in the sky measurements, when available, which were made just before and after the diaphragm increase, or by the difference in the mean count rate (averaged over 20 points) before and after the increase. The first procedure is equivalent to adding noise to the data which were edited. If the number of points adjusted was small, this will have negligible effect on the data analysis. In the case where the number of edited points exceeded 20 (e.g. a 10 minute cloud interruption), these intervals were flagged and deleted when using analysis techniques that did not require equally spaced data. The second technique is likely to preserve the oscillations except to increase the noise slightly while the third procedure will leave the oscillations unchanged and the edited points

resulting from these latter two techniques were treated as perfectly good data.

In spite of all these considerations, the number of edited points was less than 1% of the total number of points and unlikely to affect the results in any appreciable way.

6.2. The Reduction Of The Data

In discussing the way the data were reduced, it is helpful to distinguish between two quantities, the mean number of counts I_∞ that would be registered by the data acquisition system operating in the absence of the earth's atmosphere and the rapidly varying number of counts A_∞, similarly detected, and associated with the oscillations in the star. For the former quantity, mean denotes averaging over a few cycles of the longest oscillation period in the star (found to be 350 s). There was no monitoring of any kind of standard star during the observations. Consequently, since the mean number of detected counts (with sky contribution removed) is influenced by transparency changes in the atmosphere as well as variations in the sensitivity of the photomultiplier and reflectivity of the mirrors, it was impossible to prove definitely that I_∞ remained constant over the time spanned by the observations. Nevertheless, Liller and Hesser (1979) have scanned plate archives stretching back 90 years and their conclusions suggest that the mean luminosity of L 19-2, as well as the rest of the ZZ Ceti stars tested by them, has remained constant to within 0.1 mag over this period. In addition, L 19-2 was observed on two occasions immediately after fresh aluminization of the 0.75 m telescope mirrors. Since Warner (private discussions) has observed that the photomultiplier sensitivity is constant over the typical range of observing conditions found at Sutherland, and since the mean number of detected counts from the star at the same zenith distance was found to be the same on those two occasions, there is additional supporting evidence that I_∞ was constant over the 18 months spanning the observations. This assumption will be made throughout the rest of the analysis.

The edited raw data were converted to counts/sec (to allow comparison between runs of different sampling times) and the sky contribution was subtracted. Since the count rate was too low to be appreciably affected by the 52 nanosecond 'dead time' of the photomultiplier, it was not necessary to correct for co-incidence loss. The data were then corrected for atmospheric extinction by multiplying by $e^{\alpha \sec z}$ where α is the mean extinction co-efficient. Its value was determined by plotting the log of the net count rate against sec z (z the zenith distance) for a number of nights' observations and averaging the slopes of the straight lines that were fitted to the data by least squares. The result was a value of 0.4. Of course, this correction for extinction is crude, but the ratio of the amplitude of oscillation to the mean brightness of the star will be unaffected by errors in the extinction co-efficient. Excluding colour effects which will be negligible due to the low amplitude of oscillation, this ratio will also not be affected by variations in the photomultiplier sensitivity nor mirror reflectivity since both these will affect the amplitude of oscillation and mean brightness in an exactly similar way. In order to express the data in a form suited to measuring the amplitude of oscillation relative to the mean brightness of the

star, the data were further reduced in the following way : a set of mean brightnesses was found by successively averaging over 150 data points. This set was spline interpolated to provide a mean brightness for every individual data point. Finally, the mean was removed from the data (as well as long term trends) by first subtracting the interpolated value from every point and then dividing the result by the interpolated value so as to normalize the data as required. This was done separately for each run to produce a set of reduced data with zero mean and normalized in such a way that any variations in the amplitudes of any of the oscillations are due to intrinsic changes in the star rather than factors relating to the measuring process.

One problem that was difficult to circumvent was that initially, it was assumed by B. Warner that the normalization would include the sky contribution so that no sky measurements were made for some of the early runs. Because of this, it was impossible to separate the correct normalization factor, i.e. the net brightness of the star alone, from the total number of counts detected. Of course, since the photomultiplier sensitivity is constant with time, the absolute amplitude of oscillation will vary on a night to night basis due to transparency changes and, on a longer time scale, due to deterioration in the reflectivity of the mirrors. This problem was further aggravated by the use of two telescopes for the observations with mirrors that were re-aluminized at different times. As a result, a somewhat arbitrary method of normalization was adopted and will now be described.

During the early investigations of the amplitude changes in the 192 s period, it became apparent (see next chapter) that the variations were due to beating of a strong component at about 192.6 s with two weaker components separated by about 0.5 s and equally spaced in frequency about the strong one. Using data that could be normalized as described above, i.e. for which sky measurements were made, and which spanned a sufficient length of time (only about 2 days) that the strong component was well resolved from the weaker ones, it was found that the amplitude of the strong component at 192.6 s was constant to within the measurement limits over a period of at least 6 months. Assuming that this component was also constant for those runs without sky measurements, the data for those runs were normalized to yield the same amplitude at 192.6 s as obtained for the data with sky measurements. In practice, this method was not as arbitrary as it seems from the above description and was implemented as follows : from the total number of counts detected when the moon was not up and an approximate idea of the star's contribution (3300 c/s for the 0.75 m telescope and found from the data with sky measurements), an estimate of the sky contribution could be made which was suitably adjusted when it increased due to the moon rising. In this way, estimates of the sky were obtained, the data were normalized using these estimates and the amplitude of the 192.6 s oscillation component was determined. In every case, it was found that this amplitude agreed with that determined from the data with sky measurements, indicating that the calculated sky estimates were realistic. Had this not been the case, the calculated sky estimates would have been suitably altered and another iteration performed until the required consistency was achieved. In this way, the data without sky measurements were forced to be internally consistent with the data with sky points, the latter providing the only independent evidence that the 192.6 s component was indeed constant. However, the fact that the

self-consistency was easily achieved by using the measured sky values to provide realistic estimates for the unknown quantities, indicates that the affected runs were not unduly prejudiced by this procedure. As mentioned in table 6-1, the affected runs were those of weeks 3, 5 and 7, about 1/3 of the total number of integrations. This concludes the description of how the data were obtained and the technique used in the reductions. We now turn to the frequency analysis to answer the questions posed at the beginning of chapter 5.

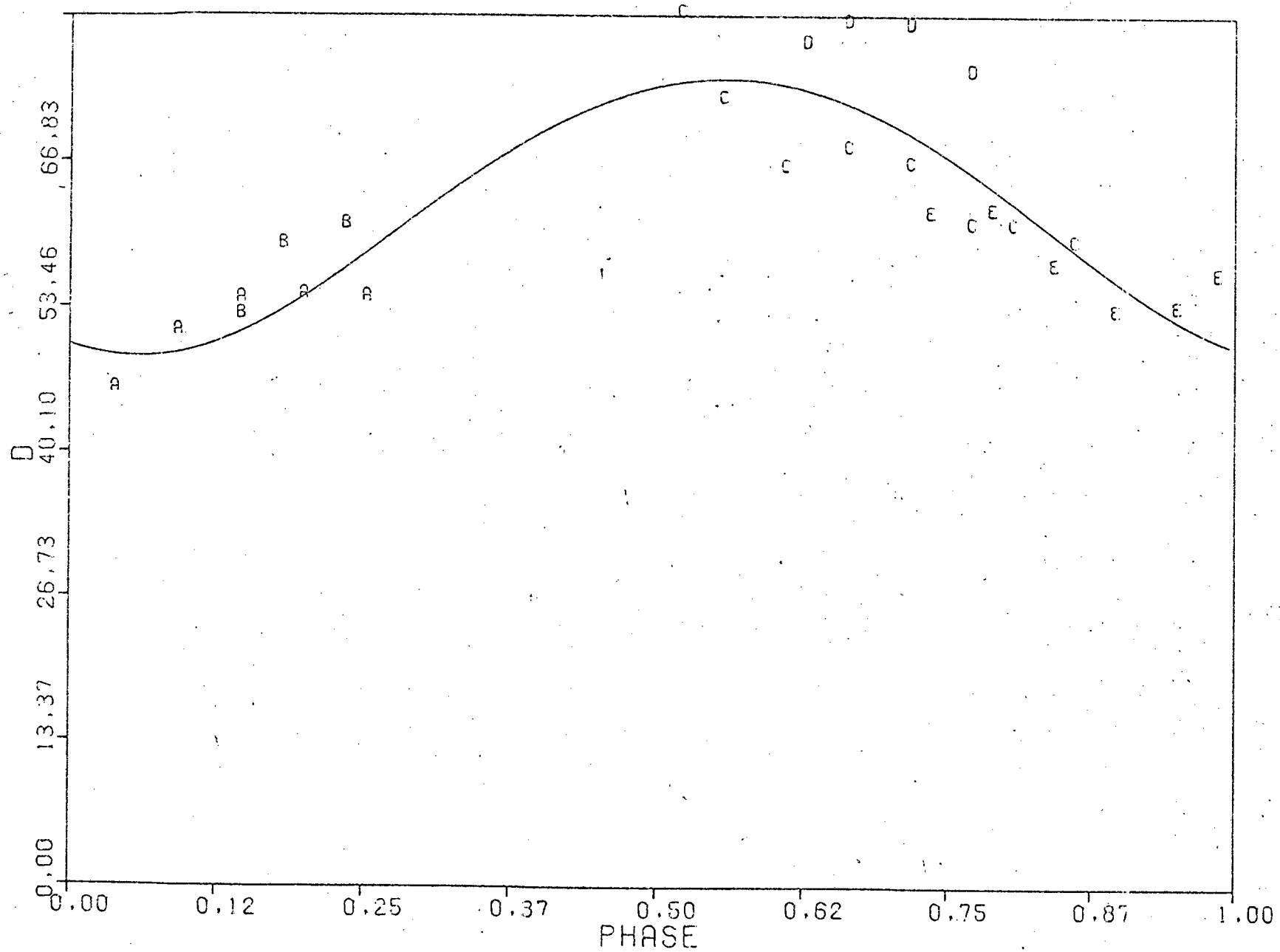

Figure 16. The measured amplitudes of the 192 s oscillation in L 19-2 for the data of week 3, folded on the beat period of 0.89 days. The solid line is the least squares fit of a sinusoid of period 0.89 days to the squared data points and replotted as the root of the sinusoid.

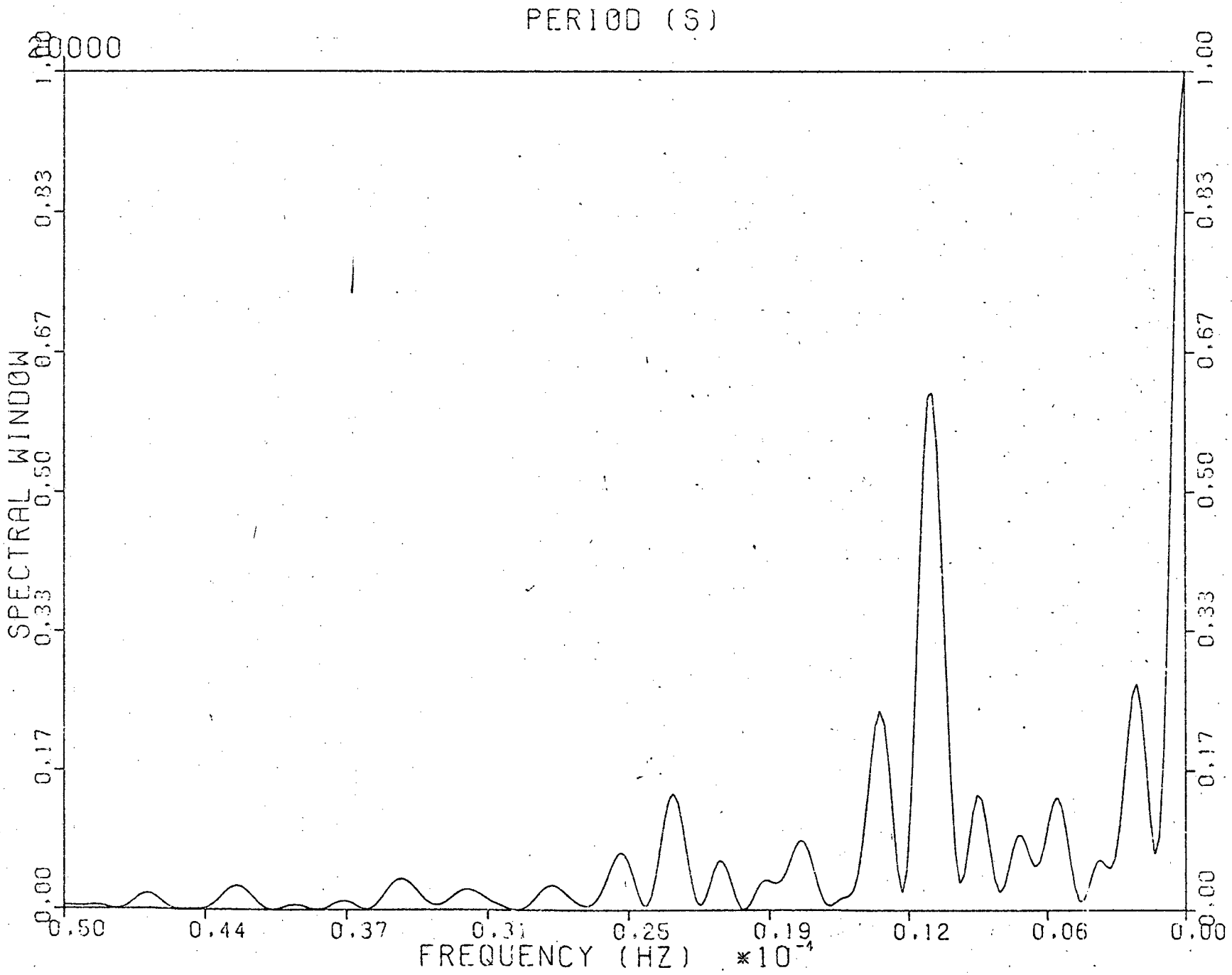

Figure 17. The power spectral window of the data for week 3.

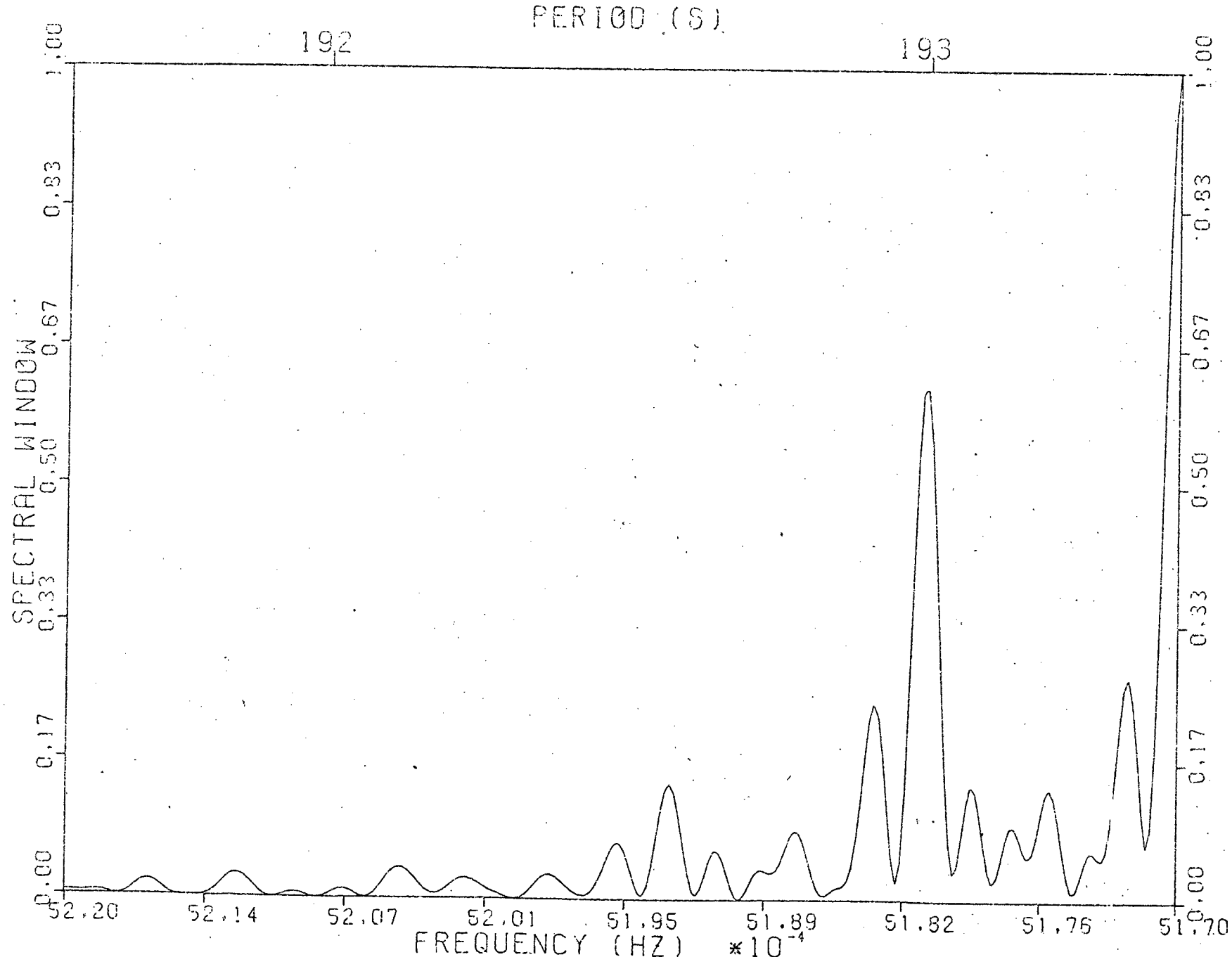

Figure 18. The power spectral window of the data for week 3 plotted at the same scale and on the same frequency axis as the power spectrum in fig. 19.

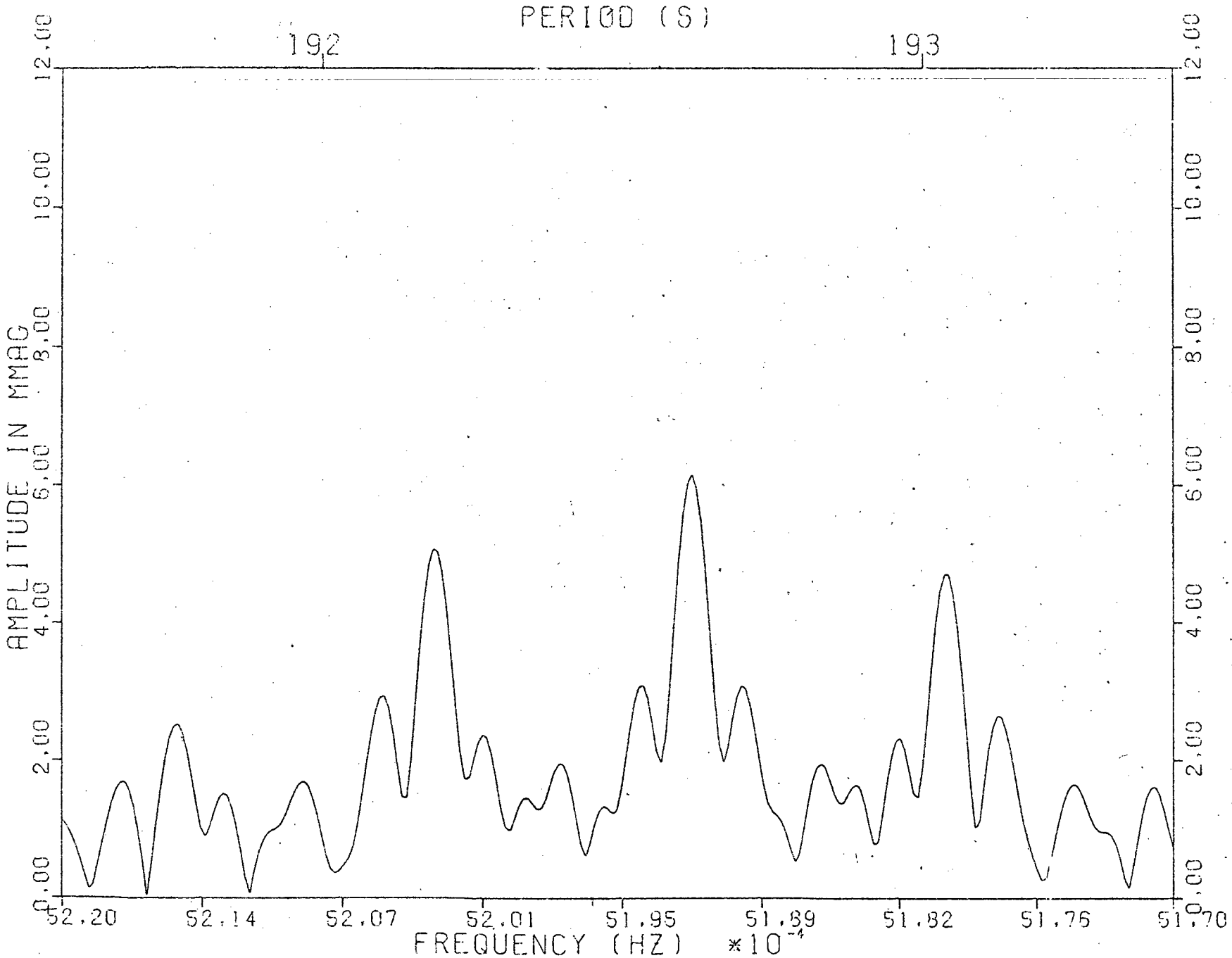

Figure 19. Power spectrum near 192 s for the data of week 3. The ordinate is the amplitude of oscillation in mmag. All the remaining figures are very similar either to this or to the power spectral window in fig. 18. Any prewhitened components will be indicated in the title so that no captions will be provided for the remaining figures.

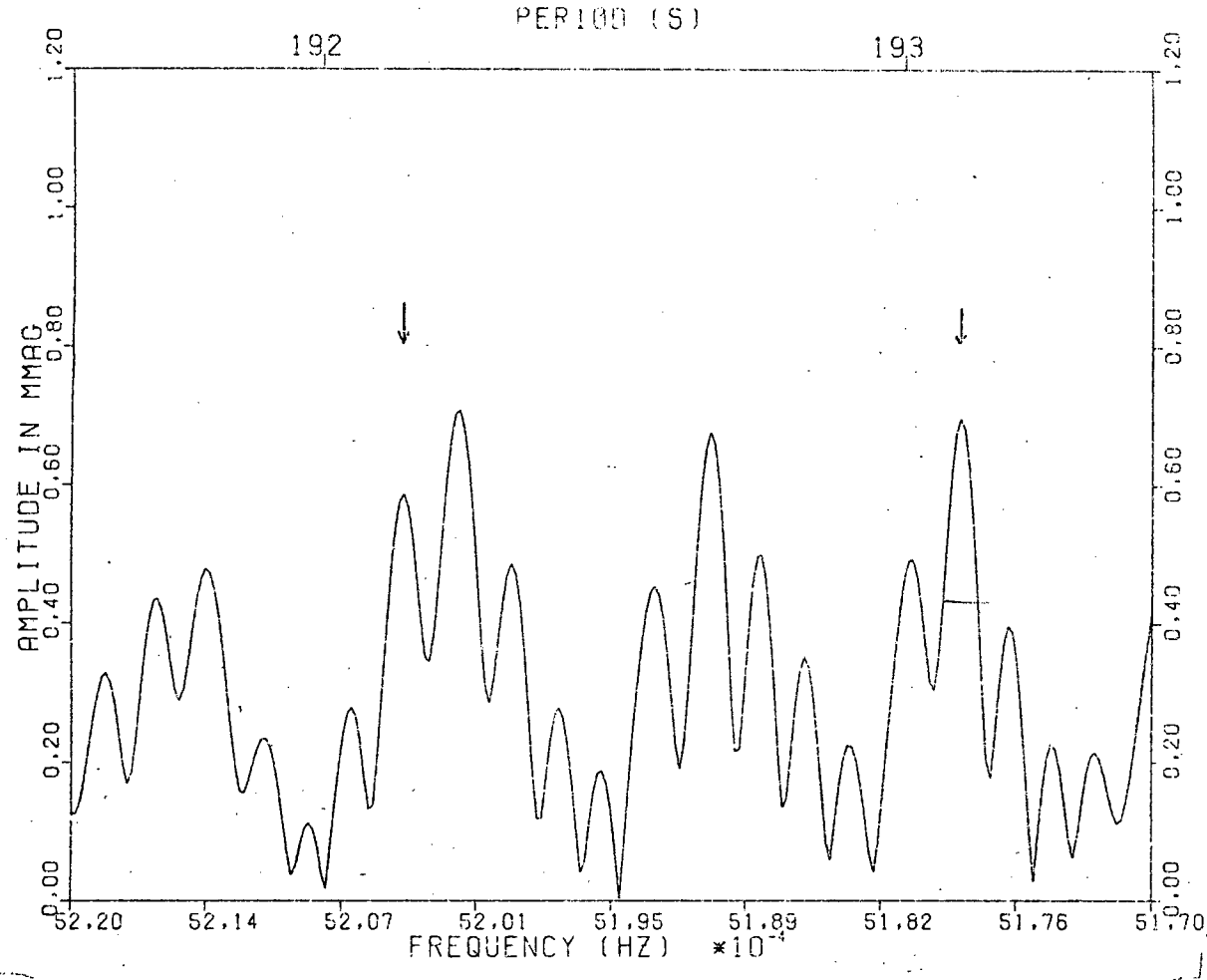

Figure 20

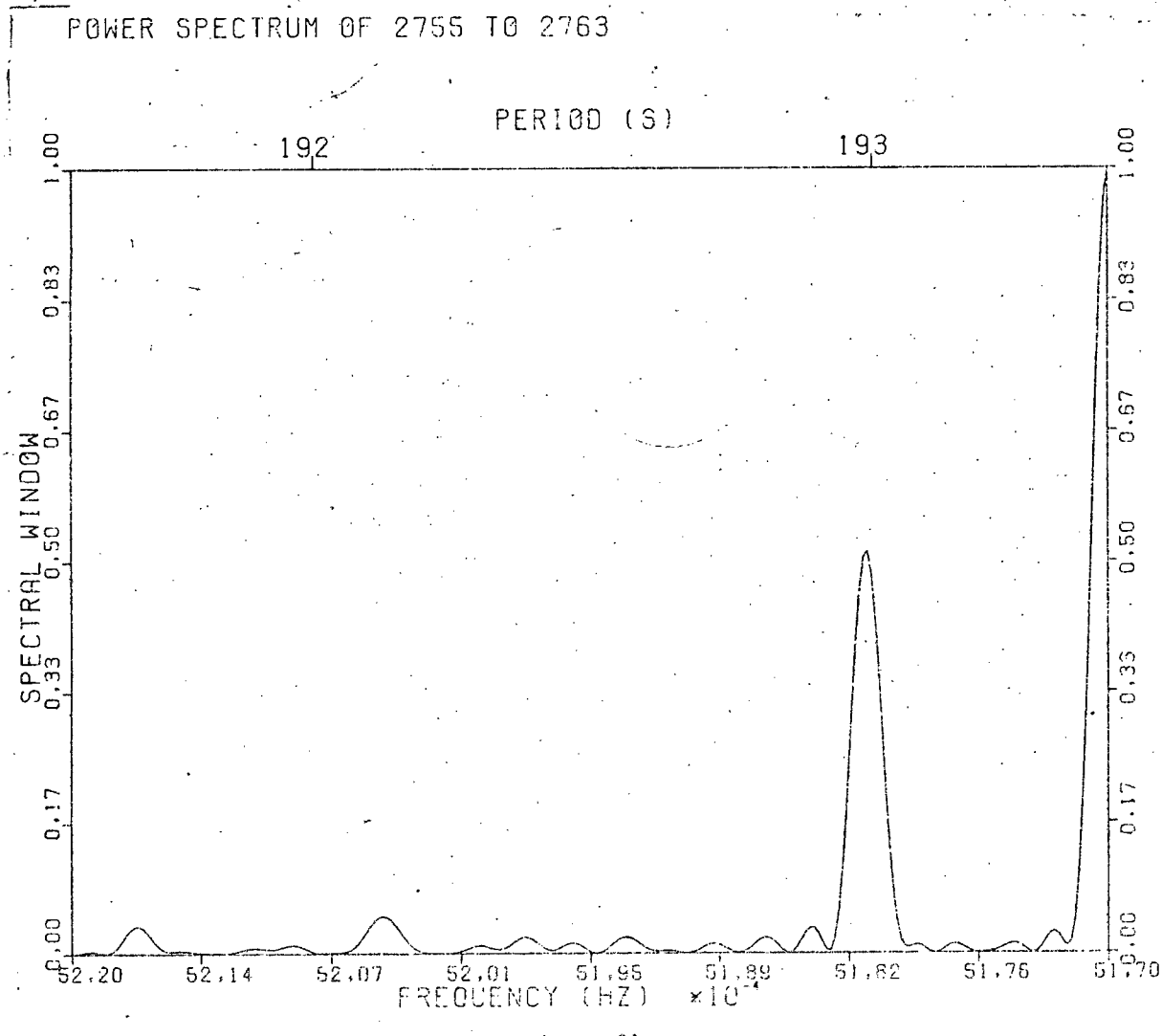

Figure 21

7. Frequency Analysis Of L 19-2

From the 1024 point power spectra that were available at the telescope, it became obvious early on that the oscillation period near 192 seconds was associated with the strongest pulsation mode in the star. It was almost always visible on the real time data display and seemed to vary smoothly in strength on a time scale of a day or aliases thereof. Besides this periodicity, three others were apparent in the above power spectra : at about 113 s, 118 s and 350 s. The former two were of lower amplitude than the 192 s period and seemed to vary in amplitude quite rapidly within a few hours while the latter was just barely detectable above the noise. A comment on the existence of the 118 s period is appropriate at this point. Since its strength is approximately the same as that at 113 s, it is surprising that it was reported in neither Mc Graw (1977) nor Hesser et al. (1977). However, Mc Graw detected it in his data and rejected it on the basis that it resulted from sidereal drive errors while our power spectra of the data of Hesser et al. also failed to detect it. This confusion is resolved by noting the following : (1) the frequency analysis below will show that the 118 s period is very clearly resolved from the approximately 120 second period normally associated with drive errors. Furthermore, both telescopes used for our observations and Mc Graw's observations have 80 s periodicities associated with their sidereal drives. Finally, besides the fact that its declination of -81° makes it unlikely that guiding errors could be responsible for the 118 s variation, one of the observers (B. Warner) noted on one occasion in the observing log that he monitored the telescope guiding during a time when the 118 s oscillation was apparent in the power spectrum and could detect no guiding errors. Thus, Mc Graw's rejection of the existence of this oscillation is not justified ; (2) the observations made by Hesser et al. were not very extensive and the frequency analysis below will show that it is quite plausible that the 118 s oscillation may have been of very low amplitude during their observations and thus undetectable. This low amplitude results from interference between the separate frequency components comprising the 118 s oscillation and causing the amplitude variability seen in the oscillation modes in ZZ Ceti itself.

Since the 192 s period was of the largest amplitude, it was decided to analyse its variations first. In order to distinguish between the 192 s period with its associated amplitude and phase variations, and the separate components which may give rise to these variations, the former will be referred to by the integer part of the period while the separate components will be referred to by their periods given to greater accuracy e.g. the 192 s oscillation on the one hand and the 192.6 s component on the other. This convention will also apply to the oscillations detected in the star. Also, following previous authors e.g. Mc Graw (1977), the units mHz (milliHertz) and mmag (millimagnitudes) will indicate 0.001 Hz and 0.001 mag respectively.

7.1. Initial Investigations Of The 192 s Period

In order to investigate the nature of the 192 s period, it was decided to follow a similar course to that of Robinson, Nather and

Mc Graw (1976) (hereinafter RNM) in their analysis of ZZ Ceti described in section 5.4. To effect this, it was necessary to measure the amplitude of oscillation of the 192 s period as a function of time and to do this, the periodogram technique of Warner and Robinson (1972) was used.

This technique consists of choosing a test period, P, and folding the light curve at that test period to produce a 'mean light curve'. If a periodicity of P is present in the data, the folding will add together points of the same phase and the mean light curve will be sinusoidal in shape. If not, the mean light curve will be random noise. A discriminating function differentiates between these cases. More specifically, the period P is divided into m bins (typically 16) and the data (which must have the mean and all low frequency trends carefully removed previously) are added into the appropriate bin depending on its phase relative to P or some integer multiple of P : e.g. the point at 1050 s from the start of a light curve has a phase of (1050 - 10 x 100) / 100 = 0.5 relative to a period of 100 s and is added into the middle bin. The discriminating function used is

$$D(P) = \frac{\sum_{i=1}^{m} \left[\frac{c_i}{n_i}\right]^2}{\sum_{i=1}^{m} n_i}$$

where c_i is the sum of all the n_i points added into the i^{th} bin. This is very similar to calculating the variance of the mean light curve so that when P is at, or close to, a periodicity in the data, points in the same bin will have the same phase and add constructively. Thus, the mean light curve will have a larger variance than when P does not fulfill the above condition which results in the points in the same bin tending to cancel. The function D(P) is calculated for a range of periods and a plot of D against these periods will reveal a peak at any periodicities in the data and random noise at others. Peaks may also appear at harmonics and sub-harmonics of any period in the data and must not be interpreted as separate periodicities.

Using D(P) as a quantity proportional to the amplitude of oscillation of the 192 s oscillation, D(P) was calculated for sets of data from week 3 (runs 2704-2717) that were 4800 s long (about 25 cycles of 192 seconds) and overlapping adjoining sets by 50%. D was plotted as a function of the time at the middle of each data set and the resulting 'amplitude time series' was searched for periodicity. A periodicity was found near 0.9 days and the amplitude data were folded back at that period to produce a 'mean amplitude curve' and this is shown in fig. 16. The letters correspond to estimates of D obtained from the data for the same run. As in the case of ZZ Ceti, the data show an approximately sinusoidal variation indicating that there exists a beat period of about 0.9 days between two components of the 192 s oscillation separated by 0.48 s. Similar plots for the other data were even noisier than fig. 16 but were consistent with the conclusion reached for the week 3 data. As shown in section 5.4. , the addition of two sine waves of amplitudes A_0, A_1 and frequencies ω_0 and $\omega_0 \pm \omega_A$ is given by

$$F(t) = A_t \sin(\omega_0 t + \phi_t)$$

$$A_t^2 = A_0^2 + A_1^2 + 2A_0 A_1 \cos\omega_A t \qquad 5.4.2$$

$$\tan \phi_t = \frac{\pm A_1 \sin\omega_A t}{A_0 + A_1 \cos\omega_A t}$$

From the above equations, the mean amplitude curve provides estimates for A_o, A_1 and $\omega_A = 2\pi/T$ where T is the beat period. The ratio A_1 to A_o found from this curve was about 0.25. However, the frequency ω_o and the choice between the + or - sign is not obtainable from this curve. The latter choice may be seen to be determined from the phase or ϕ_t equation and ϕ_t may be measured as a function of time by fitting a sine wave with variable amplitude A_t but fixed frequency ω_o to successive sections of the data. In practice, neither ω_o nor A_t was specified and the sinusoid was fitted by least squares using a range of values for ω_o and A_t. The variations of ϕ_t with time were determined and examined for behaviour resembling that predicted by the phase equation. Unfortunately, ϕ_t is very sensitive to the value of ω_o since an incorrect ω_o will force a linearly increasing contribution to ϕ_t and so only the non-linear or curvature behaviour of the ϕ_t-time relation could provide useful information. No pattern of ϕ_t variations, consistent with the predictions of the phase equation, could be found for any of the early data. However, the average value of ω_o that yielded the best fit for all the sinusoids was found to correspond to a period of 192.608 s.

A fresh approach was adopted and this consisted of fitting two sine waves to the complete runs, first for the week 3 data and later for the rest of the data gathered up to that time. One sine wave was of amplitude A_o and frequency ω_o while the other was of amplitude A_1 and frequency $\omega_o + \omega_A$ in one case, and $\omega_o - \omega_A$ in the other. The sine waves were fitted by the iterative least squares technique described in Bloomfield (1976). The residual sum of squares is the sum of the squares of the differences between the data and the fitted curve and is a measure of 'goodness' of fit, obviously falling to zero for a perfect fit. These quantities were compared for the fits of the two pairs of sine waves to see which gave the best fit and so determine the unknown + or - sign. The differences were found to be marginal for each run and not consistent from run to run. Most probably because of the low signal-to-noise even for the 192 s oscillation, the residual sum of squares for these fits was not much lower than that for a single constant amplitude sine wave. Hence, this technique also failed to reveal the correct sign. This result yielded the somewhat puzzling picture that the data were quite sensitive to the presence of a beating component as it affected the amplitude of oscillation, but insensitive to its effects on the phase of the pulsations. To ensure that the numerical techniques were not at fault, some noise free test data were generated with the properties associated with the above numerical model and the computer programmes indeed detected the expected phase variations.

The solution to the present impasse will be described in the next section. It is appropriate to digress at this stage and discuss some points in relation to the whole approach being used

to study amplitude variations in the 192 s oscillation.

The variations in amplitude for the 113 s and 118 s oscillations were obtained in a similar way to that described for the 192 s oscillation. As we have seen, the amplitude variations for the latter indicate a smooth , nearly sinusoidal variation. However, in the case of the former two, no consistent sinusoidal variation could be seen in any of the appropriate amplitude data, suggesting that either the variations are distorted by noise due to the low amplitude of these oscillations, or the variations themselves are non-sinusoidal possibly indicating the presence of 3 or more beating components. Thus, the technique of analysing amplitude variations to discover any hidden separate components was found to be defficient and may be criticised for the following reasons :

(1) The approach assumes that only two components are present. The existence of any other components would yield amplitude variations that contain beating on a number of time scales : one for each pair of frequencies (although two pairs with the same frequency separation will obviously have the same beat period). This may be seen from the analogous expression for A_t in 5.4.2 in the case of addition of multiple sine waves. More specifically , consider the addition of a sine wave of amplitude A_o and frequency ω to sine waves of amplitude $A_1, A_2, \ldots, A_{n/2}$ and frequency $\omega+\Delta, \omega+2\Delta, \ldots, \omega+n/2\Delta$ respectively and sine waves of amplitude $B_1, B_2, \ldots, B_{n/2}$ and frequency $\omega-\Delta, \omega-2\Delta, \ldots, \omega-n/2\Delta$. Expressing the sum in the form $A_t \sin(\omega t+\phi_t)$, lengthy but straightforward algebra yields

$$A_t^2 = A_0^2 + 2\sum_{i=1}^{n/2} A_0(A_i+B_i)\cos i\Delta t + \sum_{i=1}^{n/2}(A_i^2+B_i^2) + \sum_{i=1}^{n/2}\sum_{j=1}^{n/2}\{A_iA_j\cos(i-j)\Delta t +$$

$$B_iB_j\cos(i-j)\Delta t + A_iB_j\cos(i+j)\Delta t\} + 2\sum_{i=1}^{n/2} A_iB_i\cos 2i\Delta t$$

which, in the case of just two components, reduces to 5.4.2 and , in the case of three components, yields

$$A_t^2 = A_0^2+A_1^2+B_1^2+2A_0(A_1+B_1)\cos\Delta t + 2A_1B_1\cos 2\Delta t \qquad 7.1.1$$

The latter expression indicates beating at the frequency separation of A_o and A_1 or B_1, and additional beating at the frequency separation of A_1 and B_1. It can thus be seen that analysing amplitude variations of more than two components is difficult, if not impossible.

(2) Even in the case of two components, the approach is severely limited by noisy data. In order to measure time varying amplitudes of oscillation, a sufficiently short length of data must be used so that the variations are not smoothed out i.e. one must use lengths of data that span only a short section of the beat cycle. This limitation may hide any regular variations in the amplitude data due to such variations being distorted by noise resulting from being forced to select only a short section of data for each amplitude estimate as in the case of the 113 and 118 s oscillations. The technique to be discussed in the next section is not limited in this way.

(3) Only the curvature of the phase-time relation provides useful

information , unless the frequency ω_0 is known to very high accuracy. As a result, the information obtainable from the phase variations which is needed for a full specification of the parameters associated with the numerical model, is very difficult to extract from the data when low signal-to-noise ratios are present.

For these reasons, this approach was abandoned and the calculation of power spectra from Fourier transforms of long data strings was preferred.

7.2. Power Spectra Of Unequally Spaced Data

The detection of closely spaced frequency components may be effected by analysing the amplitude and phase variations of short sections of data to detect the underlying numerical model, or it may be carried out by the more direct method of calculating power spectra with sufficient frequency resolution that any closely spaced frequency components may be clearly resolved. Since the frequency resolution of a power spectrum $d\nu$, is related to T, the time spanned by the time series, by

$$d\nu = \frac{1}{T} \qquad 7.2.1$$

and the frequency spacing of two components produces amplitude variations on a time scale of T related by the identical expression 7.2.1, it is necessary to use a data set spanning at least the amplitude beat period in order to resolve the components responsible for the beating. Investigations by Loumos and Deeming (1978) have shown that an even longer set of data (at least 50%) is necessary to clearly resolve the frequencies. In the case of L 19-2, this means that at least two nights of observations are necessary. Extreme care must be exercised in handling such a data set because the daytime interval when no observations were possible might give rise to aliases of the true oscillation frequencies. Fortunately, the technique of Fourier transforms of unequally spaced data (Deeming,1975) is well suited to this sort of analysis.

Considering a set of N data points, arbitrarily spaced at times $t_1,\ldots,t_N$ with ordinates $f(t_1),\ldots,f(t_N)$, the discrete Fourier transform is defined as

$$F_N(\nu) = \sum_{k=1}^{N} f(t_k) e^{i2\pi\nu t_K}$$

The function $F_N(\nu)$ for a finite data set generated by a cosine wave of frequency ν_0 will generally be significantly different from zero at frequencies near ν_0 and $-\nu_0$. In addition, aliasing frequencies may arise if the data are undersampled giving rise to significant functional values $F_N(\nu)$ at frequencies other than that actually used to generate the data and dependent on the characteristics of the undersampling. The most usual type of undersampling is where the time series consists of equally spaced points separated by times much greater than the time scale responsible for variations in the time series. In the case of L 19-2, all the data consisted of separate runs with integration

times much shorter than the characteristic oscillation periods of 100-1000 s. However, in order to use multiple runs in the same data set, it is necessary to bear in mind that aliasing can also occur due to the absence of data during (a) the daylight period between runs and (b) the period of months between allocations of observing time. In order to predict in advance where aliasing might occur, Deeming (1975) defines a spectral window function $\delta_N(\nu)$ by

$$\delta_N(\nu) = \sum_{k=1}^{N} e^{i2\pi\nu t_K}$$

and shows that $F_N(\nu)$ is the convolution of the 'true' Fourier transform $F(\nu)$ with the spectral window i.e.

$$F_N(\nu) = F(\nu) * \delta_N(\nu)$$

so that any strictly periodic function, which normally transforms to the Dirac delta function at $\pm \nu_0$ say, will transform in the discrete case, to $\delta_N(\nu)$ shifted to $\pm \nu_0$. If, for example, $\delta_N(\nu)$ for a given data set consisted of the Dirac Comb function with a separation of Δ between the teeth, $F_N(\nu)$ for that set will show peaks at any frequency ν_0 in the data and additional peaks at all those frequencies ν_0, $\nu_0 \pm 2\Delta$... which must not be interpreted as separate frequencies in the data but as due to aliases resulting from undersampling. Thus the spectral window contains all the pathology of the time spacing in the data set and is an invaluable tool in interpreting power spectra resulting from discrete Fourier transforms. The various normalization procedures for $F_N(\nu)$ and $\delta_N(\nu)$ are described in Deeming (1975) and it suffices to say that the former was divided by N so that power spectra of different lengths of data could be directly compared while the latter was normalized to unity at zero frequency. The power spectra were calculated from the modulus of the real and imaginary parts of $F_N(\nu)$ to yield the amplitude of oscillation directly in mmag. The spectral window, a complex function, is not immediately helpful in interpreting power spectra but the 'power spectral window' given by $\delta_N(\nu)\delta_N^*(\nu)$ (superscript * denotes complex conjugate) is and this latter function was plotted for selected data sets where its information is important in the interpretation. The power spectral window, while revealing where aliasing frequencies may be found, generally predicts that the amplitude of the aliasing frequencies is less than actually seen in the power spectra. This arises because although 7.2.1 is strictly valid, $F_N(\nu)F_N^*(\nu)$ is not generally equal to the convolution of the true power spectrum with the power spectral window (see Deeming's discussion). It is of interest to consider some characteristics of the power spectral windows (PSW). To this end, attention will be restricted to the PSW of a typical week's data. The data for each observing week usually consisted of a number of blocks of equally spaced data (i.e. one run) starting at the same time each night. Each run is separated from the next night's by at least half a day. Thus the PSW may be expected to show aliasing due to the 1 day interval in the distribution of data for the whole week. A typical PSW for the week 3 data is shown in fig. 17. This plot is such that a single periodicity would result in a power spectrum which exhibited a shape similar to the PSW with the peak at zero

frequency in the latter at the position of the period representing the oscillation in the data. Furthermore, the PS will be symmetrical about this position. The PSW in the figure shows the peak at zero frequency normalized to unity with the one day alias separated from it by just under 1.2×10^{-5} Hz (whose inverse is 85000 seconds, slightly shorter than a day). The following points concerning the figure are noteworthy :

(1) There is a small alias near 2.4×10^{-5} Hz corresponding to a 1/2 day alias. In the PSWs of the other weeks of data, this peak is much stronger and there are additional peaks at 1/4, 1/8 day aliases etc. The presence and strength of all these peaks (including the 1 day alias), depends on the lengths of the individual runs comprising the week. For the week 3 data, run 2714 was half a day long making the alises other than the 1 day peak weak. In other weeks consisting of only short runs (e.g. week 5), these peaks were strong.

(2) Both large and small peaks in the PSW and hence in the power spectrum, have the same characteristic width dependent on the inverse of the total time spanned by the whole week's data in accordance with equation 7.2.1. Thus, any peak in the power spectrum has an uncertainty in its frequency that may be conservatively estimated as the 1/2 width of its peak at 1/2 its amplitude. The frequency is probably known to much better than this error estimate but it is a useful conservative yardstick for errors.

(3) The other subsidiary peaks in the PSW arise because of the peculiarities of the distribution of data over the week (e.g. run 2711 was very short while there were no observations on the night of 28-29 June) and are generally insignificant in interpreting the power spectrum.

The next few sections are devoted to describing the power spectra of the individual weeks of data for the frequency intervals where oscillations in the light curve have been found. Subsequently, power spectra of the complete data set (first our data alone and then including Mc Graw and Hesser's data) will be presented in order to yield the best estimates of the parameters of the individual frequency components. The approach in both cases consisted of obtaining a power spectrum which generally had some peak of largest amplitude. The data were then 'prewhitened' by this peak, i.e. a cosine wave of the corresponding frequency, amplitude and phase was subtracted out of the data, and a new power spectrum was calculated to reveal any other significant peaks corresponding to additional frequencies present in the data. This process of repeated prewhitening was pursued until a power spectrum consistent with noise was obtained. Power spectra calculated in the manner described above are computationally very expensive. However, a method of combining the individual weeks' power spectra was found which substantially reduced the amount of time needed for the power spectra of the complete data set. To make this technique work, each individual week was prewhitened with parameters obtained from the power spectrum of the complete data set and <u>not</u> from the power spectrum of the individual week. Any cases where this is likely to lead to error will be discussed in the text. It will obviously be the wrong approach should the data of any individual week be inconsistent with the complete set e.g. by having a frequency component with a phase in the individual week that is different from that of the complete data set.

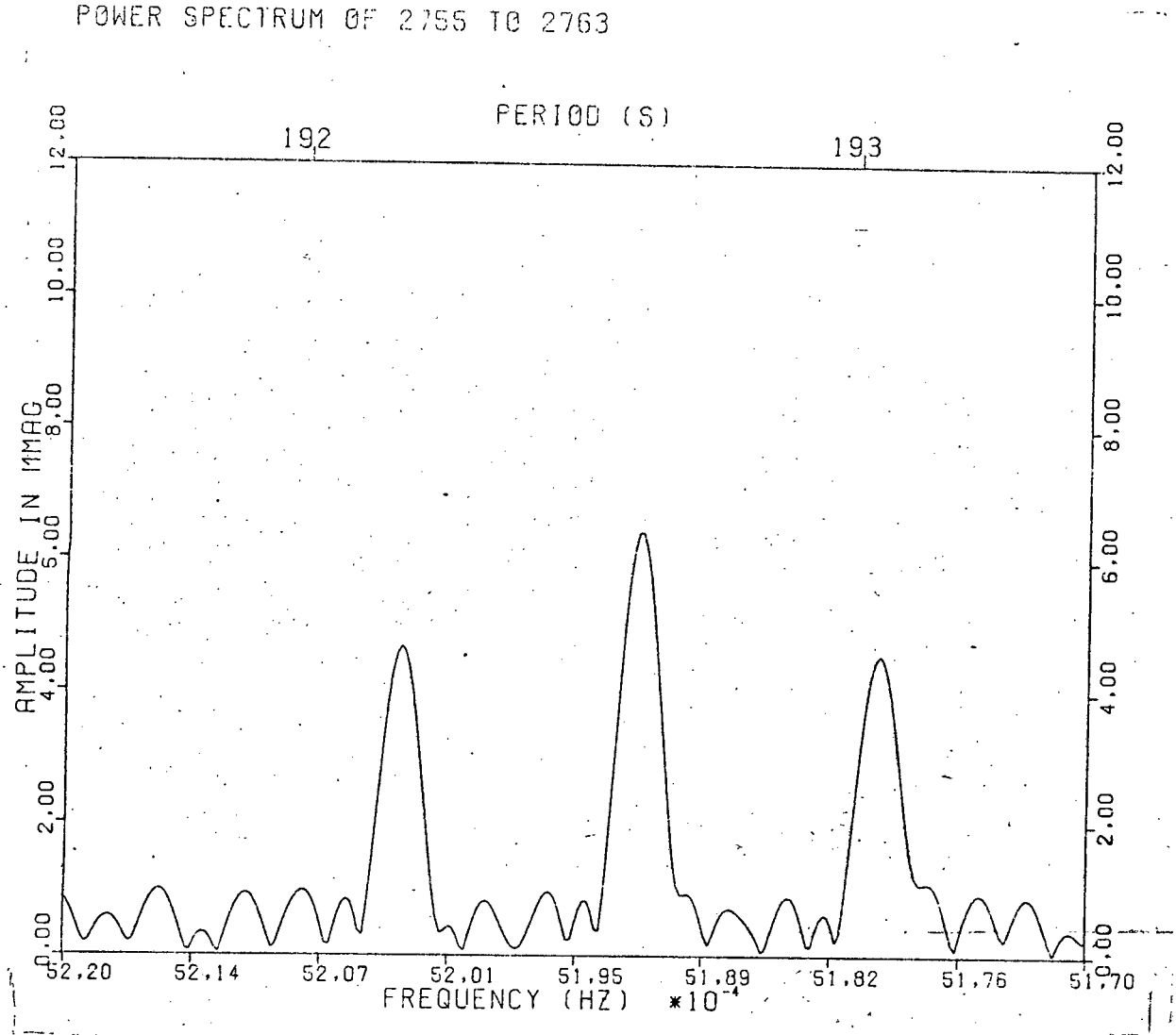

Figure 22

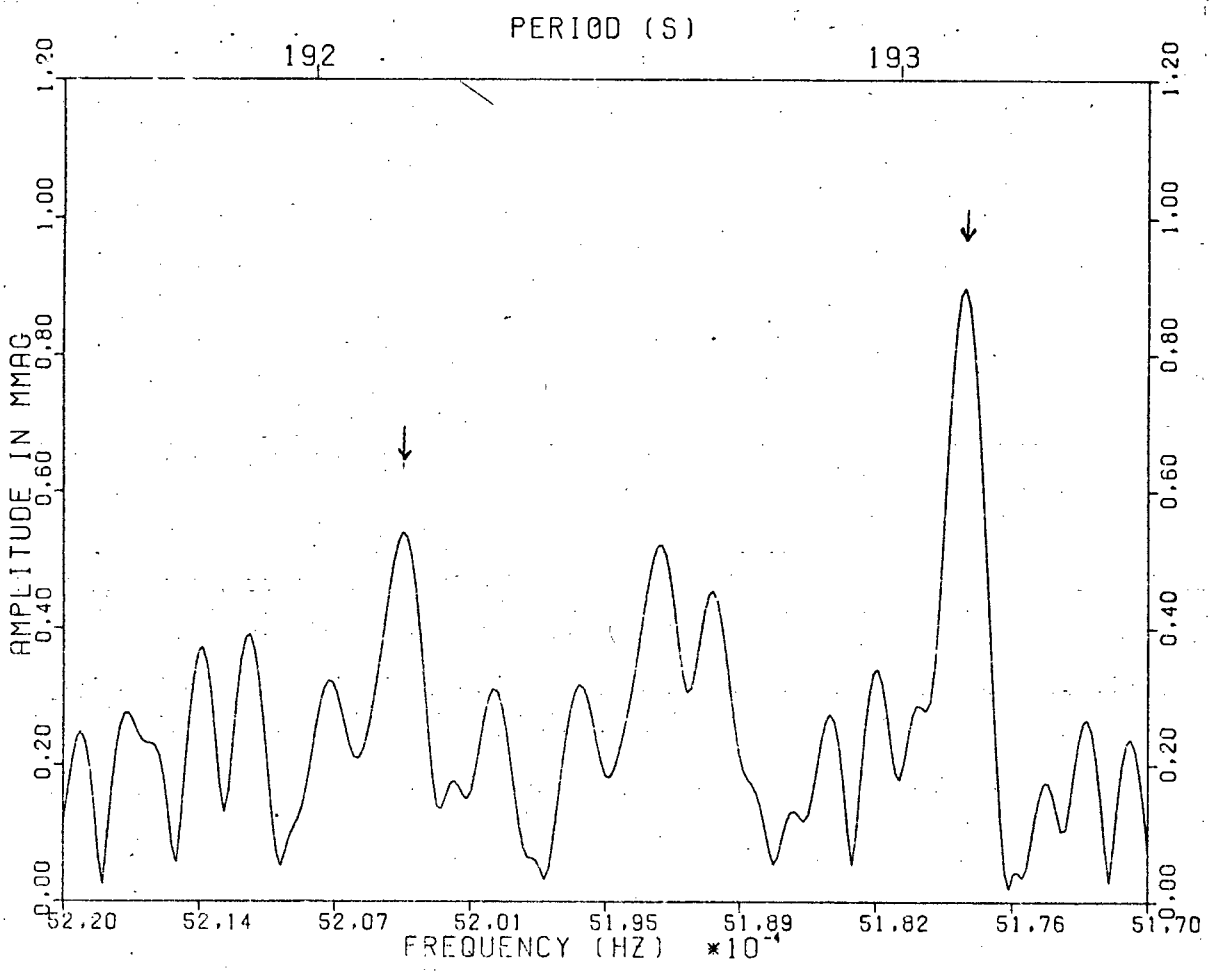

Figure 23

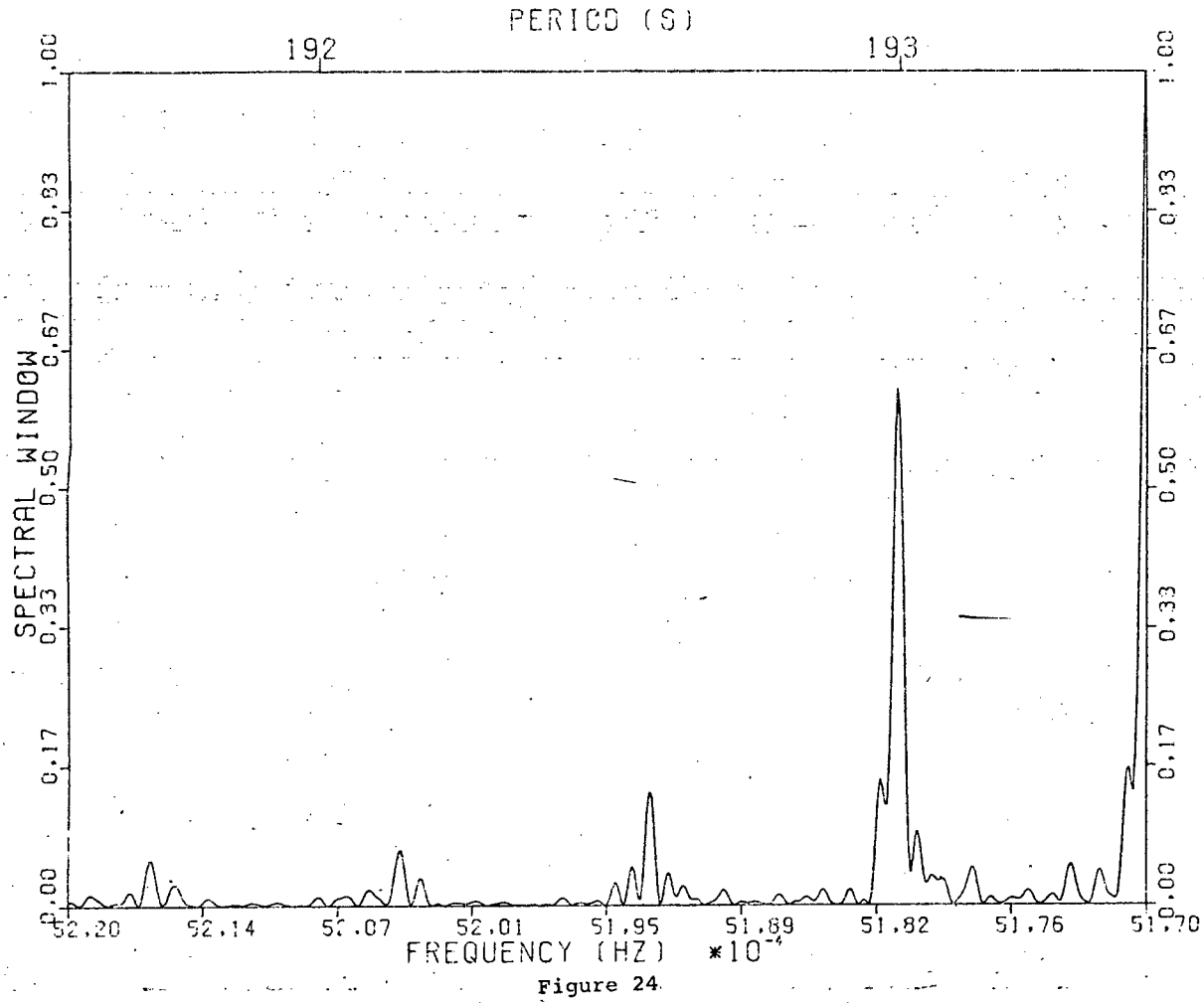

Figure 24

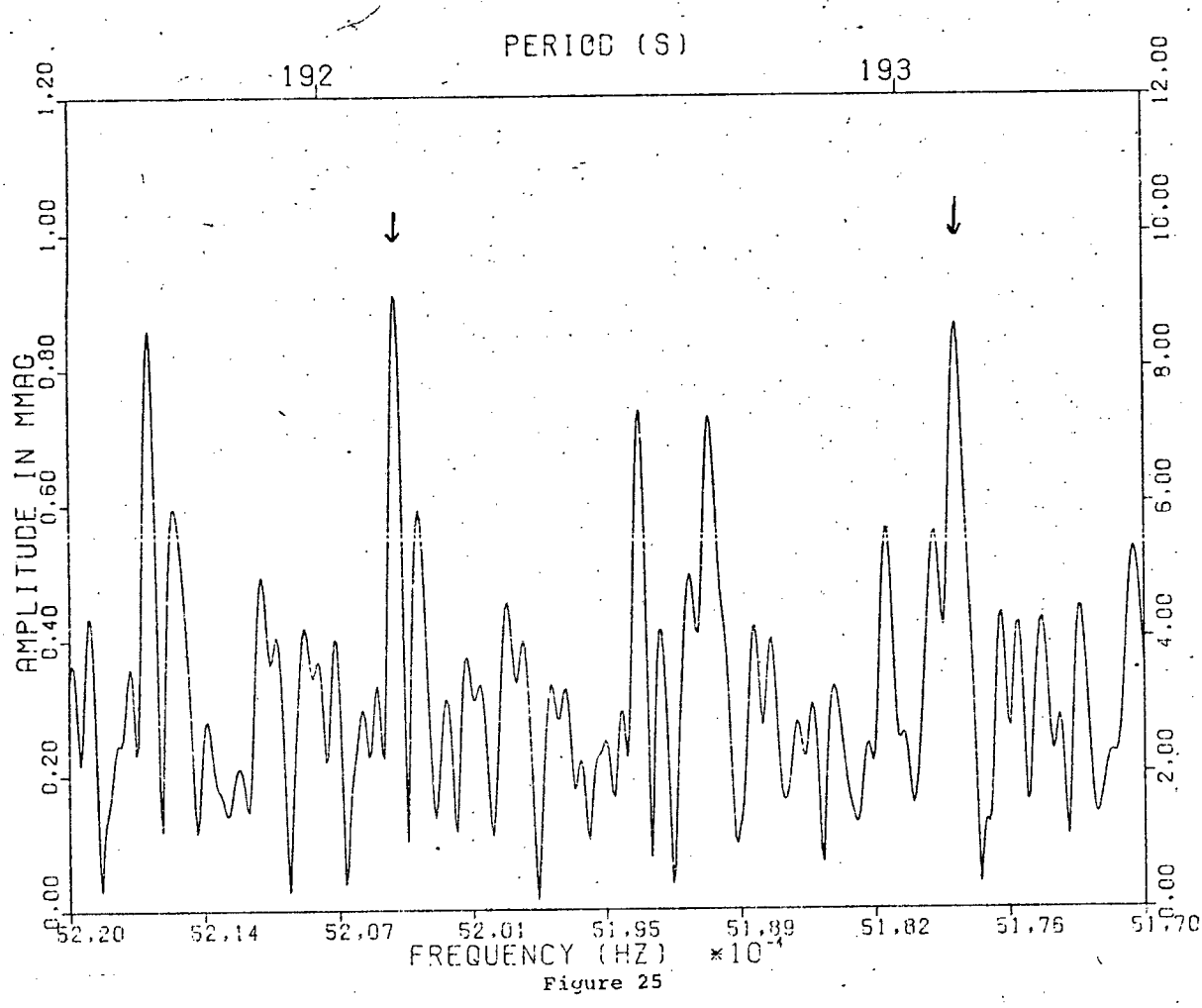

Figure 25

7.3. Frequency Structure Of The 192 s Oscillation

The power spectrum (PS) near 192 s, and its PSW, for the week 3 data are shown in figs. 18 and 19. For convenience of comparison, the PSW (previously shown in fig. 17), is replotted at the same frequency scale as the PS ; its location is, of course, arbitrary.

Fig. 19 shows a principal peak near 192.6 s, with structure on either side, very similar to the shape of the PSW, apparently indicating the presence of only one component near the frequency ω_c found in section 7.1. The secondary component found in 7.1 had $A_1 = 0.25\ A_c$, and would appear in the PS with an amplitude of about 1.5 mmag and separated from the principal peak by ≈0.5 s. Even though such an amplitude would be close to the apparent noise in the PS, some asymmetry of the pattern might have been expected from a component strong enough to produce 'beats' in the periodogram results.

In order to investigate this puzzle, the data were prewhitened with the 192.6 s principal component. The resulting PS is shown in fig. 20. Prewhitening has removed considerable power throughout the PS. There remain, however, a number of peaks significantly above the noise. Tests on artificial data with similar properties have verified that these peaks are not due to incomplete prewhitening and must consist of real frequencies and their aliases.

The arrows in fig. 20 indicate the two possible expected locations for the 'missing' component : at each there appears a peak in the PS. Prewhitening with these two frequencies removes all significant peaks from the PS, leaving only noise. This, incidentally, shows that some of the high peaks in fig. 20 are caused by the near superposition of aliases of the two frequencies.

In order to verify this result, a similar analysis was performed on data from other weeks. As an example, figs. 21 and 22 are the PSW and PS for the data from week 8. The principal component and its aliases are again evident. Fig. 23 shows the PS that results from prewhitening the data with the principal component. As before, the two secondary components (arrowed) are present ; their differences in amplitude from those seen in fig. 20 may only be as a result of the low signal-to-noise. All other PS for weeks that contained sufficient observations produce results consistent with these. While the PS of weeks with only a little data were very noisy, it was always possible to detect peaks of the right amplitude at the positions of the two side components found above.

Use of the extended data set, comprising runs 2772 to 2806, which span about 19 days, provides complete confirmation. The PSW and PS obtained by prewhitening with the principal component are shown in figs. 24 and 25. Again, prewhitening with the arrowed frequencies leaves only noise in the PS.

The frequency range on either side of that in the above PS was searched for other components but none were found. The same results were obtained from independent data sets with a variety of PSWs (and alias spacings) so we conclude :

(1) There are <u>two</u> secondary components, not one, that beat with the 192.6 s principal component. They lie equidistant either side of the latter, the spacing being just that required to explain the beat period in fig. 16.

(2) The amplitude of each secondary component is about half that deduced for the single component postulated in section 7.1.

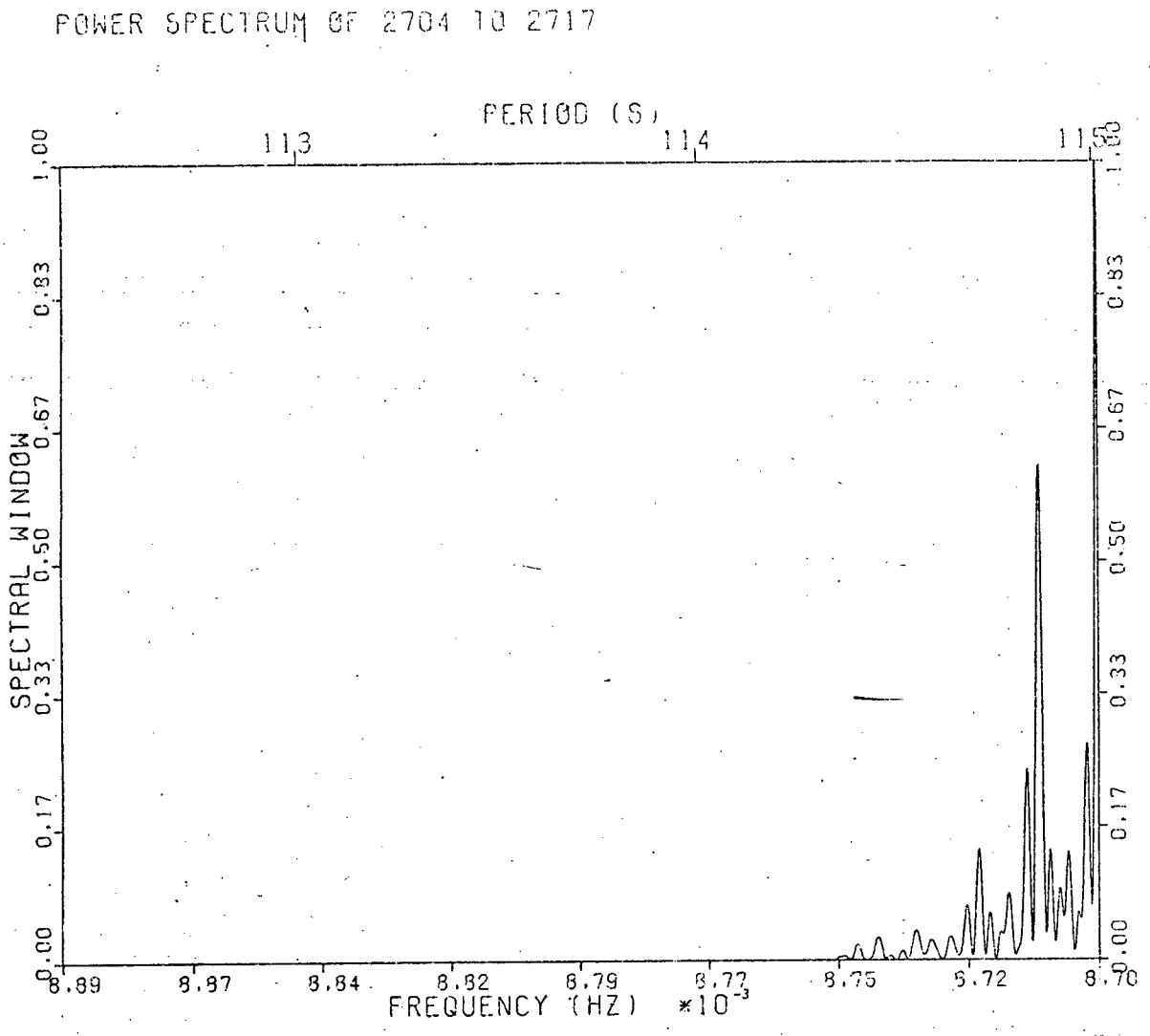

Figure 26

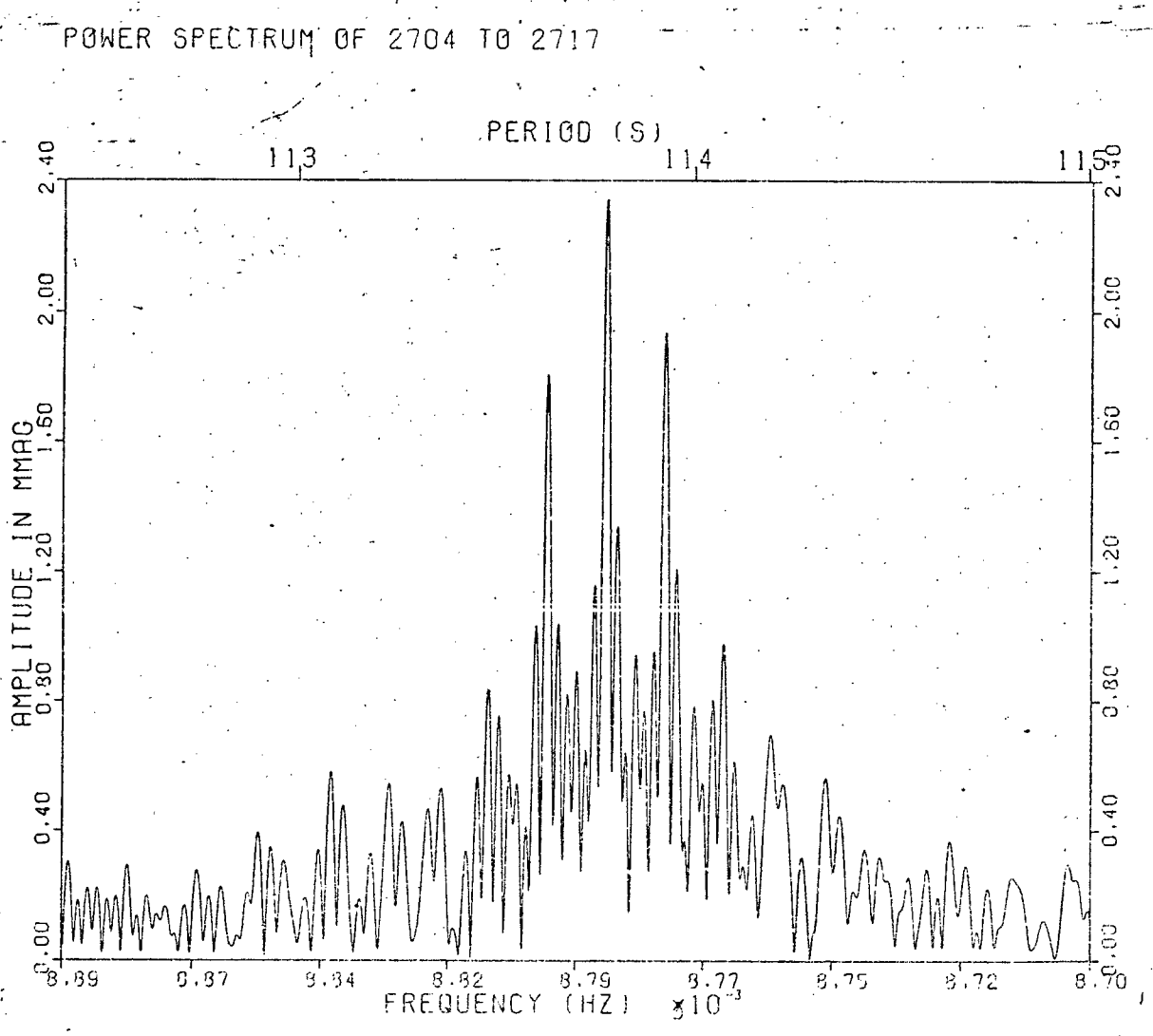

Figure 27

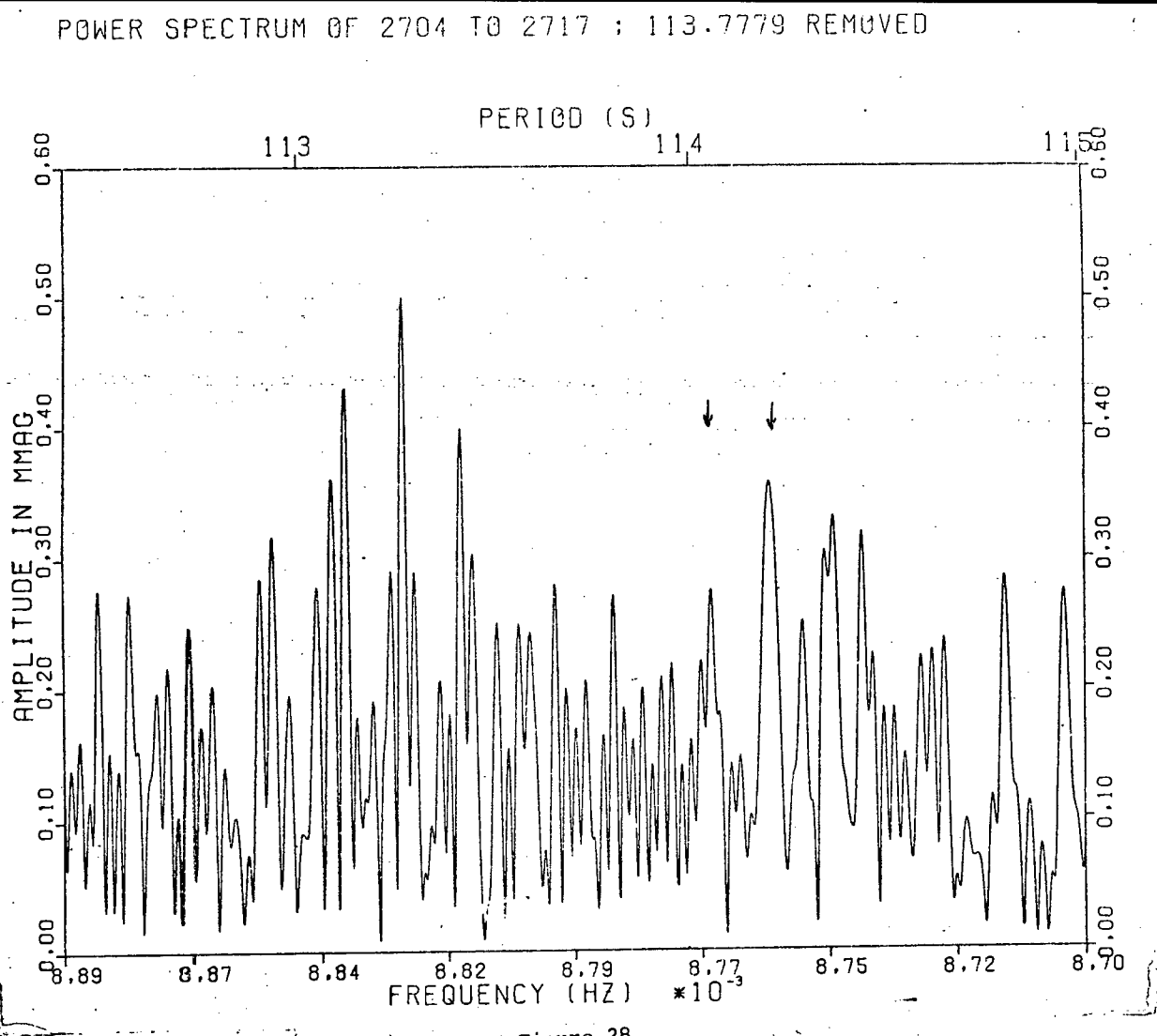

Figure 28

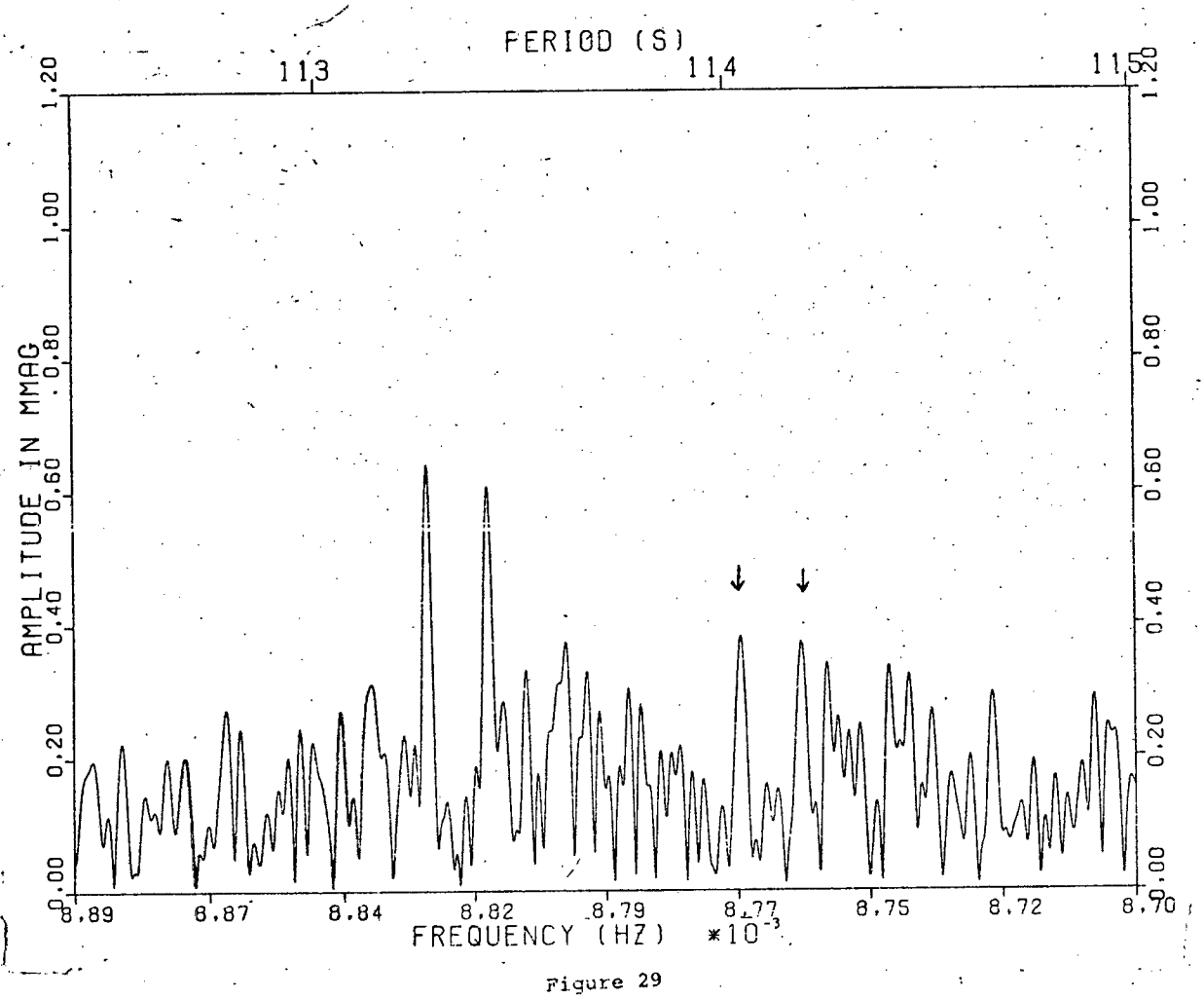

Figure 29

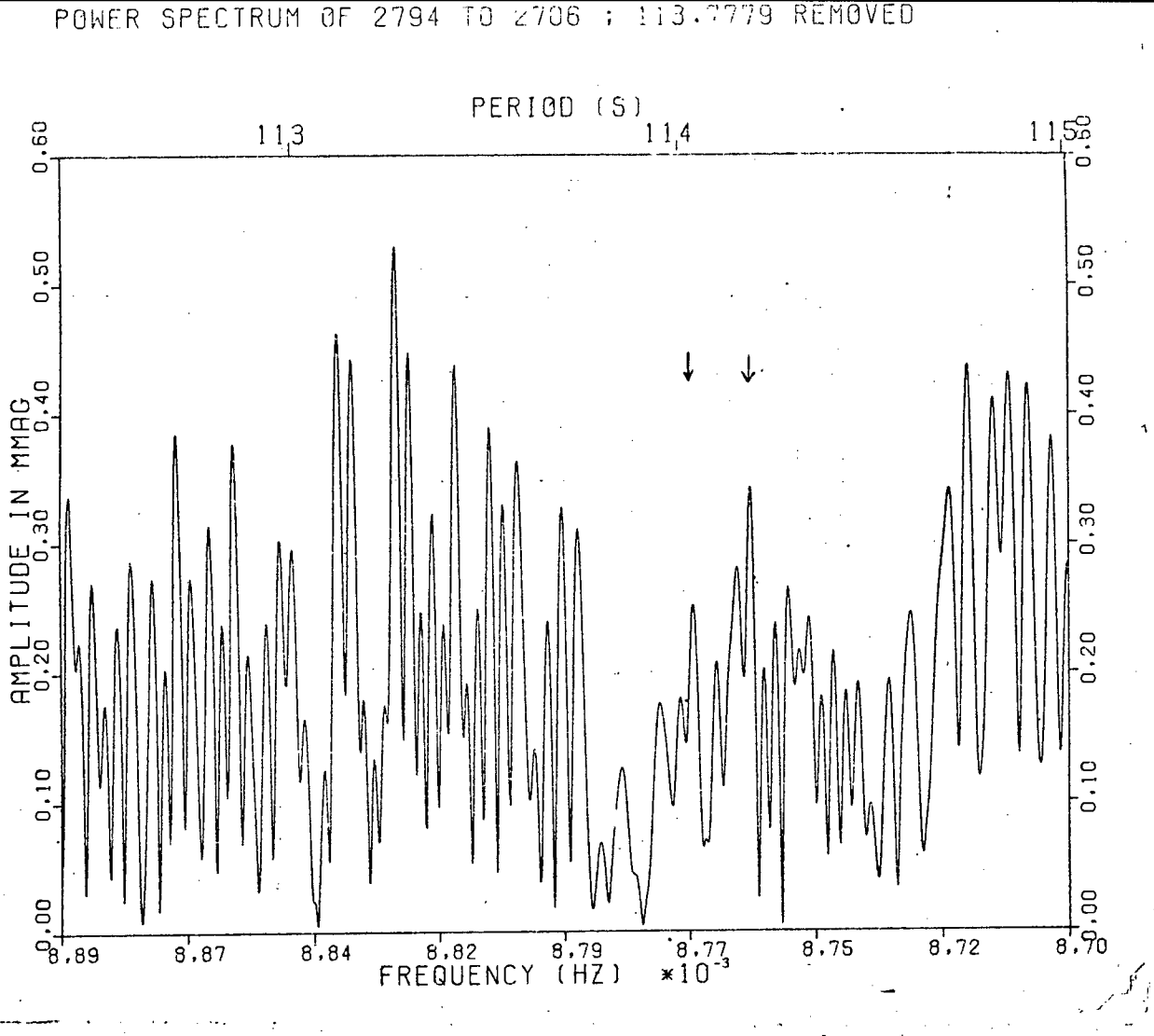

Figure 30

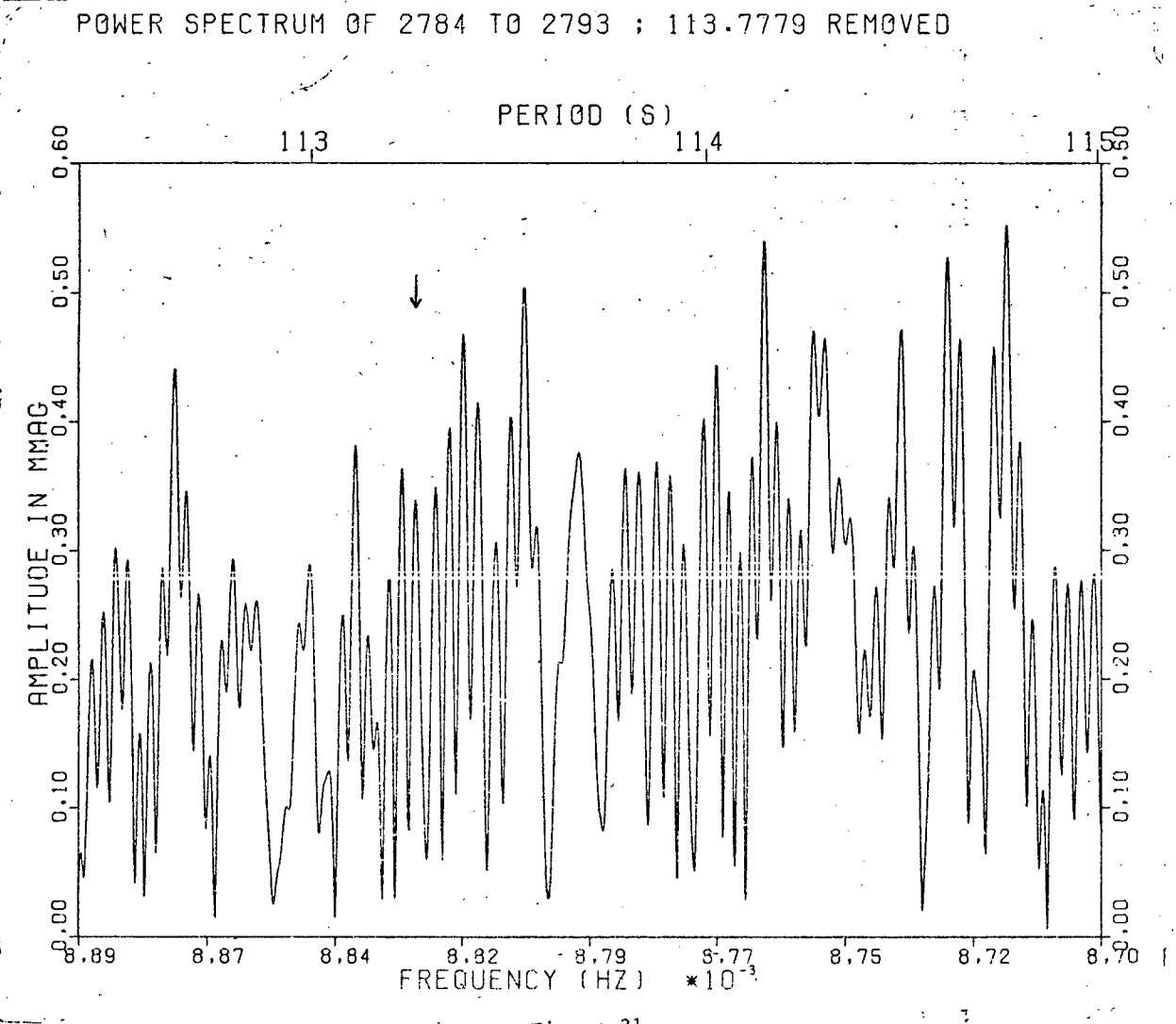

Figure 31

(3) From equation 7.1.1, modulation at 0.45 days as well as 0.9 days is predicted. However, with the values A_1 = 0.6 mmag, B_1 = 0.7 mmag and A_0 = 6.0 mmag found from the PS, the modulation amplitude $2A_1B_1$ at 0.45 d is only one twentieth of the amplitude $2A_0(A_1+B_1)$ at 0.9 d and is therefore undetectable.

(4) The tan ϕ_t equation corresponding to the amplitude equation 7.1.1, predicts that for the addition of a sine wave to two others equally split in frequency about the former and of equal amplitude, there will be no variation in ϕ_t with time as was found in section 7.1.

Final estimates of the frequency, amplitude and phase of all 3 components will be obtained from the PS of the complete data set which will be discussed later.

7.4. Frequency Structure Of The 113 s Oscillation

As we have seen, the 113 s oscillation was of lower amplitude than that at 192 s and varied more rapidly. The periodogram approach was found to be inadequate in deciphering the frequency structure so that any structure found by the direct method of using PS could not be verified by the former.

The PSW for week 3 is repeated in fig. 26 at a scale appropriate to the 113 s period interval investigated. In order to conserve computer time, it was calculated for only a limited frequency range encompassing the major aliasing peaks. The PS for week 3 near 113 s is shown in fig. 27 while the PS in fig. 28 was obtained by prewhitening the data with the main peak near 113.8 s in fig. 27. With the exception of the arrowed peaks, whose significance will be seen later, removal by prewhitening of the obvious frequency component near 113.3 s resulted in a PS consistent with noise.

The PS from all the other weeks exhibited a principal component near 113.8 s. The presence of the side component is confirmed in almost all of their PS, obtained when the principal component is removed. Examples are shown in fig. 29 for the week 8 data and fig. 30 for the week 12 data. In the former, only the right hand (low frequency) alias is seen while attention is again drawn to the two arrowed components in each figure. One exception where no side component is seen is the PS in fig. 31 obtained by prewhitening the week 11 data with the principal component as usual. The arrow indicates where the 'expected' component, whose amplitude was found to be about 0.6 mmag, should lie.

Many, but not all, of the PS from the other weeks showed peaks above 114.0 s at the positions of the arrowed components mentioned above. In addition, the presence of isolated peaks or suggestive aliasing patterns well above the noise, indicated that other components may have been present. However, there was no consistent re-appearance of any of these and besides warning that there may be low amplitude components that grow and die on a time scale of weeks, nothing further will be said about these.

In summary, it seems that the 113 s oscillation consists of a large amplitude component at 113.78 s (2.4 mmag) and a smaller component of about 0.6 mmag at 113.26 s. There is possibly a third above 114.0 s. Precise determination of the parameters for these oscillations must await the discussion of the PS of the complete data set.

POWER SPECTRUM OF 2772 TO 2806

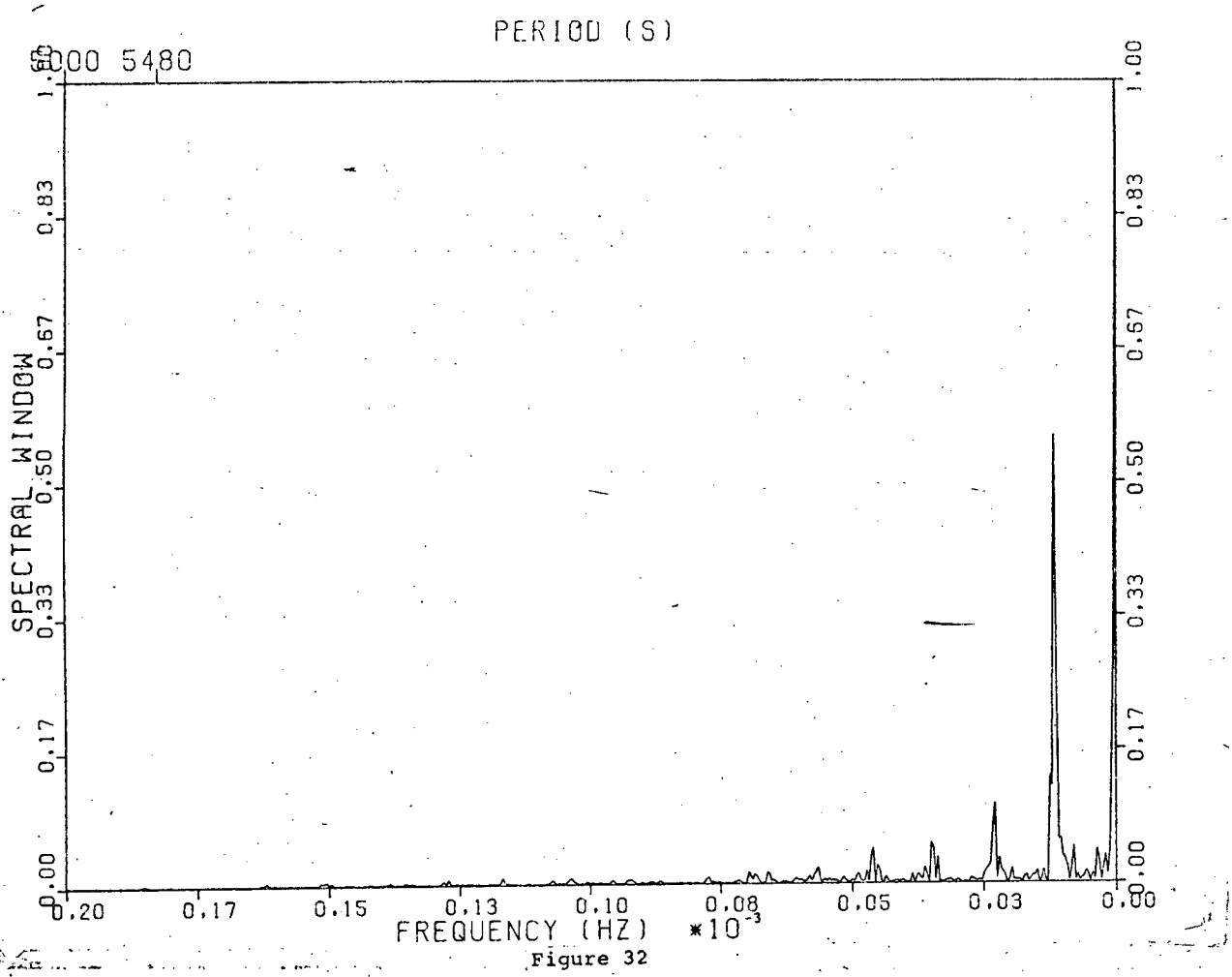

Figure 32

POWER SPECTRUM OF 2772 TO 2806

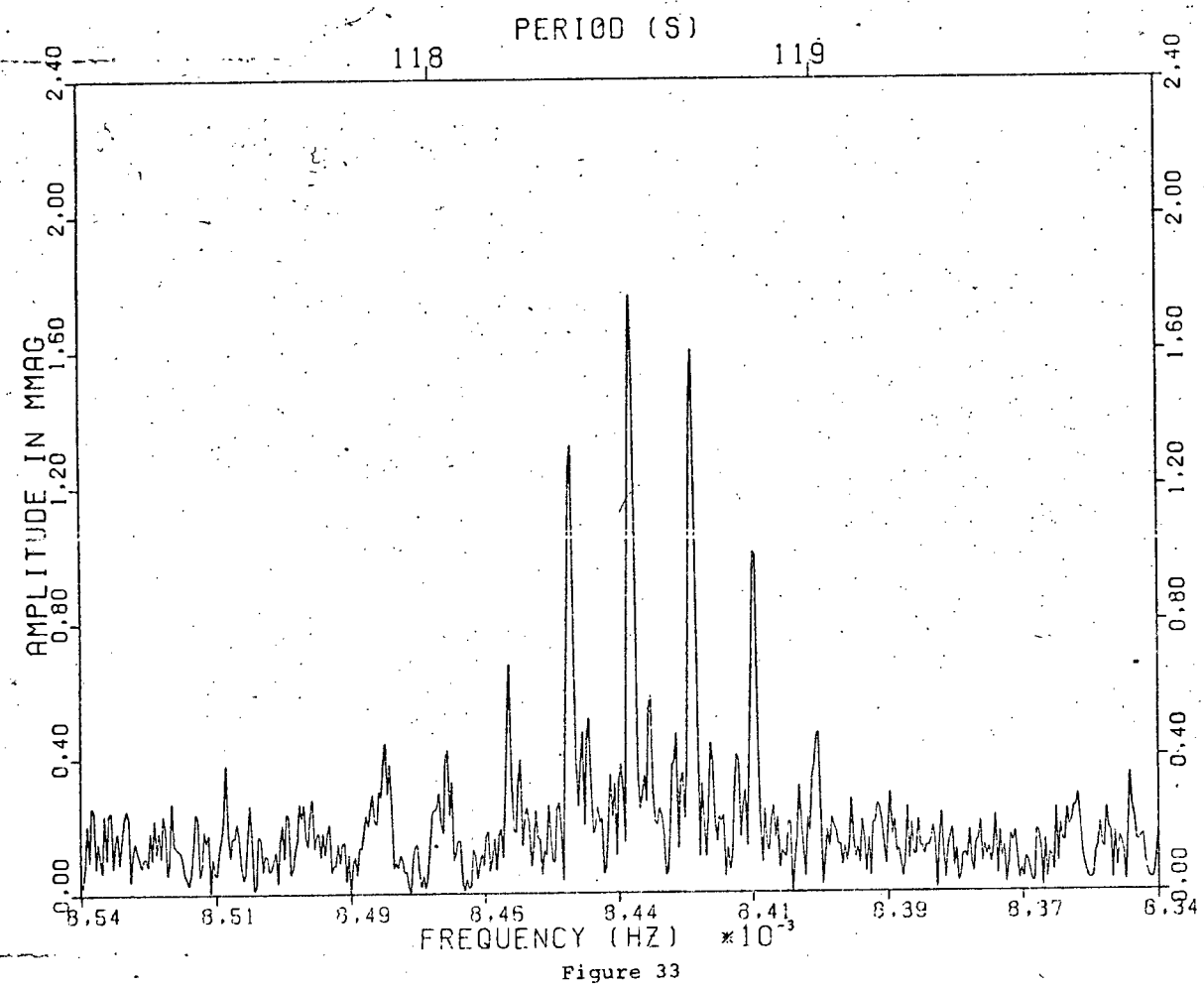

Figure 33

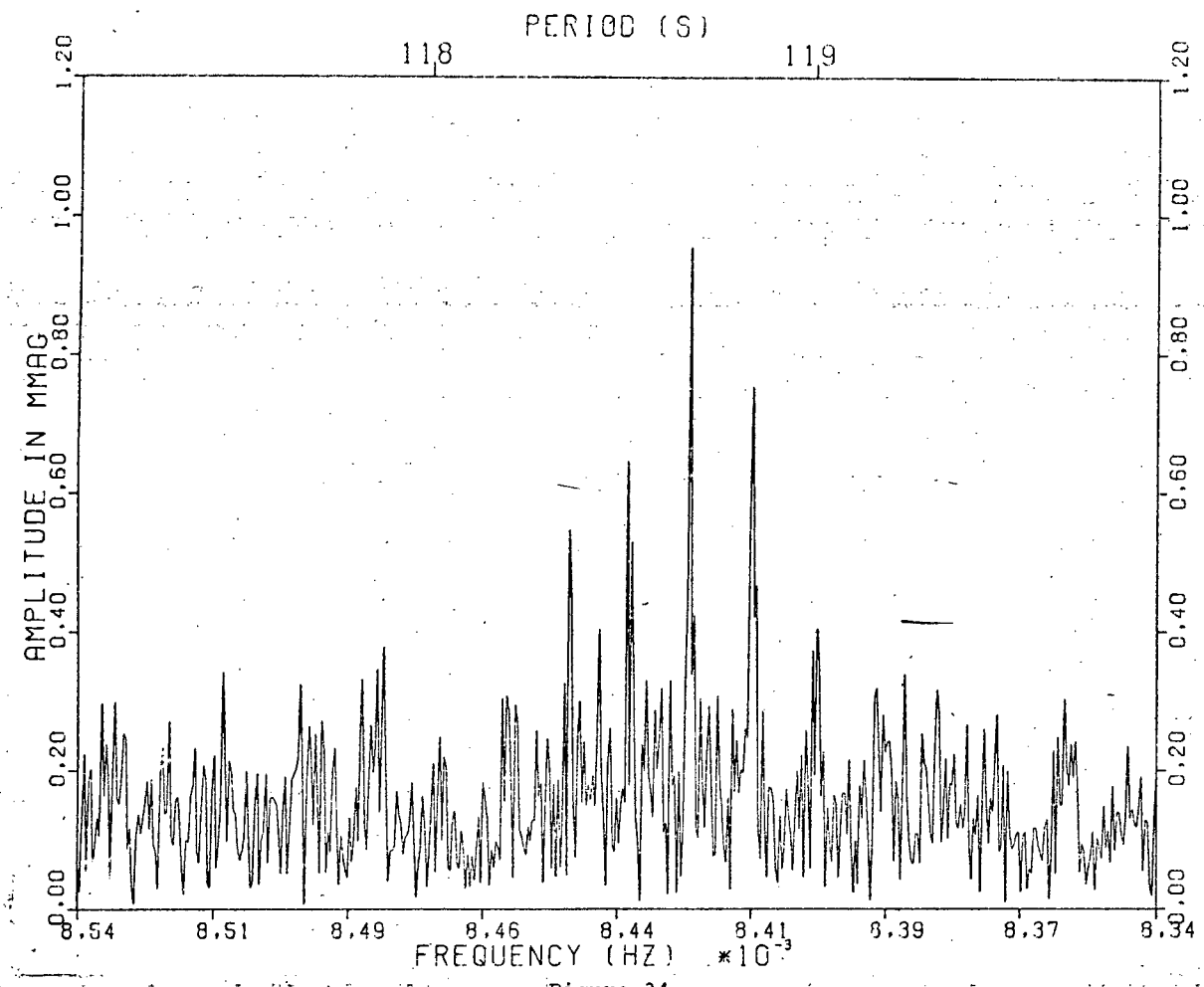

Figure 34

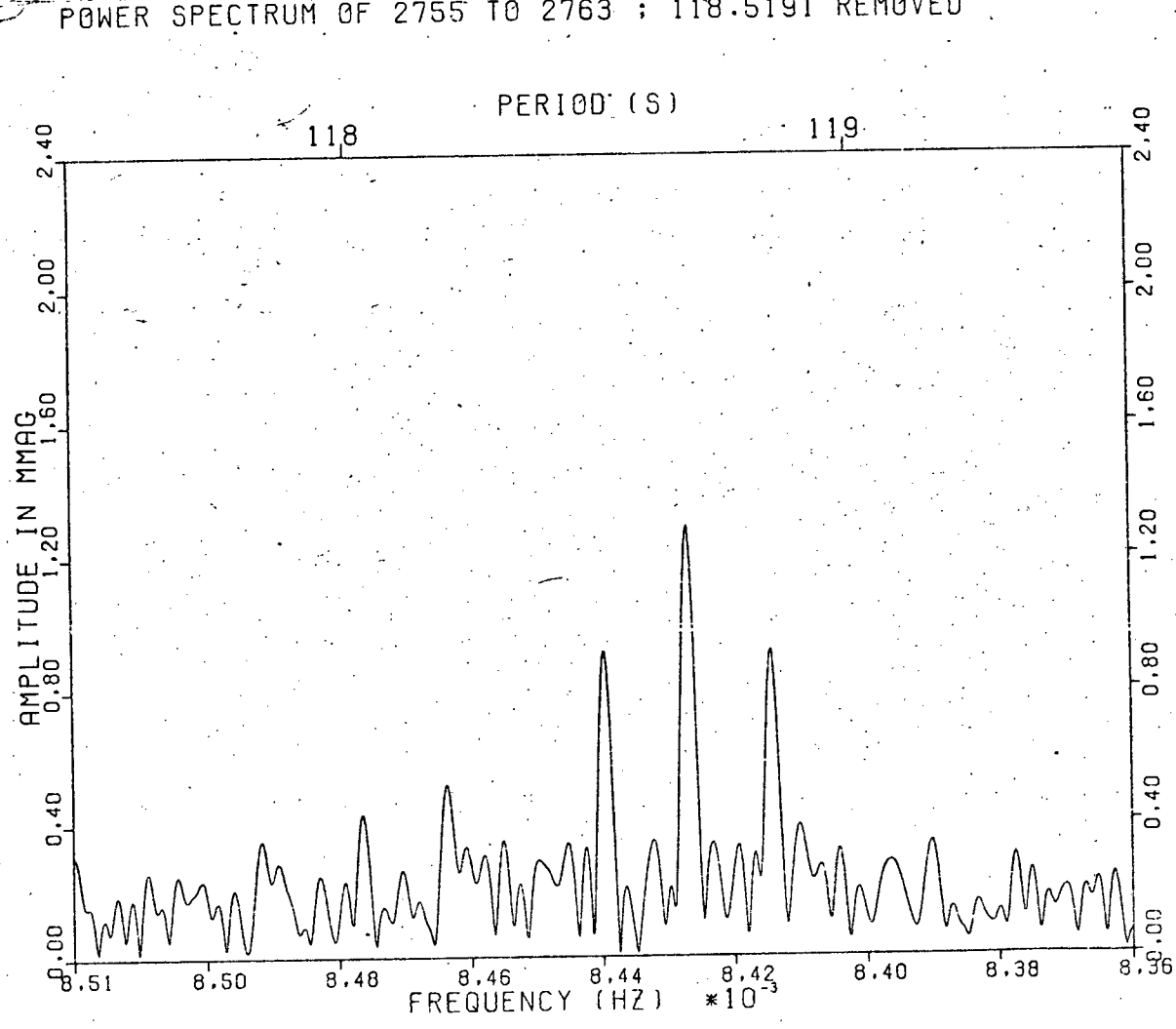

Figure 35

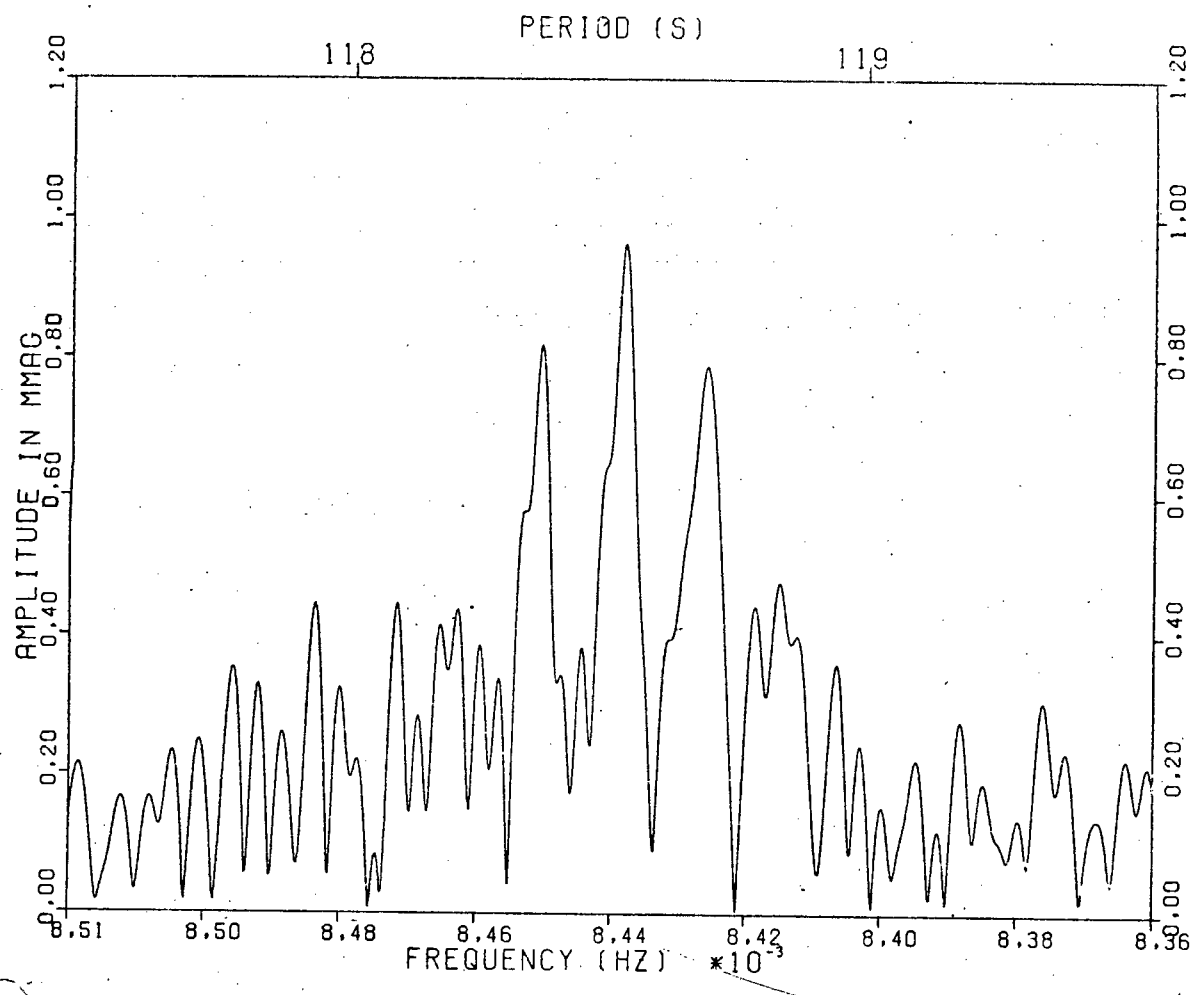

Figure 36

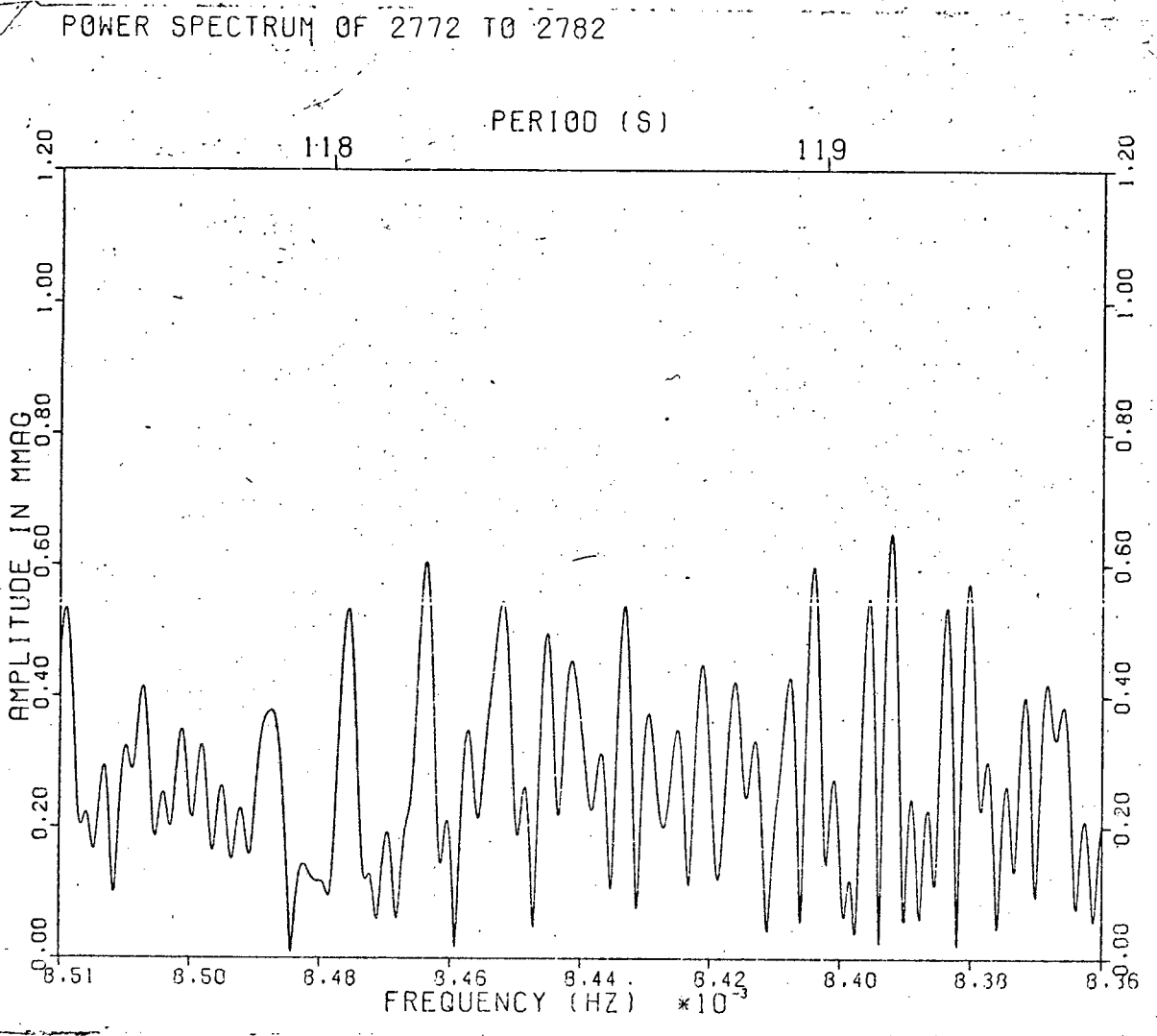

Figure 37

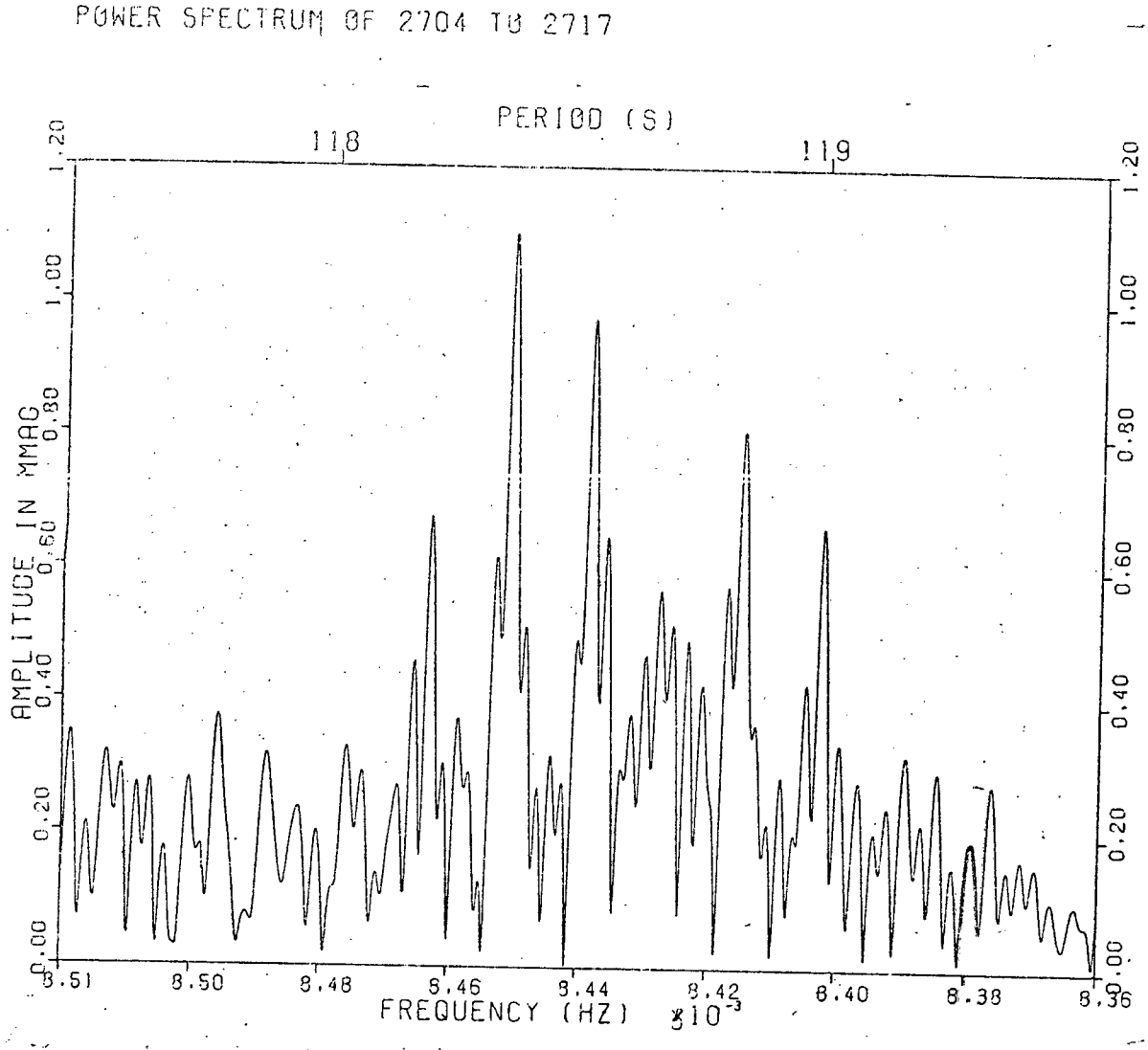

Figure 38

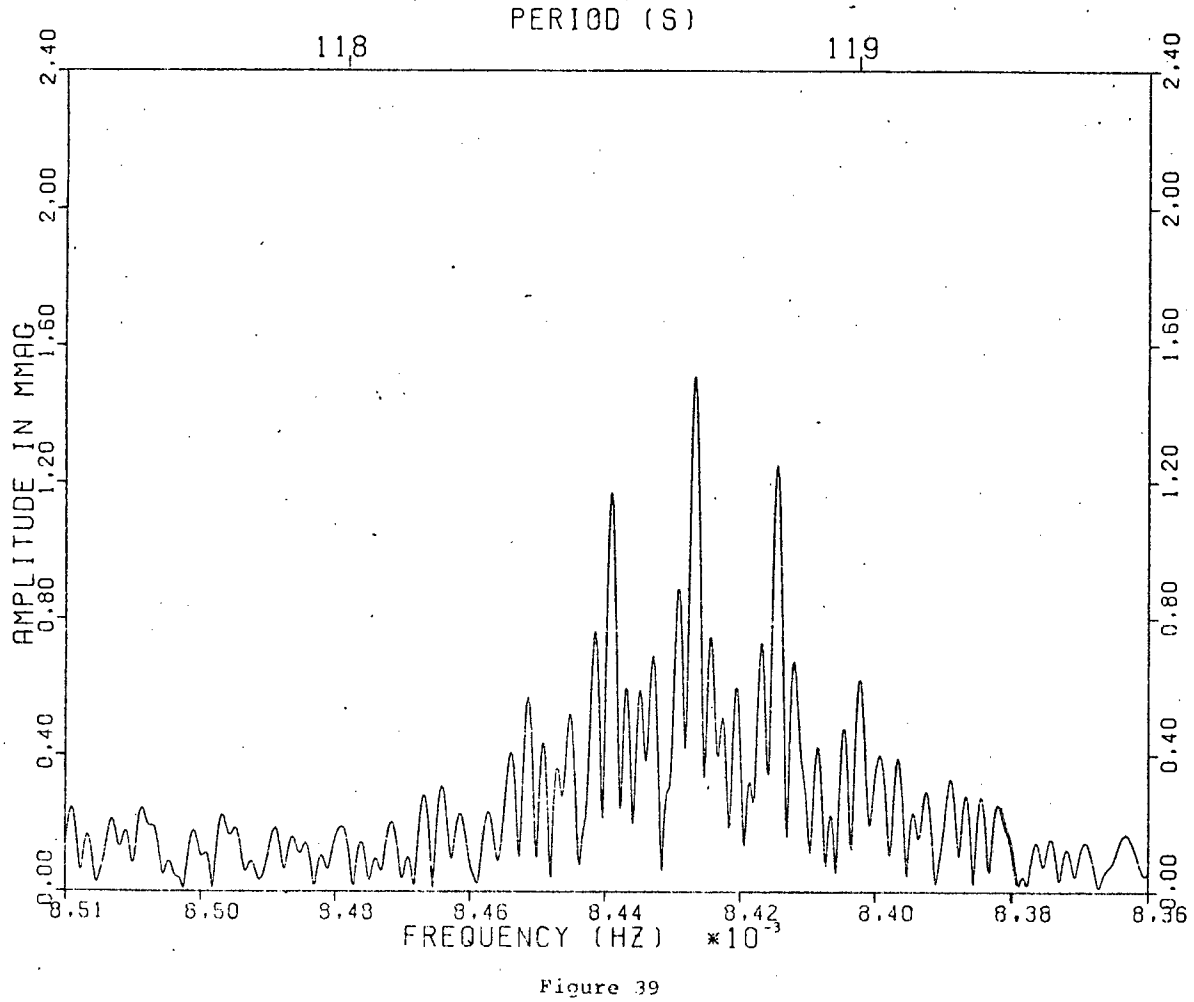

Figure 39

7.5. Fequency Structure Of The 118 s Oscillation

The PSW and PS for the 19 day run, weeks 10-12, are shown in figs. 32 and 33. The pattern of peaks in the PS is asymmetrical indicating that there is more than one component present as expected. Unfortunately, it is also apparent that the frequency separation of these components is some multiple of the separation of the aliasing peaks in the PSW so that the components and their aliases 'sit' on each other. This aliasing problem will introduce substantial uncertainty into any prewhitening because it will not be clear what portion of any peak is 'real' and what is due to the alias(es) of the other component(s). Nevertheless, the PS in fig. 34 was obtained by prewhitening the data with the principal component near 118.5 s in the previous plot. These two PS suggest that there are two components, separated by the 1 day alias, at 118.52 s and 118.68 s. Removal of this second component resulted in a PS consistent with noise.

With the exception of two which will be discussed below (weeks 10 and 3), all the other weeks showed the same asymmetrical pattern in the unprewhitened PS. For those weeks with sufficient data, removal of the principal component revealed the second component in the position found above, e.g. the PS in fig. 35 for the week 8 data, and its removal resulted in noise. The resulting noise spectrum was, however, not seen in the case of the week 7 data with both components removed and shown in fig. 36. The remaining peaks are broader than expected and situated at the positions of the principal component and its aliases, indicating that errors in the prewhitening could be responsible.

The PS of week 10 is shown in fig. 37. The absence of any significant power at all near 118 s is understandable when the following is noted : (i) the week 10 data mainly consisted of short runs beginning at the same time each night ; (ii) the two components found above will beat with a 1 day period so that the observations sample the same part of the beat cycle each night. If the components, which are of similar size, were out of phase with each other during week 10 at that time of night, no 118 s oscillation would be detected. This is the most likely explanation why the data of Hesser et al. (1977) also did not contain a 118 s oscillation.

Finally, the PS of week 3 is shown in fig. 38 and does not show the same pattern or size of peaks seen in the other PS. However, prewhitening the data with the main peak seen in the other PS (the parameters were obtained, as usual, from the PS of the complete data set), results in the PS in fig. 39 which shows the secondary component in the 'right' place and of the right size. Although the data are thus consistent with the other weeks, it is not obvious as to how the 'peculiar' first power spectrum could arise.

As before, the PS of the 'short' weeks were noisier and also suffered more acute aliasing. However, they were all interpretable in a consistent fashion with the above PS. In addition, searches for periodicity in the entire interval between the 113 and 118 s periods, and also at periods slightly greater than 118 s, failed for the weeks with relatively more data.

In summary, it appears that the 118 s oscillation consists of two roughly equal amplitude components at 118.52 and 118.68 s. Although this conclusion is not completely established, more supporting evidence will be obtained from the PS of the complete data set.

7.6. Calculating Power Spectra Of Large Data Sets

The advantages to be gained from calculating power spectra of the whole data set are (a) better determination of frequencies due to the resolution increasing proportionately to the time spanned by the observations and (b) lower noise enabling the confirmation of the low amplitude components in the three oscillation modes discussed so far. Such calculations also facilitate the analysis of the 350 s oscillation for which it will soon become apparent that even power spectra of individual weeks are inadequate in determining the frequency structure. Moreover, it was also decided to survey the interval 1.0 to 10.0 mHz (100-1000s) in order to check if there are any other oscillations in this interval (where almost all of the observed ZZ Ceti frequencies lie) whose low amplitude has prevented their detection in shorter lengths of data. This survey turned up one further oscillation mode near 143 s which later proved to be significant in the interpretation of the oscillations in terms of non-radial g-mode pulsations.

Needless to say, calculation of power spectra of over 100 000 data points at a high resolution (so as not to 'miss' any possible components) and spanning 1.0 to 10.0 mHz is likely to be a very expensive procedure. In fact, rough calculations show that about 1250 hours of Univac 1108 computer time are needed for the Deeming technique that we have used so far ! In order to solve this problem, we invented the following procedure which is specifically tailored to the case where a large quantity of data are distributed in widely spaced blocks.

Consider the definition of the discrete Fourier transform of N points which may be written as separate real and imaginary parts :

$$F_N(\nu) = \sum_{k=1}^{N} f(t_k)\cos 2\pi\nu t_k + i \sum_{k=1}^{N} f(t_k)\sin 2\pi\nu t_k \qquad 7.6.1$$

In the case of power spectra of the individual weeks, the times t_k may be taken as the time from each point to the beginning of the first run of the week. However, for power spectra of the entire data set, these times must all be placed on the same scale. This can be done by adding on to each of the original times t_k, the time T_j between the start of the first run of the j^{th} week and some arbitrary epoch within the time spanned by the data set taken as Heliocentric Julian Date 2,444,000.0 . The discrete Fourier transform is now

$$F_N(\nu) = \sum_{k=1}^{N} f(t_k)\cos 2\pi\nu(t_k+T_j) + i \sum_{k=1}^{N} f(t_k)\sin 2\pi\nu(t_k+T_j) \qquad 7.6.2$$

where T_j is appropriate to the k^{th} point. This function is slowly varying in frequency space provided that

$$d\nu << \frac{2\pi}{t_k+T_j} \qquad 7.6.3$$

while the analogous condition for equation 7.6.1 is

$$d\nu << \frac{2\pi}{t_k} \qquad 7.6.3$$

thus showing that 7.6.2 is a much higher resolution transform than 7.6.1 as expected. By writing

$$C_j = \sum_k f(t_k)\cos 2\pi\nu t$$

$$S_j = \sum_k f(t_k)\sin 2\pi\nu t$$

where the summation index k is allowed to range over only those points appropriate to week j, 7.6.2 may be rewritten

$$F_N(\nu) = \sum_j (C_j\cos 2\pi\nu T_j - S_j\sin 2\pi\nu T_j) + i(S_j\cos 2\pi\nu T_j + C_j\sin 2\pi\nu T_j) \qquad 7.6.4$$

which is just an application of the Fourier shift theorem in the discrete case. Thus the Fourier transform of the complete data set may be expressed as the sum of linear combinations of the real and imaginary parts of the Fourier transforms of the individual weeks with appropriate phase factors : $\cos 2\pi\nu T_j$, $\sin 2\pi\nu T_j$. The key to the saving of computer time lies in this expression considered along with 7.6.3. The latter equations show that C_j and S_j are much more slowly varying functions than $F_N(\nu)$ in 7.6.4. In fact, since the time spanned by the data set is 564 days, nearly 100 times as great as the average of 6 days spanned by an individual week of observing, the resolution of the entire data set is 100 times as large as that of an individual week. Thus C_j and S_j vary in frequency space much more slowly than $F_N(\nu)$ in 7.6.4. Thus, provided that these quantities are calculated with at least the frequency resolution of one week's data , they may be interpolated with negligible error to provide a grid of frequencies at the much greater resolution of the whole data set. The interpolation and multiplication by the phase factors is much less expensive in computer time than calculating the greater number of frequencies directly ; in fact, this amount of time was found to be almost negligible by comparison. Thus, a factor of nearly 100 was saved in the computer time for the power spectra of the whole data set. This technique is equally applicable to the calculation of the PSW.

In order to check these ideas, a small quantity of data with appropriate time spacing was generated artificially. Power spectra were calculated for the data by the direct method and the method described above - excellent agreement was achieved. In the next few sections, we turn to applications of this technique.

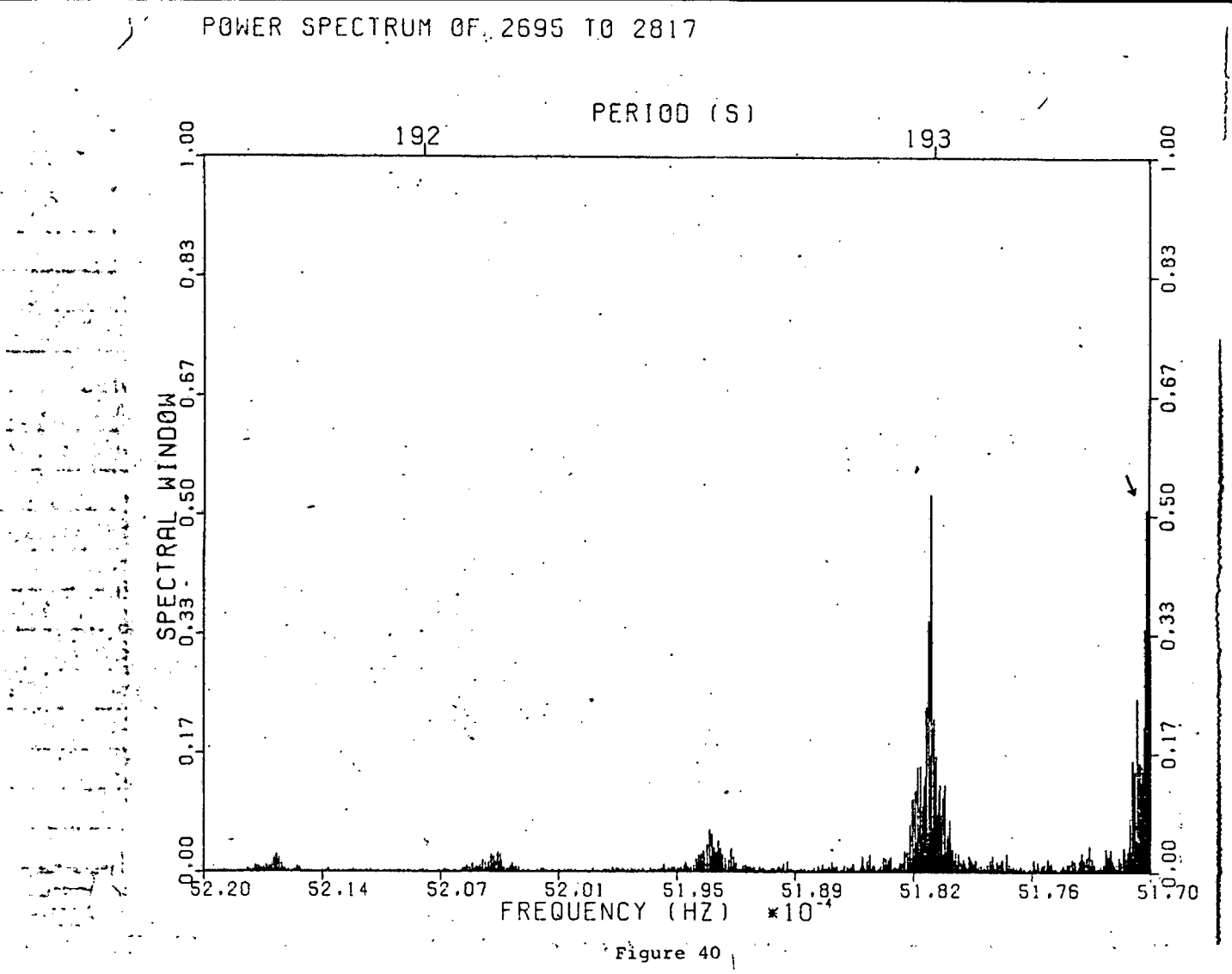

Figure 40

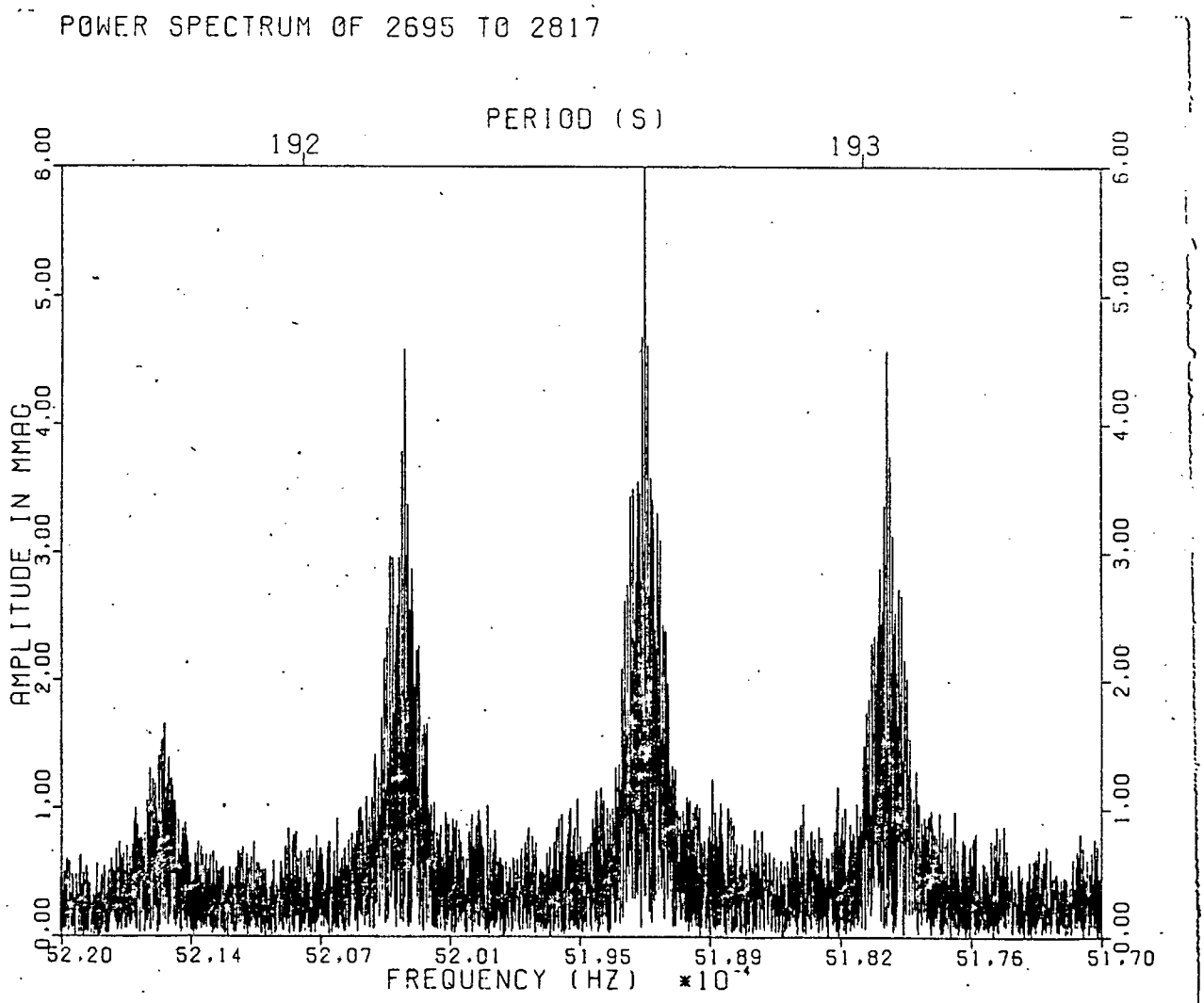

Figure 41

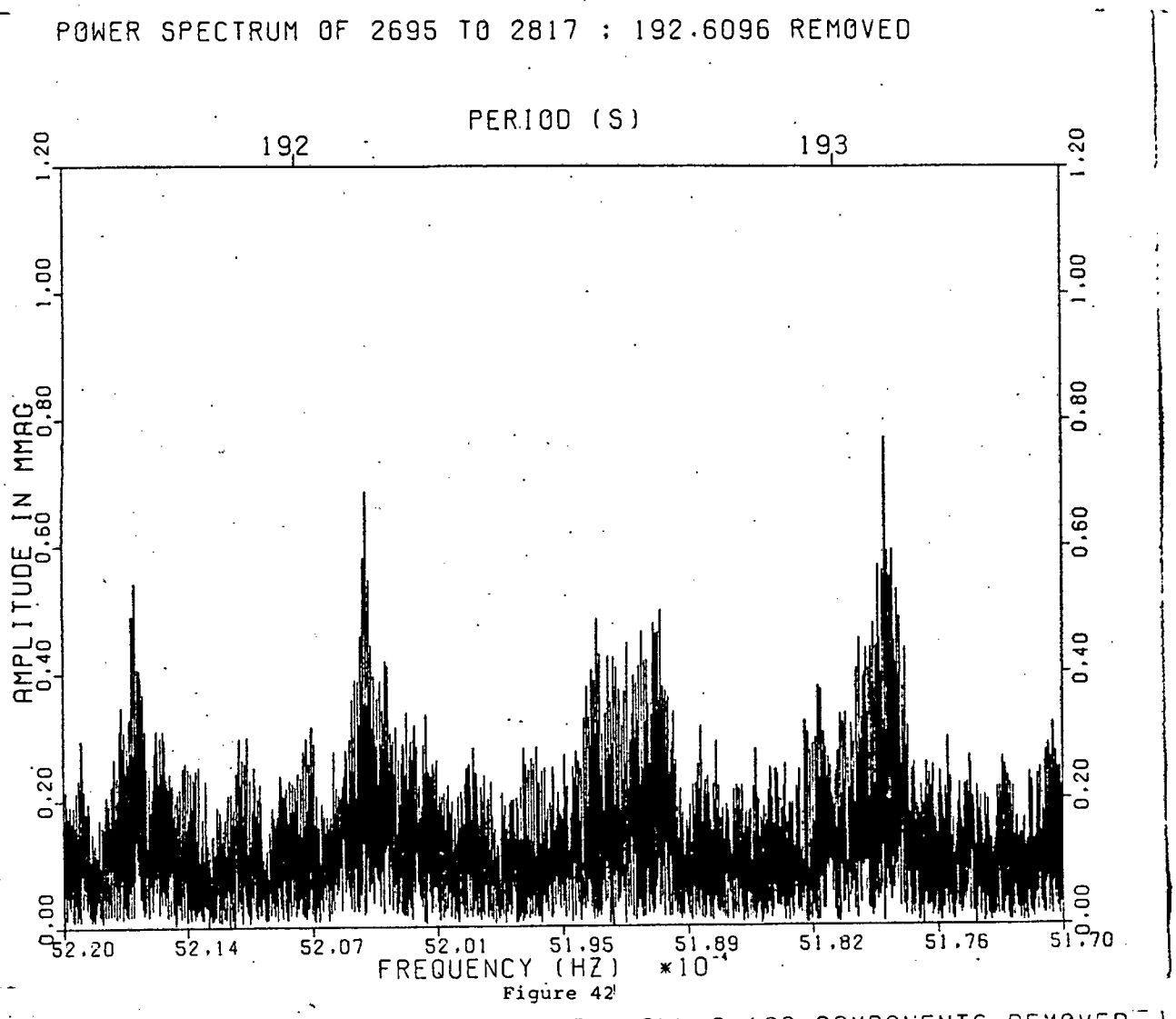

Figure 42

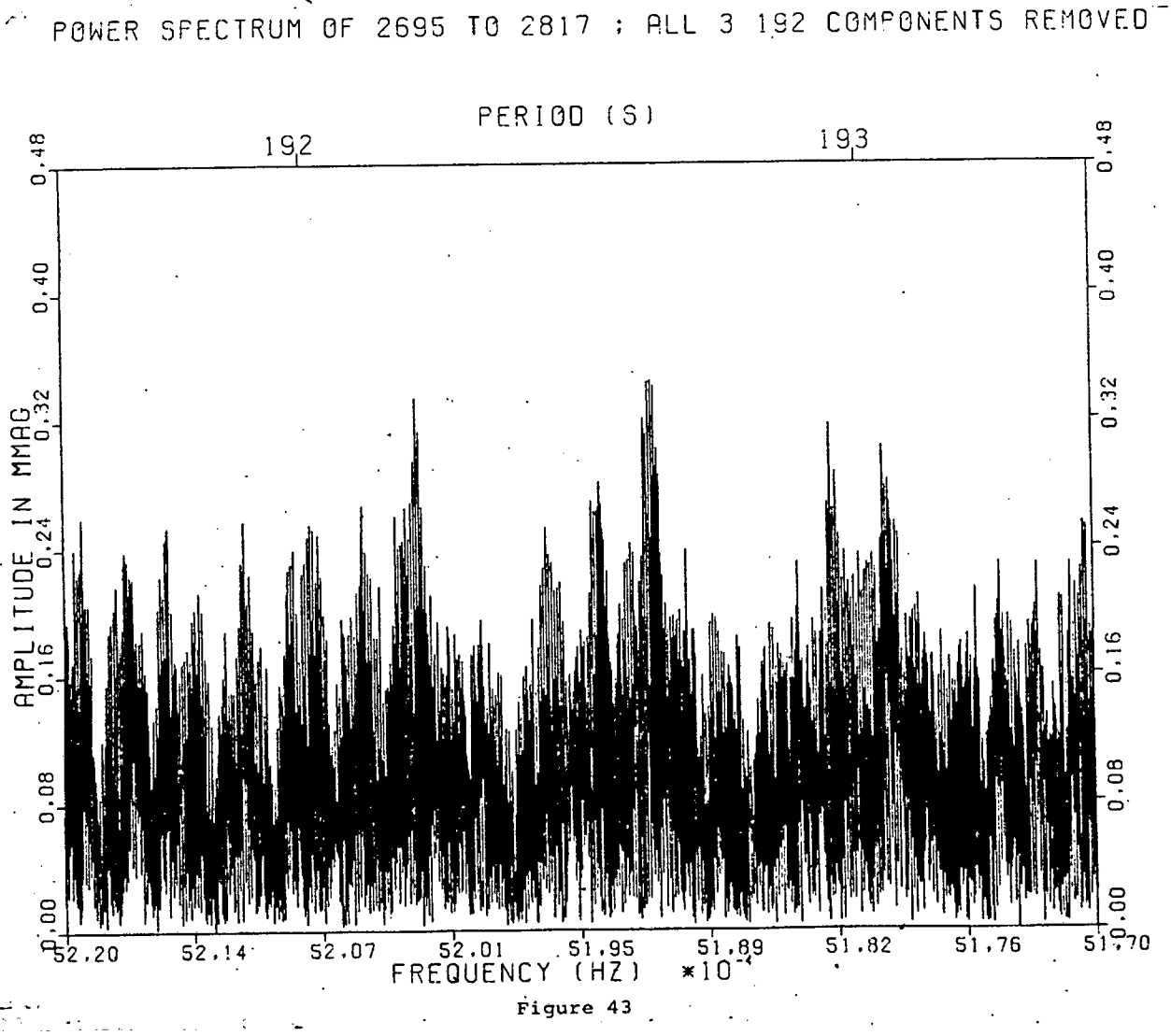

Figure 43

7.7. Power Spectra Of The Complete Data Set

7.7.1. The 192 s Oscillation

The complete data set included runs 2695 to 2817. Power spectra of week 1, runs 2693, 2695 and 2697, showed no single peak at 192.6 s but two peaks of equal height equally spaced in frequency about 192.6 s. Investigations on artificial test data showed that this situation could easily arise if there was a timing error among the three runs. Power spectra of the two runs 2695 and 2697 showed (correctly) a peak at 192.6 s indicating that the starting time of 2693 was in error. Thus, this run was excluded from consideration in the complete data set.

The PSW of these data is shown in fig. 40. It should be noted that the first aliasing peak (arrowed) is much lower than that of the zero frequency peak, thus predicting that there should be no aliasing problems in connection with picking the largest amplitude frequency component in any of the oscillations seen in the star. This is confirmed by the PS shown in fig. 41 for the 192 s interval considered before. Because their amplitudes were less than 1.0 mmag each, the presence of the two side components is hidden even in this figure by the two 1 day aliases of the main component. These components are clearly revealed when the data is prewhitened by the main component which yields the PS in fig. 42. Their peaks are also equally easy to pick and unhindered by aliasing. Finally, when all the three components are removed from the data set, the PS in fig. 43 is obtained. Except for some residual peaks near the positions of the three removed frequencies and their aliases, this figure is quite consistent with noise. The residual power is most probably due to the inaccurate removal of the components at these frequencies in the individual weeks. Each week will have some set of frequencies, amplitudes and phases which best fit the frequency components of that week. In general, because the data are noisy, this set will not precisely match the corresponding set obtained from PS for all the data. Thus, each week will have some small, residual power which contributes to the PS of the whole data set at the frequencies which were incompletely removed. This effect will also be seen in the PS of the 113 s and most acutely in the PS of the 118 s oscillation.

A most important point to make is that the peaks of the three frequency components in the PS are the same shape and width as the first peak in the PSW. This indicates that the variation in frequency of the oscillation over the observations is less than the half width of the first peak in the PSW. In this way, an upper limit on the rate of change with time of the period of each component may be placed. This Q value (dP/dt) appears in table 7-1 along with the best estimates of the amplitude, frequency, period and phase of each of the three components. The phases in the table represent the times of maximum of the pulsations relative to H.J.D. 2 444 000.0 . Since the resolution of the power spectrum of the complete data set was 2.0×10^{-9} Hz, a conservative estimate of the uncertainty in the frequency of each component was taken to be 1.0×10^{-9} Hz. Because of the low amplitude of many of these components making convergence difficult to achieve, considerable difficulty was consistently experienced

in trying to perform simultaneous least squares fits of all the frequency components in the data. In addition, a considerable amount of computer time would have been needed. Thus, no least squares fitting of the complete data set was done and no formal errors could be obtained for the amplitudes and phases. However, some idea of the uncertainty on the amplitudes is given by the size of the noise whose typical height was 0.1 mmag. The errors in the phases are more difficult to estimate but our later discussion on the linking of the present data with those of Mc Graw (1977) and Hesser et al. (1977), showed that a reasonable estimate would be ±10 s.

The conclusions reached earlier are confirmed here : the 192 s oscillation is comprised of three components - two low amplitude components equally spaced in frequency about a large amplitude component. This equal spacing is seen from table 7-1.

Table 7-1. Best Estimates For The Frequency Components In L 19-2

Period (s)	Frequency (mHz)	Amplitude (mmag) ±0.1	Phase 2444000.0+ (±10s)	Q (sec/sec) x 10^{-12}	$\Delta\nu$ (mHz)
192.6096 ±4	5.191849 ±10	6.00	-75s	8	
193.0928	5.178857	0.81	-73s	8	-0.012992
192.1288	5.204842	0.73	-45s	8	0.012993
113.7779 ±1	8.789053 ±10	2.21	45s	2	
113.26705	8.828693	0.52	-9s	2	0.039640
114.1861 ?	8.757633	0.27	52s	2	-0.031420
118.5191 ±1	8.437459 ±10	1.81	27s	2	
118.6758	8.426316	1.10	41s	2	-0.011141
118.9327 ?	8.408116	0.24	-54s	2	-0.029342
350.1484 ±12	2.855932 ±10	1.00	-72s	24	
348.7288	2.867558	0.43	-101s	24	0.011626
143.4191 ±2	6.972571 ±10	0.55	19s	4	
143.0389 ?	6.991105	0.26	8s	4	0.018534

Notes : (1) ? denotes that the existence of the component is not well established.
(2) $\Delta\nu$ is the difference in frequency between the component and the principal component in the oscillation.

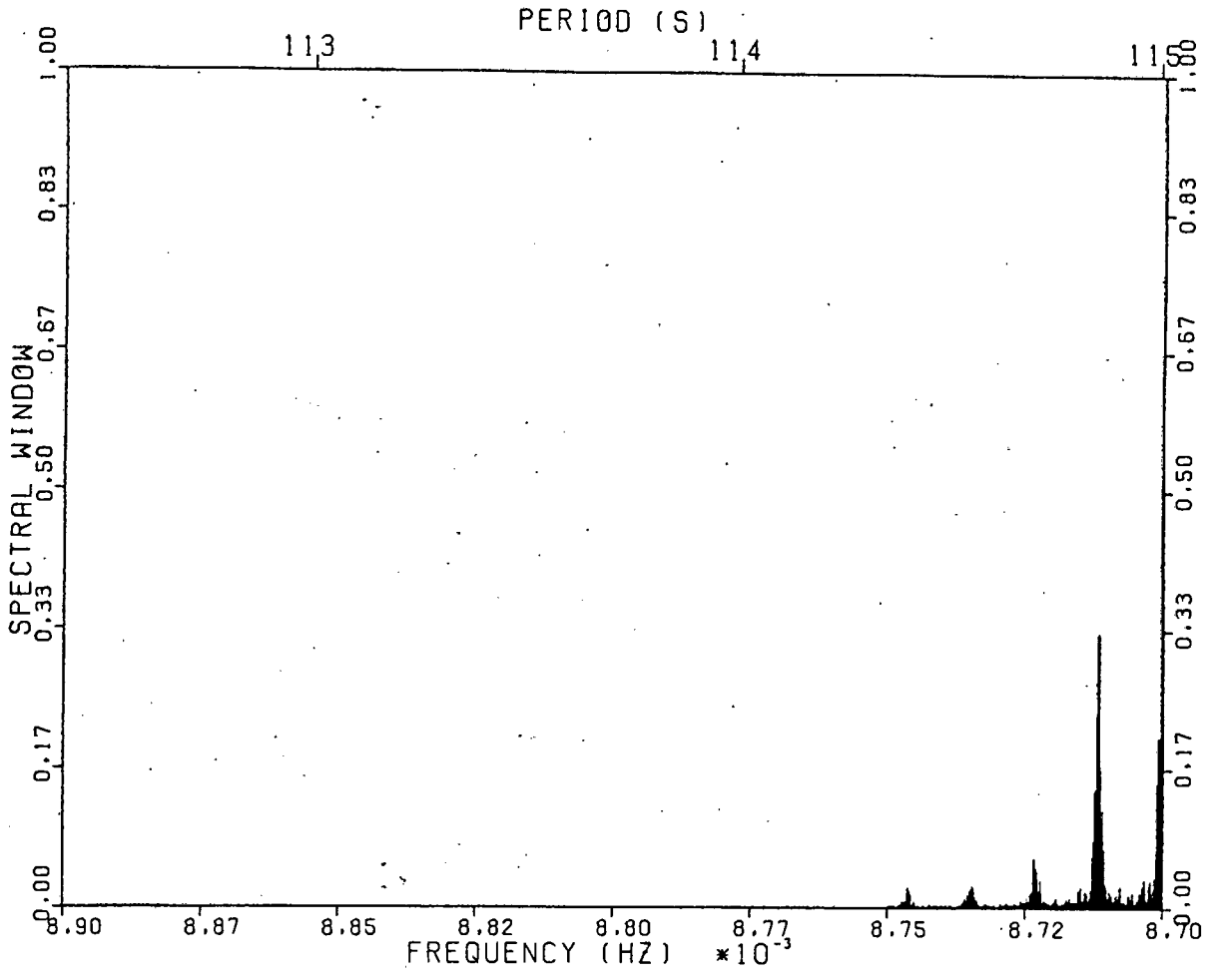

Figure 44

POWER SPECTRUM OF 2695 TO 2817

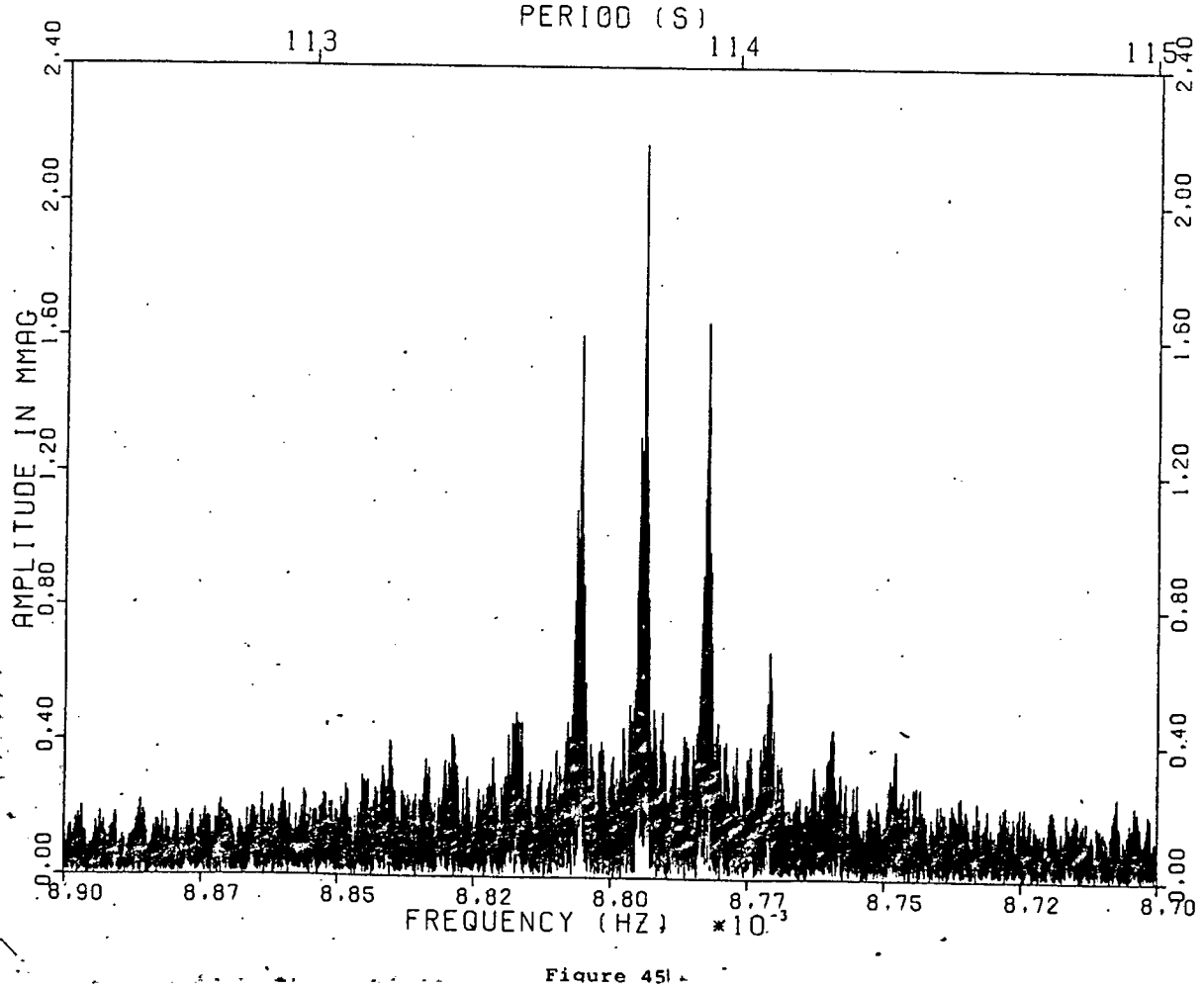

Figure 45

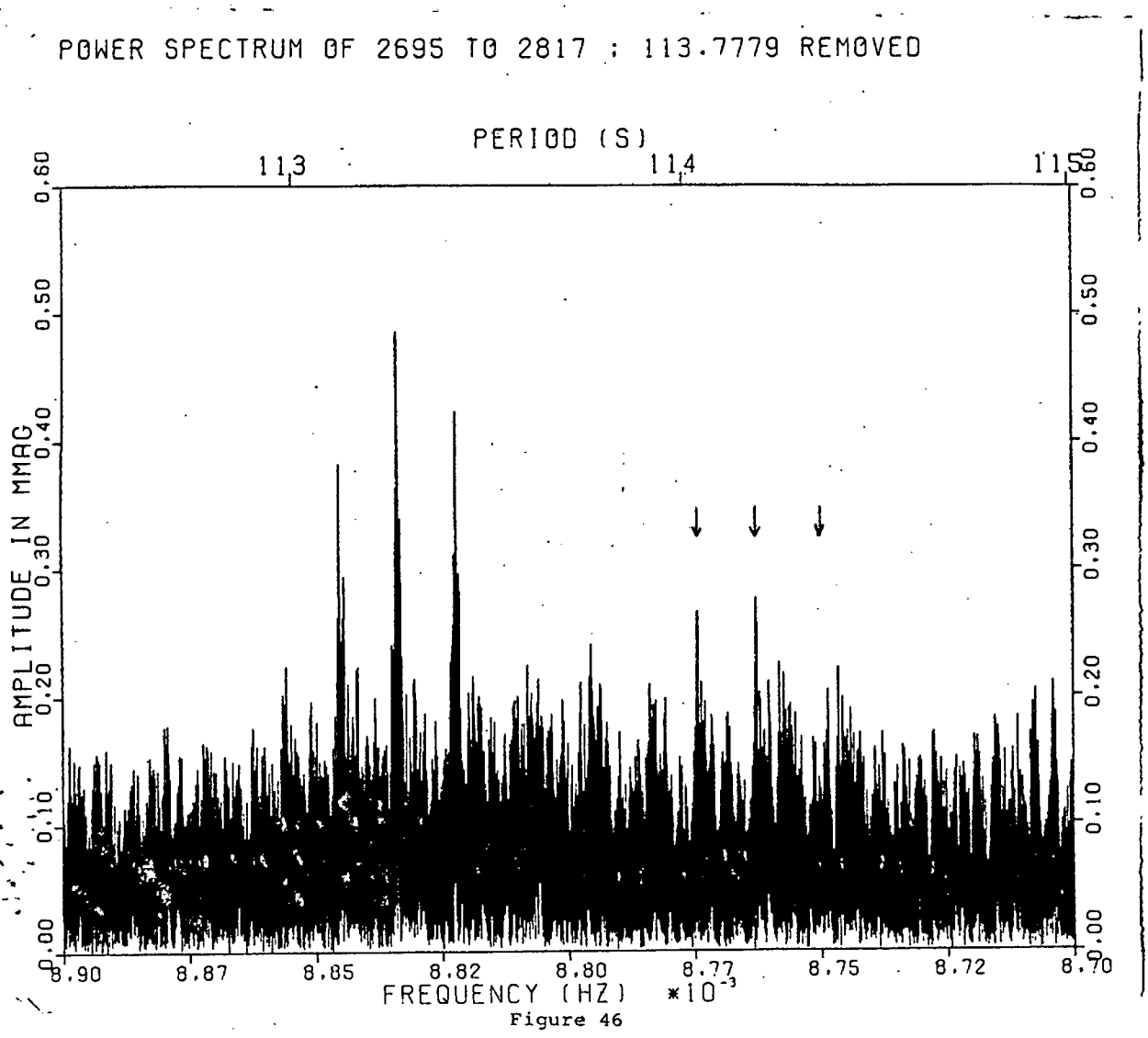

Figure 46

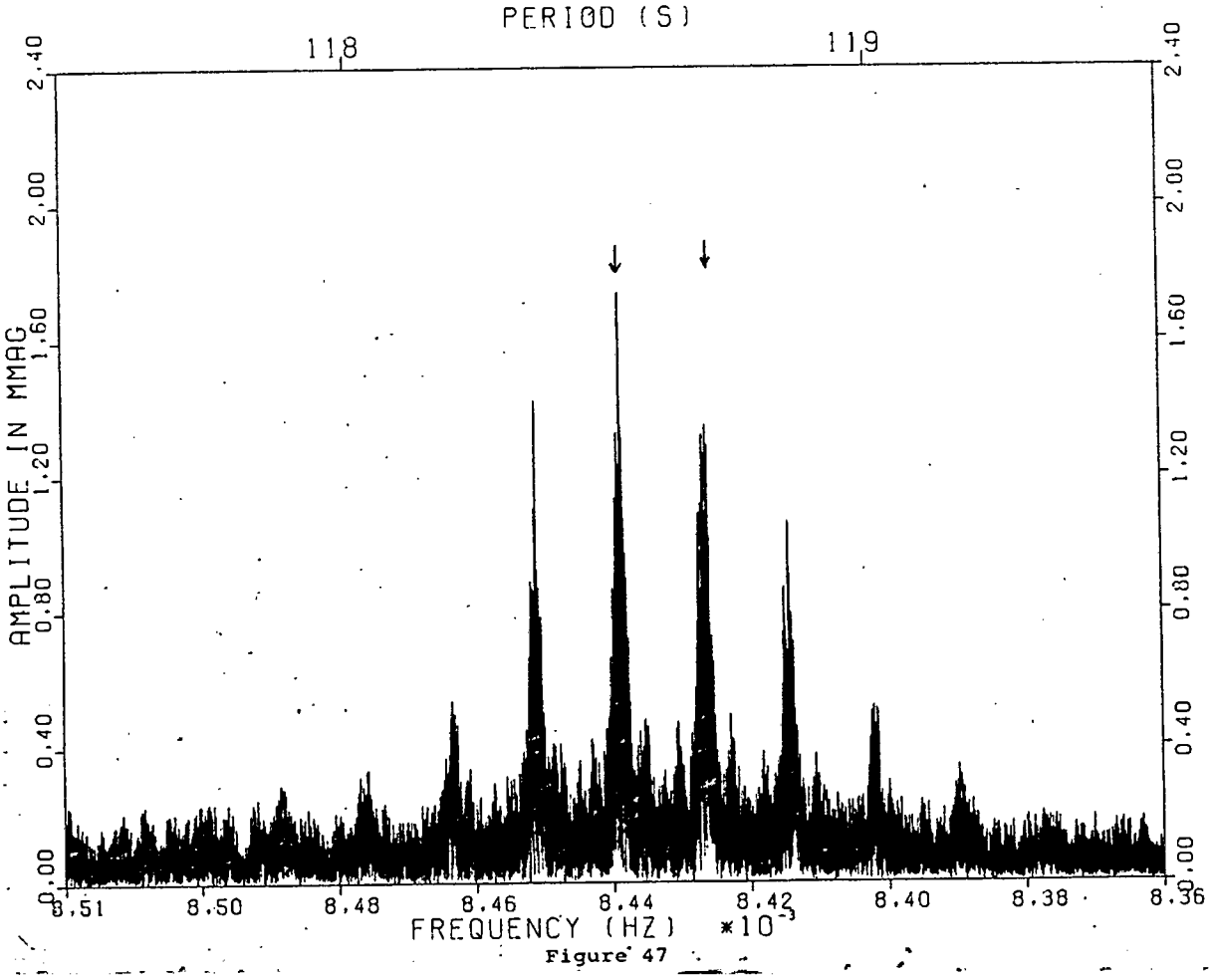

Figure 47

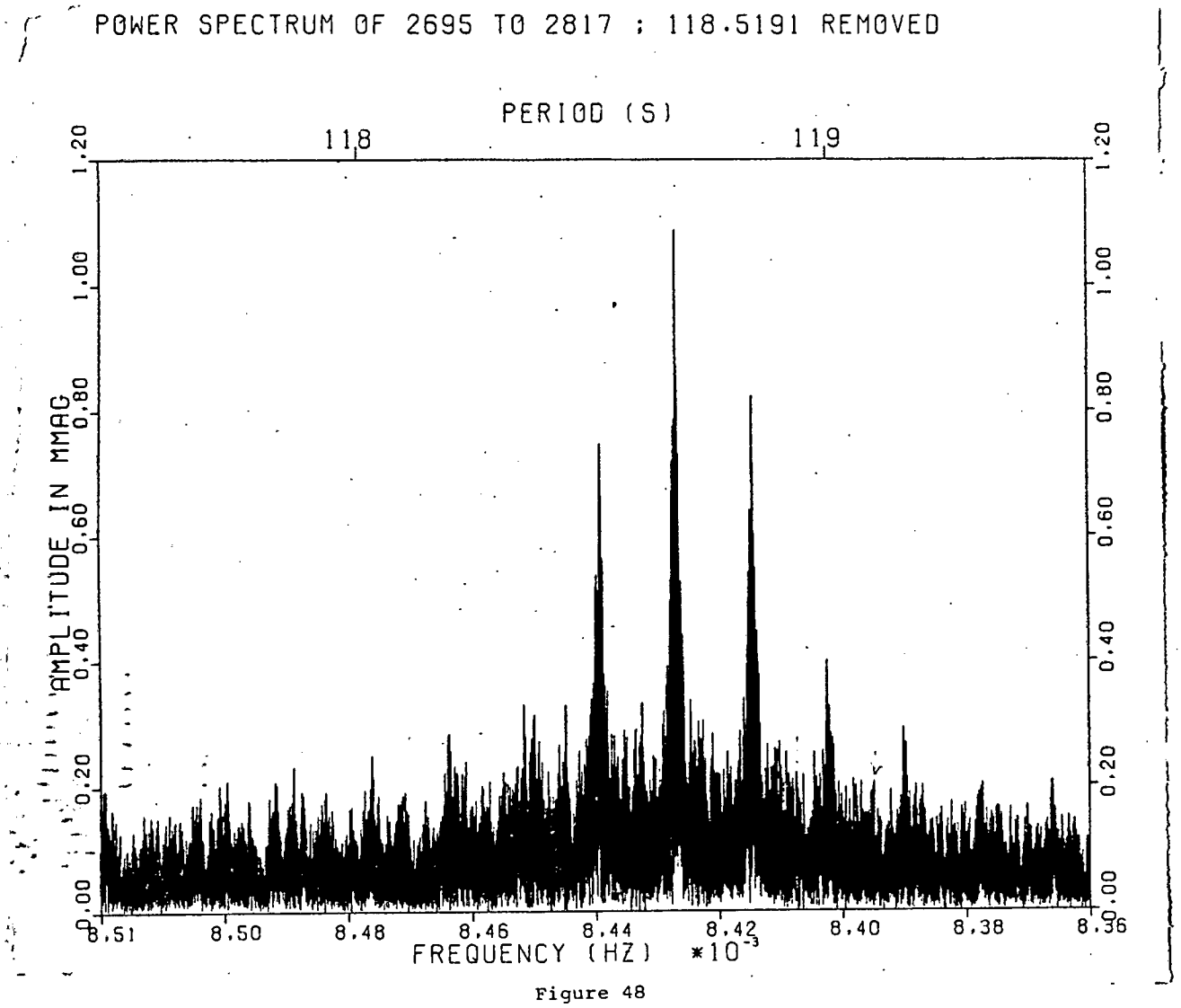

Figure 48

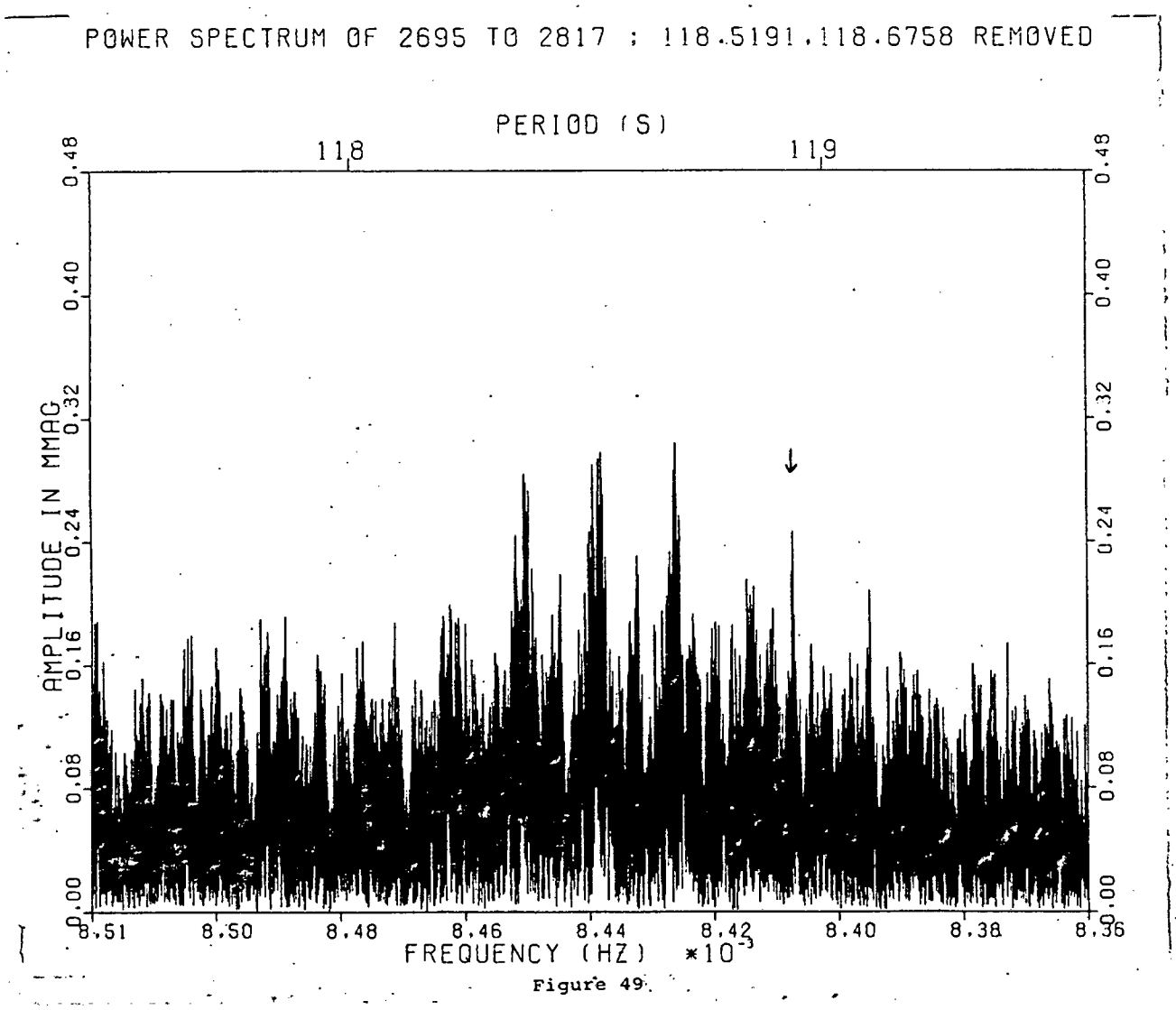

Figure 49

7.7.2. The 113 s Oscillation

The PSW is repeated in fig. 44, plotted at an appropriate scale. The PS in fig. 45 shows the previously detected large amplitude principal component near 113.78 s. Its removal from the data brings out the secondary component near 113.26 s shown in fig. 46. Except for slight residual features near the position of the principal component (presumably due to the same errors in prewhitening individual weeks as discussed in the previous section), and two peaks (arrowed), the removal of these two frequencies from the data results in a PS which is consistent with noise. The arrowed peaks were pointed out as consistently appearing in the PS of the individual weeks. The third arrow (to the right of the other two), indicates the position where the 1 day alias of the right hand peak (the middle arrow) should occur. Its separation from the principal component (113.78 s) is nearly equal to that separating the latter and the frequency at 113.26 s. However, the equality in the splitting is not nearly as precise as that seen in the 192 s oscillation. Of course, the reality of a frequency near 114.2 s is questionable and it must remain as only a 'possible' in table 7-1.

7.7.3. The 118 s Oscillation

The PS for the 118 s oscillation appears in fig. 47. This diagram is important in providing support for the contention that the two real components in the star are separated by the 1 day alias as arrowed in the figure. The significant clue is that the right hand arrowed feature does <u>not</u> have a single peak rising above all the very close aliases and it is not as high relative to the peak at 118.5 s as in most of the previous PS considered. This suggests that the resolution of the PS here is sufficient to resolve the 1 day alias of the peak at 118.5 s and the suspected real peak of similar strength at 118.67 s so that no constructive interference takes place. In addition, the next alias near 118.8 s does show a single spike adding further weight to the argument. It is difficult to see how this aliasing pattern could arise with any other frequency separation of the real components. By prewhitening the data with the peak at 118.5 s, the PS in fig. 48 is produced. Note that the remaining frequency is consistent with the above argument and does show a single spike rising above the very near aliases. By removing this frequency from the data, the PS in fig. 49 is obtained and here the remaining features near the positions of the main component and its aliases are more pronounced than in either the 192 or 113 s oscillation. This is to be expected since the aliasing problems encountered in this oscillation were worse than in the previous two, leading to greater inaccuracies in the prewhitening.

There is a possibility that there may be a remaining component just under 119 s (arrowed in the figure) but this is only marginally above the noise and does not consistently appear in the PS of the individual weeks.

It is perhaps appropriate to comment on the detectability of the 113 and 118 s oscillations. The noise in the PS of the complete data set is 0.1 to 0.2 mmag. Since this set consists of approximately 100 000 points, the noise on a 1000 point PS would

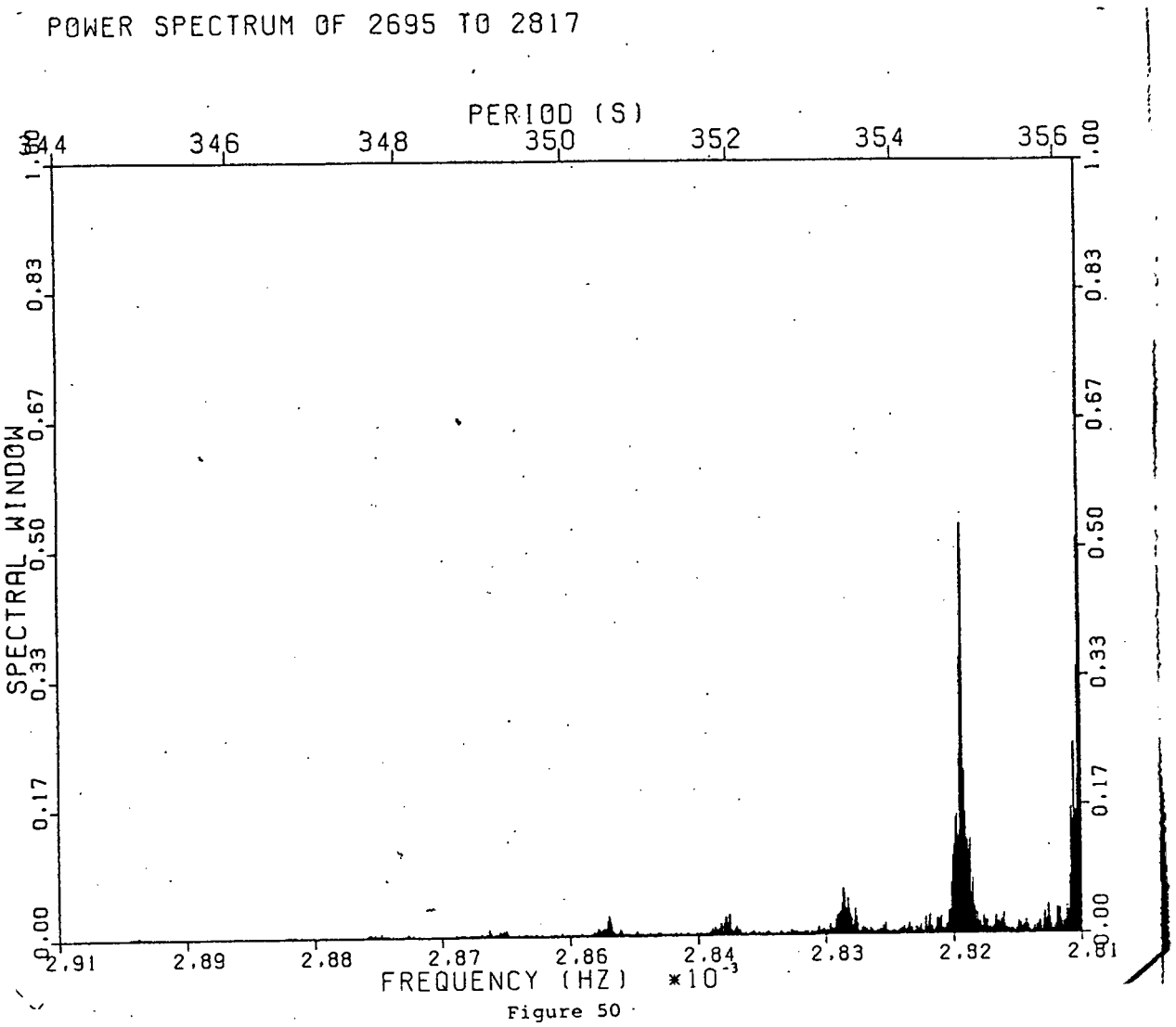

Figure 50

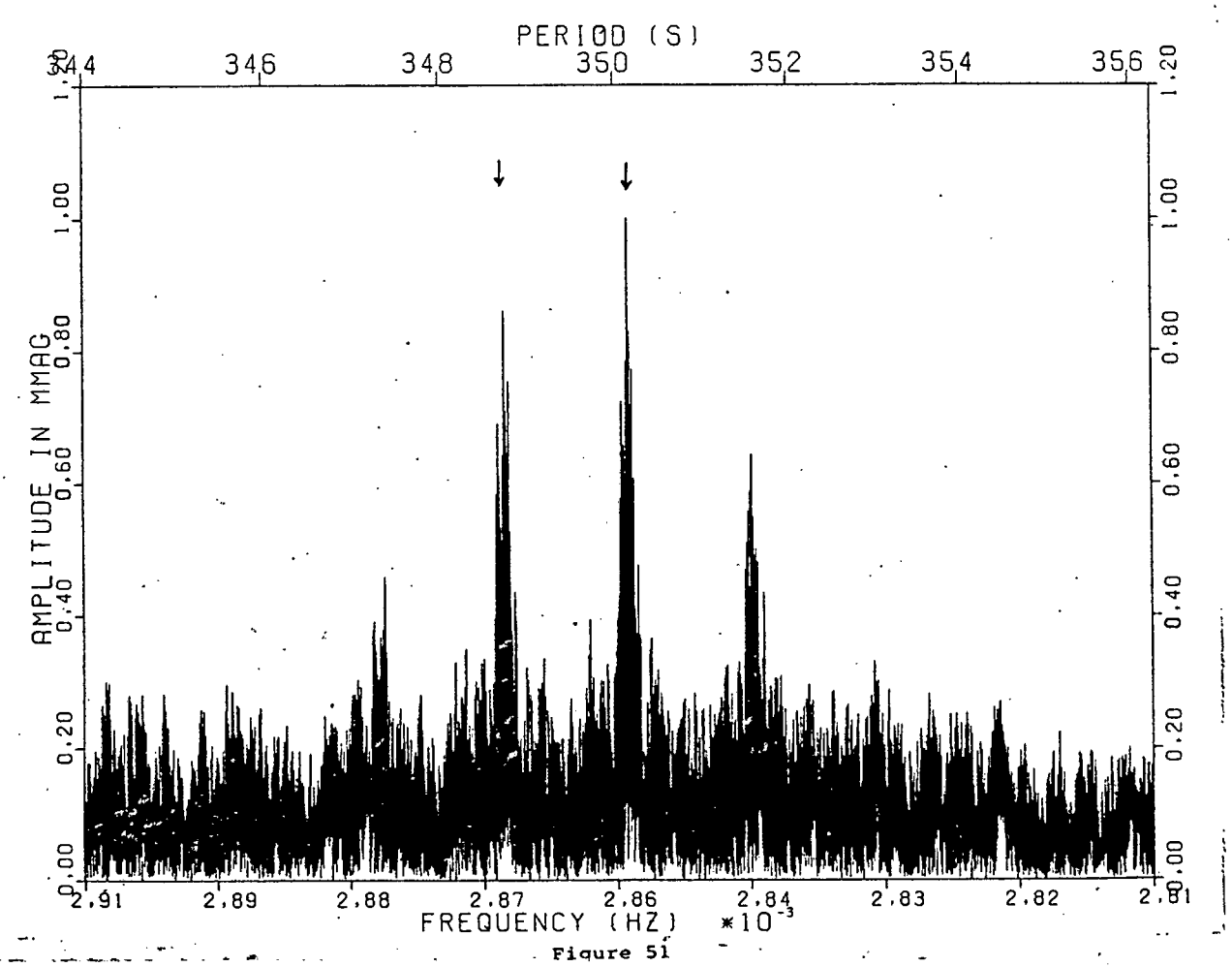

Figure 51

POWER SPECTRUM OF 2704 TO 2717

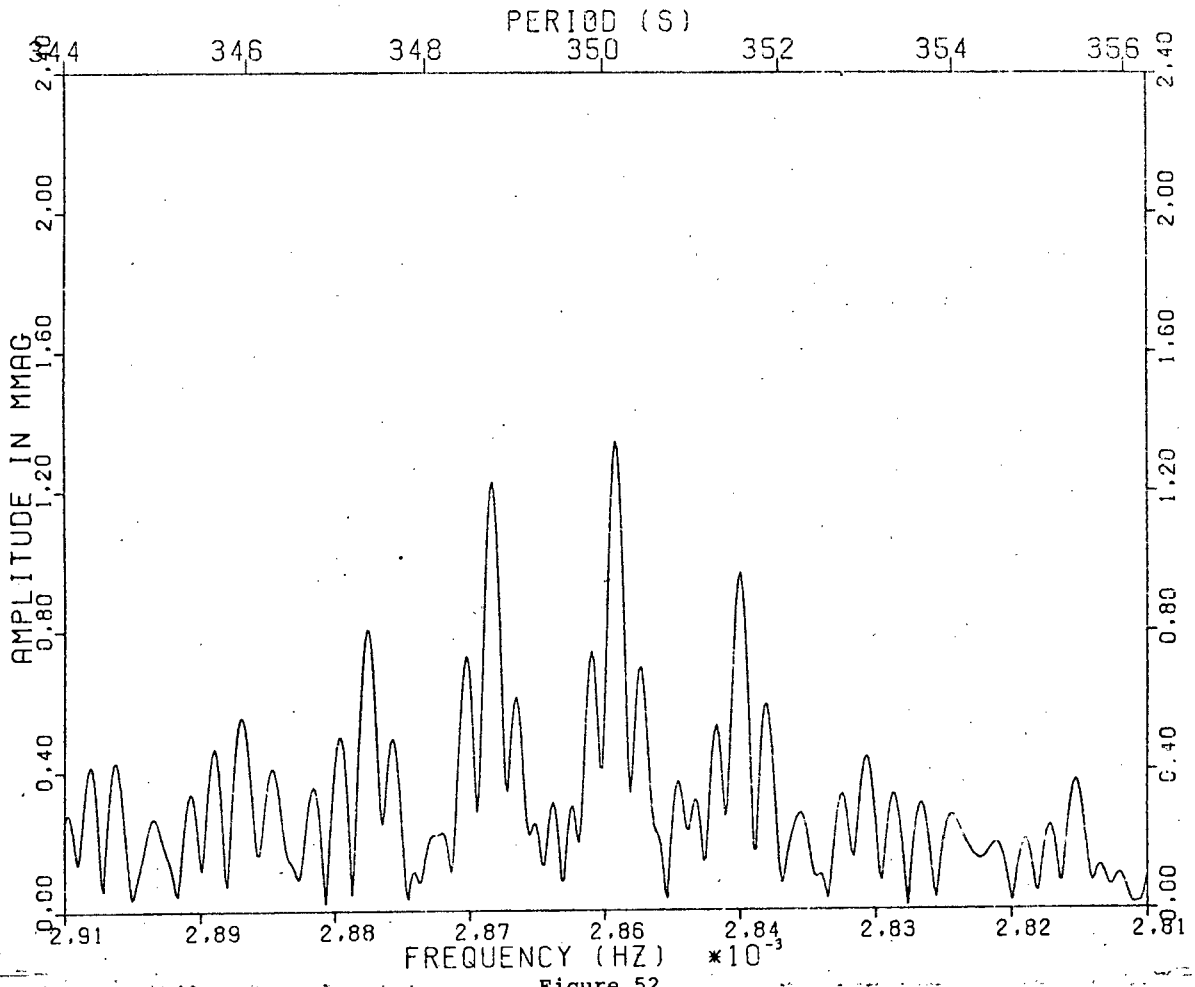

Figure 52

POWER SPECTRUM OF 2794 TO 2806

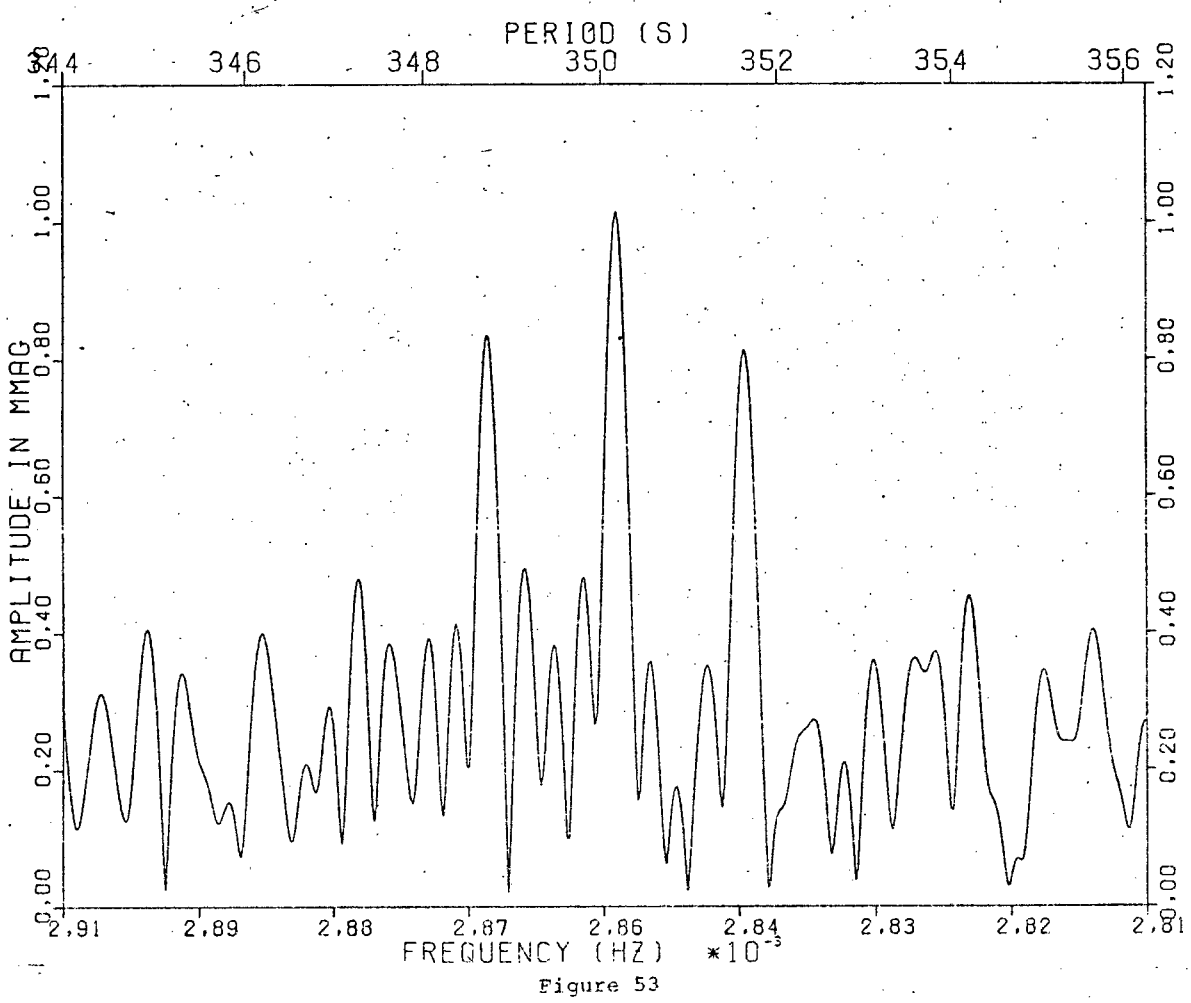

Figure 53

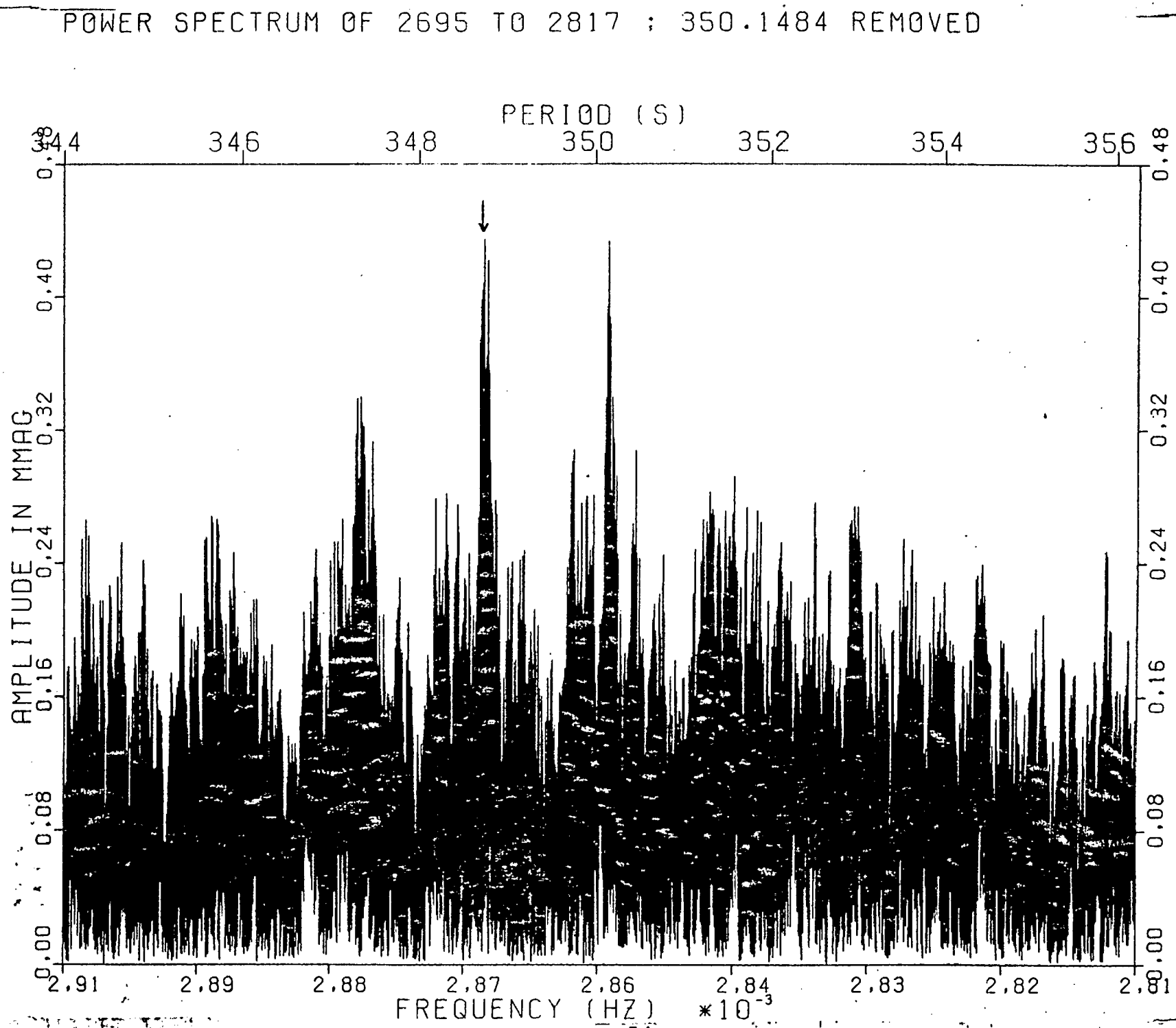
POWER SPECTRUM OF 2695 TO 2817 ; 350.1484 REMOVED
PERIOD (S)
344
346
348
350
352
354
356
AMPLITUDE IN MMAG
0,00
0,08
0,16
0,24
0,32
0,40
0,48
2,91
2,89
2,88
2,87
2,86
2,84
2,83
2,82
2,81
FREQUENCY (HZ) *10-3

Figure 54

POWER SPECTRUM OF 2704 TO 2717 ; 350.1484 REMOVED

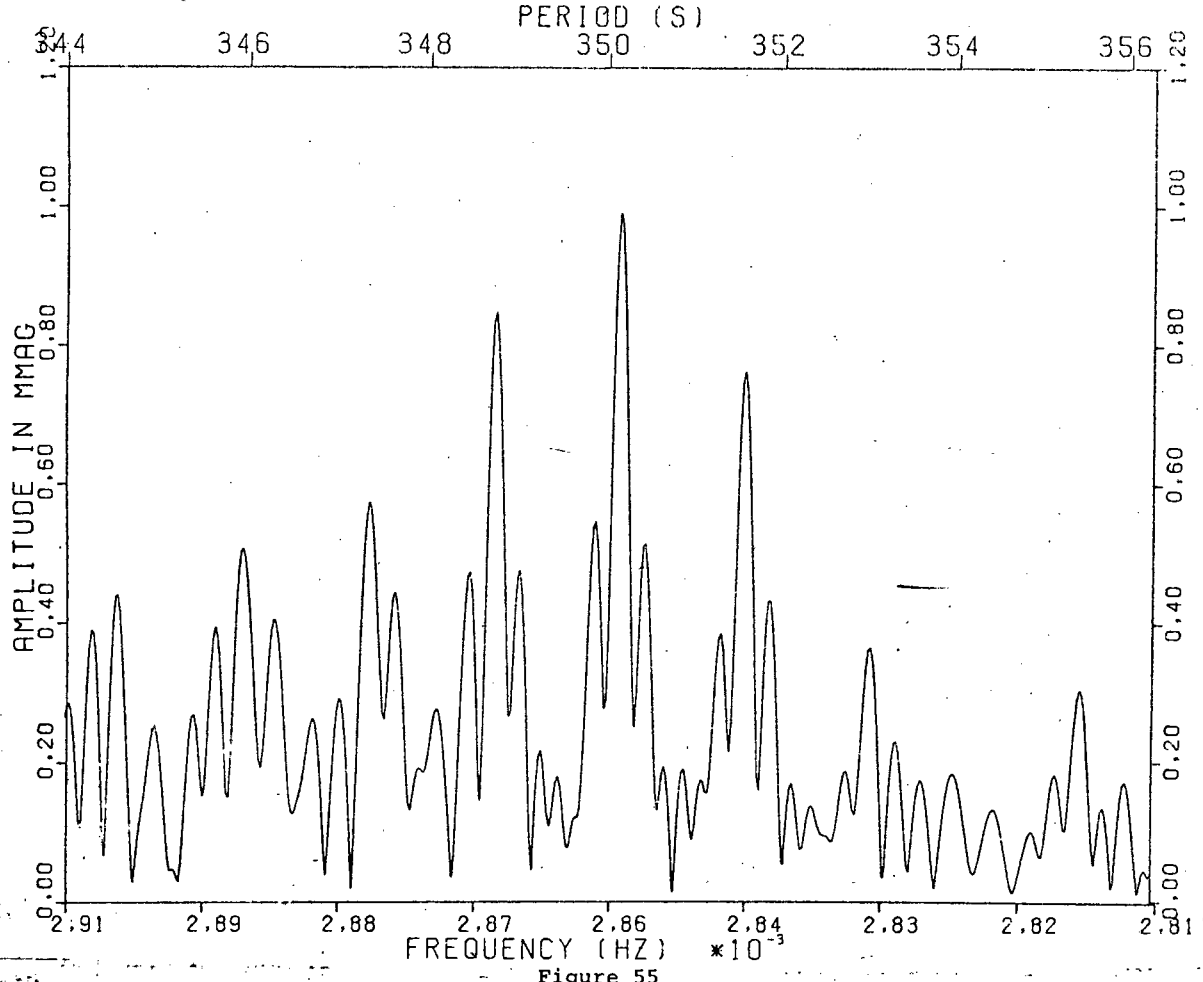

Figure 55

POWER SPECTRUM OF 2794 TO 2806 ; 350.1484 REMOVED

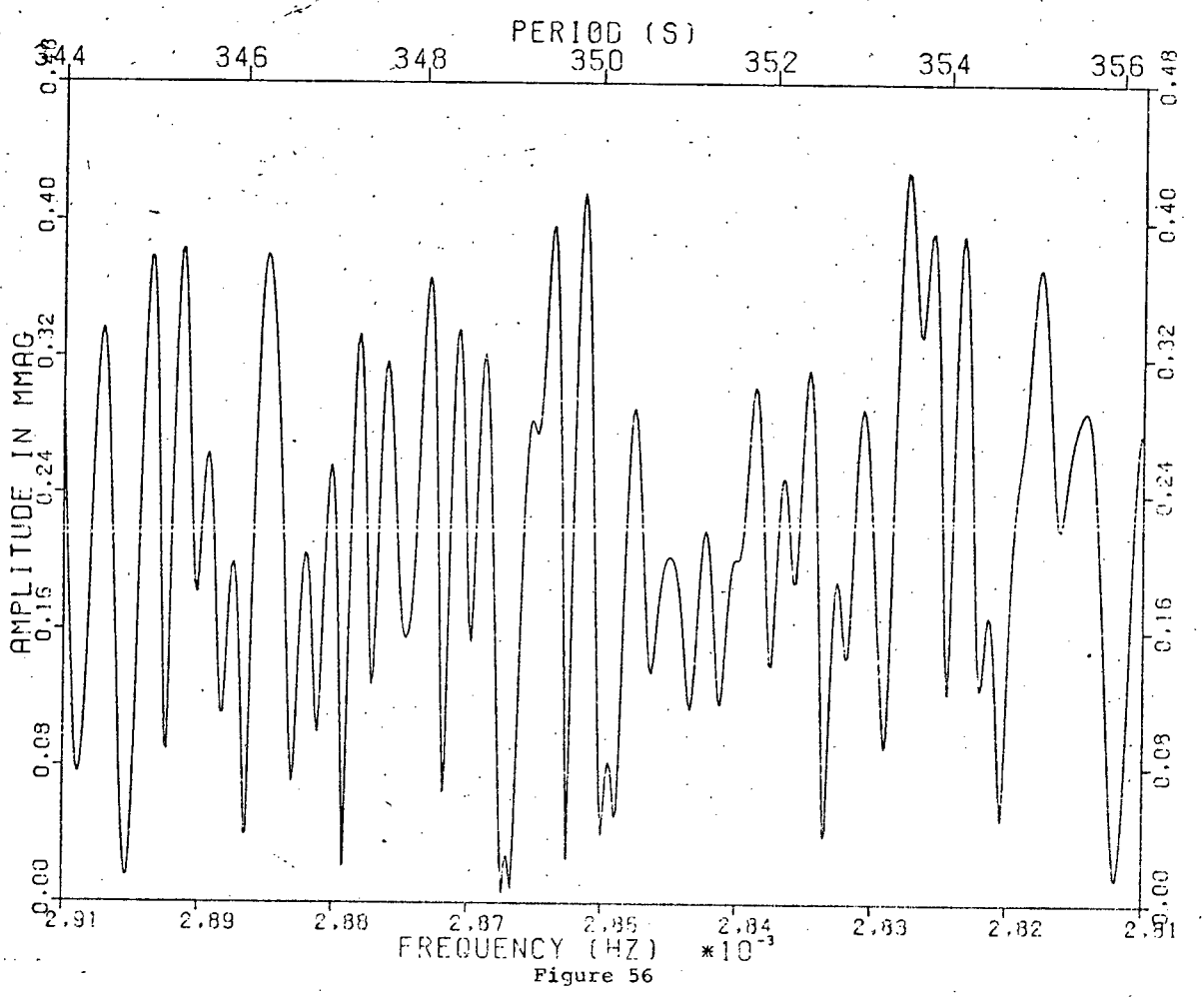

Figure 56

be 1 to 2 mmag. As the individual components of the 113 and 118 s oscillations are of similar strength (to the noise), it is very difficult to detect real variation in the strengths of these oscillations from a 1000 point data set. Thus, even though the 113 and 118 s oscillations gave the impression at the telescope that they varied rapidly within a run and sometimes disappeared altogether, these impressions are not reliable. Moreover, because the amplitude estimates from short sections of data will be swamped by noise, it can be seen quantitatively that application of the analysis technique of section 7.1 to these oscillation modes (and the weaker ones to be discussed presently) is inappropriate.

As before, the best estimates for the parameters of the components appear in table 7-1. We conclude that the evidence is strongest for the interpretation given here and note that the uncertainty introduced by the aliasing can only be removed by the scheduling of simultaneous observing weeks at different observatories widely separated in longitude.

7.8. Analysis Of The 350 s Oscillation

It will be seen presently that the 350 s oscillation suffers from the same aliasing problem seen in the 118 s oscillation. Also, the strength of this oscillation is even lower than that of any discussed previously so that the PS of individual weeks were of very little use in determining the frequency structure of this oscillation. Consequently, the PS for the complete data set will be presented immediately and the other PS (of the individual weeks) will be cited in some cases to show consistency or otherwise with the former.

The PSW and PS of the unprewhitened complete data set are shown in figs. 50 and 51. The aliasing problem is immediately apparent from the asymmetric pattern of peaks in the latter figure. It also obvious from this figure that the two real frequency components are as arrowed. This asymmetric pattern is seen in some of the individual weeks' PS such as week 3 in fig. 52, while in others, there is no suggestion of more than one component present, e.g. fig. 53 for the week 12 data. The PS shown in fig. 54 is obtained by prewhitening the complete data set by the peak at 350.15 s in fig. 51. The single spike near 350.15 s in fig. 54 is not precisely co-incident with the removed peak and is not due to inadequate prewhitening. The feature near 348.7 s is quite complex but attention is drawn to the arrowed spike in this feature. This spike is separated from the highest spike near 350.15 s by precisely the 1 day aliasing frequency interval in the PSW. Thus, this is the most likely candidate for identification with the second real component and prewhitening of the complete data set by this peak does indeed result in a noise spectrum. Because the much lower resolution of the individual weeks will result in more severe prewhitening errors, prewhitening of the individual weeks by the first component results in PS that are only marginally consistent with this interpretation. Examples of PS for the same individual weeks as above (3 and 12 respectively) prewhitened once are shown in figs. 55 and 56. In the second case, all the power was removed. In the first, the impression is given that the prewhitening was badly done.

It is obvious that the interpretation presented here is fraught

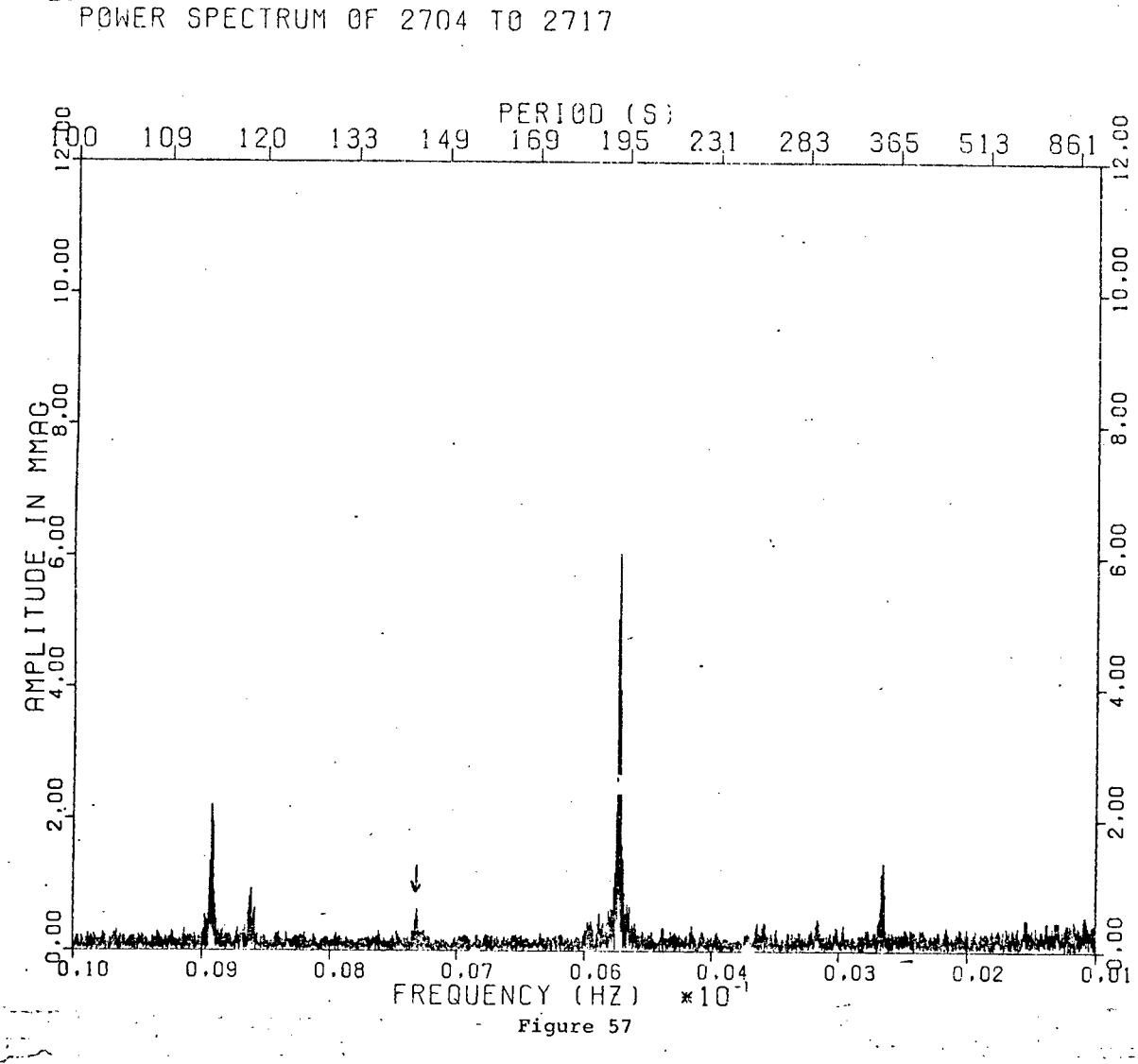

Figure 57

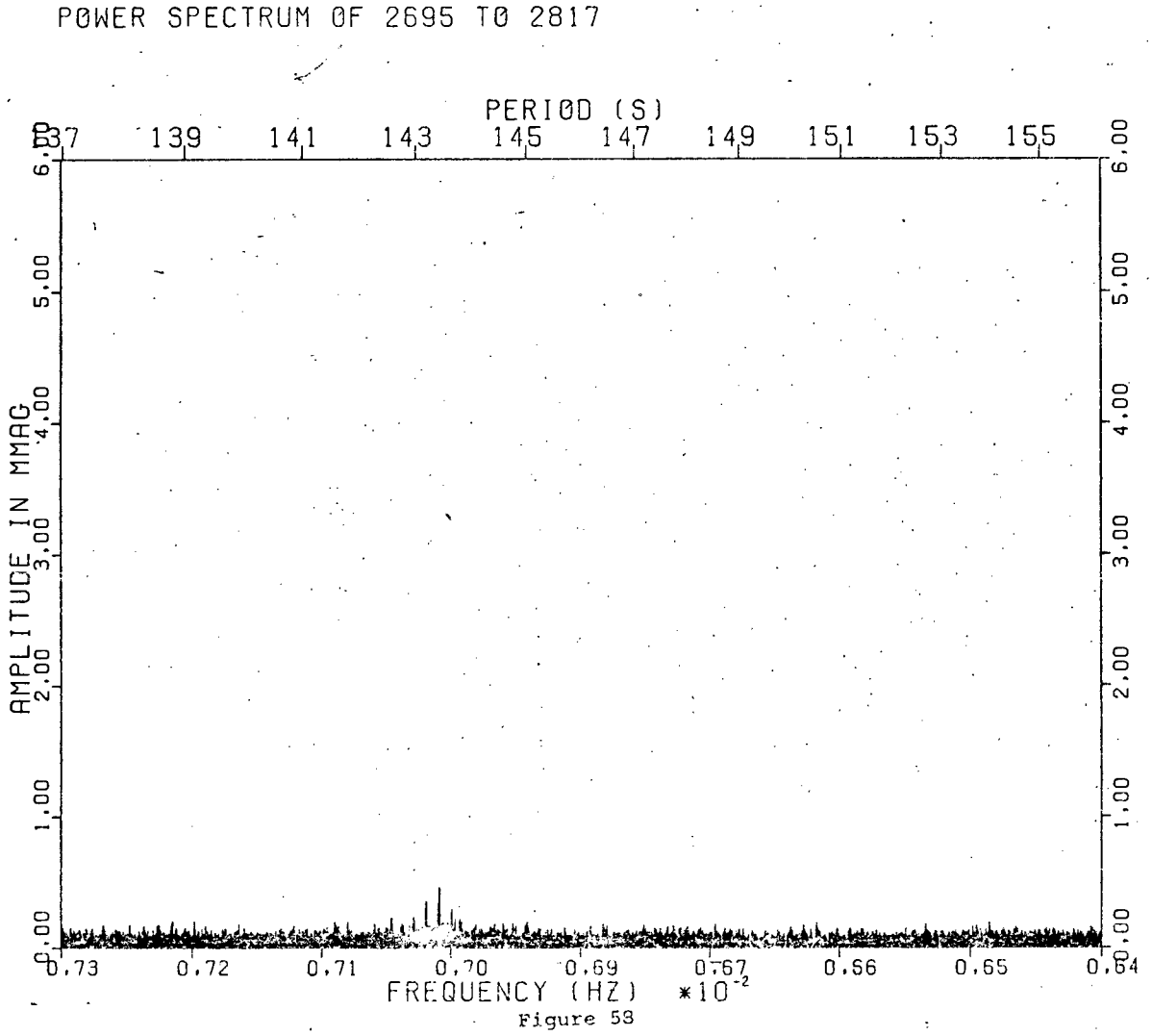

Figure 58

POWER SPECTRUM OF 2695 TO 2817

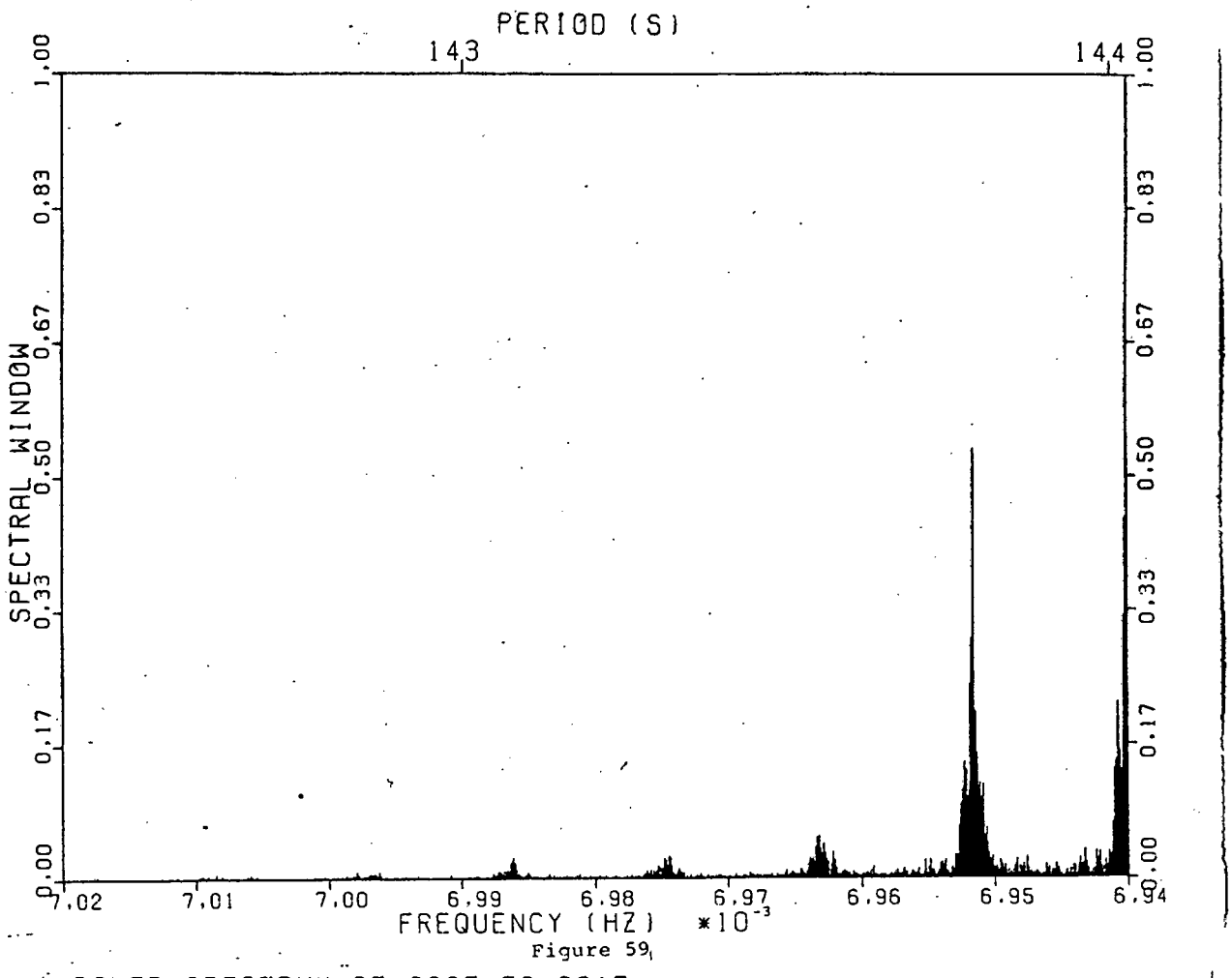

Figure 59

POWER SPECTRUM OF 2695 TO 2817

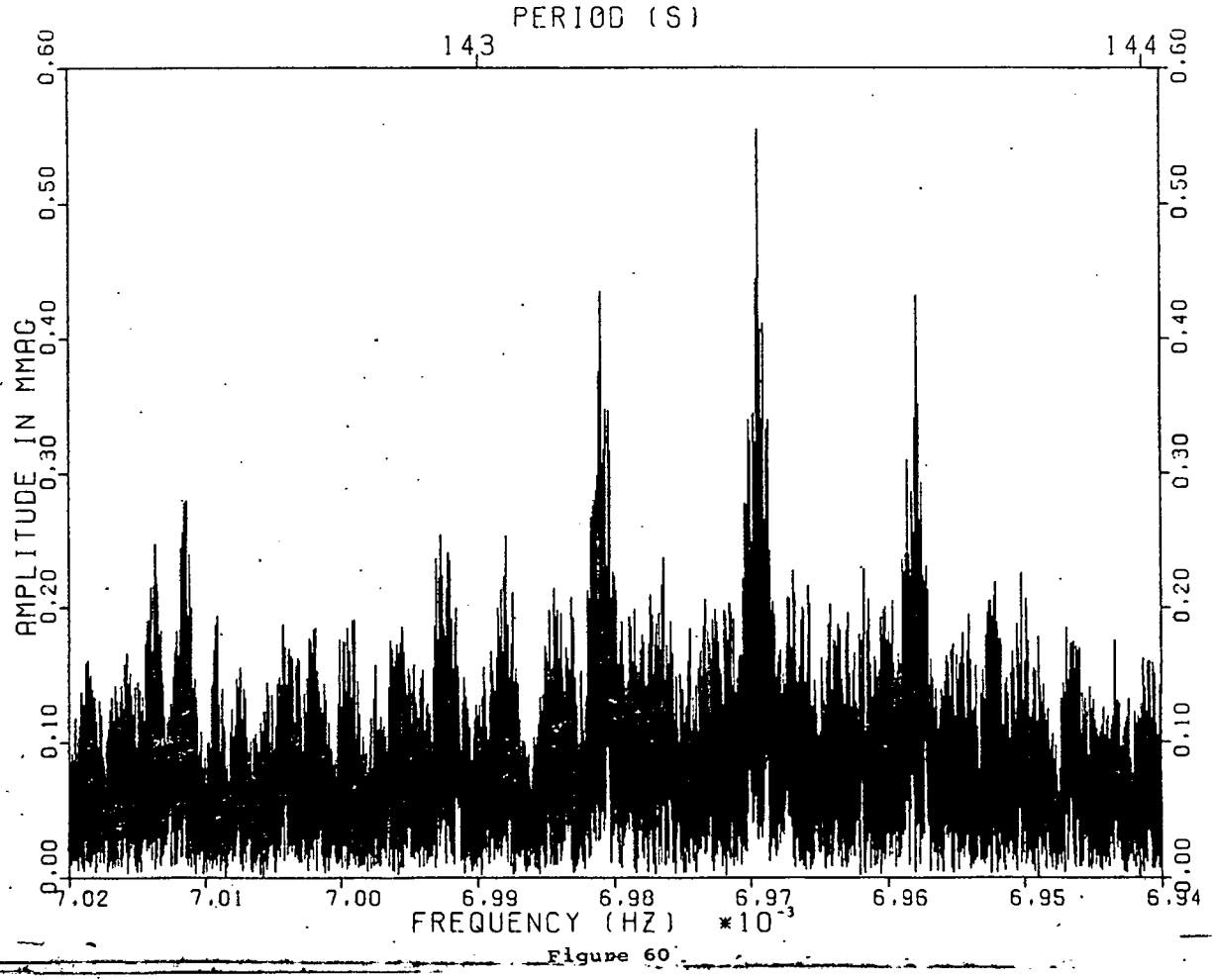

Figure 60

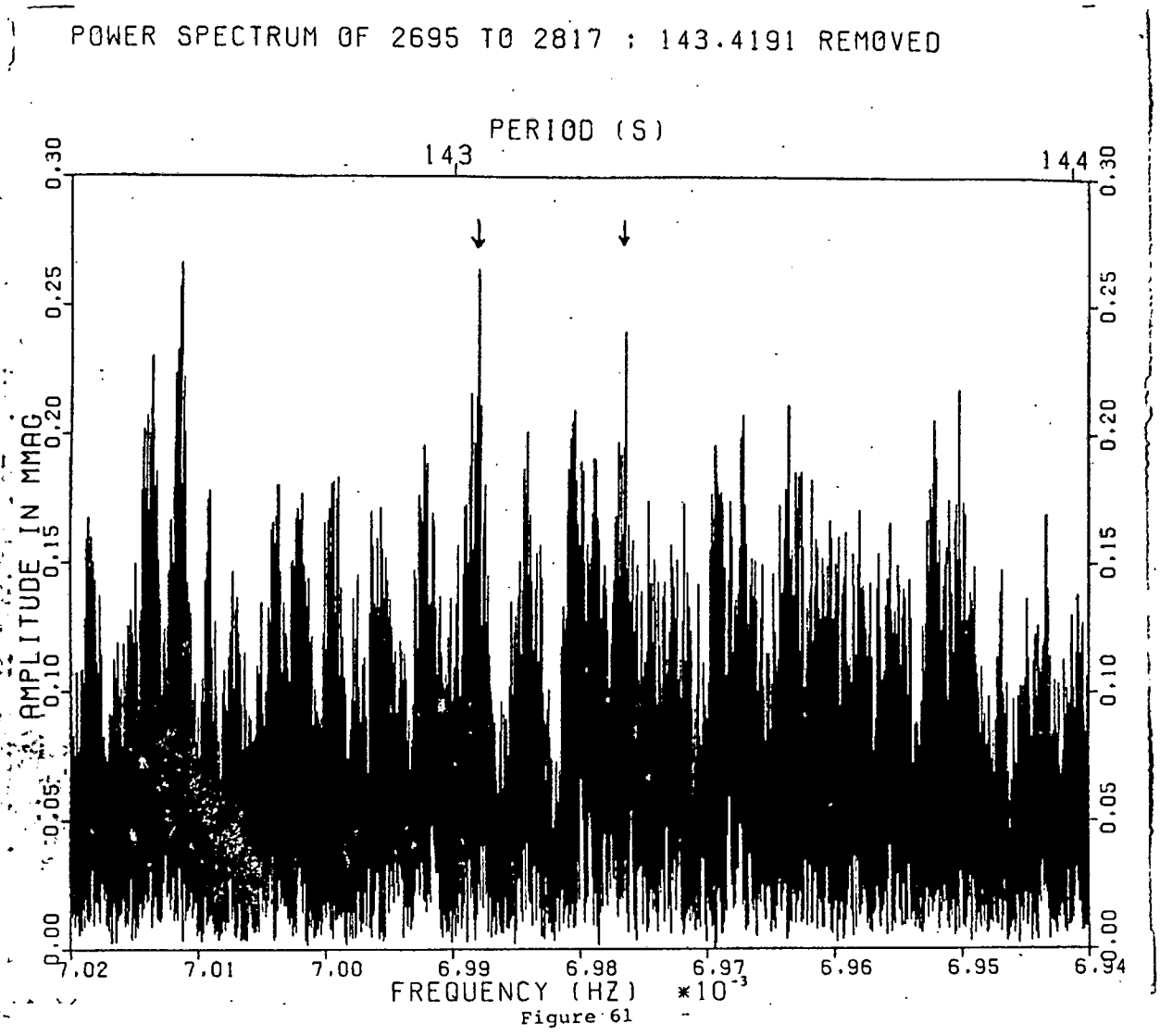

Figure 61

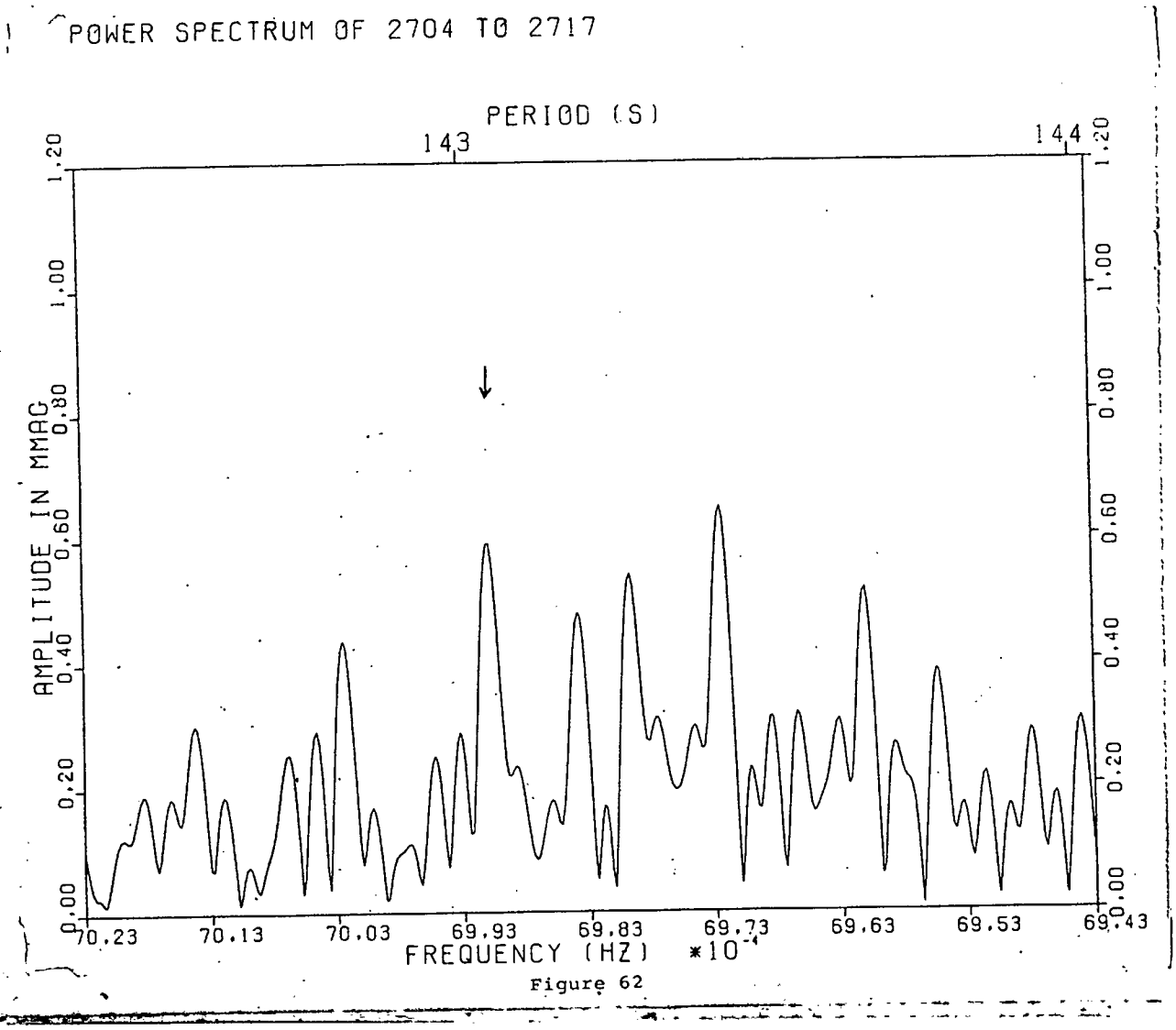

Figure 62

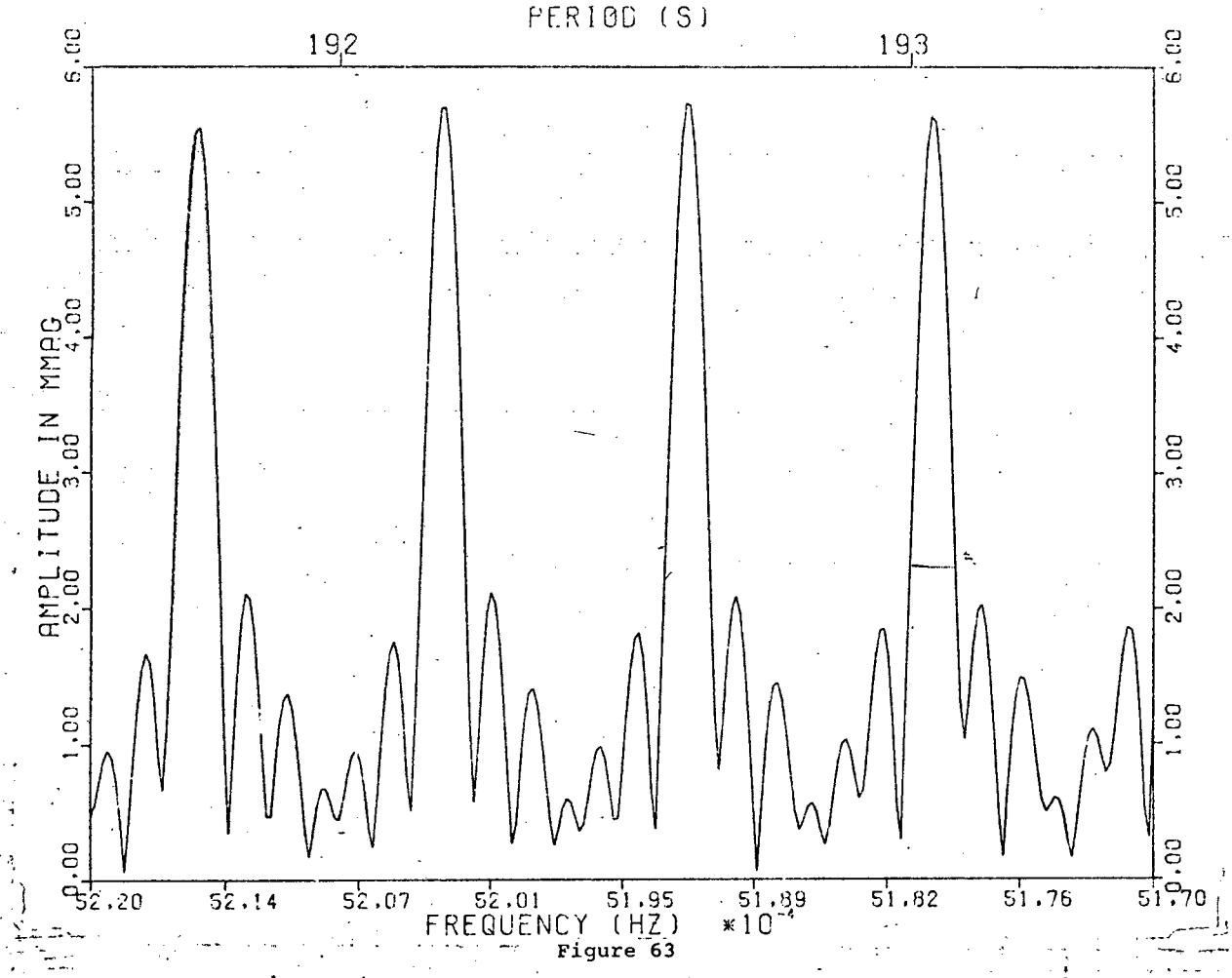

Figure 63

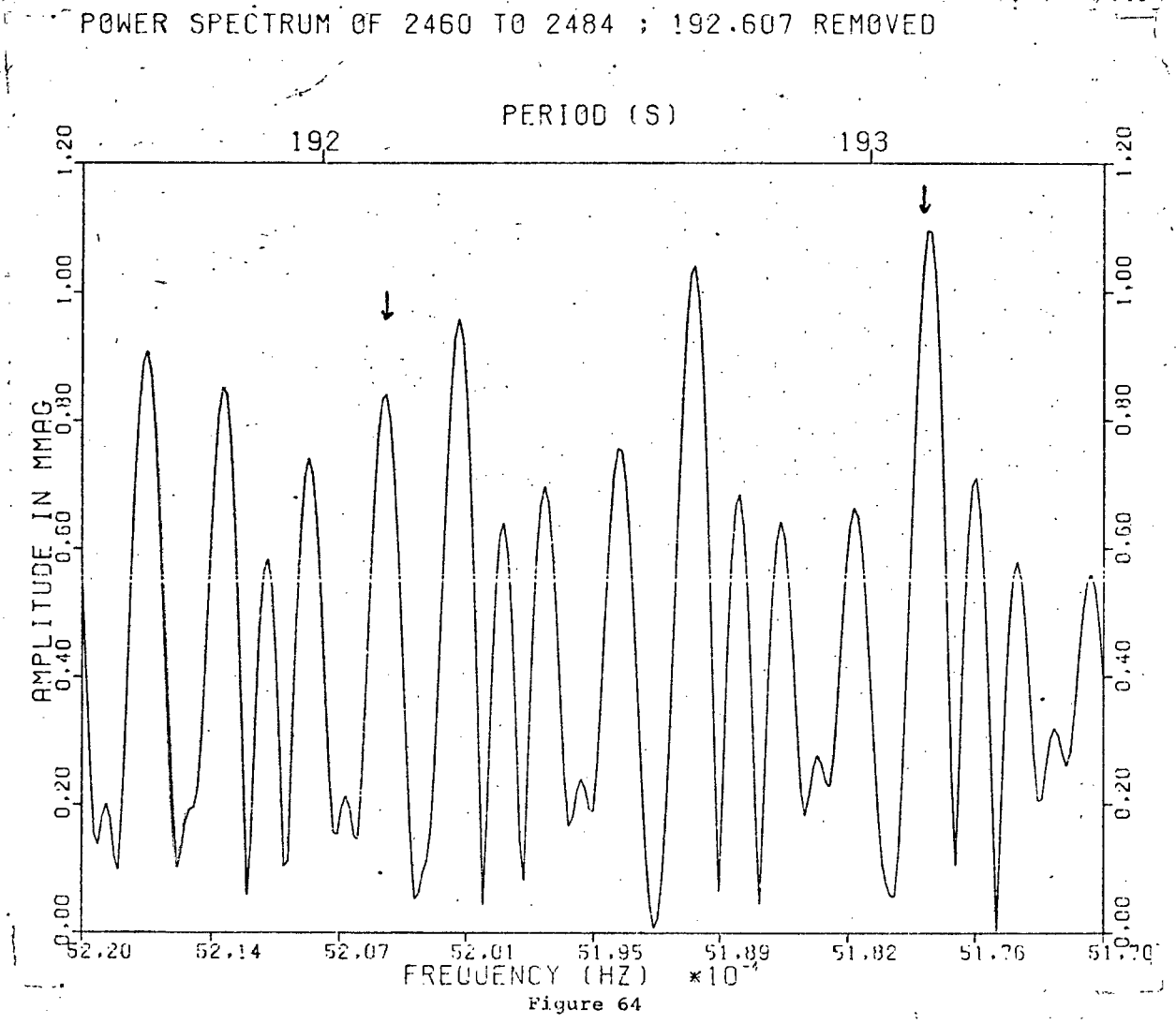

Figure 64

with difficulties but it seems the most obvious one consistent with the PS of the complete data set. Frequency, amplitude and phase values appear for the two postulated components in table 7-1.

7.9. Discovery And Analysis Of The 143 s Oscillation

Power spectra were calculated for all the individual weeks of data in the 1.0 to 10.0 mHz range ; an example is shown in fig. 57 for week 3. The low amplitude feature near 143 s is arrowed. The presence of the 143 s oscillation showed up in most of the individual weeks and is confirmed by the PS of the complete data set shown in fig. 58. Since nearly 500 000 frequencies had to be used in the 1.0 to 10.0 mHz range for the complete data set, plotting time limitations necessitated dividing up this interval into 10 sections, one of which appears in the figure. However, all the other sections showed no new frequencies and were consistent with noise.

The higher resolution PS for this oscillation, obtained from the complete data set, together with the PSW, appear in figs. 59 and 60. There is an unambiguous frequency component near 143.4 s and removal of this frequency from the complete data set results in the PS in fig. 61 which, except possibly for the arrowed component and its alias, is consistent with noise. Being so close to the noise, the reality of this component is very much in doubt, especially since it appears in the PS of only two of the individual weeks. One of these is shown in fig. 62 (for the week 3 data again) and the suspected component is arrowed. It will be included in table 7-1 as a possible.

7.10. Analysis Of The Data Of 1976

The data of Mc Graw (1977) and Hesser et al. (1977) were examinined (a) to determine whether they have the same properties discovered in the later work and (b) to improve the estimates for and stability constraints on the frequency components found above.

Firstly, it was found that the start time for run 2317 of Hesser et al. is probably incorrect : when included in a PS with the rest of their data, the amplitude of the 192.6 s oscillation was dramatically reduced from nearly 6.0 mmag to 4.2 mmag, indicating that the run's timing is incorrect relative to the other data.

Secondly, while the presence of the 192, 113 and 118 s oscillations was evident in PS of both Mc Graw's data, and all the 1976 data taken together, there was no evidence for the presence of the 350 s and 143 s variations. This is consistent with the shortness of the runs and the resultant large amount of noise.

Thirdly, because of the severe aliasing due to the data distribution, not much information was available from PS of all the 1976 taken together. Thus, only selected PS from Mc Graw's data will be considered, the first of which appears in fig. 63 for the 192 s oscillation. Note the severe aliasing and the fact that the largest peak near 192.6 s is of the same amplitude as found for the other data. When this peak is removed, the PS in fig. 64 results and, although there are many aliasing peaks, the two arrowed peaks correspond to the positions and approximate sizes of

POWER SPECTRUM OF 2460 TO 2484

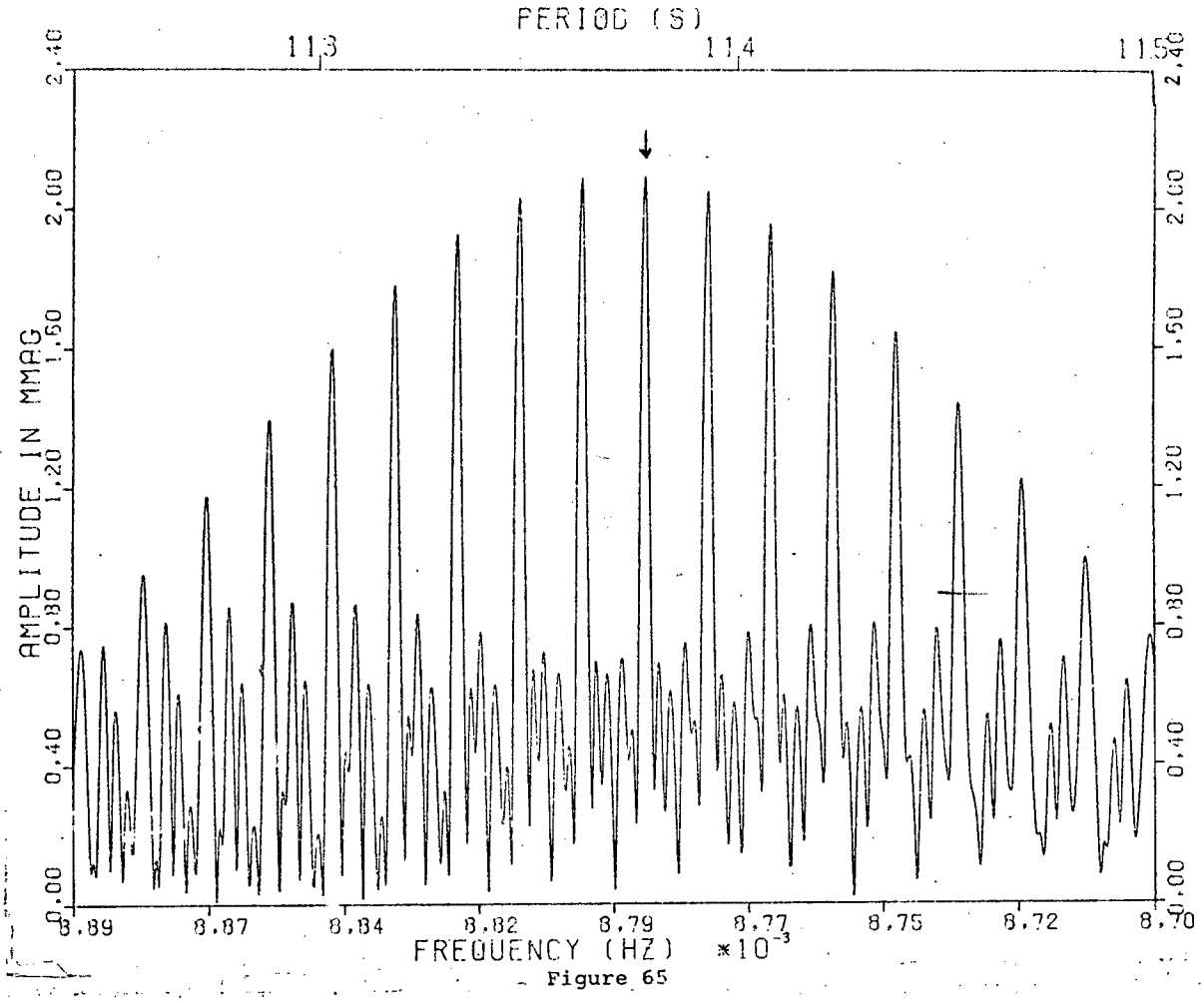

Figure 65

POWER SPECTRUM OF 2460 TO 2484 ; 113.778 REMOVED

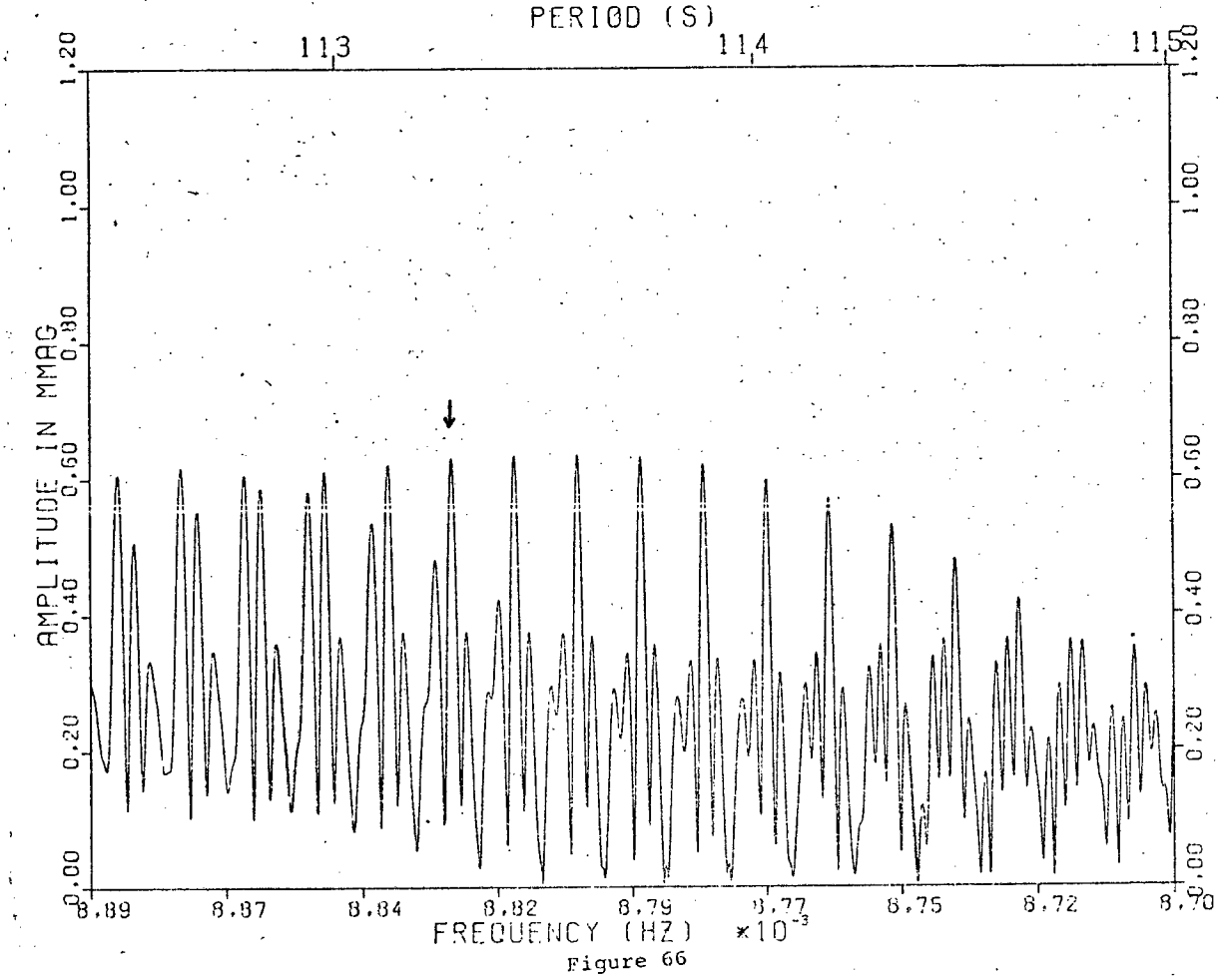

Figure 66

POWER SPECTRUM OF 2460 TO 2484

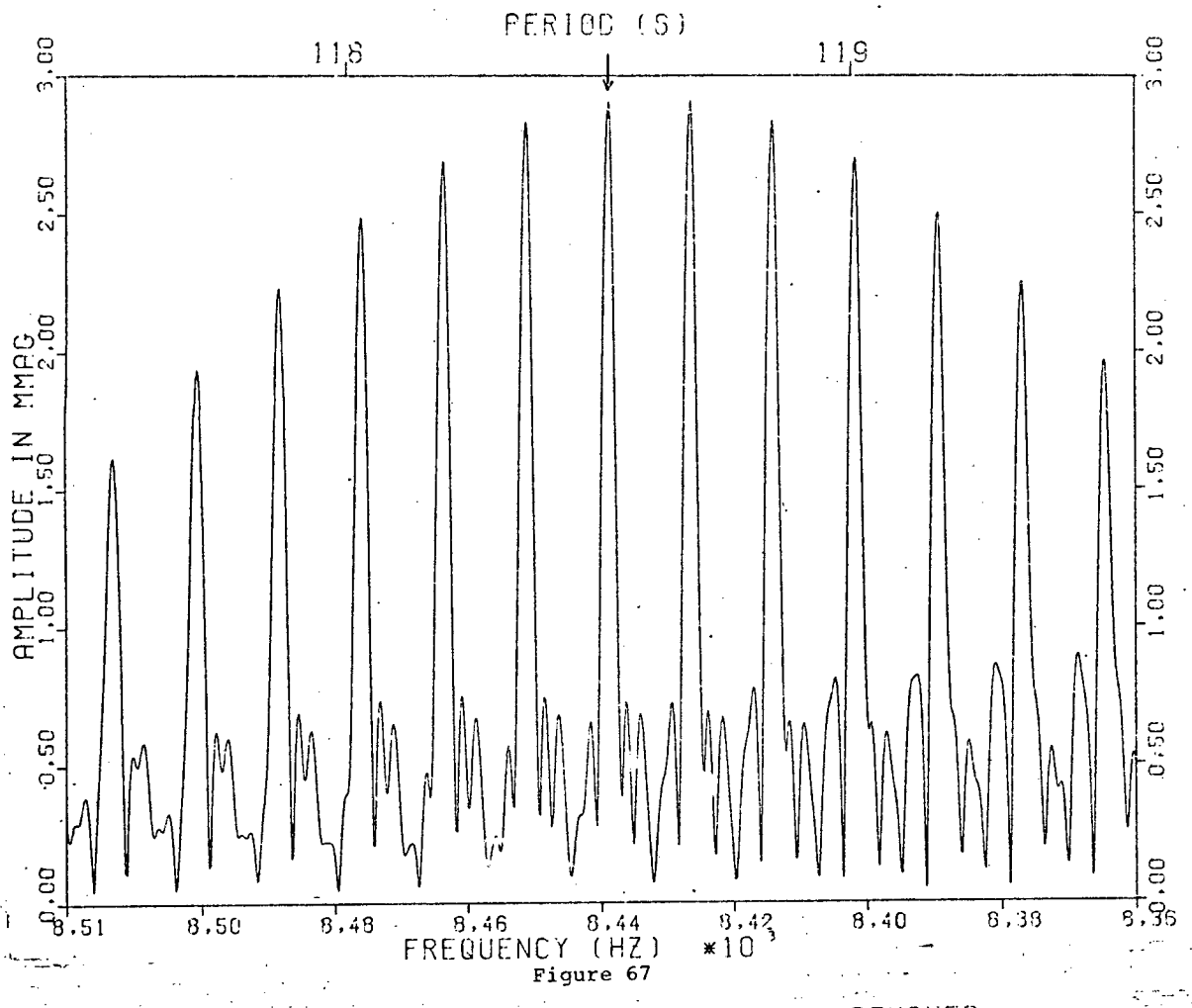

Figure 67

POWER SPECTRUM OF 2460 TO 2484 ; 118.5168 REMOVED

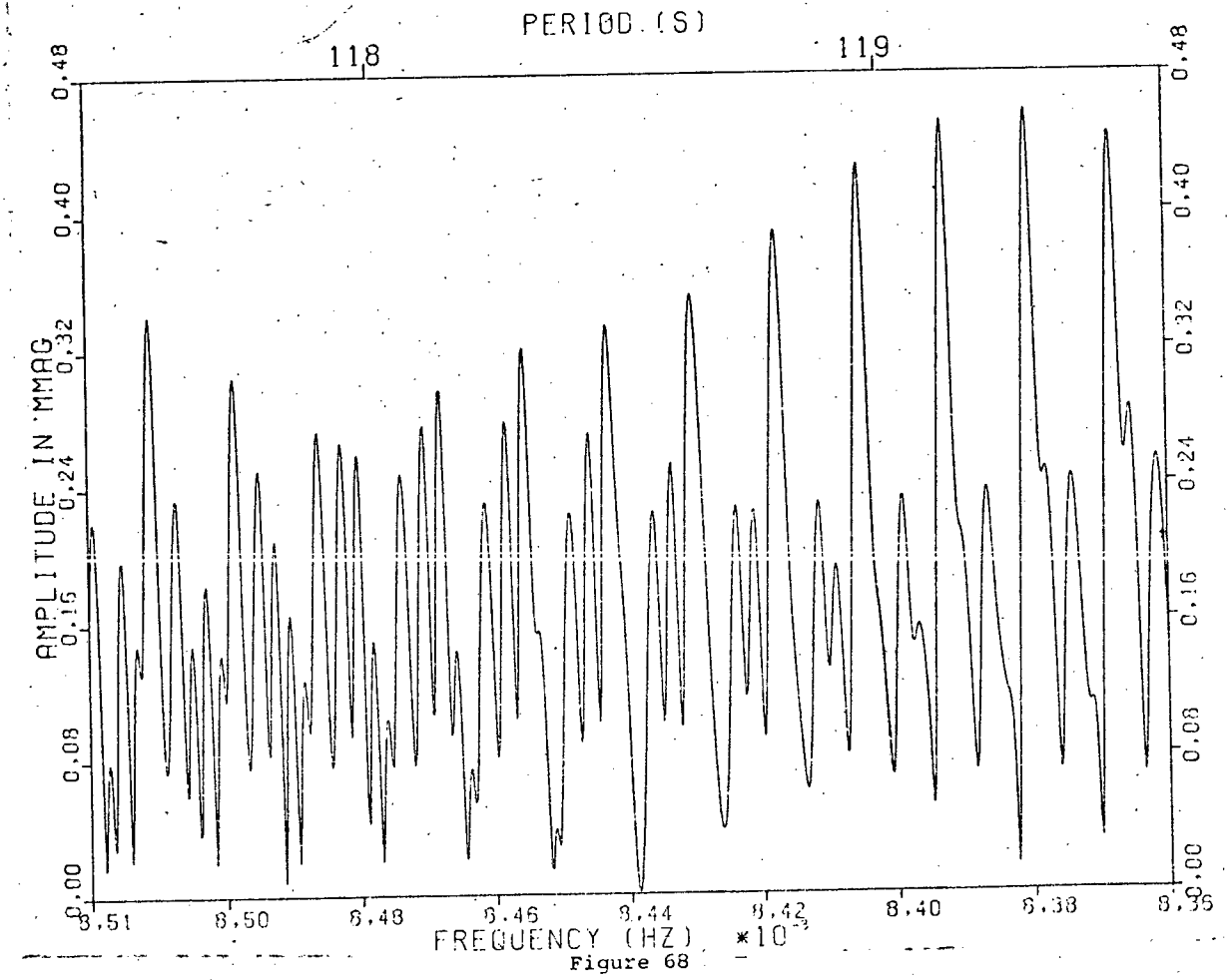

Figure 68

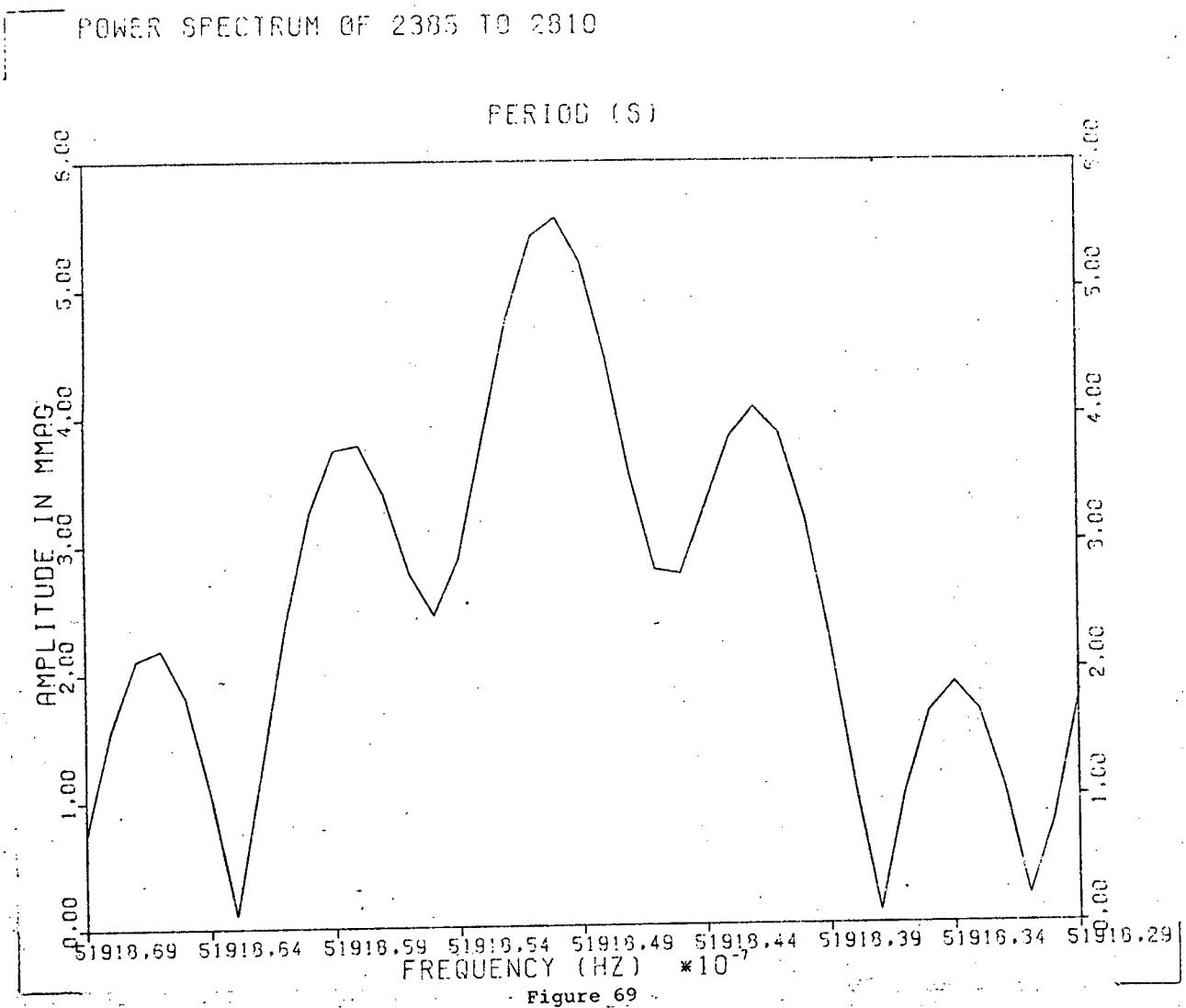

Figure 69

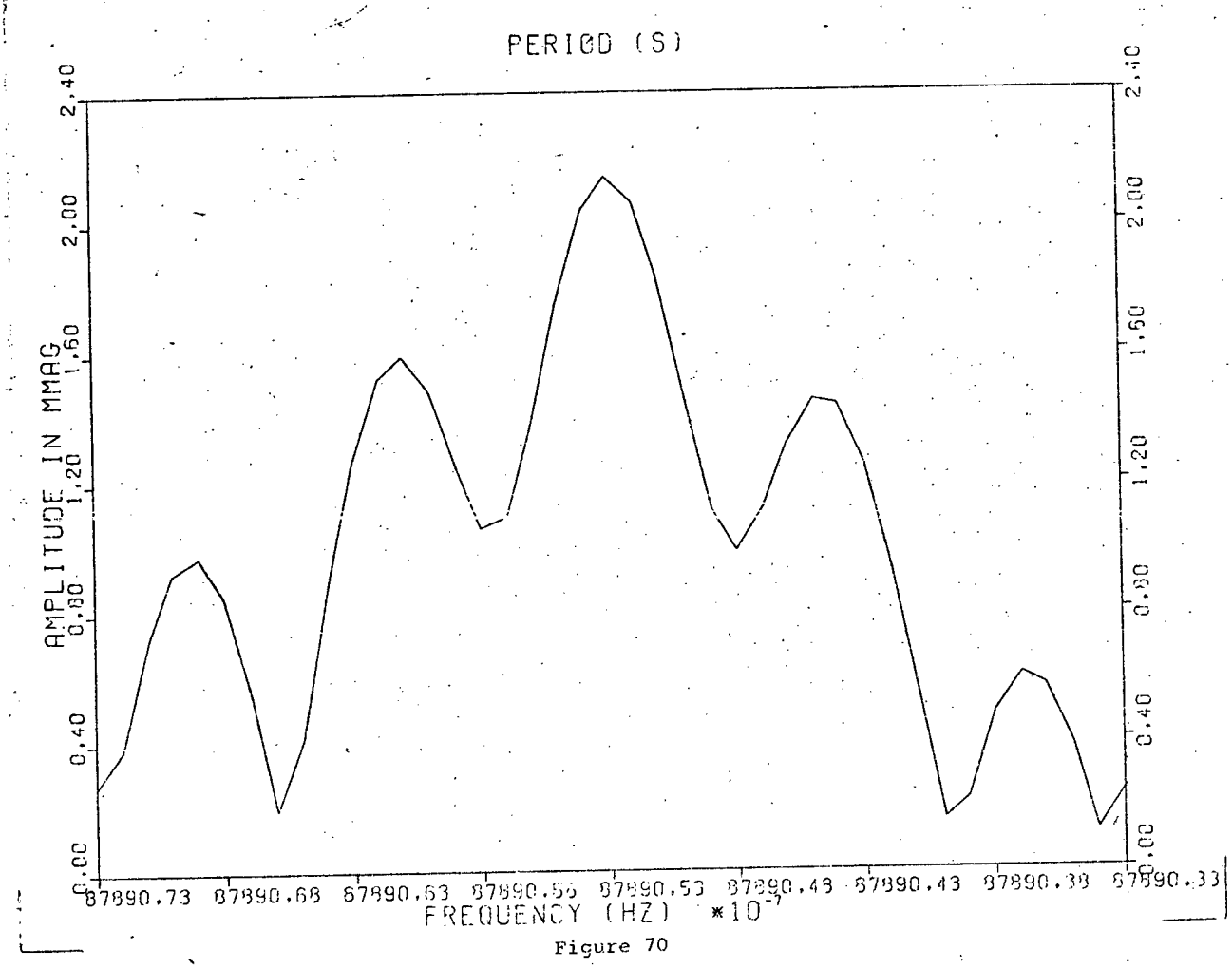

Figure 70

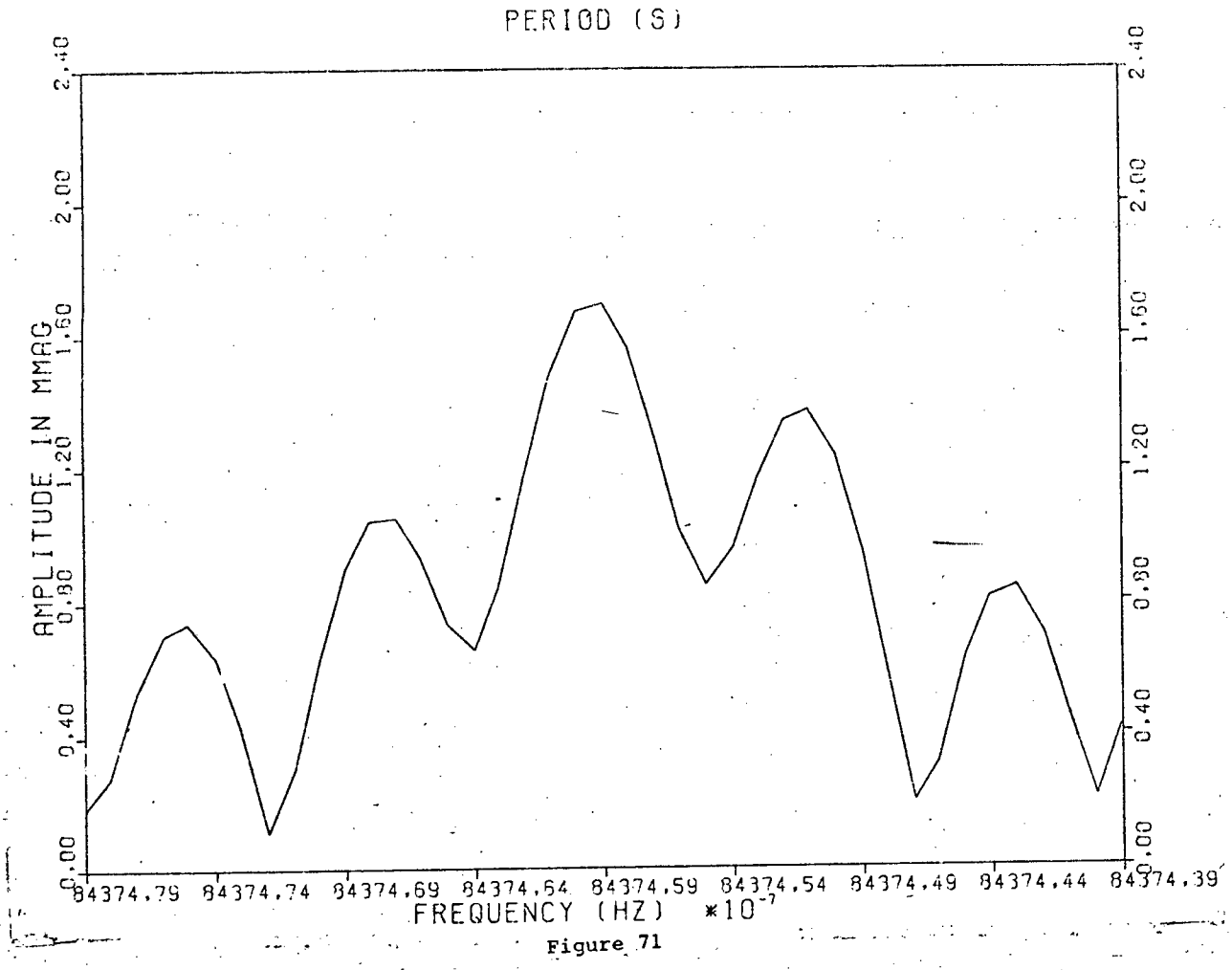
POWER SPECTRUM OF 2385 TO 2810
PERIOD (S)
AMPLITUDE IN MMAG
0.00
0.40
0.80
1.20
1.60
2.00
2.40
84374.79
84374.74
84374.69
84374.64
84374.59
84374.54
84374.49
84374.44
84374.39
FREQUENCY (HZ) *10⁻⁷

Figure 71

the side components found in the other data.

The PS in fig. 65 for the 113 s oscillation was used to prewhiten the data with the arrowed peak (close to where the principal component in the other data was found) ; the resulting PS is shown in fig. 66. The arrow corresponds to the position of the 113.26 s component found in the other data which shows that consistency is again achieved.

The PS for the 118 s oscillation is shown in fig. 67 ; the arrowed peak was used to prewhiten the data to produce the PS in fig. 68. The pattern of aliases near 119 s in the latter is consistent with noise (which also suffers aliasing) and there is no component near 118.67 s as found in the other data. This is only to be expected because this component was separated from the principal component by the 1 day aliasing interval and, in the case of this data, the aliasing is likely to result in its complete removal from the data. In support of this, it is of interest to note that the amplitude of the 118 s aliasing peaks in the previous figure are much higher than in the PS of the other data where the highest component was at about 1.8 mmag. This could come about by the aliases 'sitting' on each other more completely.

We have thus shown that Mc Graw's data is consistent with the results obtained from the later data. However, its greatest advantage lies in using it to place stricter limits on the stability of the frequency components.

In order to do this, the obvious course of action is to combine the 9000 points of all the 1976 data with the 105 000 points in the 1979-80 data to calculate a PS. However, it was found that this did not make a great difference to the PS of the 105 000 points alone : The real and imaginary parts of the PS of the total data set are weighted averages of the corresponding parts of the two component data sets. These weights are the number of points in each set (in accordance with the normalization). Since one data set overwhelms the other, including the latter has only a marginal effect. In order to correct this, a data set was composed of all the 1976 data and one run from each week of the later data set, making 36000 points in all. A PS was calculated for this data set only over the limited frequency range specified by the error limits on the principal components of the 192 , 113 and 118 s oscillations given in table 7-1. Because their amplitudes were so low, all other components were neglected. The three PS are shown in figs. 69, 70 and 71 respectively. There is no ambiguity and the correct frequency is apparent in each case. It was found from tests on artificial data, consisting of a sinusoid of slowly and linearly varying period, that although the position of the peak in the PS is sensitive to the variation, the shape does not broaden unless the frequency changes by at least the inverse of the length of the data. Thus, if the widths of the peaks are consistent with those expected in the case of completely stable periods, an upper limit can be set on the period changes over the 4.5 year baseline by the resolution of the data set. The widths of the peaks in the figures were found to fulfill this condition and the new values for the parameters of the three components appear in table 7-2. Since the phases agree with those of table 7-1, and those found from the PS of the above data set excluding the 1976 data (not shown), to within a few seconds, it can be seen that all the available data are self-consistent for the three components.

This completes the frequency analysis of L 19-2. The final

chapter deals with aspects of the physical nature of the pulsations.

Table 7-2. Best Estimates For The Frequency Components In L 19-2

Period (s)	Frequency (mHz)	Amplitude (mmag) ± 0.1	Phase 2444000.0+ (±10s)	Q (sec/sec) x 10^{-13}
192.6096 ±2	5.191850 ±5	5.55	-80s	10
113.77790 ±6	8.789053 ±5	2.14	37s	4
118.51909 ±6	8.437459 ±5	1.70	20s	4

8. Discussion And Conclusions

We have provided strong evidence for the existence of ten separate frequency components in the light curve of L 19-2 and suggested that up to three more may exist. Other than these, there is no evidence for stable frequency components with amplitudes greater than 0.2 mmag and periods in the range 100 to 1000 s. There is a possibility of some short-lived frequency components in the light curve but the evidence is weak and such variability would be unexpected for a high-Q ZZ Ceti star. The final step is to make some remarks about the physical nature of the light variations.

Using equilibrium models of white dwarfs, the set of equations describing stellar pulsation has been solved to yield the periods of the various g-modes and their growth rates (Osaki and Hansen,1973 ; Brickhill,1975 ; Dziembowski,1977a ; Dziembowski ,1979). However, because the interior structure of white dwarfs is not well known, complete confidence in these models has not been established. Despite this, some important points may be made :

(1) As discussed previously, it is widely believed that the pulsations in ZZ Ceti stars are non-radial g-mode pulsations and this interpretation is consistent with the qualitative agreement found between the theoretical periods and those detected in the light curve of L 19-2.

(2) Models of varying complexity have been made for the ZZ Ceti stars and, subject to reasonable simplifying assumptions, the periods of the various g-modes have been obtained from the solution to the non-radial oscillation equations (see above references). However, it has been found that these periods are very sensitive to the interior chemical composition of the white dwarf models, which is not directly observable. Hence, in spite of the good qualitative agreement between the two, it is not possible to fit quantitatively the observed periods of any specific star with those of the models calculated so far (except by good fortune).

(3) It is possible to put some constraints on the values of k and l describing the non-radial g-modes. By integrating the spherical harmonic associated with any l over the stellar surface, Dziembowski (1977b) and Buta and Smith (1979) find that the net flux associated with the light variation, decreases sharply as l increases. This is as a result of the cancellation of 'bright' and 'dark' zones of opposite phase distributed over the stellar surface. As a result, in the case of the large amplitude ZZ Ceti stars, it is highly likely that the value of l is small (< 4,say). However, in the case of the low amplitude stars, because the low pulsation amplitude may be due to incomplete cancellation of zones of large intrinsic light variation, it is not possible to be certain that the above restriction on l is valid. Assuming that this is not the case and that l is small, it can be seen from all the published models cited above, together with the recent models of Dziembowski (1979), Winget et al. (1981) and Dolez and Vauclair (1981), that the value of k must be low for a g-mode with period less than 200 seconds. It may thus be expected, subject to the above caveat, that the 113, 118, 143 and probably the 192 s oscillations are all g-modes with low k and l.

(4) Two relationships among the periods of different k and l are of interest. The first relates the periods of the same k but

differing l :

$$\frac{P_{k\ell}}{P_{k\ell'}} = \left[\frac{\ell'(\ell'+1)}{\ell(\ell+1)}\right]^{\frac{1}{2}} \qquad 8.1$$

while the second relates periods of the same l but differing k :

$$P_{k\ell} = P_{1\ell}\left(1 + \frac{k-1}{h}\right) \qquad 8.2$$

where h is a constant lying between 3 and 4 (Brickhill,1975). Using these relationships, it is possible to put forward the following mode identifications for the various oscillations in L 19-2

Table 8-1. Possible Scheme Of Mode Identification In L 19-2

Observed Period	k	l	R_1	R_2	
350s	1	1			347.3s
192s	1	2	1.82	1.73	200.5s
143s	1	3	2.45	2.45	141.8s
113s	1	4	3.10	3.16	109.8s
118s	2	5	2.97		112-119s

In the above table, R_1 is the ratio of the observed period to 350 s while R_2 is the expected ratio from equation 8.1 using the values of l in the table. A set of periods which are strictly related by the theoretical ratios and, at the same time, minimise the differences between themselves and the observed periods is shown in the last column of the table. The uncertainty in the last value of this column arises from the adopted value of h. The calculated periods for the k=1 , l=2 mode in Dziembowski (1979) and Winget et al. (1981) is quite near to 192 s indicating that the observed periods could be matched by models similar to theirs. In spite of the above, there are probably many other sets of periods which will match the set of periods observed in L 19-2 (although most will include modes with large k and/or l), so the above scheme is by no means well established. This point emphasises one of the principal problems in the observational analysis of the ZZ Ceti stars : mode identification on the basis of the observed periods and their relationships.

(5) Apart from the equal splitting among the 192 s oscillation components, there are no obvious suggestive frequency separations among the other components. The 118 s and 350 s oscillation exhibit the same splitting which gave rise to the aliasing problems encountered in the frequency analysis. As mentioned above, the frequency associated with a g-mode of indices k,l,m is shifted by rotation by an amount $m\Omega(1-C_{kl})$ (to first order). Chlebowski (1978) has calculated the value of C_{kl} for some ZZ Ceti type models and finds that, with the exception of isolated values of k, C_{kl} is insensitive to the value of k for a particular l. This means that modes of the same l but different k may be split into components with frequency spacings which are integral

multiples of one another. In this connection, it is of interest to note that the frequency splitting of the 113.26 s and 113.78 s components is almost 3 times that of the components of the 192 s oscillation. This is some evidence that these modes are of equal l but differing k contrary to the scheme proposed above. It is also of slight interest to note that the frequency splitting between the doubtful components and their respective principal components is similar for both the 113 and 118 s oscillations.

The most significant frequency splitting is among the components of the 192 s oscillation where the equality is established to well within the limits of the measurements. The most obvious explanation for this splitting is rotation. Since C_{kl} tends to $1/[l(l+1)]$ as $k \to \infty$ and Chlebowski has found C_{kl} to be insensitive to k, Ω corresponds to a rotation period of 0.9 d or less ; L 19-2 is thus another example of a slowly rotating white dwarf. Since the central component of the 192 s triplet is of so much larger size than the side components, themselves nearly equal in size, it is reasonable to assume that the central components has m = 0 while the side components have m values of the same size but opposite sign. It is by no means certain that m has the values ± 1 for these two components ; the exact values must remain unknown at present.

An interesting point arises concerning the existence of modulation in the 192 s oscillation amplitude. In the derivation of equation 7.1.1 on page 7-4, it was assumed that the phases of all 3 components are equal i.e. all are in phase at time t = 0. However let us suppose that the phases are such that when the components associated with A_0 and A_1 are in phase, those associated with A_0 and B_1 are exactly out of phase. Further assuming that the splitting is precisely equal so that the beat periods are equal, and that $|A_1| = |B_1|$, these conditions are equivalent to writing $A_1 = -B_1$ in 7.1.1. Thus, the modulation associated with the beating of the main component and the side components will vanish. Relating these considerations to the 192 s oscillation, we have seen that the modulation of the 0.45 d variation is much smaller than that of the 0.9 d variation and undetectable in the mean amplitude curve in fig. 16. Furthermore, since the amplitudes of the side components are nearly equal, any inequality in the frequency splitting will result in modulation of the beat amplitude on a time scale given by the inverse of the difference between the frequency splittings. Assuming that the splittings among the three components are not exactly equal, the amplitude equation for A_t analogous to 7.1.1 is

$$A_t^2 = A_0^2 + A_1^2 + B_1^2 + 2A_0(A_1\cos(\Delta t+\epsilon t) + B_1\cos(\Delta t)) + 2A_1B_1\cos(2\Delta t+\epsilon t)$$

where Δ is the splitting between the frequencies associated with A_0 and B_1 and $\Delta+\epsilon$ is the splitting between the frequencies associated with A_0 and A_1 and $\epsilon << \Delta$. The last term is associated with the 0.45 d modulation and may be ignored for the present. This equation predicts that the size of the 0.9 d amplitude modulation will vary with a period of $1/\epsilon$ and maximum and minimum values given by $2A_0(A_1+B_1)$ and $2A_0(A_1-B_1)$ respectively (assuming $A_1 > B_1$). In order to try to detect any such variations, the amplitude of the 192 s oscillation was measured for 40 cycles of

data from weeks 3, 7, 8 and 10-12 and 20 cycles for the 1976 data. These amplitudes were then squared and the resultants were fit with a sinusoid of 0.892 d period (found from the measured splitting of the three components in table 7-1) for each week separately. The means and amplitudes of these fits, k_1 and k_2, are shown in table 8-2. The quantities k_3 and k_4 are found from the expressions $A_0^2+A_1^2+B_1^2$ and $2A_0(A_1+B_1)$, where the values in the latter expressions are the amplitudes of the three components of the 192 s oscillation found from the PS of the individual weeks.

Table 8-2. Parameters Of The Fits To The Beat Cycles

Week	Time Yr	k_1	k_2	A_0	A_1	B_1	k_3	k_4
		$(\text{mmag})^2$		(mmag)			$(\text{mmag})^2$	
10-12	1980.7	38	13	6.0	0.9	0.9	39	22
8	1980.4	44	8	6.0	0.9	0.6	37	18
7	1980.2	38	11	6.0	0.9	0.9	39	22
3	1979.5	40	16	6.0	0.6	0.7	38	17
Hesser*	1976.6	39	26	6.0				
Mc Graw	1976.58	38	22	6.0	0.9	1.1	37	18

* (i) PS of the 3 days (excluding run C2317) of the data of Hesser et al. could not give reliable estimates for A_1 and B_1 due to noise ;

(ii) The data only spanned the lower half of the beat cycle so that k_1 was forced to be 39 $(\text{mmag})^2$ to give a realistic fit. The value of k_2 for this data must thus be given a low weight.

Thus k_3, k_4 are the values of k_1, k_2 expected if no inequality in the splitting exists. While there is an uncertainty of the order of 2 to 5 mmag^2 say, on the k's in the table, it is clear from the difference between k_2 and k_4 for weeks 7, 8 and 10-12 that some variation in the size of the amplitude modulation is taking place. As mentioned above, the minimum of k_2 should be $2A_0(A_1-B_1)$. However, because A_1 and B_1 are nearly equal and their values are uncertain to the same order as their difference, there is a large uncertainty on this minimum. Thus three reasonable possibilities for the type of variation that is taking place are that 1976 is a maximum of the size of the amplitude modulation and 1979 is near phase either (i) 0.25 or (ii) 0.50 or (iii) 0.75. This results in a period of about 20, 10 or 5 years respectively due to a non-zero ϵ whose corresponding values are 1.6×10^{-6} or 3.2×10^{-6} or 6.3×10^{-6} mHz. The latter value is likely to be detectable in the measured frequencies in table 7-1 and so is less probable. Following Chlebowski (1978), it is easy to show that the theoretical difference between the splittings is given by the expression :

$$\epsilon = 2(C^{(2)}_{k\ell m} - C^{(2)}_{k\ell o})\Omega^2$$

$$= \frac{2(C^{(2)}_{k\ell m} - C^{(2)}_{k\ell 0})\, d\nu^2_{obs}}{m^2(1-C_{k\ell})^2}$$

where $d\nu_{obs}$ is the observed splitting (to first order) and $C^{(2)}_{klm}$ is the co-efficient analogous to C_{kl} in the second order term in Chlebowski's equation 3. Chlebowski has also calculated $C^{(2)}_{klm}$ for low values of k and l=1,2 using Dziembowski's 1977a models. For l=1, k=1, m=1, ϵ is approximatley 17×10^{-6} mHz which increases as k increases. For l=2, k=1 and m=1 or 2, ϵ is approximately 1×10^{-6} mHz and this value is typical for the various values of k calculated by Dziembowski. The former value would easily have been detected in the data, while the latter value is in satisfactory agreement with the above measured values and predicts a period of 30 years for the variation. On the basis of Dziembowski's models the l=1, k=1 mode may be excluded from identification with the 192 s oscillation. Two points are important relative to the above discussion : (i) the theoretical ϵ is sharply reduced by any sizeable value of m through the dependence of ϵ on the square of m ; (ii) it is not clear how the value of $C^{(2)}_{klm}$ will be affected by the more realistic chemically-stratified models to be discussed below.

We conclude that we have detected second order effects in the frequency splitting of the 192 s oscillation. This effect and the pattern of components in the 192 s oscillation is unique as yet among the low amplitude ZZ Ceti stars and constitutes the most conclusive evidence to date that rotational splitting is the cause of the amplitude variability in the oscillations of these stars.

As for the assignment of m to the other frequency components, the picture is even more uncertain, although probably the principal component of the 113 s variation has m = 0 because of its relatively much greater amplitude than the other components in this oscillation. It is puzzling why triplets etc. are not seen in the frequency structure of these oscillations nor those in ZZ Ceti. Further theoretical work on excitation of surface harmonics is awaited to determine if some selection effect is involved in the excitation of modes of differing m.

(6) Another important question is whether or not the g-modes are self-excited. The growth rate, determined from the imaginary part of the eigenfrequency, must be sufficiently large that the oscillations can grow in a time much shorter than the lifetime of the white dwarf determined by the rate of cooling. When this condition is fulfilled, together with the obvious restriction that the growth rate must be positive, i.e. the star must be vibrationally unstable to perturbations around the equilibrium position, the appearance of oscillations in the ZZ Ceti stars can be accounted for. Early attempts in testing for instability in white dwarfs (Vauclair,1971 ; Osaki and Hansen,1973) were not specifically directed at white dwarfs with the physical properties of the ZZ Ceti stars. The first such attempt, by Dziembowski (1977a), failed to find any unstable g-modes with periods in the range of those seen in the ZZ Ceti stars. The only unstable modes were those of very large l. Some success was achieved by including the Stellingwerf 'bump' opacity in the models. Dziembowski (1979) and Keeley (1979) both reported detecting low order unstable g-modes with periods in the appropriate range. However, these models did not relate to the DA character of the ZZ Ceti stars and predicted similar growth rates for many g-modes which contrasts with the comparatively small number seen in the low amplitude ZZ Ceti stars. Even in the large amplitude stars, provided that the hypothesis that the so-called principal frequencies are the only independently excited ones is accepted, the number of independent g-modes is small. In three recent

preprints, Winget et al. (1981) , Dziembowski and Koester (1981) and Dolez and Vauclair (1981), a very promising solution to the above difficulties is emerging. The rationale behind this is that the diffusion time scale is relatively short in ZZ Ceti stars, which allows the envelopes, where the amplitude of oscillation is greatest, to become chemically stratified as a result of the gravitational settling of helium and the heavy elements. Many g-modes with the correct periods are now found to be unstable ; the driving mechanism is associated with the ionisation zones of helium and hydrogen. Winget et al. also report preferential excitation of a small number of modes due to a resonance between the characteristic wavelength associated with the excited mode and the depth of the hydrogen layer in the model. In this connection, it is remarkable that the three low amplitude ZZ Ceti stars analysed to date all have their largest amplitude oscillations near 200 s. This work is still in its preliminary stages but offers hope for the solution to the problem of why the ZZ Ceti stars pulsate.

The frequency structure of L 19-2 is unlike any of the other low amplitude stars analysed to date. As we have seen, G 117-B15A has a peculiar pattern of frequencies suggestive of r-modes. While more similar to ZZ Ceti, L 19-2 has more frequency components and a triplet structure which are not seen in the former. It is not clear whether this indicates a significantly different physical nature or that L 19-2 merely has more energy available for mode excitation. An obvious similarity between the two stars which is confirmed by the present study is the linearity of the oscillations. This is established by the absence of harmonics of or cross-coupling between any of the oscillation modes in L 19-2.

Finally, the stability of the oscillation periods (see tables 7-1 and 7-2) places L 19-2 firmly in the category of very stable white dwarf pulsators. In spite of the fact that the observations of L 19-2 span roughly the same time interval as those of the latter, the limits on the period changes are larger than those for both R 548 and G 117-B15A. This is because the low amplitude of many of the frequency components precluded the least squares fitting procedure used in the above two stars. The approach used here is less sensitive to period changes than least squares fitting. A better way of using Fourier transforms would be to take advantage of the sensitivity to period changes of the positions of the peaks in the power spectra. This would necessitate dividing up the data into blocks and searching for systematic period changes with time. With the present data distribution, where the largest subdivision would be determined by the 1976 data, the resolution would be too low to allow its application. The expected time scale of variations in the periods, obtained from the theory of cooling white dwarfs, is estimated to be $P/\dot{P} = 1.5 \times 10^9$ years or about 4.5×10^{16} seconds (Kepler and Robinson,1980). The ratio of this quantity to the measured upper limit on $P/\dot{P}$ is about 200. Since this limit decreases as the square of the observing time, a total of 60 years observing is needed to detect period changes. This might be shortened by judicious planning of the length of observing time per year (see Kepler and Robinson,1980). Nevertheless, at the moment, the other two stars are better candidates for long term observation.

This completes the study of L 19-2. The field of ZZ Ceti stars provides much work to keep astronomers busy. On the observational side, efforts should be made to discover more ZZ Ceti stars in

order to improve the statistics for the ratio of variable to non-variable DAs. This would also improve the definition of the instability strip. The other known variable stars should be extensively observed, particularly the large amplitude variables where a start could be made on the task of trying to find a deterministic model of their light curves. In addition, the separation of properties of the large and small amplitude stars is worth investigating : one idea that could be tested is whether the low amplitude stars are on the edges of the instability strip while the large amplitude variables occupy the centre. Highly accurate photometry would be needed. Another unexplained phenomenon is the tendency for the low amplitude stars to have short periods and the large amplitude stars to have long periods.

For theoreticians, there is no lack of work either. Many grids of models might have to be made to enable the identification of the modes of a particular star with theoretical models - surely one of the most pressing of problems. On the other hand, other techniques of mode identification should be sought which might give observers a better foundation for identification than those currently available. Another problem needing the attention of theoreticians is to answer the questions : what values of m are seen when degeneracy is lifted and why ? On a broader front, the apparent low rotation rates of white dwarfs present a challenge to evolutionary models as do the low surface magnetic fields seen in most white dwarfs. Perhaps the same mechanism is responsible for the loss of angular momentum and magnetic flux.

In conclusion, the magnetic and pulsating white dwarfs are fascinating sub-groups within the white dwarfs as a whole. The latter promise to be valuable probes into the interiors of white dwarfs which are hidden from direct observation. It is a testimony to the uniformity of nature that the same mathematics applies in objects of such different dimensions - the removal of degeneracy by the effect of a magnetic field on the energy levels of a hydrogen atom, and the removal of degeneracy by the effect of rotation on the oscillation modes of an entire star.

Aller, L.H. 1963, The Atmospheres of the Sun and Stars, Ronald Press, New York.

Angel, J.R.P. 1972, Ap. J. (Letters), 171, L17.

Angel, J.R.P. 1977, Ap. J., 216, 1.

Angel, J.R.P. 1978a, private communication to E.L. Robinson.

Angel, J.R.P. 1978b, Ann. Rev. Astron. Astroph., 16, 487.

Angel, J.R.P., Carswell, R.F., Strittmatter, P.A., Beaver, E.A. and Harms, R. 1974b, Ap. J. (Letters), 194, L47.

Angel, J.R.P., Hintzen, P. and Landstreet, J.D. 1975, Ap. J. (Letters), 196, L27.

Angel, J.R.P., Hintzen, P., Strittmatter, P.A. and Martin, P.G. 1974a, Ap. J. (Letters), 190, L71.

Angel, J.R.P., Illing, R.E. and Landstreet, J.D. 1972, Ap. J. (Letters), 175, L85.

Angel, J.R.P. and Landstreet, J.D. 1970a, Ap. J. (Letters), 162, L61.

Angel, J.R.P. and Landstreet, J.D. 1970b, Ap. J. (Letters), 160, L147.

Angel, J.R.P. and Landstreet, J.D. 1971, Ap. J. (Letters), 165, L71.

Angel, J.R.P. and Landstreet, J.D. 1972, Ap. J. (Letters), 178, L21.

Angel, J.R.P. and Landstreet, J.D. 1974, Ap. J., 191, 457.

Angel, J.R.P., Landstreet, J.D. and Oke, J.B. 1972, Ap. J. (Letters), 171, L11.

Avrett, E.H. and Krook, M. 1963, Ap. J., 137, 874.

Beckers, J.M. 1969, Solar Phys., 9, 372.

Bessell, M.S. and Wickramasinghe, D.T. 1978, Mon. Not. R. Astron. Soc., 182, 275.

Bloomfield, P. 1976, Fourier Analysis Of Time Series : An Introduction, J. Wiley, New York.

Bohm-Vitense, E. 1964, in Proceedings First Harvard-Smithsonian Conference on Stellar Atmospheres, Smithsonian Astrophys. Obs. Rep. 167, p. 99.

Borra, E.F. 1973, Ap. J., 183, 587.

Borra, E.F. 1976, Ap. J., 209, 858.

Brickhill, A.J. 1975, Mon. Not. R. Astron. Soc., 170, 405.

Brown, D.N., Rich, A., Williams, W.L. and Vauclair, G. 1977, Ap. J., 218, 227.

Buta, R.J. and Smith, M.A. 1979, Ap. J., 232, 213.

Cayrel, R. and Traving, G. 1960, Zeits. f. Ap., 50, 239.

Chanmugam, G. 1972, Nature, 236, 83.

Chanmugam, G., O'Connell, R.F. and Rajagopal, A.K. 1972, Ap. J., 177, 719.

Chlebowski, T. 1978, Acta Astronomica, 28, 442.

Cox, J.P. 1976, Ann. Rev. Astron. Ap., 14, 247.

Cox, J.P. 1980, Theory of Stellar Pulsation, Princeton University Press, Princeton.

Cox, J.P. and Hansen, C.J. 1979, in White Dwarfs and Variable Degenerate Stars, I.A.U. Colloq. No. 53, ed. by H.M van Horn and V. Weidemann, University of Rochester, New York, p. 392.

Deeming, T.J. 1975, Astophys. Space Sci., 36, 137.

Dolez, N. and Vauclair. G. 1981, preprint.

Dziembowski, W. 1977a, Acta Astronomica, 27, 1.

Dziembowski, W. 1977b, Acta Astronomica, 27, 203.

Dziembowski, W. 1979, in White Dwarfs and Variable Degenerate Stars, I.A.U. Colloq. No. 53, ed. by H.M. van Horn and V. Weidemann, University of Rochester, New York, p. 359.

Dziembowski, W. and Koester, D. 1981, preprint.

Eggen, O.J. 1968, Ap. J. Suppl., 16, 97.

Fontaine, G., Mc Graw, J.T. and Gustafson, J. 1981, preprint.

Fontaine, G., Mc Graw, J.T., Coleman, L., Lacombe, P., Patterson, J. and Vauclair, G. 1980, Ap. J., 239, 898.

Green, R., Schmidt, M., Stockman, H.S., Angel, J.R.P., Thompson, R., Landstreet, J.D. and Beaver, E.A. 1978, preprint quoted in Angel (1978b).

Greenstein, J.L. 1970, Ap. J. (Letters), 162, L55.

Greenstein, J.L. 1974, Ap. J. (Letters), 194, L51.

Greenstein, J.L. and Boksenberg, A. 1978, Mon. Not. R. Astron. Soc., 185, 823.

Greenstein, J.L. and Trimble, V.L. 1967, Ap. J., 149, 283.

Greenstein, J.L., Gunn, J. and Kristian, J. 1971, Ap. J. (Letters), 169, L63.

Greenstein, J.L., Schmidt, M. and Searle, L. 1974, Ap. J. (Letters), 190, L27.

Harper, R.V. and Rose, W.K. 1970, Ap. J., 162, 963.

Hesser, J.E., Lasker, B.M. and Neupert, H.E. 1976, Ap. J., 209, 853.

Hesser, J.E., Lasker, B.M., and Neupert, H.E. 1977, Ap. J. (Letters), 215, L75.

Ingham, W.H., Brecher, K. and Wasserman, I. 1976, Ap. J., 207, 518.

Keeley, D.A. 1979, in White Dwarfs and Variable Degenerate Stars, I.A.U. Colloq. No. 53, ed. by H.M. van Horn and V. Weidemann, University of Rochester, New York, p. 388.

Kemic, S.B. 1974, Joint Inst. Lab. Ap. Report No. 113.

Kemp, J.C. 1970a, Ap. J., 160, 169.

Kemp, J.C. 1970b, Ap. J. (Letters), 162, L69.

Kemp, J.C. 1977, Ap. J., 213, 794.

Kemp, J.C., Coyne, G.V., Swedlund, J.B. and Wolstencroft, R.D. 1974, Ap. J. (Letters), 189, L79.

Kemp, J.C. and Swedlund, J.B. 1970, Ap. J. (Letters), 162, L69.

Kemp, J.C., Swedlund, J.B., Landstreet, J.D. and Angel, J.R.P. 1970, Ap. J. (Letters), 161, L77.

Kemp, J.C., Swedlund, J.B. and Wolstencroft, P.D. 1971, Ap. J. — (Letters), 164, L17.

Kepple, P. and Griem, H. 1968, Dept. of Physics and Astronomy, Univ. of Maryland, Tech. Rep. No. 831.

Kolb, A.C., Griem, H. and Shen, K.Y. 1959, Phys. Rev., 116, 4.

Kurucz, R.L. 1970, Smithsonian Astrophysical Observatory, Special Report 309.

Lamb, F.K. and Sutherland, P.G. 1974, I.A.U. Symposium No. 53, Physics of Dense Matter, ed. C.J. Hansen, D. Reidel, Dordrecht, Holland.

Landi Degl'Innocenti, E. 1976, Ap. J., 209, 208.

Landi Degl'Innocenti, E. and Landi Degl'Innocenti, M. 1975, Nuovo Cim., 134, 27B.

Landolt, A.U. 1968, Ap. J., 153, 151.

Landstreet, J.D. and Angel, J.R.P. 1971, Ap. J. (Letters), 165, L67.

Landstreet, J.D. and Angel, J.R.P. 1975, Ap. J., 196, 819.

Lasker, B.M. and Hesser, J.E. 1971, Ap. J., 163, 289.

Ledoux, P. and Walraven, Th. 1958, Handbuch der Physik, 51, 353.

Liebert, J. 1976, Pub. Astron. Soc. Pac., 88, 490.

Liebert, J., Angel, J.R.P. and Landstreet, J.D. 1975, Ap. J. (Letters), 202, L139.

Liebert, J., Angel, J.R.P., Stockman, H.S., Beaver, E.A. 1978, Ap. J., 225, 181.

Liebert, J., Angel, J.R.P., Stockman, H.S., Spinrad, H. and Beaver, E.A. 1977, Ap. J., 214, 457.

Liebert, J. and Strittmatter, P.A. 1977, Ap. J. (Letters), 217, L59.

Liller, M.H. and Hesser, J.E. 1979, in White Dwarfs and Variable Degenerate Stars, I.A.U. Colloq. No. 53, ed. by H.M. van Horn and V. Weidemann, University of Rochester, New York, p. 376.

Loumos, G.L. and Deeming, T.J. 1978, Astrophys. Space Sci., 56, 285.

Martin, B. and Wickramasinghe, D.T. 1978, Mon. Not. R. Astron. Soc., 183, 533.

Martin, B. and Wickramasinghe, D.T. 1979, preprint.

Mc Graw, J.T. 1976, Ap. J. (Letters), 210, L35.

Mc Graw, J.T. 1977, Ph.D. Thesis, University of Texas, Austin.

Mc Graw, J.T. 1979, Ap. J., 229, 203.

Mc Graw, J.T. 1980, in Stellar Hydrodynamics, I.A.U. Colloq. No. 58, ed. by A.N. Cox and D.S. King, D. Reidel, Dordrecht, Holland, p. 601.

Mc Graw, J.T., Fontaine, G., Starrfield, S.G., Dearborn, D.S.P. and Gustafson, J. 1980, preprint.

Mc Graw, J.T. and Robinson, E.L. 1975, Ap. J. (Letters), 200, L89.

Mestel, L. 1967, in The Magnetic and Related Stars, ed. R.G. Cameron, Mono Book Corporation, Baltimore.

Nather, R.E. 1973, Vistas in Astronomy, 15, 91.

Nather, R.E. and Warner, B. 1971, Mon. Not. R. Astron. Soc., 152, 209.

Osaki, Y. and Hansen, C.J. 1973, Ap. J., 185, 277.

Papaloizou, J. and Pringle, J.E. 1978, Mon. Not. R. Astron. Soc., 182, 423.

Preston, G.W. 1970, Ap. J. (Letters), 160, L143.

Richer, H.B. and Ulrych, T.J. 1974, Ap. J., 185, 277.

Robinson, E.L. 1979, in White Dwarfs and Variable Degenerate Stars, I.A.U. Colloq. No. 53, ed. by H.M. van Horn and V. Weidemann, University of Rochester, New York, p. 343.

Robinson, E.L. 1980, in N.A.S.A Tech. Mem. 80625, Current Problems in Stellar Pulsational Instabilities, ed. by D. Fischel, J.R. Lesh and W.M. Spooks, p. 423.

Robinson, E.L and Kepler, S.O. 1980, in Stellar Hydrodynamics, I.A.U. Colloq. No. 58, ed. by A.N. Cox and D.S. King, D. Reidel, Dordrecht, Holland, p. 601.

Robinson, E.L. and Mc Graw, J.T. 1976, Ap. J. (Letters), 207, L37.

Robinson, E.L., Nather, R.E. and Mc Graw, J.T. 1976, Ap. J., 210, 211.

Robinson, E.L., Stover, R.J., Nather, R.E. and Mc Graw, J.T. 1978, Ap. J., 220, 614.

Rosi, L.A., Zimmermann, R.L. and Kemp, J.C. 1976, Ap. J., 209, 868.

Sazonov, V.N. and Chernomordik, V.V. 1975, Astrophys. Space Sci., 32, 355.

Schulov, O.S. and Kopatskaya, E.N. 1973, Astrofizika (S.S.R.), 10, 117.

Shipman, H.L. 1971, Ap. J., 167, 165.

Shipman, H.L. 1972, Ap. J., 177, 723.

Shipman, H.L. 1979, Ap. J., 228, 240.

Sion, E.N., Lupie, O.L. and Young, K.N. 1978, Pub. Astron. Soc. Pac., 90, 154.

Stover, R.J., Hesser, J.E., Lasker, B.M., Nather, R.E. and Robinson, E.L. 1980, Ap. J., 240, 865.

Swedlund, J.B., Wolstencroft, R.D., Michalsky, J.J. and Kemp, J.C. 1973, Ap. J. (Letters), 187, L121.

Terashita, Y. and Matsushima, S. 1969, Ap. J., 156, 203.

Unno, W. 1956, Pub. Astron. Soc. Jap., 8, 108.

Unno, W., Osaki, Y., Ando., H. and Shibahashi, H. 1980, Nonradial Oscillations of Stars, University of Tokyo, Tokyo.

Vauclair, G. 1971, in I.A.U. Symp. No. 42, White Dwarfs, ed. by C.J. Luyten, D. Reidel, Dordrecht, Holland, p. 145.

Warner, B. and Robinson, E.L. 1972, Nature Phys. Sci., 239, 2.

Wegner, G. 1971, Pub. Astron. Soc. Pac., 83, 205.

Wegner, G. 1976, Mon. Not. R. Astron. Soc., 174, 191.

Wegner, G. 1977a, Mem. Soc. Astr. Ital., 48, 27.

Wegner, G. 1977b, Mon. Not. Astron. Soc. S. Afr., 36, 63.

Wegner, G. 1980, Astron. J., 85, 538.

Weidemann, V. 1975, in Problems in Stellar Atmospheres and Envelopes, eds. B. Baschek, W.H. Kegel and G. Traving, Springer-Verlag, New York, p. 173.

Wickramasinghe, D.T. and Bessell, M.S. 1976, Ap. J. (Letters), 203, L39.

Wickramasinghe, D.T. and Bessell, M.S. 1979, Mon. Not. R. Astron. Soc., 186, 399.

Wickramasinghe, D.T. and Martin, B. 1979, Mon. Not. R. Astron. Soc., 188, 165.

Wickramasinghe, D.T. and Strittmatter, P.A. 1972, Mon. Not. R. Astron. Soc., 160, 421.

Wickramasinghe, D.T., Thompson, R.I. and Strittmatter, P.A. 1972, Ap. J., 178, 763.

Wickramasinghe, D.T., Whelan, J.A.J. and Bessell, M.S. 1977, Mon. Not. R. Astron. Soc., 180, 377.

Winget, D.E., van Horn, H.M. and Hansen, C.J. 1981, Ap.J., in press.